MOTION RESPONSE SIMULATION OF DAMAGED FLOATING PLATFORMS

Muhittin Söylemez, B.Sc., M.Sc.

Thesis submitted for the Degree of Doctor of Philosophy

Department of Naval Architecture and Ocean Engineering
University of Glasgow

January 1990

ProQuest LLC.
789 East Eisenhower Parkway
P.O. Box 1346
Ann Arbor, MI 48106 – 1346

DEDICATED

TO

MY PARENTS

DECLARATION

Except where reference is made to the work of others,
this thesis is believed to be original.

ACKNOWLEDGEMENTS

The research study reported in the thesis was made possible with the assistance of the members of the Department of Naval Architecture and Ocean Engineering at the University of Glasgow.

The author would like to thank the following;

Professor D. Faulkner, Head of Department, for allowing him to carry out this study and for his constructive guidance and encouragement.

Dr. A. Incecik for his excellent supervision, his continuous assistance with many aspects of the study, and his encouragement.

Professor S. M. Çalışal, for his valuable discussions on the time-domain simulation techniques during his visit to the University of Glasgow.

Dr. M. Atlar for his assistance which I received for the work presented in Chapter 2.

Mr. İsmail H. Helvacıoğlu for his stimulating discussions and valuable assistance in completing the thesis.

Mr James R. MacGregor, research colleague, with whom I have enjoyed working at the Hydrodynamics Laboratory.

Mr. Oğuz Yılmaz for his contribution towards the completion of the thesis.

Mr. D. Percival for his assistance during the development of the computer software routines.

Mr. R. Christison and the technicians at the Hydrodynamic Laboratory, for their help during the experiments.

Finally, the financial support in the form of a scholarship from the Turkish Ministry of Education is gratefully acknowledged.

CONTENTS

LIST OF FIGURES

Page

CHAPTER 2

CHAPTER 3

CHAPTER 4

CHAPTER 5

CHAPTER 6

APPENDICES

LIST OF TABLES

CHAPTER 5

CHAPTER 6

APPENDICES

SUMMARY

This thesis describes a computer based method and a procedure to simulate the motion response of a damaged platform under wave, wind and current effects. The aim of the study was to develop an analysis procedure which could be a useful tool to designers and certifying authorities in assessing the safety of mobile platforms in extreme environmental and damaged conditions.

The thesis begins by explaining the benefits of using floating structures in developing oil fields. Basic stability requirements for floating production vessels are summarised. Recent and past damage simulation studies in the literature are reviewed. Some information about the number of accidents involving floating offshore platforms operated world-wide is presented. A few of the disasters occurring in recent years are given as examples to emphasise the importance of the subject.

The Morison approach and 2D source-sink distribution technique are reviewed, and calculations of wave forces acting on a semi-submersible are carried out in order to make comparisons between the two methods. Theoretical derivations of wave forces in the frequency domain based on the Morison approach are carried out in detail for a twin-hulled semi-submersible. The development of computer programs based on both methods is summarised.

A general method for calculating wave forces and moments on circular cylinders of offshore structures is derived. By using the developed method one can calculate the wave loading on cylindrical members of fixed or floating offshore structures orientated randomly in waves. This method also provides a basic tool for determining the wave forces and moments that a floating structure is subjected to as it experiences large amplitude oscillations in six degrees of freedom.

A general method is established in this chapter to calculate the hydrodynamic loading due to the rigid body motion of the platform. The calculation of restoring forces

is discussed: a detailed description of the methods used to calculate hydrostatic forces, mooring stiffness coefficients and wind forces is given in the appendices. The calculation of inertia forces and moments defined from Newton's second law is introduced as part of a general calculation procedure. The derivation and the solution of motion equations in the time domain are presented.

Details of model tests carried out to validate the non-linear large amplitude motion calculation procedures are presented.

A description of a circular twin-hulled semi-submersible model and the loading conditions is given. The test setup and instrumentation are presented briefly. Test procedures for inclining, natural period and motion tests in waves are discussed. Methods of analysis of motion response measurements in six degrees of freedom in intact, transient and damaged conditions for head and beam seas are given. The results of motion response measurements are presented in time histories. In order to validate the numerical prediction procedures and the software based on these procedures, the physical test conditions are simulated numerically and a comparison of test results with numerical predictions is presented.

Simulation studies based on the non-linear motion equations are presented with the aim of providing comparisons to illustrate the effects of non-linearities in wave and motion induced forces. A summary of the systematic study carried out to illustrate the effects of non-linear terms on the solution of the motion response equations is given. The results of the parametric studies to investigate the effects of flooding rate and of size of damaged compartment on motion response characteristics are also discussed.

The other aspects of roll motion such as the effects of non-linear drag force, first order wave elevation, different wave heights and GM's, and non-linear added mass and damping forces on the motion behaviour and the steady tilt of semi-submersibles are investigated. The variations of GM and GZ values as a function of heel angle are also presented.

CHAPTER 1

INTRODUCTION

1.1 OIL AND GAS PRODUCTION FACILITIES

The development of small oilfields is common not only in the North Sea but also in other parts of the world. Development forecasts (Goodfellow Associates Limited, 1986) suggest that 80% of future production will be from fields with recoverable reserves of 100 million barrels or less. Proposed early production and subsea systems for small oilfields are as follows:

i) Semi-submersible exporting crude oil through offshore loading,
ii) Semi-submersible exporting crude oil through submarine pipeline,
iii) Tankers with storage, and shuttle tankers,
iv) Articulated columns,
v) Jack-up rigs.

Since the fixed production platforms are not cost-effective for deep waters, floating production platforms together with subsea systems are accepted as being more feasible solutions for deep water application.

The increasing incidence of small field development has highlighted the importance of floating production systems as opposed to more conventional jacket systems. The benefits of using a floating production system are as follows:

i) Low initial capital investment
ii) Early production and thus early return on investment
iii) Low abandonment costs
iv) Ease of relocation at end of field life
v) Good mobility allows system to be moved from politically unstable areas or after change of perceived reservoir.

The semi-submersible was designed in the 1950's primarily as an exploratory drilling vessel. The use of the semi-submersible has since been extended to include floating production facilities, and construction and diving support platforms. Moreover,

the semi-submersible hull has been proposed for use as a mobile radar tracking ocean platform for NASA, the USAF and the Navy. It has also been proposed for use to support combat training systems (Shields et al. 1987, Shields and Zueck, 1984). New generation semi-submersibles have been proposed for use in deep water and hostile environments (Deepwater Drilling Report Aug., 1982). Innovative semi-submersibles were designed to help some of the service problems on fixed platforms and subsea pipelines (Deepwater Drilling Report June, 1982). Recently, the development of a new multi-purpose semi-submersible design proposed by Seaways Engineering (U.K.) Ltd. was assisted by the Department of Naval Architecture and Ocean Engineering at the University of Glasgow (Faulkner et al. 1989). While the use of semi-submersibles has increased, the incidence of two major offshore disasters has led to a focus on the damaged stability of semi-submersibles.

1.2 STABILITY AND PAYLOAD OF FLOATING OFFSHORE UNITS

Basic Stability Requirements

A major consideration of any floating production vessel is the weight of payload required. With this payload onboard, the vessel must meet certain stability requirements.

The offshore structure should experience minimal movement to provide a stable work station for operations such as drilling and producing oil.

Moreover, from the motion response point of view the main reason for adopting the semi-submersible geometry in preference to a monohull vessel is probably the better motion response that can be achieved in a relatively small unit.

There are worldwide a variety of semi-submersible vessels available (Martinovich and Praught, 1986). The dynamics and performance of these vessels are of great importance in overall field development.

Historical Development of Stability Work on Semi-Submersibles

As the demand for floating offshore vessels for the development of marginal oil fields in deeper waters increased in the mid 1970's, studies on the stability of semi-submersibles were initiated in an effort to provide safer stability limits for existing and new design semi-submersibles. Pioneering work on the problem was conducted by Numata and Michel (1974), Numata and McClure (1975) and Numata et al (1976). The work carried out by Numata et al (1976) was directed by SNAME Panel MS-3 and concerned with the effects of underdeck clearance and wave-induced steady heel on the stability of semi-submersibles. Similar effects on the stability assessment was also investigated by Kuo et al (1977), and De Souza and Miller (1978). The importance of damaged stability was highlighted by Dahle (1981) and Abicht (1982) after Alexander Kielland floating platform disaster in the North Sea in 1980. The objective of the research performed by Hineno et al (1982) was to identify a method to predict the minimum underdeck clearance of a semi-submersible platform in irregular waves. The influence of mooring lines on the stability of semi-submersible platforms was investigated by Takarada et al (1982). McIver et al (1983) highlighted the requirements for a more general approach to the total stability analysis, that is, static and dynamic stability. A quasi-dynamic stability assessment procedure based on the energy-balance method was introduced by Vassalos et al (1985). Takarada et al (1986) investigated the possibility of capsizing in survival sea conditions, such as steady heeling moment, and proposed a new computational approach for determining the required minimum GM. A pilot study on the intact stability of semi-submersibles, undertaken by ABS was presented by Chen et al (1986). Takai et al (1987) examined the characteristics of static stability of semi-submersibles using the results of parametric studies. After the capsize of two semi-submersibles (Alexander L. Kielland and Ocean Ranger) with substantial loss of life in the early 1980's, the ABS initiated the pilot study mentioned above which was continued as a joint industry project in order to develop a dynamic-response-based criterion. The new criterion will be studied by the IMO with a view to replacing the present IMO MODU code. ABS work which was summarised by Shark et al (1989) gave examples of dynamic motion simulations. These dynamic motion analyses were carried out for the

generic offshore units comprising three or four column-stabilised semi-submersibles. The analyses only considered post-flooding conditions in establishing the new stability criterion. However, transient conditions are also important in assessing the stability of a mobile platform as emphasized by several researchers.

The literature reviewed in the preceding section, apart from the last reference, refers to the intact stability of semi-submersibles. There are also published studies carried out over the years on dynamic motion analysis of damaged semi-submersibles. The first time-domain simulation study for a semi-submersible was reported by Paulling (1977), and aimed at analysing the non-linear terms in the motion equations. Experiments with a semi-submersible platform having a large list angle were carried out by Huang et al (1982) and Huang and Naess (1983). Stability and dynamics of semi-submersibles after accidental damage (post-flooding condition) were also investigated experimentally by Clauss (1984), Nakamura et al (1984) and Naes et al (1985). Naess and Hoff (1984) presented a non-linear time-domain simulation method to predict the motions of a platform with large list angles. A brief methodology in predicting the behaviour of a damaged platform in progressive and post-flooding conditions is also reported by Moncarz et al (1985). Huse and Nadrelid (1985) stated in their work that the effect of waves and dynamic wind forces should be taken into account when the dynamic stability of a semi-submersible is examined. The need to perform a dynamic analysis for both intact and damaged platform conditions in order to evaluate proper locations of floodable openings was highlighted by Dahle (1985). The transient (progressive flooding or sudden breaking of mooring lines) behaviour of a semi-submersible type platform was studied both theoretically and experimentally by Adachi and Kagemoto (1986). Kagemoto et al (1987) emphasized the importance of dynamic effects in the prediction of the behaviour of semi-submersibles after damage. Mourelle et al (1987) investigated the non-linear uncoupled motions of a semi-submersible anchored with catenary moorings. The stabilisation of a heavily listed semi-submersible by adjusting the ballast water was proposed by Takaki et al (1987).

The studies referred to above did not present a complete motion simulation procedure which takes into account intact, progressive flooding and post-flooding

conditions in coupled six-degrees of freedom. The development of generalised non-linear motion equations (coupled in six-degrees of freedom) to study intact, progressive and post-flooding behaviour of a floating structure was presented by the author (1988).

1.3 REQUIREMENT FOR DYNAMIC MOTION ANALYSIS

The damaged stability criteria based on the experience gained with ships over many years have been applied to floating platforms. However, these rules, based on the calm water level assumption, are not necessarily realistic recommendations for floating structures having different geometrical configurations from ships.

Loss of, or damage to, any buoyant compartment due to accidents, including collisions, structural failure, explosions, etc. can cause submergence of non-watertight openings. Classification rules combine static stability properties with dynamic wind load. These rules appear to be unrealistic since high waves are not taken into account. Additionally, a damage zone is defined as an area bounded by horizontal lines 5 m above and 3 m below the waterline (Springett and Praught, 1986), whereas flooding can start anywhere on the platform, for instance due to structural failure, as happened in the Alexander L. Kielland disaster (Rusaas, 1982), and in the Ocean Ranger disaster (Dudgeon, 1986), where chain lockers were damaged and high waves subsequently caused the flooding.

Present classification society rules for damaged stability can be summarised as follows:

The damaged platform's metacentric height in calm water is calculated. A wind heeling moment for a wind speed of 100 knots or more is used in connection with metacentric height of damaged platform to determine the tilt or list angle without taking into account the effects of the waves. With such high winds, the assumption of calm water and static attitude of the platform are obviously unrealistic.

Due to the considerable differences between the geometrical configurations of the floating platforms and those of ships, global criteria based on the experience gained from ships may not be appropriate.

With today's modern technology, i.e. fast computers, it is possible to develop more realistic mathematical models for floating platforms or ships by simulating their behaviour in a damaged condition, taking into account effects of waves, winds, currents, etc.

Flooding rate and associated changes in the vessel buoyancy are significant factors in rescue programmes or in planning remedial action. Since flooding rate is a time-dependent process with the vessel submergence and the sea-state history, a time-domain analysis is necessary to approach the problem more realistically.

In the frequency domain analysis of motion, it is assumed that the platform motions are small and the member configurations are symmetrical. All hydrodynamic coefficients are calculated and the motion equations are also solved by assuming that the platform remains at the calm water level. These assumptions can be relaxed when motion equations are derived and solved in the time-domain.

In the time-domain simulation procedure, damaged condition can be considered in two stages, i.e. progressive flooding and post damage. During progressive flooding, mass, all hydrodynamic coefficients and excitation forces and moments vary with time and consequently with position. In solving large amplitude non-linear coupled motion equations in the time-domain, one needs to carry out a step-by-step integration procedure. In this study, the Runge-Kutta method was adopted.

Since the step-by-step technique to solve the motion response will require the calculation of hydrodynamic, hydrostatic and forcing function many times over a given wave cycle, one has to select an appropriate method to determine these values so that the computational task will be feasible.

Methods to be considered are:

a) Morison approach,
b) 2-D sink-source distribution technique,
c) 3-D sink-source distribution technique.

The method chosen should permit the time-domain simulations to be carried out accurately and quickly by a computer. With this in mind, calculations were carried out by the author to compare the Morison approach with the 2-D sink-source distribution technique. In this study, 3-D sink-source distribution technique is not considered.

The reason behind the idea of the comparison is to ascertain whether the calculations can be accurate enough if the Morison approach is used and to check that computing time and space will also be manageable.

In these calculations the Morison approach considers the inertia forces and drag(velocity) forces whereas the 2-D sink-source distribution technique does not take into account drag forces.

1.4 STUDY OBJECTIVES

The purpose of the study is to develop a prediction technique to simulate the motion response of a damaged platform under wave, wind and current forces.

Approach Adopted

The analysis technique employs large displacement non-linear motion equations. Solutions were obtained in the time-domain to predict the motion characteristics. In this study, analysis procedures were developed to calculate:

a) Wave loading on asymmetrical structural configurations

b) Hydrodynamic reaction forces (inertia or moment of inertia, damping and restoring forces) on asymmetrical shapes.

During the damage simulation, change in the mass of the structure as well as wave and hydrodynamic reaction forces, were taken into account.

The expected benefits of the study to designers and to the certifying bodies may be summarised as follows:

a) Simulation of the motion response and dynamic stability of a damaged floating structure in order to determine the adequacy of watertight spacings and openings for a given structure,

b) The provision of an accurate tool to predict the behaviour of a damaged platform in order to assess the adequacy of existing damaged stability rules,

c) The provision of a reliable tool to determine the ultimate strength of the members of a damaged structure.

1.5 STRUCTURE OF THESIS

The work presented in the thesis begins by comparing the methods intended to be employed in the calculation of external forces acting on the semi-submersible. Therefore, Chapter 2 is devoted to a review of the Morison and 2-D source-sink distribution techniques and to a presentation of a comparison between the two methods. In Chapter 3, the derivation of a general method to calculate wave forces on the cylindrical members of offshore structures is given.

A general method is established in Chapter 4 to calculate the hydrodynamic loading due to the rigid body motion of the platform. A discussion is given on the calculation of restoring forces. The calculation of inertia forces and moments defined from Newton's

second law are introduced in a general calculation procedure. The derivation and the solution of motion equations in the time-domain are presented.

In chapter 5, details of the model tests carried out to validate the non-linear large amplitude motion calculation procedures are presented. Methods of analysis of motion response measurements in six degrees of freedom in intact, transient and damaged conditions for head and beam seas are given. Finally, in Chapter 6, a summary of the systematic study carried out to illustrate the effects of non-linear terms on the solution of the motion response equations is given.

CHAPTER 2

REVIEW OF THE METHODS

2.1 INTRODUCTION

The calculation of hydrodynamic load on offshore structures is of great importance to designers involved in offshore engineering. The hydrodynamic load calculations for design form a very difficult task because the environmental conditions are very complex and, because interaction occurs between waves and structure. Although ocean waves are of a random nature, it is of great interest to designers to investigate the environmental forces and resulting motions of offshore structures under regular sea conditions. This is known as the design wave approach. This type of analysis technique is fully deterministic and considers two parameters which are the period and the height of a given wave. However, there is another approach which works with the wave-energy spectrum by using probabilistic theory. The statistical design parameters; extreme forces and significant motion responses, etc. could be predicted by employing this approach.

There are a wide variety of offshore structures to accomplish various tasks. Among them are; jacket type platforms which are composed of small tubular members; concrete gravity type platforms; semi-submersibles and tension-leg platforms. Depending on the type and size of the members of an offshore structure in comparison with the wave length, different calculation methods are employed in predicting the hydrodynamic forces and resulting responses.

The existing methods for the hydrodynamic loads on offshore structures are mainly based on one of the following: Morison's Equation, two dimensional (2-D) and three dimensional (3-D) source-sink distribution techniques. Among these methods, the 3-D method is used generally for structures comprising large structural members. If a structure consists of small members, the strip approach utilising Morison's equation or 2–D source-sink distribution method provides an adequate tool for design and analysis calculation.

Oo and Miller (1976) examined the heave motion aspect of several different type of semi-submersible design. The sensitivity of motion responses of a semi-submersible and a tension leg platform to different calculation methods in use for computing the

hydrodynamic loads on floating platforms was discussed by Paulling, J.R. (1981). A comparison of methods for calculating the motion of a semi-submersible was carried out by the 17th ITTC Ocean Engineering Committee. A summary of the results of the project in which 34 computer programs from 28 different organisations were used was reported by Takagi et al. (1985). The results of the study predicting wave and motion induced forces on a tension leg platform, which was initiated by the 9th ISSC, were published by Eatock Taylor and Jefferys (1986). The study reported by Standing (1987) examined the effects of wave spreading on the motion response of a transportation barge. Two different offshore platforms: a semi-submersible and an articulated tower, were considered in quantifying the effects of different design parameters and analysis methods on motion and structural response predictions by Incecik et al. (1987). Östergaard and Schellin (1987) presented hydrodynamic calculations as applied to a variety of offshore structures and discussed the validity and accuracy of predicted results by comparison with closed form solutions or model test measurements. In these studies, it was concluded that the Morison approach and those based on the potential theory compare favourably with each other and with measurements.

In the following sections of this chapter, the Morison approach and 2D source-sink distribution technique are compared in calculating the wave forces on a semi-submersible. Theoretical derivations of wave forces in the frequency domain based on the Morison approach are carried out in detail for a twin-hulled semi-submersible given in Fig.2.2.

In this study, the calculation of the wave kinematic properties is based on the Airy wave theory. The reasons for choosing the linear Airy wave theory instead of a non-linear wave theory were due to the following factors:

a) In a pilot study carried out with the Stokes fifth-order theory it was found that there was not any converging solution in lower wave frequency range. Dean (1970) also indicated that if $D/T^2<0.1$ (D is defined in meter), Stokes fifth-order theory does not yield converging solutions. For water depth of 150 metres this corresponds to $\omega<0.2$ rad/s. Since one of the objectives of this study is to investigate the large motions around the natural frequencies the use of Stokes fifth-order theory would have not made motion

predictions possible around the natural roll and pitch frequencies.

b) Another high-order wave theory developed by Dean (1965) was considered and found that implementation of this theory into a time-domain simulation program will not be feasible due to very extensive computer time requirements.

The development of computer programs based on both methods is summarised. A summary of and conclusions arising from the results are presented at the end of the chapter.

2.2 REVIEW OF THE METHODS

2.2.1 HYDRODYNAMIC FORCES

The hydrodynamic forces to which an offshore structure is subject are the result of various physical mechanisms. They can linearly be decomposed into the following components:

1) *Froude-Krylov force*: This force is due to the hydrodynamic pressure change below the surface of a wave train while the wave is proceeding. It is assumed that the presence of the structure does not interfere with the flow field. The Froude-Krylov force can be calculated from the dynamic pressure which is derived from the incident wave potential.

2) *Diffraction force*: If the interaction between the structure and the waves is taken into account, (assuming that the structure is motionless) the potential called scattering wave potential must be added to the incident wave potential within the limits of linear theory.

3) *Radiation force*: The radiation potential resulting from the oscillation of the structure in calm water gives rise to the radiation force (or motion induced force). This

must also be added to those described above with the linear theory assumption.

4) *Drag force*: The force in-line with the velocity which is proportional to the square of the velocity due to the separation of the boundary layer.

5) *Lift force*: Lift force is generated when two separation points behind the cylinder are not symmetrical about the direction of wave particle velocity or if the vortex shedding is in non-symmetrical order. Lift forces act on the structure transversely to the velocity direction.

6) *Other forces*: The wave forces are non-linear in nature. Those described in 1-2-3 are linear and first order. There are also forces of second or higher order which could induce significant motions of some platform configurations. For example compliant platforms (i.e. tension leg, articulated tower and SALM systems) could experience large motions due to the second-order forces.

2.2.2 EVALUATION OF WAVE FORCES ON CYLINDERS BY MORISON EQUATION

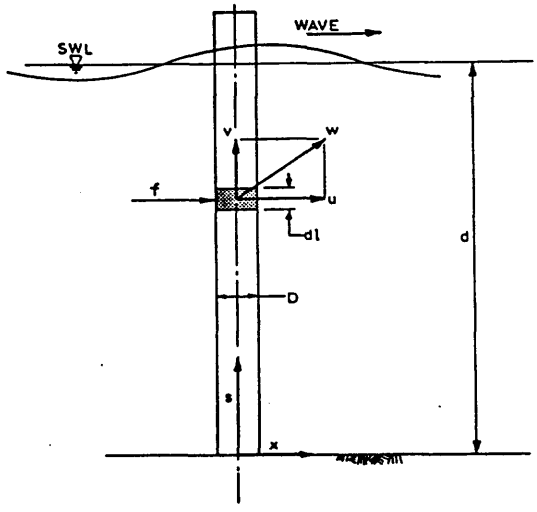

Fig.2.1 Definition sketch for wave forces on small diameter cylinder (Chakrabarti,1987)

The Morison equation was first proposed by Morison et al. (1950) where the authors described the horizontal wave forces acting on a vertical pile which extends from the sea-bed up to the free surface (Fig.2.1). Morison et al. (1950) suggested that one may superimpose the two flow regimes, which generate inertia and drag forces to obtain the total time-varying load per unit length of a cylinder which is stationary in a plane flow field with arbitrary free stream velocity $u(t)$.

The interpretation of the inertia force is that in principle a water particle moving in a wave pattern creates a momentum due to its motion. The water particle acceleration changes as it passes around a circular cylinder. According to Newton's law the change of the momentum with respect to time results in an excitation force acting on the cylinder. The inertia force acting on a segment (ds) of a cylinder can be expressed in terms of the wave particle acceleration at the centre of cross-section of a small diameter cylinder as follows:

$$df_M = C_M \rho \frac{\pi}{4} D^2 \frac{\partial u}{\partial t} ds \tag{2.1}$$

where

df_M	Inertia force on the segment ds of the vertical cylinder
D	Cylinder diameter
$\frac{\partial u}{\partial t}$	Local water particle acceleration at the centre line of the cylinder
C_M	Inertia coefficient
ρ	Water density

The wake region behind the cylinder gives rise to the drag force component. Since the pressure in the wake field is dropped compared to that in the region where the cylinder faces oncoming stream, a pressure differential is created in an instant. The change in the pressure causes drag or velocity force acting in the direction of the instantaneous water particle velocity. The drag force component in the Morison Equation is given in the following form:

$$df_D = \tfrac{1}{2} C_D \rho D u |u| ds \tag{2.2}$$

where

df_D	Drag force on the segment ds on the vertical cylinder
u	Instantaneous water particle velocity
C_D	Drag coefficient

C_D coefficients for the drag force calculations in waves are not only the function of the Reynolds Number which changes throughout one wave cycle, but they are also related to the inertia coefficients with the Keulegan-Carpenter Number which is defined as uT/D. Therefore, the most accurate viscous force prediction in the waves could be obtained from the experimental results with time averaging where flow is sinusoidally oscillating or from real wave data. For the prediction of drag forces in waves, C_D values obtained from the steady flow results may be used, although the values of drag coefficients in waves show similarity to the drag coefficients in steady flow, where C_D decreases considerably with Reynolds Number over the approximate range $10^4<Re<10^6$. It should be noted that special care must be taken if steady flow results are applied to sea-wave flows due to the two main flow phenomena which do not exist neither in steady flow nor in the sinusoidally oscillating flow:

i) The water particle motions are orbital,

ii) Irregularities of sea-waves.

If a member of the structure is relatively large with respect to the wave height, the viscous drag coefficient becomes less sensitive to Reynolds Number and steady flow results may be more suitable.

The drag force is proportional to the square of the flow particle velocity and in the case of an oscillatory flow the flow velocity is multiplied by the absolute value of the flow velocity to ensure that a correct sign will be assigned to the velocity force.

When the characteristic dimensions of members of a structure are equal to 0.2 times the wave length or greater, wave force calculations should take into account the scattering potential. Wave force calculation on large arbitrary geometries utilising the 3-D sink-source distribution method is also described by several authors (see Hogben and Standing, 1974; Faltinsen and Michelsen 1974; Garrison 1978).

It was proved that wave forces due to water particle velocity and accelerations can be computed by Morison equation only, if the characteristic dimensions of the members of a structure do not exceed 0.2 times the wave length. Various flow regimes are summarised as follows (Hallam et al. 1978):

$D/\lambda>1$	Conditions approximate to pure reflection	
$D/\lambda>0.2$	Diffraction increasingly important	
$D/\lambda<0.2$	Morison approach is valid	
$D/W>0.2$	Inertia increasingly predominant	Within Morison Equation
D/W<0.2	Drag predominant	

where

D The diameter or width of the member

λ The wave length

W The orbit width of the water particle.

$$= \frac{H}{\tanh\left(\frac{2\pi d}{\lambda}\right)} \tag{2.3}$$

where

H the wave height

d the water depth.

Final form of the Morison equation is obtained by summing inertia and drag forces given in Eqs.(2.1-2.2).

$$dF_T = C_M \rho A_S \dot{u} ds + \tfrac{1}{2} \rho C_D D u |u| ds \tag{2.4}$$

where

D	Diameter of the member
A_S	Cross section area
$\dot{u}$	$\partial u/\partial t$
L	Length of the member

or

$$F_T = \int_L C_M \rho A_S \dot{u} ds + \int_L \frac{1}{2} \rho C_D D u |u| ds \tag{2.5}$$

2.2.3 REVIEW OF THE 2D SOURCE-SINK METHOD

In combination with the strip theory approach the 2D source-sink distribution technique was first introduced for the calculation of semi-submersible motions by Kim et al. (1973), as an alternative to the Morison equation. In this approach, a floating structure is divided into several elements (i.e. lower hulls, columns, bracings etc.) and each element is considered individually. The hydrodynamic interference between the members of the structure is neglected. A comparison of the approach proposed by Kim et al. (1973) with improved 2-D source-sink distribution technique as well as with 3-D source-sink distribution technique was given by Mathisen et al. (1980).

The forces calculated using the strip method given by Kim et al. (1973) take into account the free surface effect. The use of the strip method for twin-hulled semi-submersible is satisfactory for main hulls since their longitudinal dimensions in the direction normal to wave propagation are large compared to its other dimensions. However the use of this method for vertical column sections, bracings etc. is open to question since the strip theory rules are not satisfied for such members of the semi-submersible.

In this study the beamwise strip theory was utilised in combination with the 2D source-sink distribution technique which is known as Frank Close-Fit method as explained in detail by Atlar (1985 a). The Frank-Close Fit method will be applied to a

semi-submersible platform geometry shown in Fig.2.2 to determine the wave and motion induced forces acting on the structure.

The method employs linearised potential theory. Evaluation of the wave exciting forces including wave diffraction requires the solution of a boundary value problem which is identical to the problem of an oscillating body in proximity to an initially calm free surface. The semi-submersible is split into many beamwise strips as shown in Fig.2.3 to calculate the motion (added mass and damping) and wave induced forces. The source and sinks (Green's Functions) which satisfy the various boundary conditions represent the velocity potential of the fluid at each location point around each strip. The fluid disturbance due to the body motions which is represented by the radiation potential is utilized to obtain the sectional motion-induced force (added mass and damping) coefficients. In order to obtain the sectional wave–induced (exciting) forces which consist of diffraction and the Froude-Krylov components, incident wave potential and diffraction potential are combined within the kinematic boundary condition.

In order to perform the sectional hydrodynamic force calculations for the semi-submersible model, two available computer programs, based on the Frank-Close Fit technique, BURAK for the motion induced coefficients and AYHANR for the wave induced forces were used, Atlar and Lai (1985 b). A numerical integration procedure were carried out to obtain total hydrodynamic loads acting on the structure. The motion equations were derived from Newton's second law. The inverse matrix technique is used to solve the coupled motion equations.

In this study the following points were highlighted:

i) The effects of hydrodynamic interference between the sectional hull and column forces,

ii) The effect of hydrodynamic coupling on the motion response,

iii) The comparisons of the forces, moments and motion responses obtained from the calculations based on the Morison equation and the 2D source-sink distribution technique.

2.2.4 FORMULATION OF HYDRODYNAMIC LOADS AND DERIVATION OF MOTION EQUATIONS IN FREQUENCY DOMAIN

In this section, theoretical derivations for the calculations of wave exciting forces and moments acting on a twin hull semi-submersible are carried out by using Morison's Equation. The forces and resulting motions of the semi-submersible derived in this section include head and beam sea conditions.

The inertia force term given in Eq.(2.1) can be expressed in terms of pressure (F_P) and acceleration (F_A) components as follows:

$$F_I = F_P + F_A \tag{2.6}$$

where

$$F_P = \rho A_S \dot{u} L \tag{2.7}$$

and

$$F_A = \rho k_M A_S \dot{u} L \tag{2.8}$$

where

k_M Added mass coefficient

In the following, the derivation of vertical and horizontal forces and moments to predict heave, surge, roll and pitch mode of motions using the Morison approach will be summarised.

Derivation of Vertical Forces for Head Sea Condition

Vertical forces on the hull:

Pressure force: From Eq.(2.7)

$$F_P = -\int_{-L/2}^{L/2} \rho \pi R_H^2 \, 0.5 H_\omega \omega^2 e^{-kH} \cos(kx - \omega t)\, dx \tag{2.9}$$

where

R_H	Radius of hull
H_ω	Wave height
ω	Wave frequency
ρ	Water density
k	Wave number
H	Distance between calm water level and centre of hull

Acceleration force: From Eq.(2.8)

$$F_A = -\int_{-L/2}^{L/2} k_M \rho \pi R_H^2 \, 0.5 H_\omega \omega^2 e^{-kH} \cos(kx - \omega t)\, dx \tag{2.10}$$

Velocity (Drag) force: From Eq.(2.2)

$$F_V = -\int_{-L/2}^{L/2} \frac{1}{2} C_D \rho A_L (0.5 H_\omega \omega)^2 e^{-2kH} \sin(kx - \omega t) \left|\sin(kx - \omega t)\right| dx \tag{2.11}$$

Total vertical force acting on the hull is written as a summation of the three components given above, in the following form:

$$F_{TH} = -\int_{-L/2}^{L/2} C_M \rho \pi R_H^2 0.5 H_\omega e^{-kH} \cos(kx - \omega t)dx$$

$$+ \tfrac{1}{2} C_D \rho A_L (0.5 H_\omega \omega)^2 e^{-2kH} \int_{-L/2}^{L/2} \sin(kx - \omega t)\left|\sin(kx - \omega t)\right| dx \qquad (2.12)$$

where

$$C_M = 1 + k_M$$

Vertical forces on the column,

Pressure force:

$$F_p = p_d \pi R_c^2$$

or

$$F_P = \rho g \pi R_C^2 0.5 H_\omega e^{-kH_c} \cos(kx_C - \omega t) \qquad (2.13)$$

where

p_d	Dynamic pressure
R_C	Radius of column
x_C	Horizontal distance between centre of column and the vertical axis

Acceleration force:

$$F_A = M_{AVM,V} \ddot{u}_y$$

$$F_A = -\tfrac{4}{3} \rho R_C^2 0.5 H_\omega \omega^2 e^{-kH_c} \cos(kx_C - \omega t) \qquad (2.14)$$

where

$M_{AVM,V}$ Vertical added mass

$= \frac{4}{3}\rho R_C^3$

given by Hooft (1972).

Velocity force:

$$F_V = \tfrac{1}{2}\rho \pi R_C^2 C_D u_y |u_y|$$

$$F_V = \tfrac{1}{2} C_D \rho \pi R_C^2 (0.5 H_\omega \omega)^2 e^{-2kH_C} \sin(kx_C - \omega t) |\sin(kx_C - \omega t)| \quad (2.15)$$

Total vertical force acting on a column is written as

$$F_{TC} = \rho\, 0.5 H_\omega (g\pi - \tfrac{4}{3}\omega^2 R_C) e^{-kH_C} \cos(kx_C - \omega t) - \tfrac{1}{2} C_D \rho \pi R_C^2 (0.52 H_\omega \omega)^2 e^{-2kH_C} \sin(kx_C - \omega t) |\sin(kx_C - \omega t)| \quad (2.16)$$

The summation of F_{TH} and F_{TC} for each member of the semi-submersible is carried out to calculate the total vertical force.

The motion equation to obtain heave displacements can be written as:

$$(m + a)\ddot{y} + c\dot{y} + k y = F \cos \omega t \quad (2.17)$$

where

m	mass of the structure
a	added mass of the structure
c	damping coefficient
k	stiffness coefficient

If it is assumed that F is constant for a given frequency, the usual solution for a linear single degree of freedom system is

$$x = Y_0 e^{-i\omega t} \tag{2.18}$$

where

$$Y_0 = \frac{F}{\sqrt{(k - (m + a)\omega^2)^2 + (c\omega)^2}} \tag{2.19}$$

It is possible to write X_0 in terms of frequency and damping ratio as follows:

$$Y_0 = \frac{F / k}{\sqrt{(1 - r^2)^2 + (2r d)^2}} \tag{2.20}$$

where

$$r = \frac{\omega}{\omega_n} \tag{2.21}$$

$$\omega_n = \sqrt{\frac{k}{(m + a)}} \tag{2.22}$$

$$d = \frac{c}{c_c} \tag{2.23}$$

where critical damping is

$$c_c = 2\sqrt{(m + a)k} \tag{2.24}$$

Derivation of Vertical Forces for Beam Sea Condition

The vertical forces for beam sea condition can be derived by following a similar procedure to that of the head sea condition.

Total vertical force on the hull for beam sea condition can be written as follows:

$$F_{TH} = -C_M \rho \omega^2 \pi R_H^2 0.5H_\omega e^{-kH} L_H \cos(kx_C - \omega t) + \tfrac{1}{2} C_D \rho A_L (0.5H_\omega \omega)^2 e^{-2kH} L_H \sin(kx_C - \omega t) \left| \sin(kx_C - \omega t) \right| \quad (2.25)$$

where

L_H Length of hull

Total vertical force on the column for beam sea condition can be written as:

$$F_{TC} = \rho 0.5H_\omega (g\pi - \tfrac{4}{3}\omega^2 R_C) R_C^2 e^{-kH_C} \cos(kx_C - \omega t) - \tfrac{1}{2} C_D \rho A_L (0.5H_\omega \omega)^2 e^{-2kH_C} \sin(kx_C - \omega t) \left| \sin(kx_C - \omega t) \right| \quad (2.26)$$

Derivation of Horizontal Forces for Head Sea Condition

The total horizontal force on the hull can be written as follows:

$$F_{TH} = \rho \pi R_H^2 0.5H_\omega g e^{-kH} \cos(k x_C - \omega t) + k_M 0.5H_\omega \omega^2 e^{-kH} L_H \sin(k x_C - \omega t) + \tfrac{1}{2} C_D \rho A_L (0.5H_\omega \omega)^2 e^{-2kH} \cos(k x_C - \omega t) \left| \cos(k x_C - \omega t) \right| \quad (2.27)$$

where

$$k_M = \tfrac{4}{3} \rho R_H^3 \quad (2.28)$$

Total horizontal force on the column can be written in the following form:

$$F_{TC} = C_M \rho \pi R_C^2 0.5H_\omega g (1 - e^{-2kH_C}) \sin(k x_C - \omega t)$$

$$+ \tfrac{1}{2} C_D \rho R_C (0.5H_\omega)^2 g (1 - e^{-2kH_C}) \cos(k x_C - \omega t) \left| \cos(k x_C - \omega t) \right| \quad (2.29)$$

The total horizontal wave forces on the structure is

$$F_H = F_{TH} + F_{TC} \quad (2.30)$$

Derivation of the Horizontal Forces for Beam Sea Condition

Total force on the hull for beam sea condition is given by the following equation:

$$F_{TH} = C_M \rho 0.5H_\omega \pi R_H^2 \omega e^{-kH} L_H \sin(k x_C - \omega t)$$

$$+ \tfrac{1}{2} C_D \rho R_H (0.5H_\omega \omega)^2 e^{-2kH} L_H \cos(k x_C - \omega t) \left| \cos(k x_C - \omega t) \right| \quad (2.31)$$

Total force on the column for beam sea condition is as follows

$$F_{TC} = C_M \rho \pi R_C^2 0.5H_\omega g (1 - e^{-kH_C}) \sin(k x_C - \omega t)$$

$$+ \tfrac{1}{2} C_D \rho R_C (0.5H_\omega)^2 g (1 - e^{-2kH_C}) \cos(k x_C - \omega t) \left| \cos(k x_C - \omega t) \right| \quad (2.32)$$

The total horizontal forces acting on the structure become

$$F_H = F_{TH} + F_{TC} \quad (2.33)$$

Derivation of Pitching Moments

Moments acting on the hull:

$$M_{T_H} = -\rho C_M 0.5H_\omega \pi R_H^2 \omega^2 e^{-kH} \sin \omega t \left[-\frac{L}{k}\cos k\frac{L}{2} + \frac{2}{k^2}\sin k\frac{L}{2}\right]$$

$$+\frac{1}{2}\rho A_L C_D (0.5H_\omega \omega)^2 e^{-2kH}\frac{8}{3\pi}\{\cos \omega t \left[-\frac{L}{k}\cos k\frac{L}{2} + \frac{2}{k^2}\sin k\frac{L}{2}\right]$$

$$-\frac{1}{5}\cos \omega t \left[-\frac{L}{3k}\cos 3k\frac{L}{2} + \frac{2}{9k^2}\sin 3k\frac{L}{2}\right]\}$$

$$+\{-\rho g H_\omega \pi R_H^2 e^{-kH} \sin k\frac{L}{2}\sin \omega t$$

$$-k_M H_\omega \omega^2 e^{-kH}\cos k\frac{L}{2}\sin \omega t$$

$$+\frac{1}{2}\rho C_D \pi R_H^2 (0.5H_\omega \omega)^2 e^{-2kH}[\cos(k\frac{L}{2} - \omega t)\left|\cos(k\frac{L}{2} - \omega t)\right|$$

$$+[\cos(k\frac{L}{2} + \omega t)\left|\cos(k\frac{L}{2} + \omega t)\right|\}l_v \qquad (2.34)$$

Moments acting on the column:

$$M_{T_C} = [\rho g 0.5H_\omega \pi R_C^2 e^{-kH_C}\cos(k x_C - \omega t)$$

$$+\frac{4}{3}\rho R_C^3 0.5H_\omega \omega^2 e^{-kH_C}\cos(k x_C - \omega t)$$

$$-\frac{1}{2}\rho A_L C_D (0.5H_\omega \omega)^2 e^{-2kH_C}\sin(k x_C - \omega t)\left|\sin(k x_C - \omega t)\right|]x_C$$

$$+C_M \rho \pi R_C^2 g 0.5H_\omega \sin(k x_C - \omega t)[(H_C + \frac{1}{k})e^{-kH_C} - \frac{1}{k}]$$

$$+\rho C_D R_C (0.5H_\omega)^2 g \cos(k x_C - \omega t)\left|\cos(k x_C - \omega t)\right|[e^{-2kH_C}(\frac{H_C}{2} + \frac{1}{4k}) - \frac{1}{4k}] \qquad (2.35)$$

Derivation of Rolling Moments

Moments acting on the hull:

$$M_{T_H} = [- C_M \rho \omega^2 \pi R_H^2 0.5 H_\omega e^{-kH} L_H \cos(k x_C - \omega t)$$

$$+ C_D \rho R_H (0.5 H_\omega \omega)^2 e^{-2kH} L_H \sin(k x_C - \omega t) \left|\sin(k x_C - \omega t)\right|] x_C$$

$$+ [C_M \rho 0.5 H_\omega \omega^2 \pi R_H^2 L_H \sin(k x_C - \omega t)$$

$$+ [C_D \rho R_H (0.5 H_\omega \omega)^2 e^{-2kH} \cos(k x_C - \omega t) \left|\cos(k x_C - \omega t)\right|] y_C \tag{2.36}$$

Moments acting on the column:

$$M_{T_C} = [\rho g \pi R_C^2 0.5 H_\omega e^{-kH_C} \cos(k x_C - \omega t)$$

$$+ \tfrac{4}{3} \rho R_C^3 0.5 H_\omega e^{-kH_C} \cos(k x_C - \omega t)$$

$$- \tfrac{1}{2} C_D \rho \pi R_C^2 (0.5 H_\omega \omega)^2 e^{-2kH_C} \sin(k x_C - \omega t) \left|\sin(k x_C - \omega t)\right|] x_C$$

$$+ C_M \rho 0.5 H_\omega \pi R_C^2 g [(1 - e^{-kH_C}) (\overline{OG} - \tfrac{1}{k}) + H_C e^{-kH_C}] \sin(k x_C - \omega t)$$

$$+ C_D \rho R_C (0.5 H_\omega)^2 g [\tfrac{1}{2}(1 - e^{-2kH_C}) (\overline{OG} - \tfrac{1}{2k}) + \tfrac{1}{2} H_C e^{-2kH_C}] \cos(k x_C - \omega t) \tag{2.37}$$

where

$$A_L = 2 R_H$$

$l_v = L_H / 2$

$y_C = \overline{KG} - R_H / 2$

H_C Distance between calm water level and bottom of column

$\overline{OG}$ Distance of C.O.G from calm water level

2.3 DEVELOPMENT OF COMPUTER PROGRAMS

In order to carry out wave force and motion response calculations for the semi-submersible geometry shown in Fig.2.2 a number of routines were developed as summarised in the following.

The program HEAVE calculates the total vertical force acting on the semi-submersible and solves the single degree of freedom system. The program SWAY calculates the horizontal hull, column and hull+column forces for beam sea condition. The program SURGE performs the horizontal force calculations in head sea condition. The program BEAM was written for the estimation of vertical forces and heave response for the beam sea condition. The program MORHP was written to calculate pitching moments. The coupled heave and pitch motion equations were solved by using the results from MORHP as input to the program HPCM. The program MORHR was developed for predicting wave induced roll moments. Results from the program MORHR are used as input to the program HPCM and coupled heave and roll motion equations were solved.

The same calculations were carried out by using 2D source-sink distribution technique in order to compare the two different methods. In utilising the programs based on the 2D source-sink distribution technique the semi-submersible was represented by 7 typical sections. These sections were chosen so that 3 typical sections can represent each of inner and outer columns and one typical section can represent the main hull. One of the sections is shown in Fig.2.3. The co–ordinates of segments on each section were generated using the program BISCONT. Sectional added mass and damping values were calculated by running program BURAK. In order to calculate sectional wave-excitation forces AYHANR was run for the seven sections. Program PM was written to calculate

total pitch moment of the semi-submersible. This program integrates the sectional wave-excitation forces and pitching moments along the length of the semi-submersible. Similarly program ADC integrates the sectional added mass and damping values. The coupled heave-pitch motion equations were solved in program HPC using the output data obtained from PM and ADC.

2.4. SUMMARY OF THE RESULTS OBTAINED USING MORISON EQUATION AND 2D SOURCE-SINK DISTRIBUTION TECHNIQUE

In Figs.2.4-2.9 the variation of damping, added mass coefficients and wave exciting forces with the wave frequency are presented. The results of the study to investigate the effect of interference between the hull and the column are shown by Figs.2.4-2.7.

Figs.2.10-2.11 show the variation of total damping, and added mass values which were obtained by the integration of the sectional values over the length of the semi-submersible.

As shown in Fig.2.4 the variation of added mass coefficients of typical sections taken from the column members with different aspect ratios for the heave mode of motion has a significant decrease of up to 3 rad/s. The added mass values become constant in the range of high frequencies. However, added mass coefficients for the submerged hull show a constant trend for the whole range of frequencies. The effect of the free surface tends to be more significant on the surface piercing column members in the lower frequencies.

Variation of damping force coefficients shown in Fig.2.5 has a peak at about 2 rad/s for the surface piercing sections whereas the peak for the submerged hull section appears to be at a frequency of 7 rad/s. There is a large difference of magnitude in damping values of the most slender (i.e. min H/R) and of the most bluff section (i.e. max H/R) up to 8 rad/s. Damping coefficients for the submerged hull section are

almost constant up to 2 rad/s.

In order to study the importance of the hydrodynamic interaction between the hull and columns, Figs.2.4-2.6 which show added mass and damping values being obtained with and without interaction are presented. Comparison of Fig.2.4 and Fig.2.6 reveals that the effect of interaction between the hull and the column is to increase the added mass values particularly in the high frequency range.

In Fig.2.7 variation of damping force coefficients with frequency without the interaction effect being taken into account between hull and column sections is shown. Comparisons between Fig.2.7 and Fig.2.5 shows that there is on average a 25% increase in the maximum damping forces for the sections with different aspect ratios at 2 rad/s if the interaction effects are not taken into account.

Variation of sectional wave forces with frequency for head sea condition is given in Fig.2.8. The sectional column forces have a minimum of between 6 and 10 rad/s and when the columns become larger in diameter, wave forces increase. In Fig.2.9 variation of wave forces is given for beam sea condition. The difference between Fig.2.8 and Fig.2.9 is that the wave forces acting on the hull are at a minimum at about 6 rad/s for the beam sea condition.

The total added mass values of the semi-submersible with and without the interaction effects being taken into account are compared in Fig.2.10. The total added mass values increase by about 20% if the interaction between the hull and columns is not taken into account. Similarly the total damping forces on the structure are compared in Fig.2.11. The interaction between the members appears to have no effect on total damping forces below the frequency of 2 rad/s. However, the difference between the two cases increases as the wave frequencies increase. The maximum difference is about 33% and occurs at a frequency of 6 rad/s.

The variation of the vertical hull and column forces (calculated using the Morison equation) with frequency in the beam sea condition is shown in Fig.2.12. Fig.2.13

shows the heave response of the semi-submersible in the beam sea condition. As can be seen from Fig. 2.13 the magnitude of damping ratio affects the motion response significantly in the region of the natural frequency.

Fig.2.14 shows the horizontal hull and column forces for the head sea condition. The vertical hull and column forces for the head sea condition are shown in Fig.2.15. Fig. 2.16 shows the heave response of the semi-submersible. The effect of damping in heave response in head seas is illustrated in Fig.2.16. The total sway forces as well as hull and column force components are shown in Fig.2.17.

The total vertical forces in head seas calculated using the Morison approach and 2D source-sink method are compared in Fig.2.18. As can be seen in Fig. 2.18 the two methods correlate very well except for the frequency range below 2 rad/s. This can be attributed to large discrepancy in sectional forces between the column sections with different aspect ratios as shown in Fig.2.8.

Pitching moments obtained from the Morison approach and 2-D source-sink distribution method are compared in Fig.2.19. Since with Morison approach the pitching moments due to the surge forces can be calculated and 2D source-sink distribution technique does not have the facility to incorporate the surge forces, a significant difference arises between the results of the two methods as illustrated in Fig.2.20.

Coupled heave and pitch motions as well as coupled heave and roll motion response values obtained from both methods are shown in Fig.2.21-2.24.

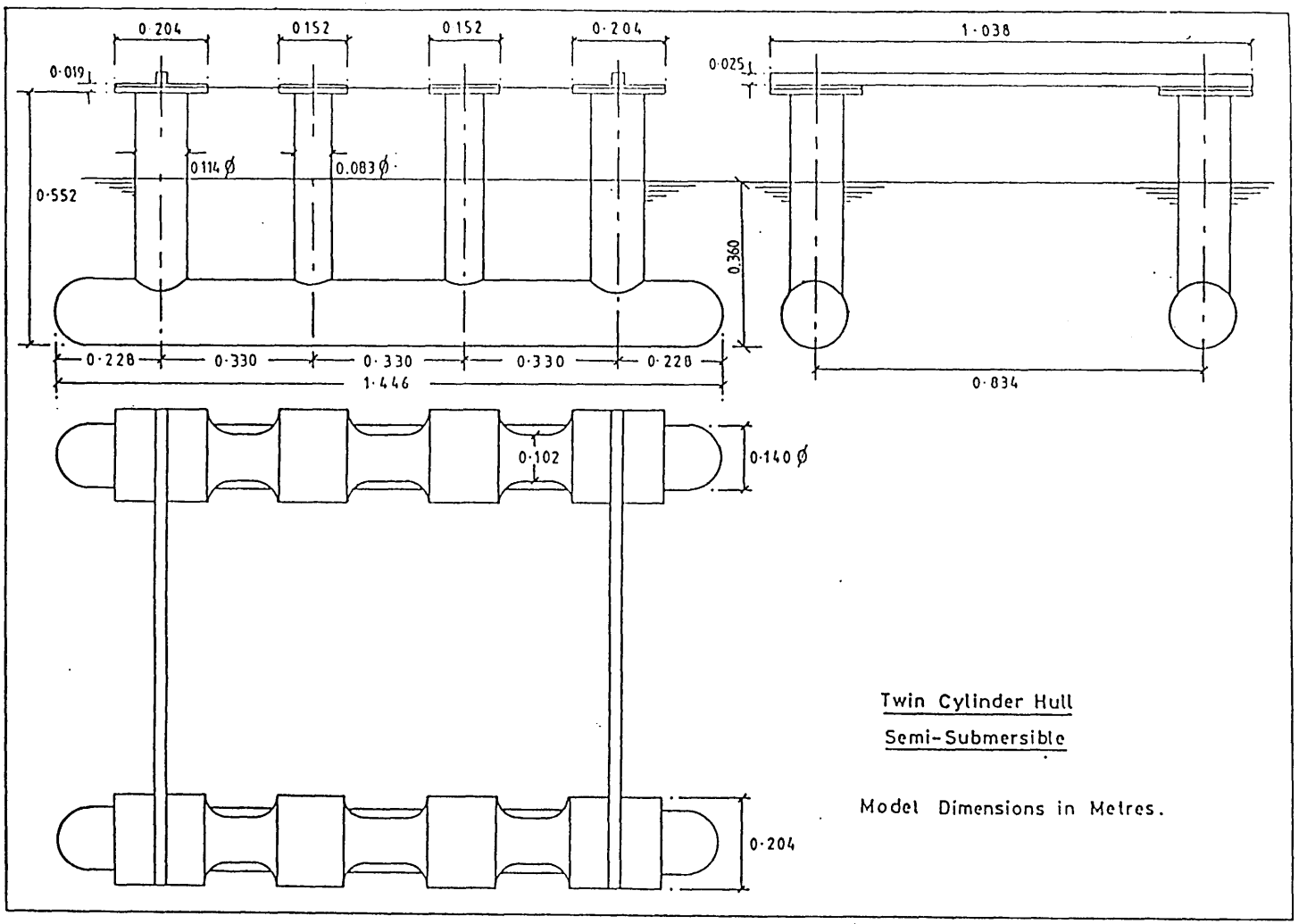

Fig.2.2 General arrangement of the semi-submersible model tested

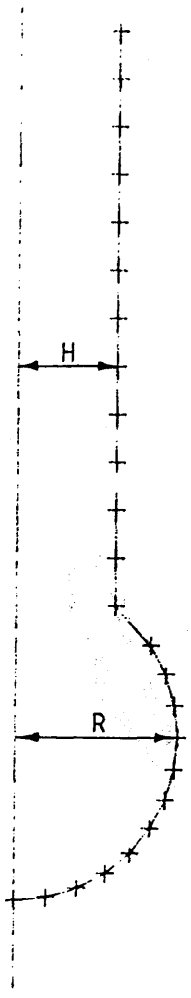

HULL GEOMETRY	:	CIRCULAR
NO OF SEGMENTS	:	24
HULL RADIUS	:	0.0700 M
H/R (ASPECT RATIO)	:	0.6069
DRAUGHT	:	0.3600 M

Fig.2.3.Segment distributions of the typical cross-section of the semi-submersible

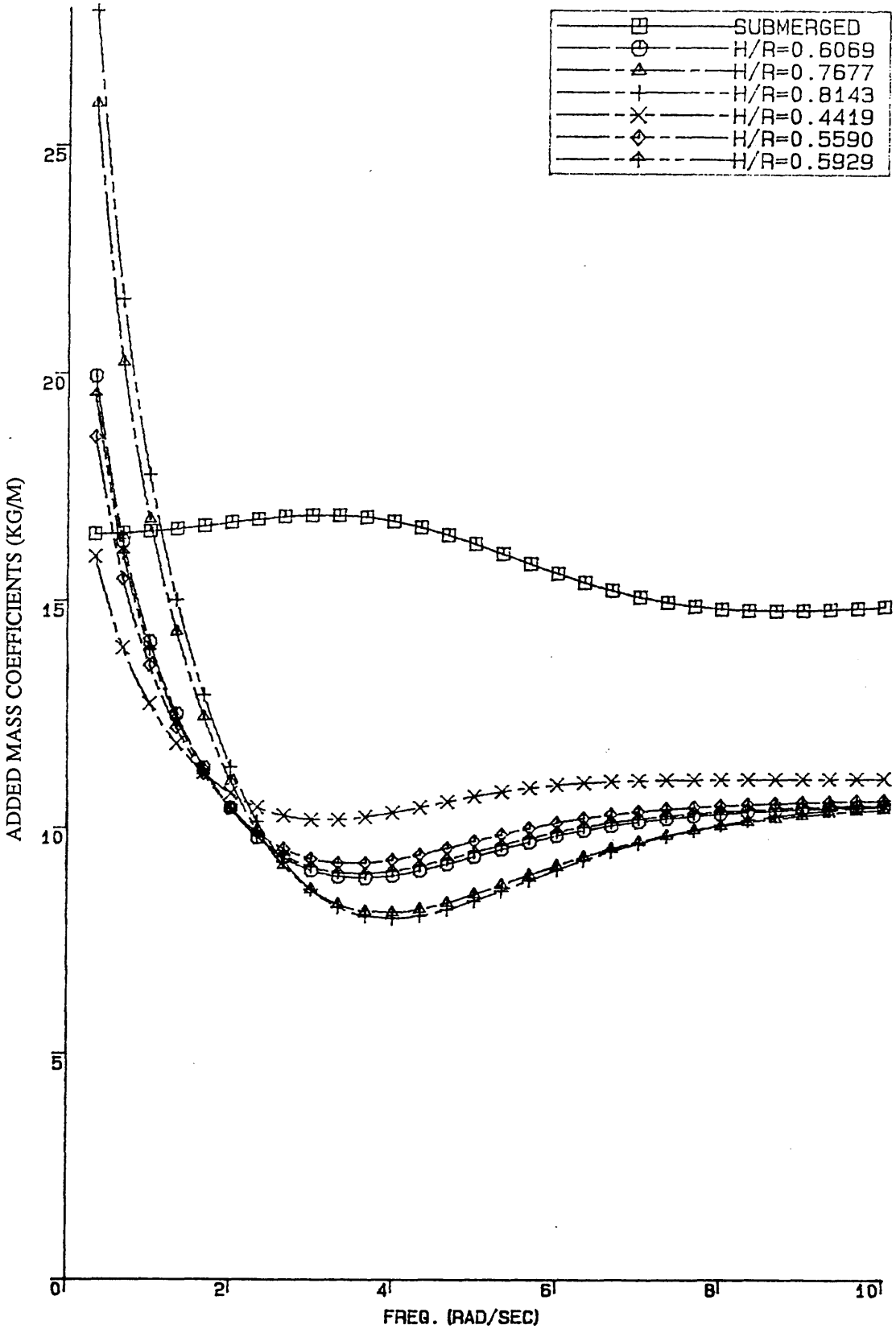

Fig.2.4 Sectional added mass coefficients for the heave mode in the presence of the hydrodynamic interaction between hull and column

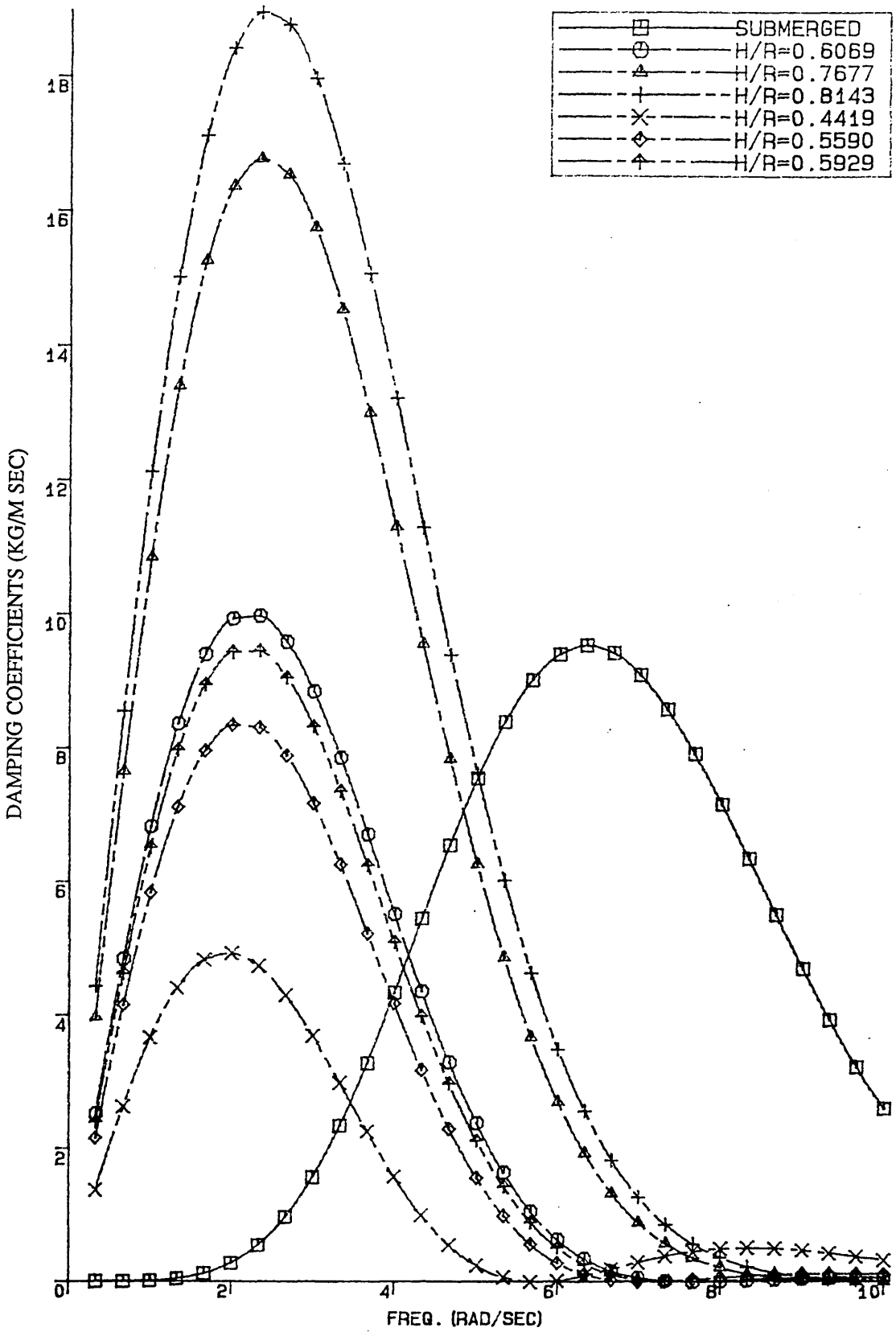

Fig.2.5 Sectional damping coefficients for the heave mode in the presence of the hydrodynamic interaction between hull and column

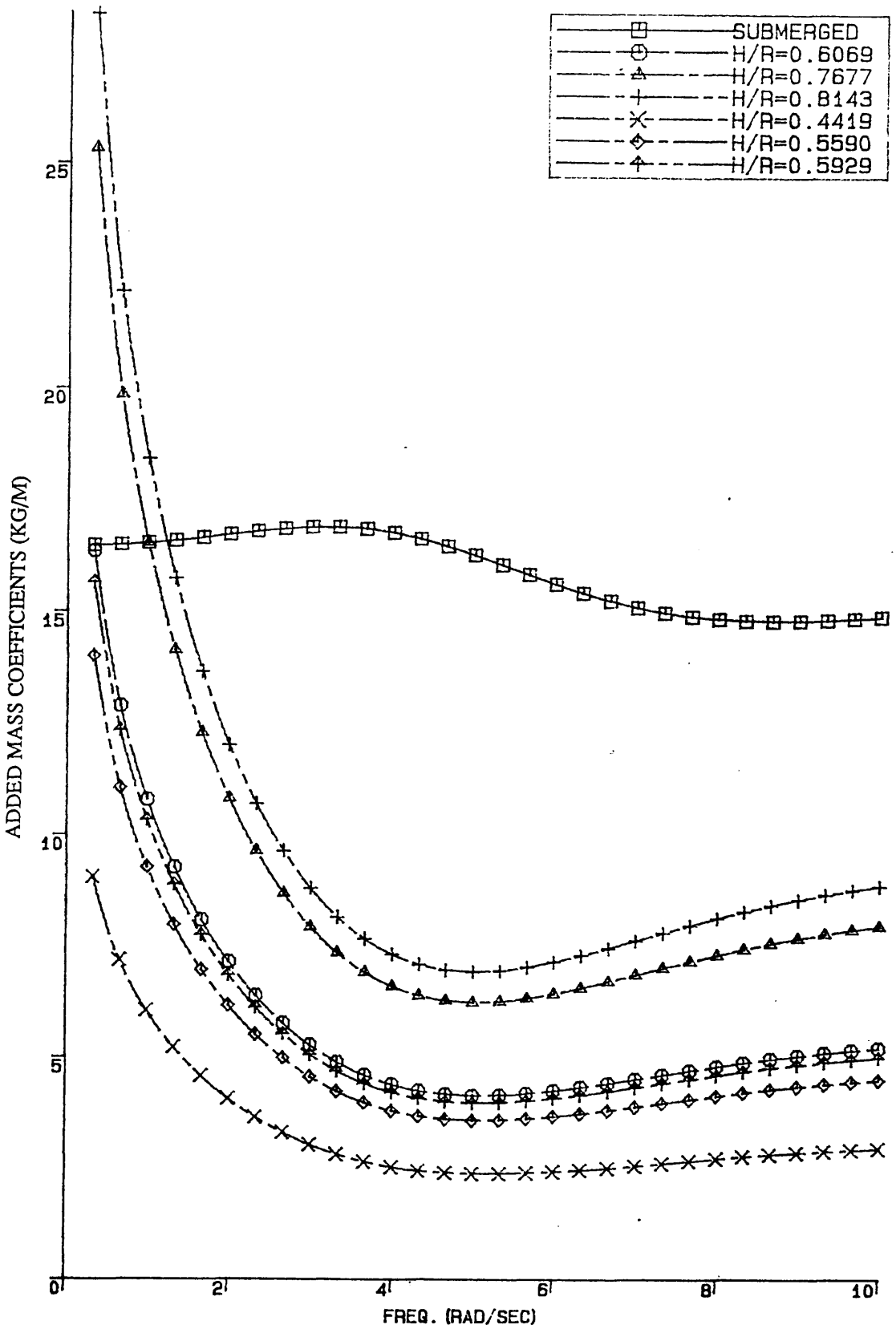

Fig.2.6 Sectional added mass coefficients for the heave mode in the absence of the hydrodynamic interaction between hull and column

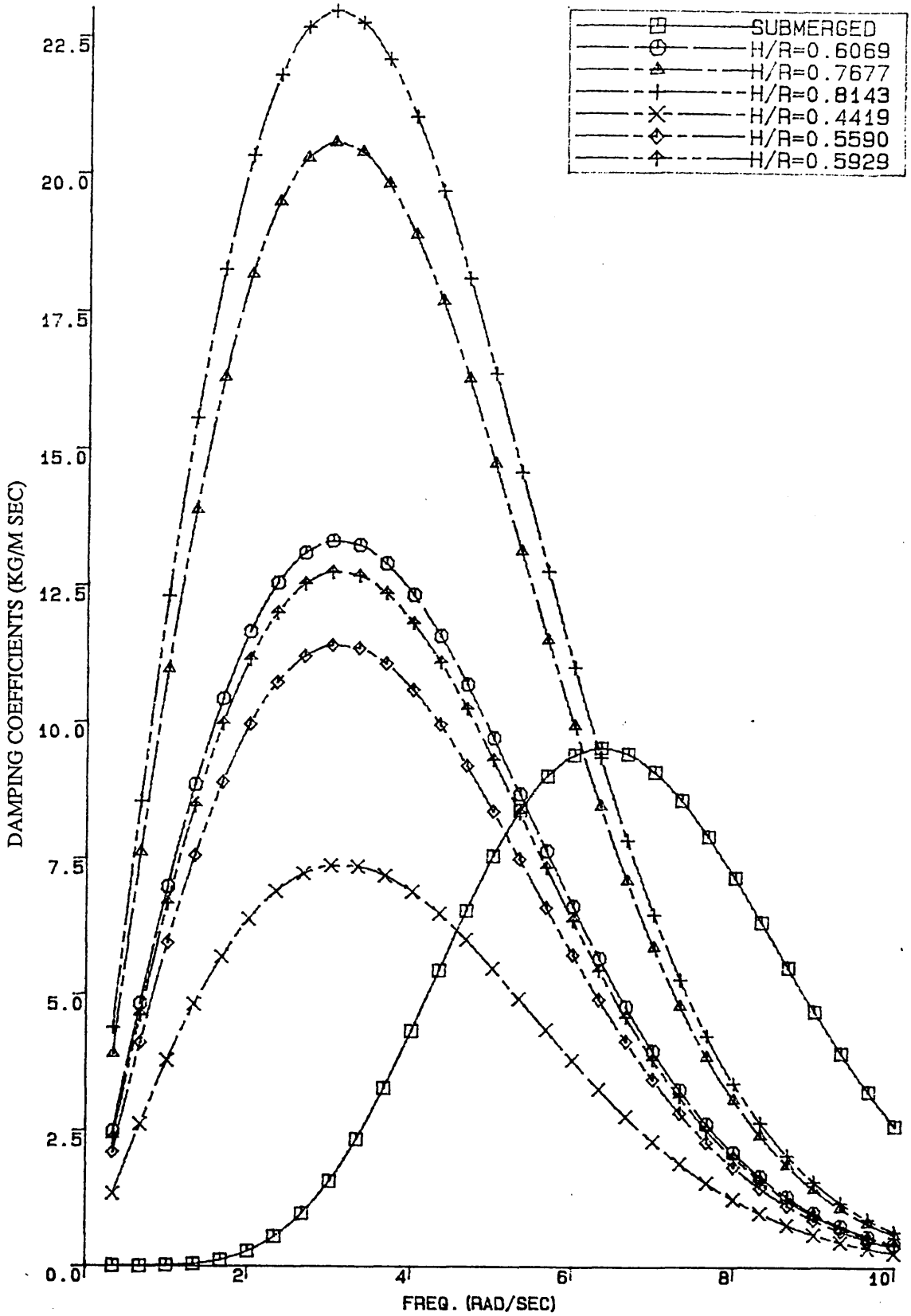

Fig.2.7 Sectional damping coefficients for the heave mode in the absence of the hydrodynamic interaction between hull and column

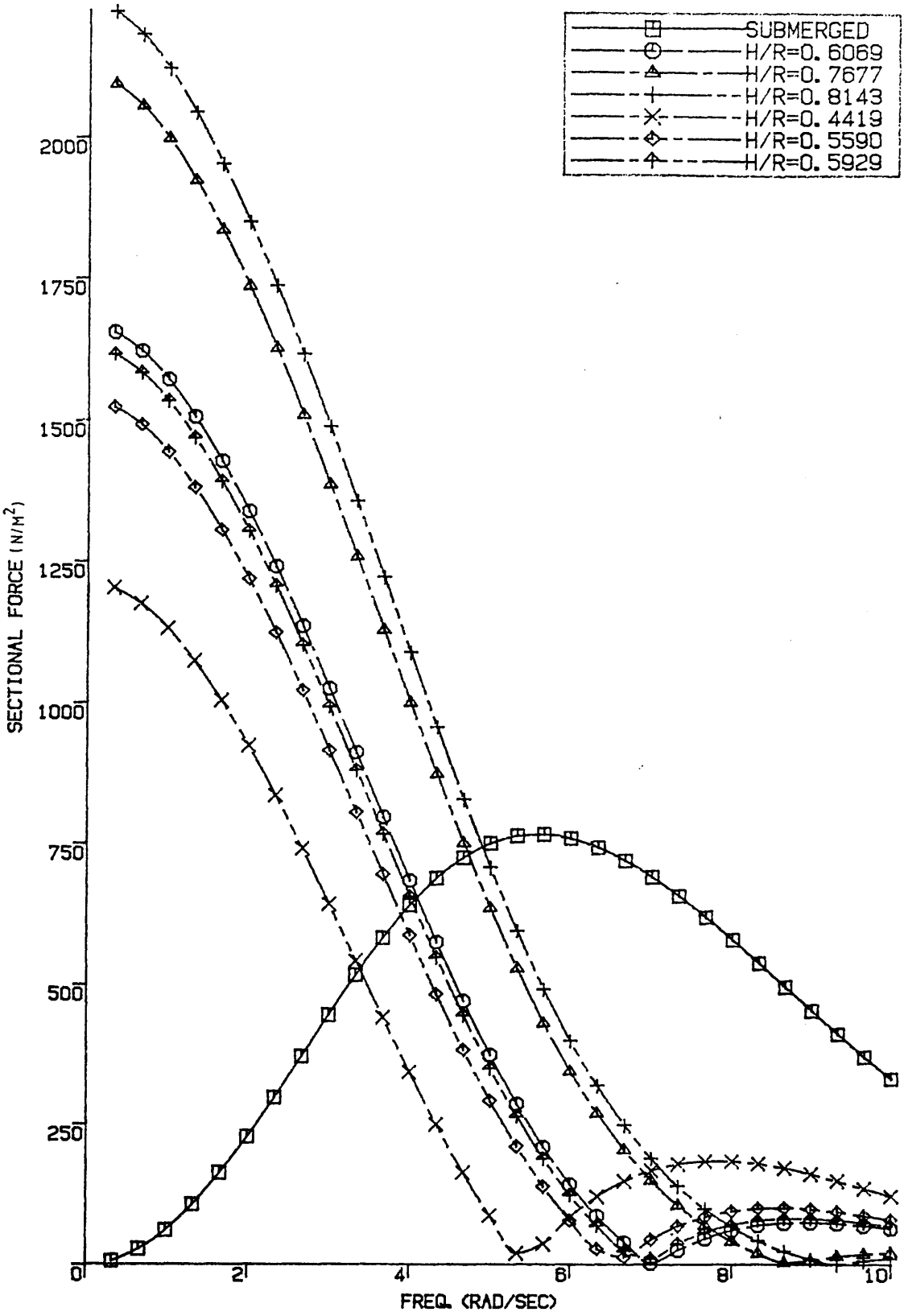

Fig.2.8 Sectional wave-induced coefficients for the heave mode in the presence of the hydrodynamic interaction between hull and column for head sea condition

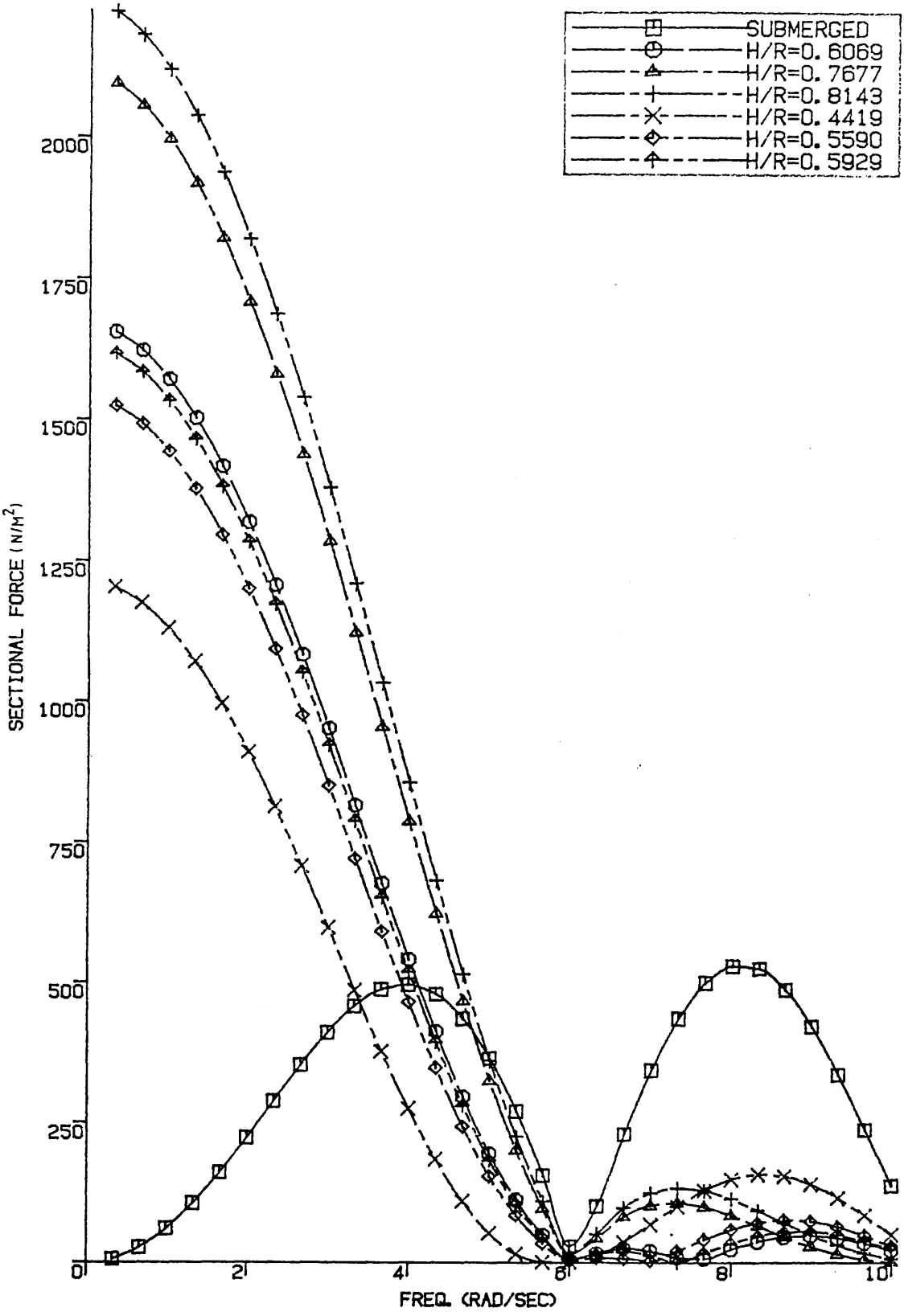

Fig.2.9 Sectional wave-induced coefficients for the heave mode in the presence of the hydrodynamic interaction between hull and column for beam sea condition

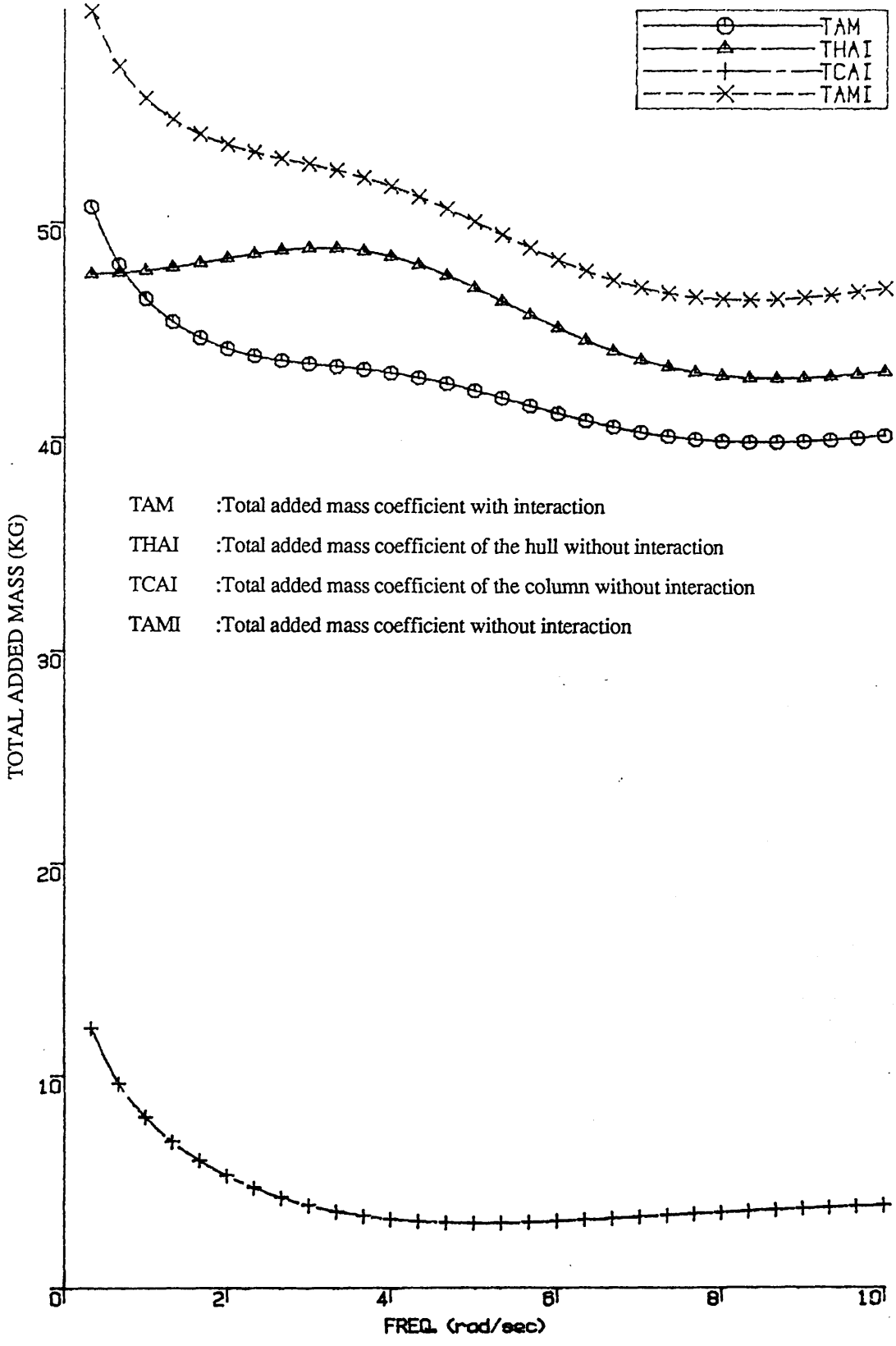

Fig.2.10 Comparison of the total added mass coefficients

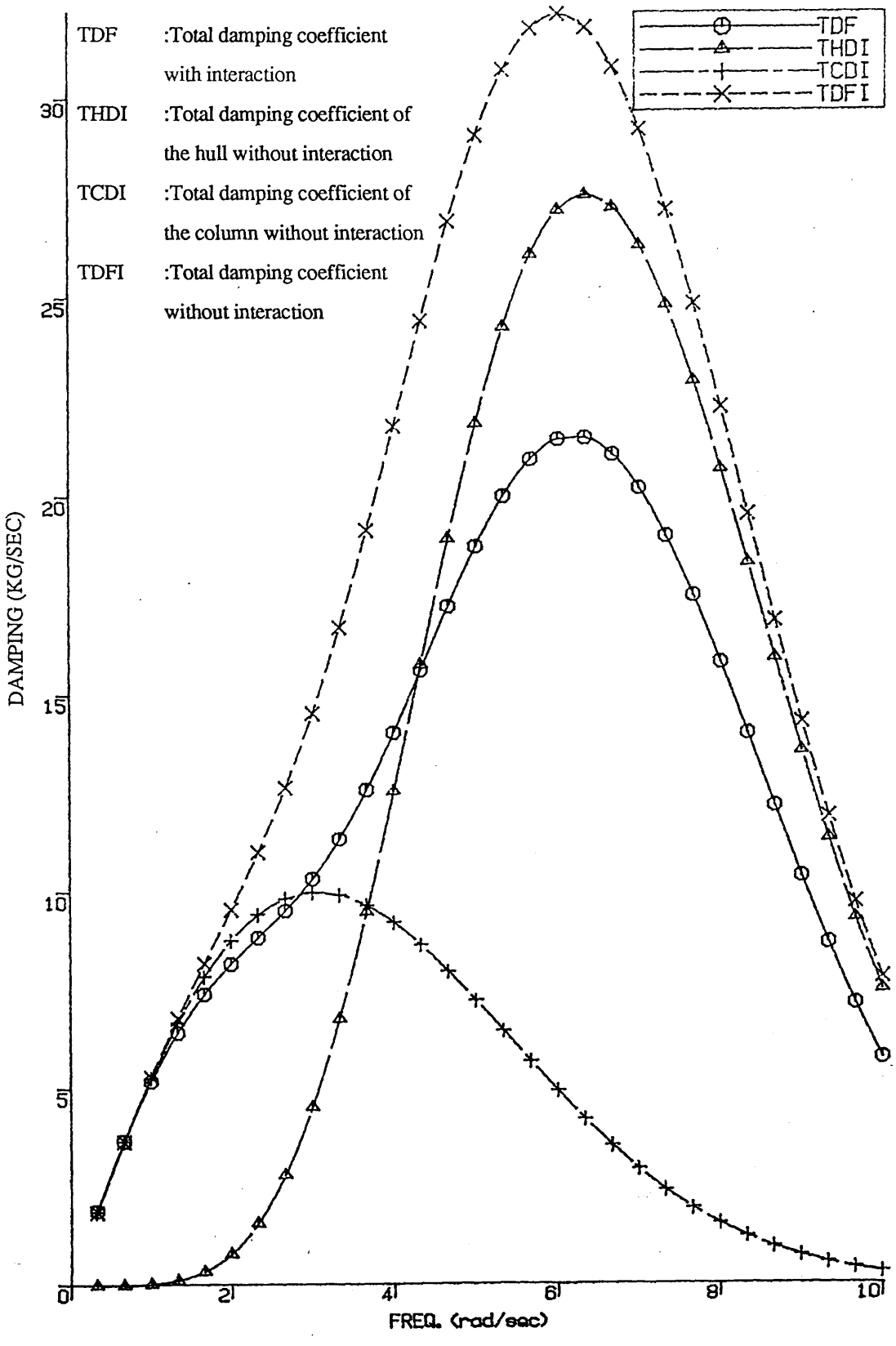

Fig.2.11 Comparison of the total damping coefficients

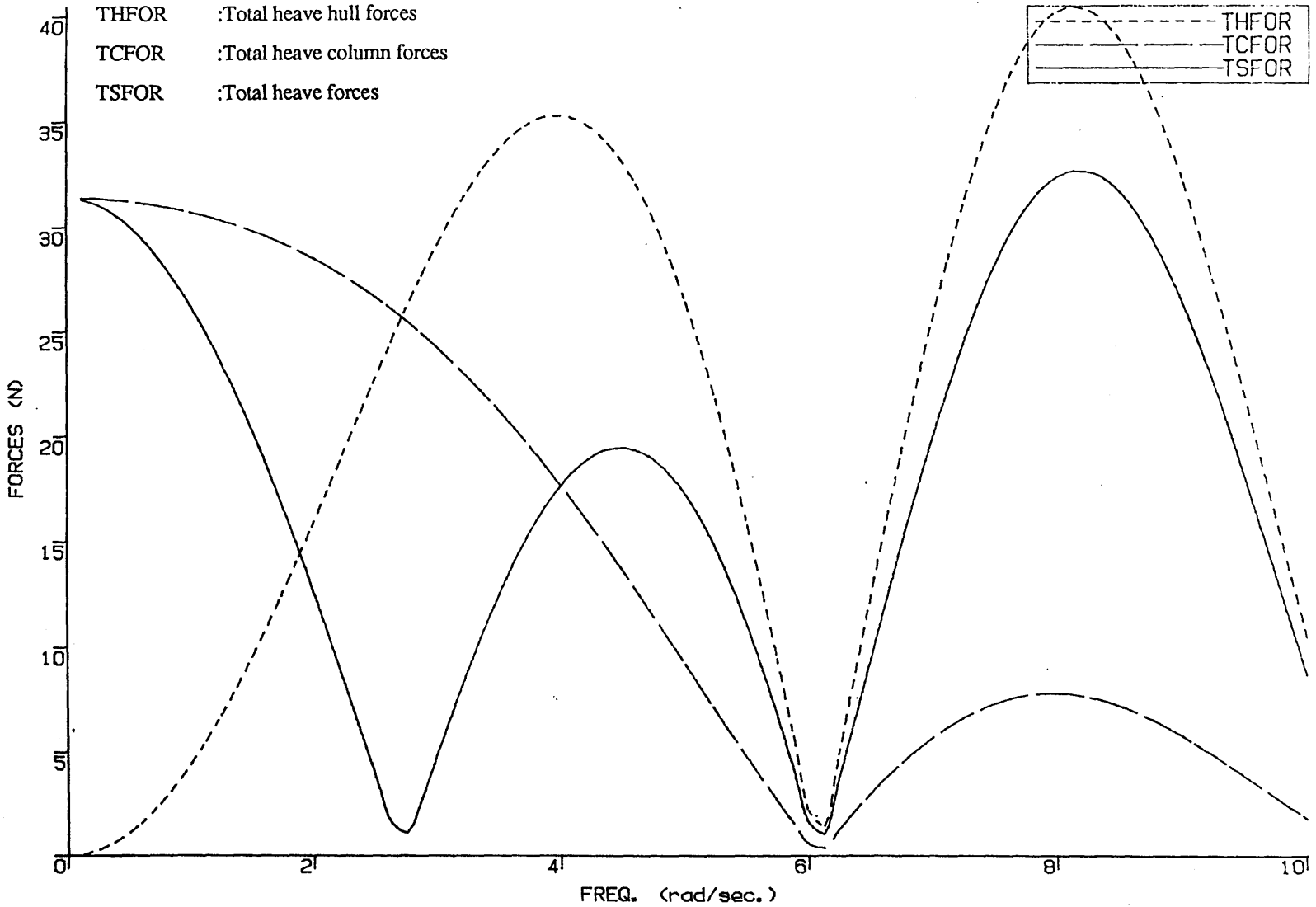

Fig.2.12 Heave forces for beam sea condition

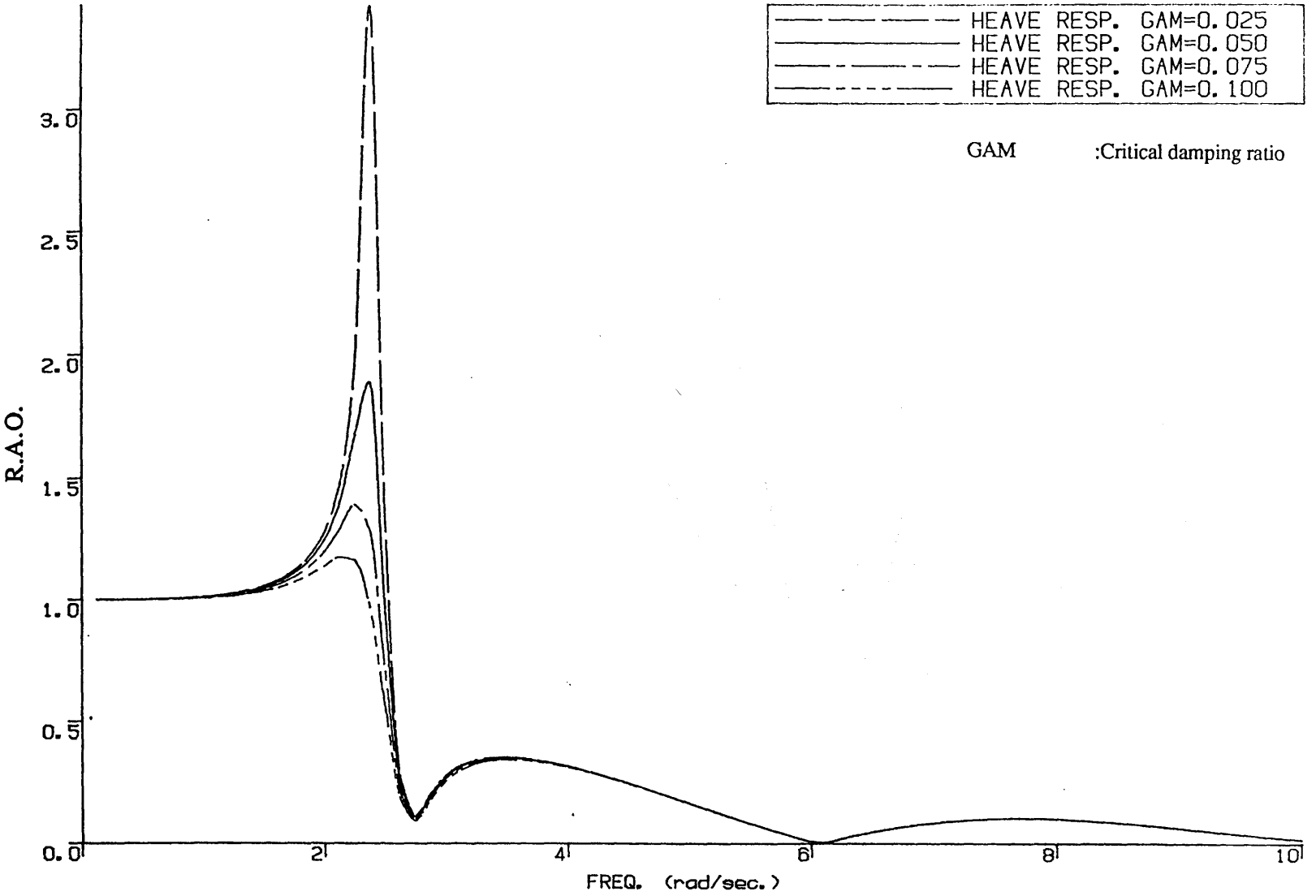

Fig.2.13 Heave response for beam sea condition

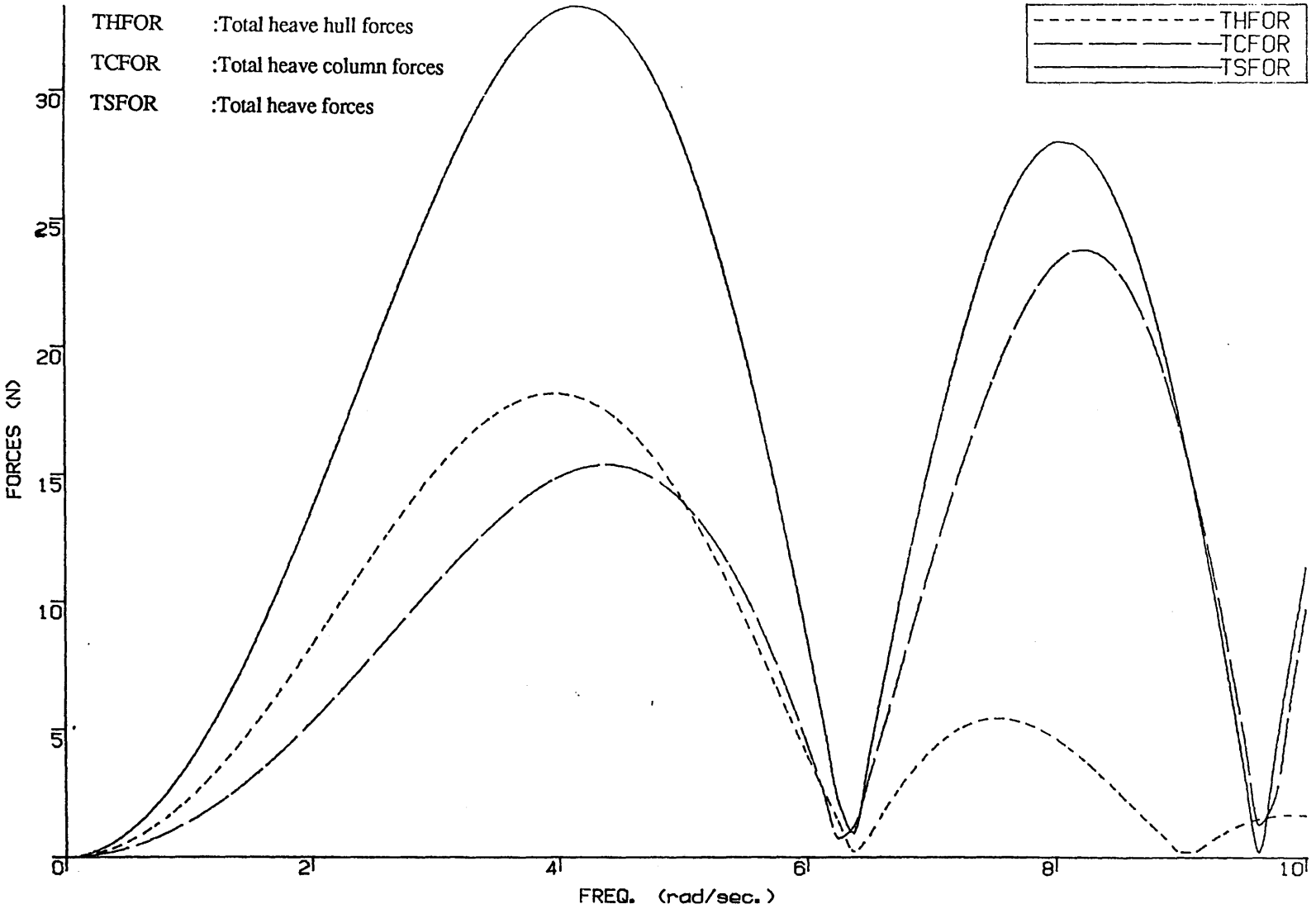

Fig.2.14 Surge forces

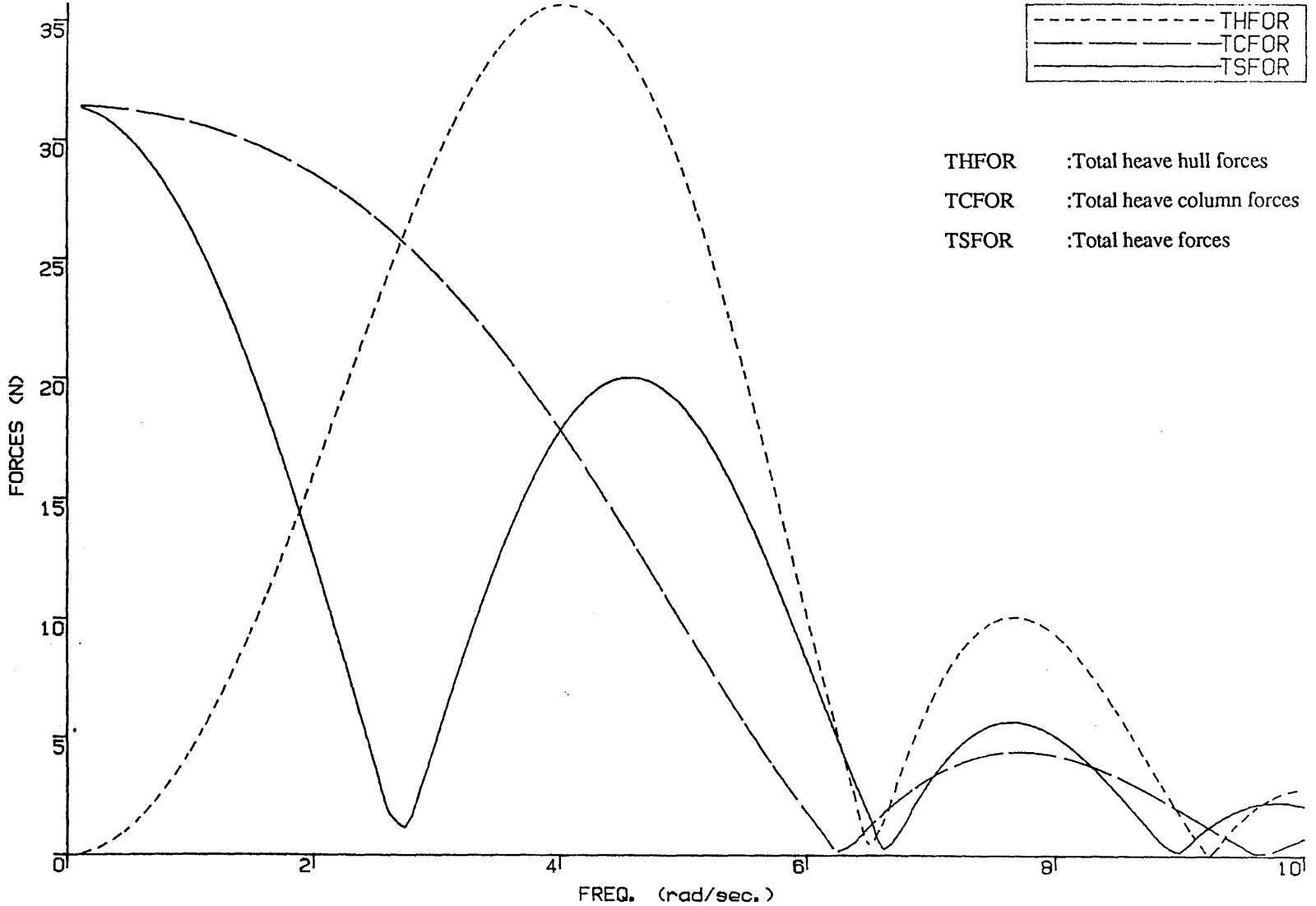

Fig.2.15 Heave forces for head sea condition

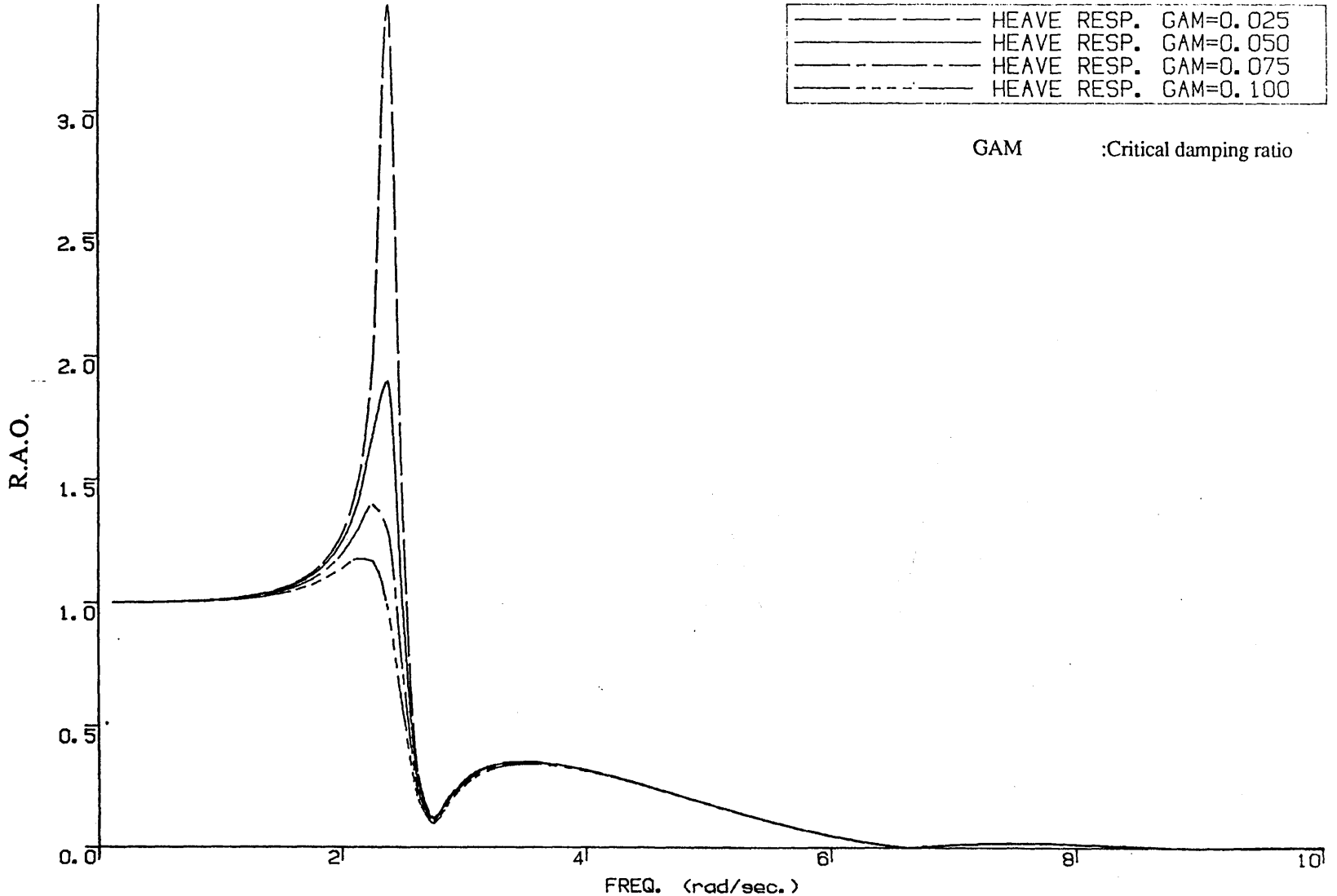

Fig.2.16 Heave response for head sea condition

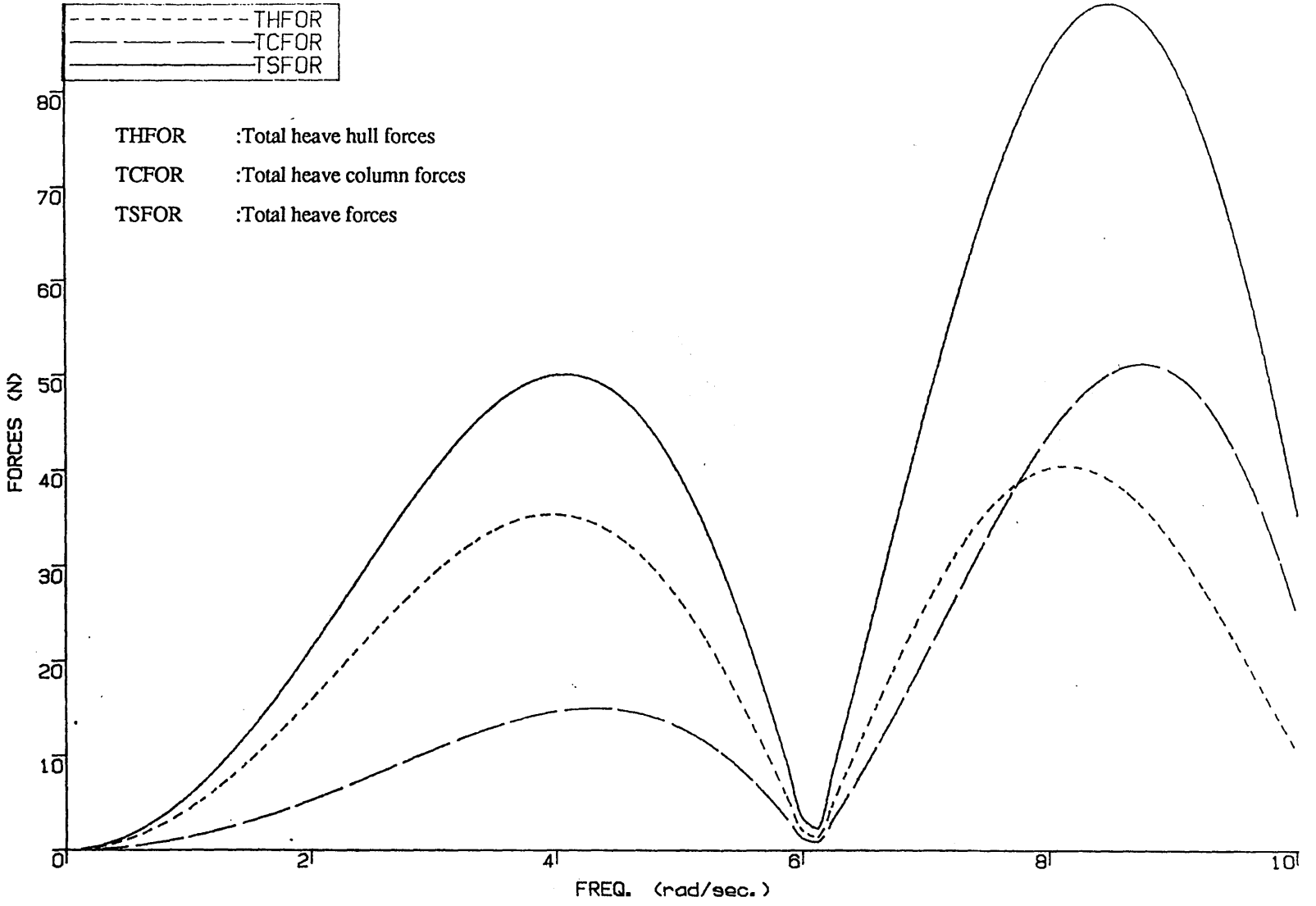

Fig.2.17 Sway forces

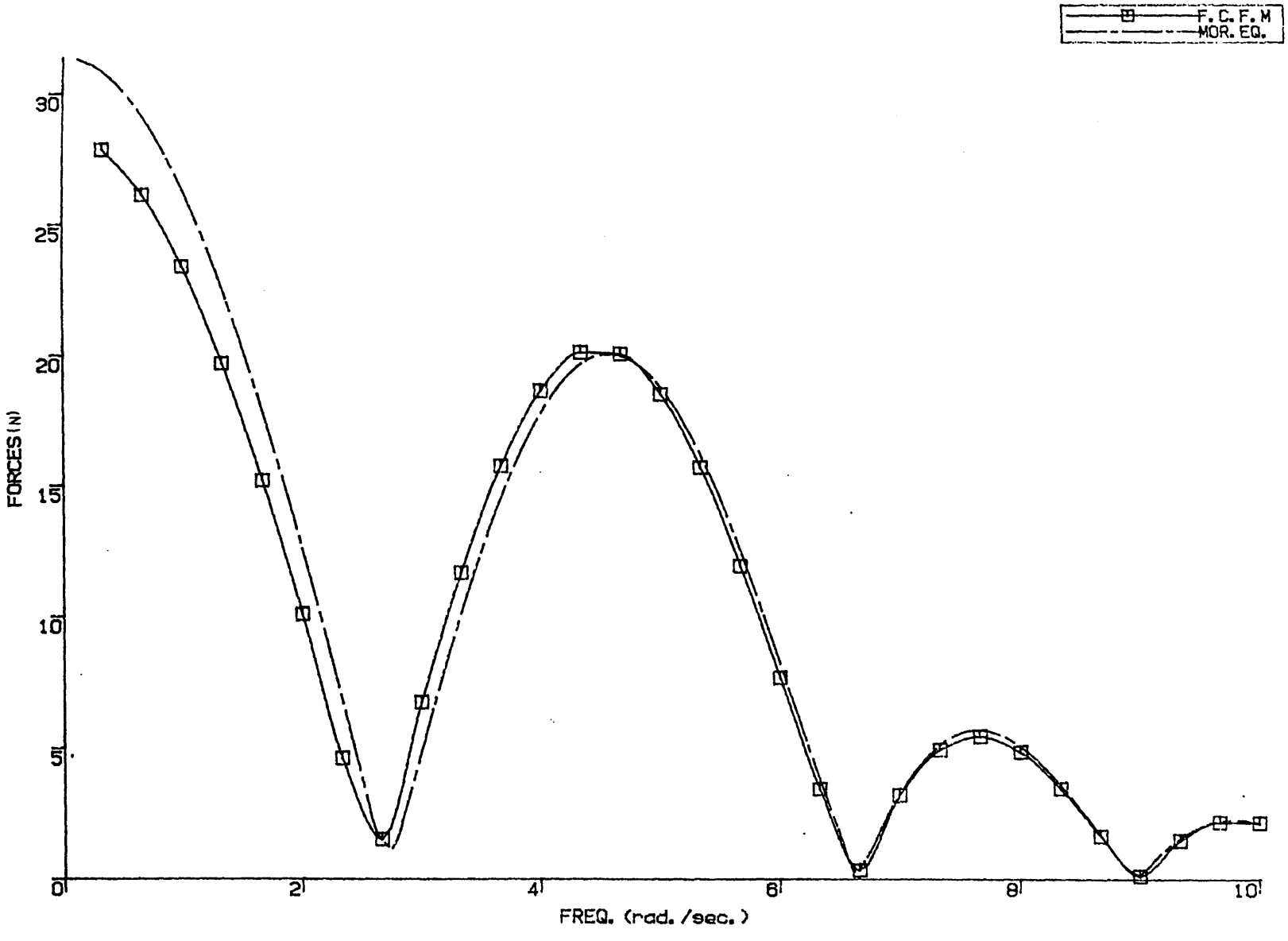

Fig.2.18 Comparison of the heave forces for head sea condition between two methods

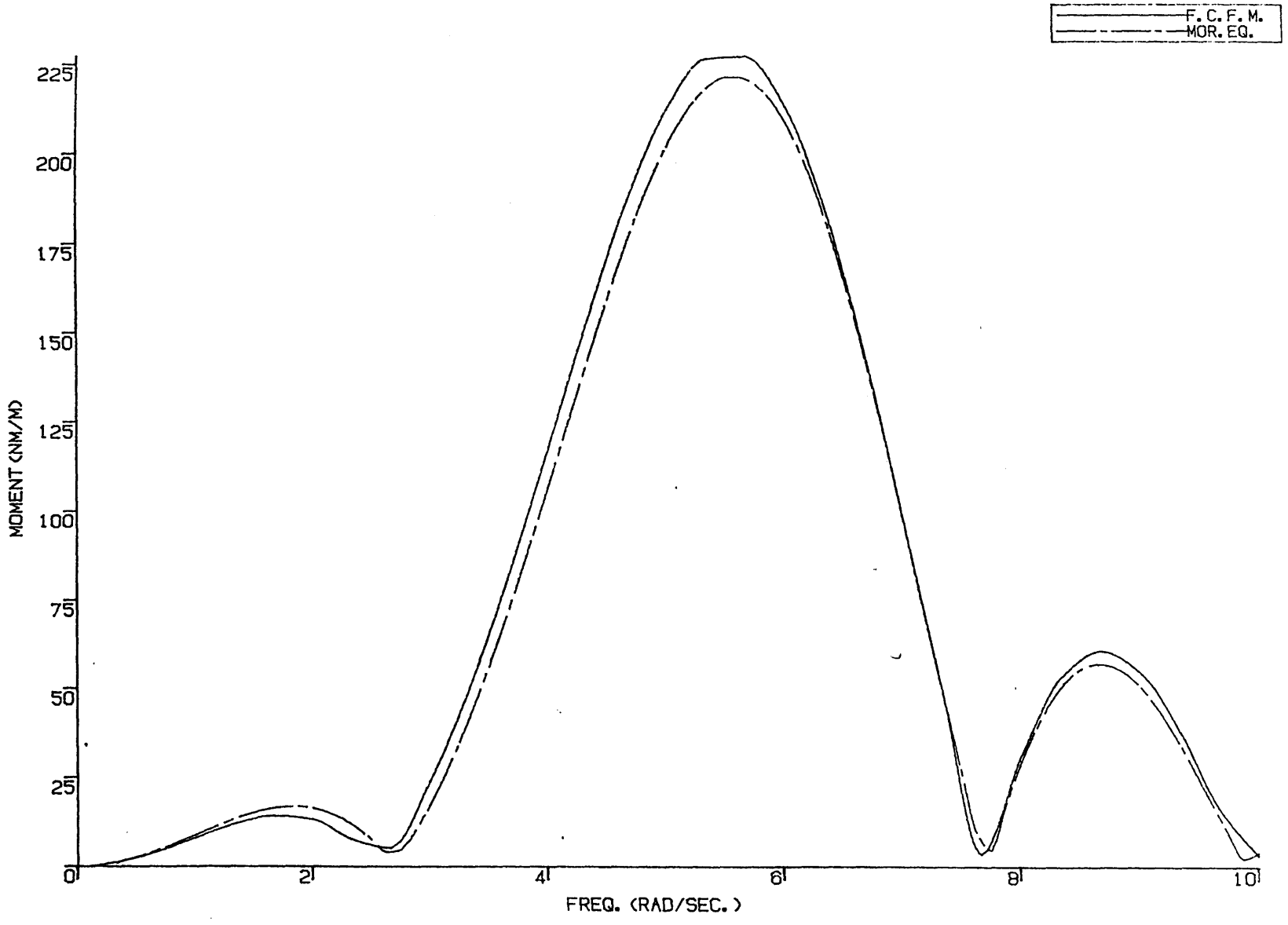

Fig.2.19 Comparison of the pitch moments between two methods without the effect of surge forces

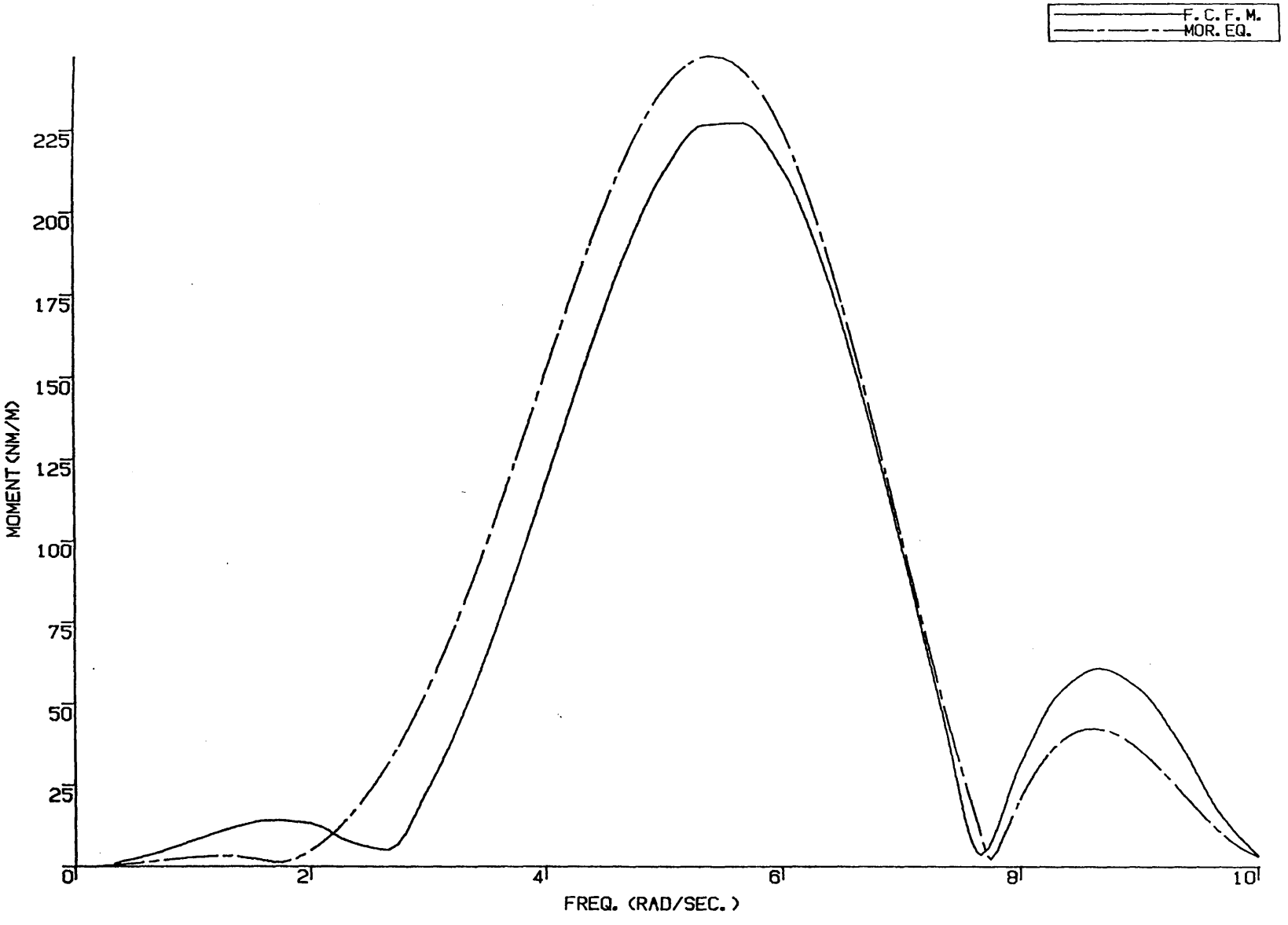

Fig.2.20 Comparison of the pitch moments between two methods with the effect of surge forces

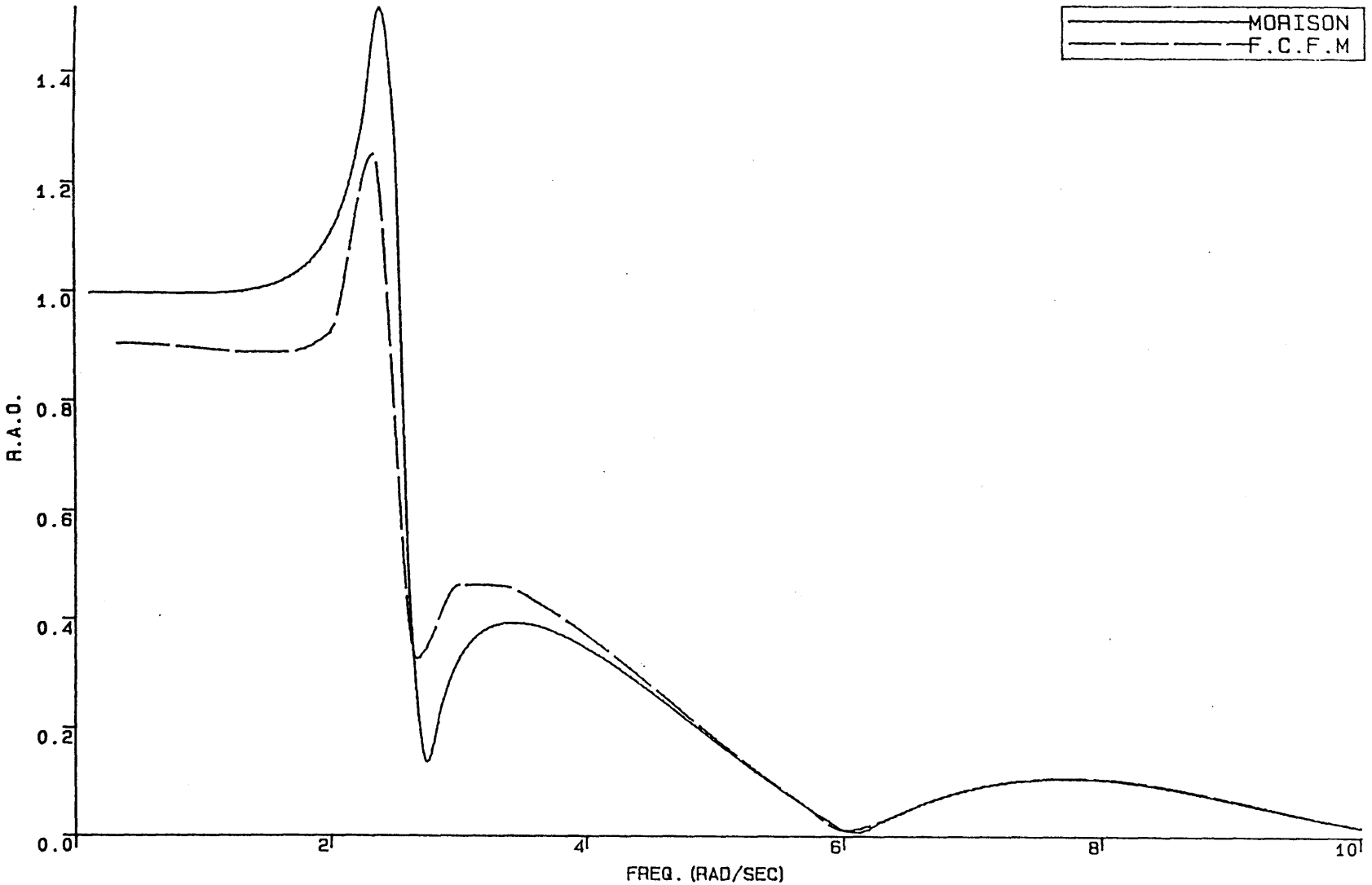

Fig.2.21 Comparison of the heave responses between two methods

Coupled Heave-Roll Modes

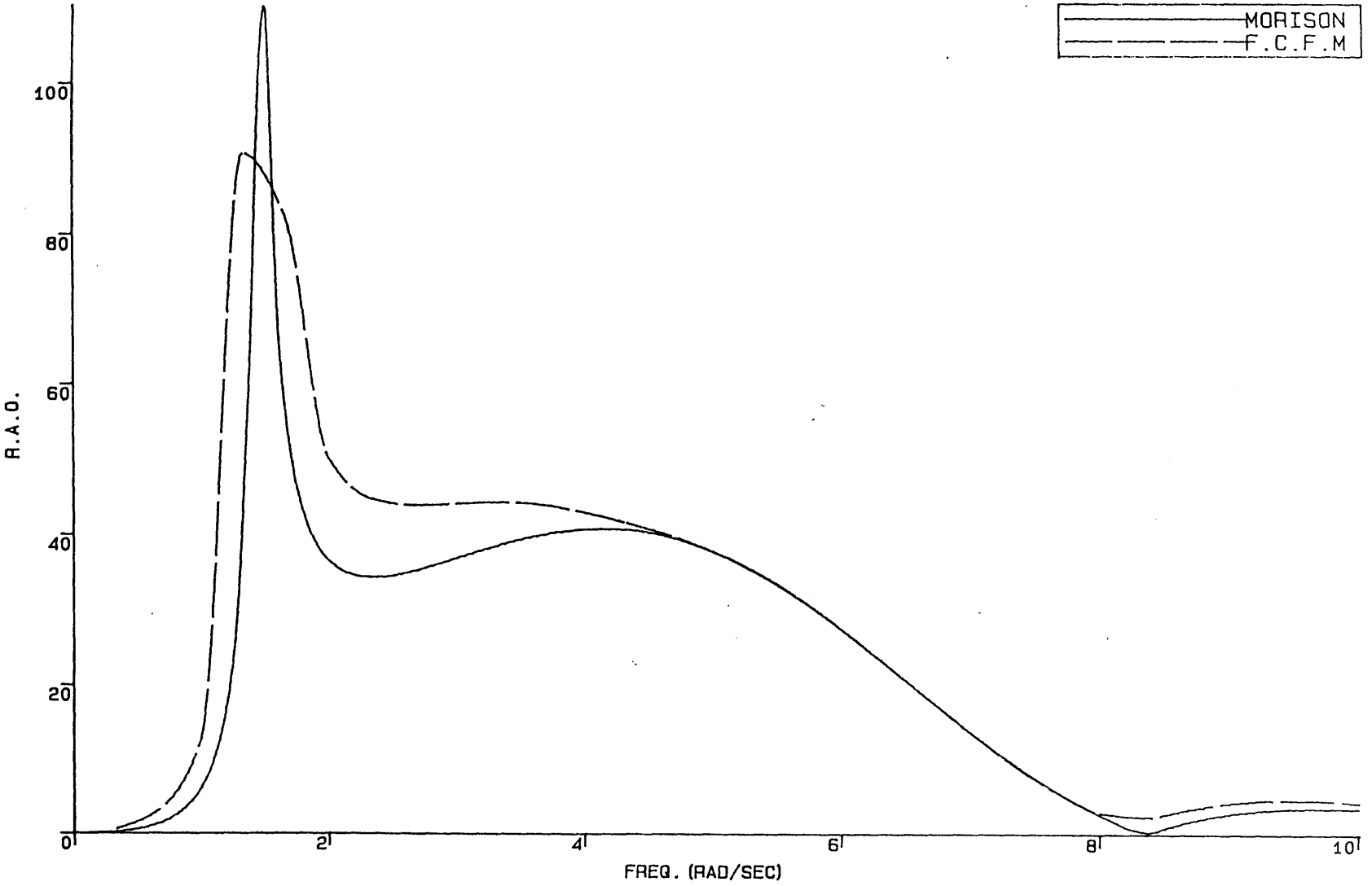

Fig.2.22 Comparison of the roll responses between two methods

Coupled Heave-Roll Modes

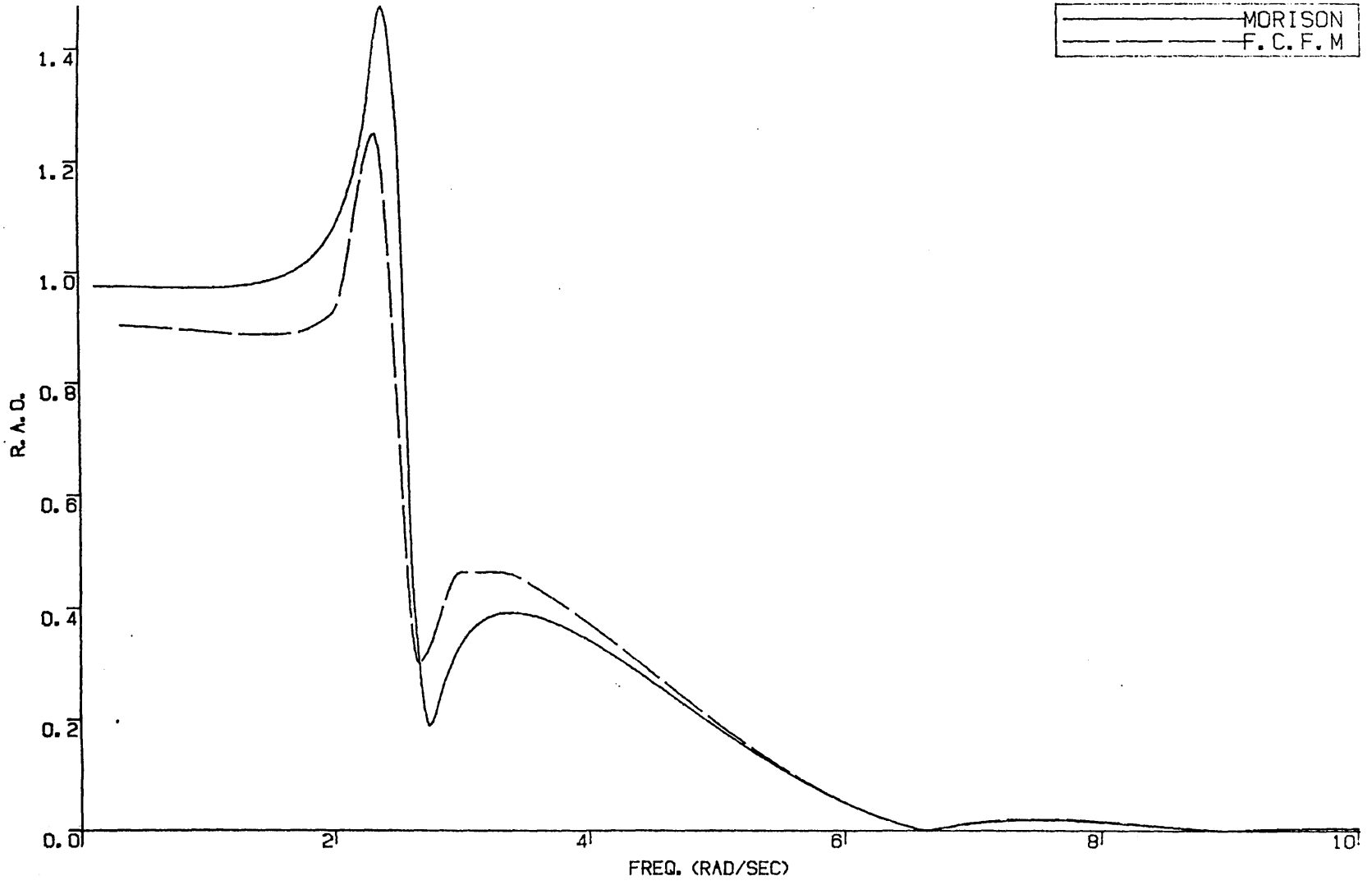

Fig.2.23 Comparison of the heave responses between two methods

Coupled Heave-Pitch Modes

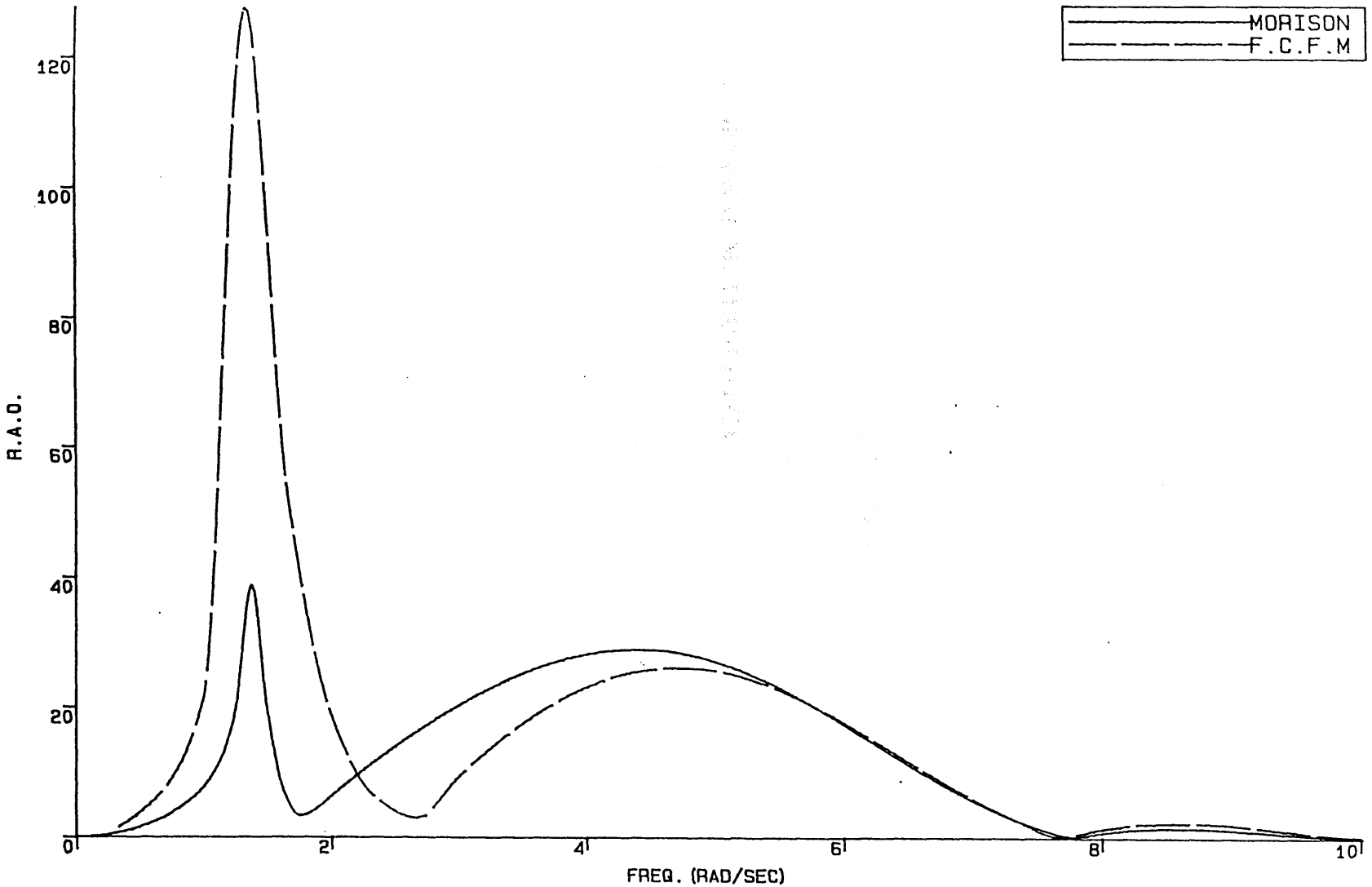

Fig.2.24 Comparison of the pitch responses between two methods

Coupled Heave-Pitch Modes

CHAPTER 3

A GENERAL METHOD TO CALCULATE HYDRODYNAMIC LOADING

3.1 INTRODUCTION

In this chapter the derivation of a general method to calculate wave forces on the cylindrical members of offshore structures is presented. By means of the developed method one can calculate the wave loading on cylindrical members of fixed or floating offshore structures orientated randomly in waves. The method is based on the hydrodynamic theory and the calculation procedure summarised by Incecik (1982).

In the following sections, a general method for calculating wave forces and moments on circular cylinders is derived. This method will provide a basic tool for determining the wave forces and moments that a floating structure is subjected to as it experiences large amplitude oscillations in six degrees of freedom. In addition, in Chapter 4 the non-linear motion equations of the platform will be derived and solved by utilising these force and moment calculations.

The following force components will be taken into account in calculating the wave forces and moments. Detailed discussion on these force components has also been given in Section 2.2.1.

1) *Dynamic Pressure Force (Froude-Krylov Force)*: Dynamic Pressure Force is due to the hydrodynamic pressure change below the surface of a wave while the wave propagates. It is assumed that there is no interference between the flow field and the structure.

2) *Acceleration Force*: The presence of the structure (or its components) fixed relative to the waves gives rise to an acceleration force which is calculated as the product of the added virtual mass of the structure (or of its components) and the acceleration of the fluid particles. In order to calculate the wave acceleration forces on the ends of cylindrical members, an approach given by Hooft (1972) is used. Using this approach the acceleration forces are calculated by multiplying the acceleration of the water particles at the centre of top or bottom cross-sections of the cylinder by the added mass of a disk which has the same diameter as the cylinder in question. The method may be formulated

as follows:

$$F_y = \frac{4}{3}\rho R^3 \dot{u}_y$$

3) *Drag Force*: The drag force mainly results from the turbulent flow downstream of the body due to viscous effects which are significant when diameter/wave height<0.125 for circular cylinders.

The following basic philosophy which was given by Incecik (1982) is employed in the derivation of a general three dimensional method for wave loading calculations:

a) All the wave properties, i.e. dynamic pressure, velocity and acceleration of water particles which are defined in the fixed wave reference system are first transferred to the structure reference system (which moves relative to the wave reference system) and from the structure reference system to the member reference system (which is fixed relative to the structural reference system).

b) All force and moment calculations are carried out in the member reference system.

c) The results of the force and moment calculations are transferred back to the structure reference system and moments are summed along the principle axes of the structure reference system to obtain pitch, roll and yaw moments. Forces are transferred to the wave reference system and summed along the principle axes of the wave reference system to obtain heave, surge and sway forces.

3.2 DERIVATION OF A GENERAL METHOD TO CALCULATE WAVE FORCES ON THE CIRCULAR CYLINDRICAL MEMBERS OF OFFSHORE STRUCTURES

3.2.1 DEFINITION OF REFERENCE SYSTEMS

The wave properties, i.e. pressure,velocity and acceleration of water particles may be defined in the wave reference system (Oxyz).

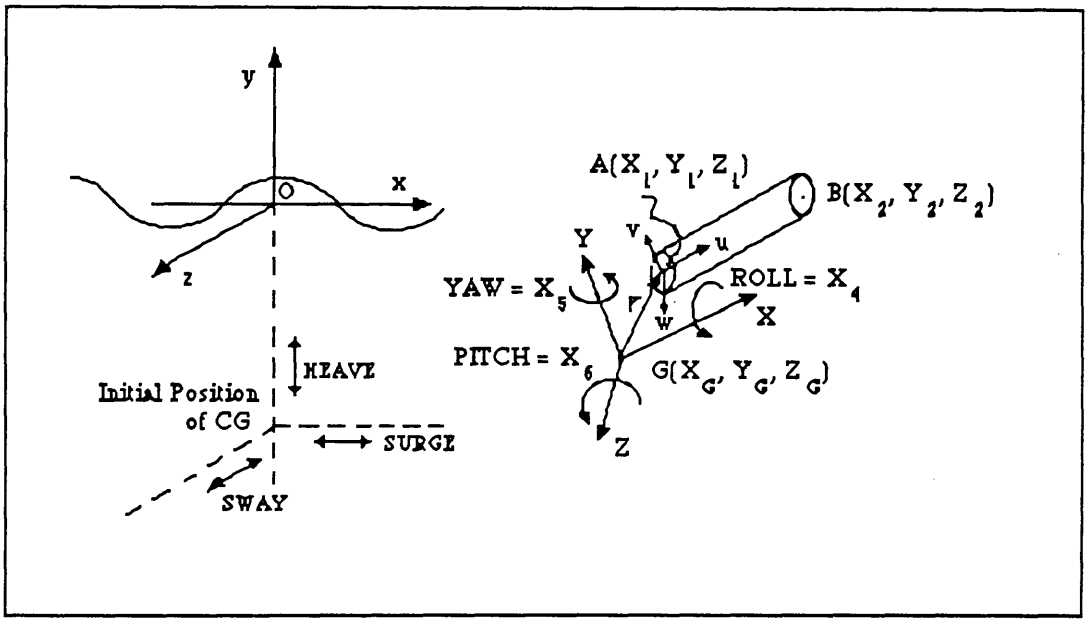

Fig.3.1 Co-ordinate system used in hydrodynamic force calculation

The structural global reference system (GXYZ) is chosen at the centre of gravity of a floating structure. (Auvw) are the reference axes for an individual member within the structure (see Fig.3.1).

3.2.2 CALCULATION OF WAVE FORCES

In order to calculate pressure,acceleration and velocity forces coordinates defined in the (Oxyz) system are transferred to the (GXYZ) system using the following transformation matrix:

$$\begin{bmatrix} x \\ y \\ z \end{bmatrix} = \begin{bmatrix} \beta_{11} & \beta_{12} & \beta_{13} \\ \beta_{21} & \beta_{22} & \beta_{23} \\ \beta_{31} & \beta_{32} & \beta_{33} \end{bmatrix} \begin{bmatrix} X \\ Y \\ Z \end{bmatrix} + \begin{bmatrix} X_G \\ Y_G \\ Z_G \end{bmatrix} \tag{3.1}$$

where

X_G , Y_G and Z_G are the vessel's C.O.G at initial position.

$$\begin{aligned}
\beta_{11} &= \cos X_5 \cos X_6 \\
\beta_{12} &= -\cos X_5 \sin X_6 \\
\beta_{13} &= \sin X_5 \\
\beta_{21} &= \cos X_4 \sin X_6 + \sin X_5 \cos X_6 \sin X_4 \\
\beta_{22} &= \cos X_6 \cos X_4 - \sin X_4 \sin X_5 \sin X_6 \\
\beta_{23} &= -\sin X_4 \cos X_5 \\
\beta_{31} &= \sin X_4 \sin X_6 - \cos X_4 \sin X_5 \cos X_6 \\
\beta_{32} &= \sin X_4 \cos X_6 + \cos X_4 \sin X_5 \sin X_6 \\
\beta_{33} &= \cos X_4 \cos X_5
\end{aligned} \tag{3.2}$$

Using the transformation Eqs.(3.1), the wave particle velocity, acceleration and pressure equations, by referring to the structure reference system can be written as follows:

Horizontal Wave Particle Velocity

$$u_{x,(s)} = 0.5 H_w \omega e^{k(\beta_{21}X + \beta_{22}Y + \beta_{23}Z + Y_G)} \cos[k(\beta_{11}X + \beta_{12}Y + \beta_{13}Z + X_G) - \omega t] \tag{3.3}$$

where

k Wave number given by $\frac{\omega^2}{g}$

ω Angular wave frequency

H_ω Wave height

Subscript (s) denotes structure reference system.

Vertical Wave Particle Velocity

$$u_{y,(s)} = 0.5 H_w \, \omega \, e^{k(\beta_{21}X + \beta_{22}Y + \beta_{23}Z + Y_G)} \sin[k(\beta_{11}X + \beta_{12}Y + \beta_{13}Z + X_G) - \omega t] \quad (3.4)$$

Horizontal Wave Particle Acceleration

$$\dot{u}_{x,(s)} = 0.5 H_w \, \omega^2 e^{k(\beta_{21}X + \beta_{22}Y + \beta_{23}Z + Y_G)} \sin[k(\beta_{11}X + \beta_{12}Y + \beta_{13}Z + X_G) - \omega t] \quad (3.5)$$

Vertical Wave Particle Acceleration

$$\dot{u}_{y,(s)} = -0.5 H_w \, \omega^2 e^{k(\beta_{21}X + \beta_{22}Y + \beta_{23}Z + Y_G)} \cos[k(\beta_{11}X + \beta_{12}Y + \beta_{13}Z + X_G) - \omega t] \quad (3.6)$$

Dynamic Pressure

$$p_{(m)} = 0.5 H_w \, \rho \, g \, e^{k[\beta_{21}X + \beta_{22}Y + \beta_{23}Z + Y_G]} \cos[k(\beta_{11}X + \beta_{12}Y + \beta_{13}Z + X_G) - \omega t] \quad (3.7)$$

where

ρ Density of water

g Gravity acceleration

In order to carry out force and moment calculations on an individual member of the structure one has to transfer these wave particle velocity, acceleration and pressure equations, which have been written in the structure reference system, to the member reference system using the following matrix equation:

$$\begin{bmatrix} X \\ Y \\ Z \end{bmatrix} = \begin{bmatrix} \alpha_{11} & \alpha_{12} & \alpha_{13} \\ \alpha_{21} & \alpha_{22} & \alpha_{23} \\ \alpha_{31} & \alpha_{32} & \alpha_{33} \end{bmatrix} \begin{bmatrix} u \\ v \\ w \end{bmatrix} + \begin{bmatrix} X_1 \\ Y_1 \\ Z_1 \end{bmatrix} \tag{3.8}$$

where

α_{11} : The cosine of the angle between X and u

α_{12} : The cosine of the angle between X and v

α_{13} : The cosine of the angle between X and w

α_{21} : The cosine of the angle between Y and u

α_{22} : The cosine of the angle between Y and v

α_{23} : The cosine of the angle between Y and w

α_{31} : The cosine of the angle between Z and u

α_{32} : The cosine of the angle between Z and v

α_{33} : The cosine of the angle between Z and w

The direction cosines are calculated by following the procedure described by Incecik (1982). The relationships between the direction cosines and the unit vectors are given in the following:

$$\alpha_{11} = \boldsymbol{i} \cdot \boldsymbol{e}_1 \qquad \alpha_{12} = \boldsymbol{i} \cdot \boldsymbol{e}_2 \qquad \alpha_{13} = \boldsymbol{i} \cdot \boldsymbol{e}_3$$

$$\alpha_{21} = \boldsymbol{j} \cdot \boldsymbol{e}_1 \qquad \alpha_{22} = \boldsymbol{j} \cdot \boldsymbol{e}_2 \qquad \alpha_{23} = \boldsymbol{j} \cdot \boldsymbol{e}_3$$

$$\alpha_{31} = \boldsymbol{k} \cdot \boldsymbol{e}_1 \qquad \alpha_{32} = \boldsymbol{k} \cdot \boldsymbol{e}_2 \qquad \alpha_{33} = \boldsymbol{k} \cdot \boldsymbol{e}_3 \tag{3.9}$$

3.2.3 CALCULATION OF PRESSURE FORCES

The dynamic pressure change with depth below the surface of a wave in the structural reference system is given in Eq.(3.7). This equation can be transformed to the member reference system, using matrix Eq.(3.8) to calculate the dynamic wave pressure forces acting on an individual member as follows:

$$p_{(m)} = 0.5 H_w \rho g e^{kB} \cos(k A - \omega t) \tag{3.10}$$

where

$$\begin{aligned} A &= \beta_{11} X + \beta_{12} Y + \beta_{13} Z + X_G \\ B &= \beta_{21} X + \beta_{22} Y + \beta_{23} Z + Y_G \end{aligned} \tag{3.11}$$

The total pressure force in a member's reference system can be determined using the following integration equation

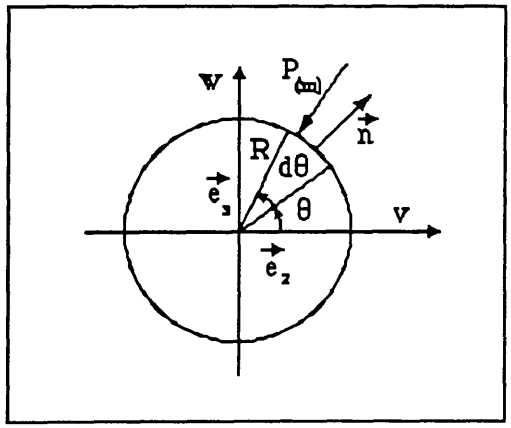

Fig.3.2 Pressure definition on circular cylinder

$$\boldsymbol{FP}_{i,(m)} = -\int_{u=0}^{l} \int_{\theta=0}^{2\pi} (p_{(m)} R \cos\theta \, d\theta \, du \, \boldsymbol{e}_2 + p_{(m)} R \sin\theta \, d\theta \, du \, \boldsymbol{e}_3) \tag{3.12}$$

where subscript m indicates member reference system

Since

$$dS = R\, d\theta\, du \tag{3.13}$$

$\boldsymbol{n}$: unit normal vector to surface (positive outwards)

$$= \cos\theta\, \boldsymbol{e}_2 + \sin\theta\, \boldsymbol{e}_3 \tag{3.14}$$

$\boldsymbol{FP}_{i,(m)}$ may be written as follows:

$$\boldsymbol{FP}_{i,(m)} = -\int_S p_{(m)}\, \boldsymbol{n}\, dS \tag{3.15}$$

Using the divergence theorem of Gauss, the surface integral form of $\boldsymbol{FP}_{i,(m)}$ can be converted to a volume integral:

$$\boldsymbol{FP}_{i,(m)} = -\int_S p_{(m)}\, \boldsymbol{n}\, dS = -\iiint_V \nabla\, p_{(m)} dV \tag{3.16}$$

where V is the volume bounded by a closed surface S and

$$\nabla = \frac{\partial}{\partial u}\boldsymbol{e}_1 + \frac{\partial}{\partial v}\boldsymbol{e}_2 + \frac{\partial}{\partial w}\boldsymbol{e}_3 \tag{3.17}$$

The pressure force components along the w and v axes can be written in the form of a volume integral as follows

$$\boldsymbol{FP}_{w\,i,(m)} = -\iiint_V \frac{\partial}{\partial w} p_{(m)} dV\, \boldsymbol{e}_3 \tag{3.18}$$

or

$$\boldsymbol{FP}_{w\,i,(m)} = -\iiint_V \frac{\partial}{\partial w} [0.5 H_w\, \rho\, g\, e^{kB} \cos(k\,A - \omega\, t)] dV\, \boldsymbol{e}_3 \tag{3.19}$$

Since $dV = r\, d\theta\, dr\, du$

$v = r\cos\theta$

$w = r\sin\theta$ (3.20)

The following equation can be written from the transformation matrix Eq.(3.8):

$$X = \alpha_{11}u + \alpha_{12}(r\cos\theta) + \alpha_{13}(r\sin\theta) + X_1$$
$$Y = \alpha_{21}u + \alpha_{22}(r\cos\theta) + \alpha_{23}(r\sin\theta) + Y_1$$
$$Z = \alpha_{31}u + \alpha_{32}(r\cos\theta) + \alpha_{33}(r\sin\theta) + Z_1 \quad (3.21)$$

Since $kv<<1$ and $kw<<1$ in the case of small diameter cylinders ($D/\lambda<0.2$) the terms involving kv and kw can be neglected and therefore further simplifications can be made in Eq.(3.19).

$$\boldsymbol{FP}_{w_{i,(m)}} = -0.5H_w\,\omega^2 \int_{u=0}^{l}\int_{r=0}^{R}\int_{\theta=0}^{2\pi} [C\,e^{kB}\cos(k\,A - \omega\,t) - D\,e^{kB}\sin(k\,A - \omega\,t)]\,r\,d\theta\,dr\,du\,\boldsymbol{e}_3 \quad (3.22)$$

where

$$C = \beta_{21}\alpha_{13} + \beta_{22}\alpha_{23} + \beta_{23}\alpha_{33}$$
$$D = \beta_{11}\alpha_{13} + \beta_{12}\alpha_{23} + \beta_{13}\alpha_{33} \quad (3.23)$$

Having carried out the integrations with respect to r and θ in Eq.(3.22), the pressure force in w direction can be written in the following form:

$$\boldsymbol{FP}_{w_{i,(m)}} = -0.5H_w\,\rho\,\omega^2\pi R^2 \int_{u=0}^{l} [C\,e^{kE}\cos(k\,F - \omega\,t) - D\,e^{kE}\sin(k\,F - \omega\,t)]\,du\,\boldsymbol{e}_3 \quad (3.24)$$

where

$$E = \beta_{21}(\alpha_{11}u + X_1) + \beta_{22}(\alpha_{21}u + Y_1) + \beta_{23}(\alpha_{31}u + Z_1) + Y_G$$
$$F = \beta_{11}(\alpha_{11}u + X_1) + \beta_{12}(\alpha_{21}u + Y_1) + \beta_{13}(\alpha_{31}u + Z_1) + X_G \quad (3.25)$$

Similarly, the pressure force along the v direction can be obtained as follows:

$$\boldsymbol{FP}_{v_{i,(m)}} = -\iiint_V \frac{\partial}{\partial v} p_{(m)} dV \, \boldsymbol{e}_2 \quad (3.26)$$

$$\boldsymbol{FP}_{v_{i,(m)}} = -\iiint_V \frac{\partial}{\partial v} [0.5 H_w \rho g e^{kB} \cos(kA - \omega t)] dV \, \boldsymbol{e}_2 \quad (3.27)$$

$$\boldsymbol{FP}_{v_{i,(m)}} = -0.5 H_w \rho \omega^2 \int_{u=0}^{l} \int_{r=0}^{R} \int_{\theta=0}^{2\pi} [G e^{kB} \cos(kA - \omega t) - H e^{kB} \sin(kA - \omega t)] r \, d\theta \, dr \, du \, \boldsymbol{e}_2 \quad (3.28)$$

where

$$G = \beta_{21}\alpha_{12} + \beta_{22}\alpha_{22} + \beta_{23}\alpha_{32}$$
$$H = \beta_{11}\alpha_{12} + \beta_{12}\alpha_{22} + \beta_{13}\alpha_{32} \quad (3.29)$$

Similarly, the pressure force in *v* direction can be written in the following form:

$$\boldsymbol{FP}_{w_{i,(m)}} = -0.5 H_w \rho \omega^2 \pi R^2 \int_{u=0}^{l} [G e^{kE} \cos(kF - \omega t) - H e^{kE} \sin(kF - \omega t)] du \, \boldsymbol{e}_2 \quad (3.30)$$

The pressure forces at the bottom and at the top of a cylindrical member can be written as follows:

$$FP_{u_{i,(m)}} = \int_{r=0}^{R} \int_{\theta=0}^{2\pi} p_{(m)} r \, dr \, d\theta \tag{3.31}$$

Since the dynamic pressure change may be assumed to be constant across the diameter of the cylindrical member, Eq.(3.31) can take the following form

$$FP_{u_{i,(m)}} = 0.5 H_w \rho g \pi R^2 e^{kB} \cos(kA - \omega t) \tag{3.32}$$

Pressure force on the bottom of a cylindrical member:

$$\boldsymbol{FP}_{u=0,(m)} = 0.5 H_w \rho g \pi R^2 e^{kI} \cos(kJ - \omega t) \boldsymbol{e}_1 \tag{3.33}$$

where

$$\begin{aligned} I &= \beta_{21} X_1 + \beta_{22} Y_1 + \beta_{23} Z_1 + Y_G \\ J &= \beta_{11} X_1 + \beta_{12} Y_1 + \beta_{13} Z_1 + X_G \end{aligned} \tag{3.34}$$

Similarly, the pressure force at the top end of the cylindrical member will be:

$$\boldsymbol{FP}_{u=l,(m)} = -0.5 H_w \rho g \pi R^2 e^{kK} \cos(kL - \omega t) \boldsymbol{e}_1 \tag{3.35}$$

where

$$\begin{aligned} K &= \beta_{21}(\alpha_{11} l + X_1) + \beta_{22}(\alpha_{21} l + Y_1) + \beta_{23}(\alpha_{31} l + Z_1) + Y_G \\ L &= \beta_{11}(\alpha_{11} l + X_1) + \beta_{12}(\alpha_{21} l + Y_1) + \beta_{13}(\alpha_{31} l + Z_1) + X_G \end{aligned} \tag{3.36}$$

When the total pressure force acting on a member in the member and structure reference systems are written the following equations are obtained:

$$FP_{i,(m)} = FP_{w_{i,(m)}} e_3 + FP_{v_{i,(m)}} e_2 + (FP_{u=0_{i,(m)}} - FP_{u=l_{i,(m)}}) e_1 \tag{3.37}$$

$$FP_{i,(s)} = (FP_{i,(m)} i)i + (FP_{i,(m)} j)j + (FP_{i,(m)} k)k \tag{3.38}$$

Using the direction cosines the pressure equation given above can also be written in the following form:

$$\underbrace{FP_{i,(s)} = [FP_{w_{i,(m)}} \alpha_{13} + FP_{v_{i,(m)}} \alpha_{12} + (FP_{u=0_{i,(m)}} - FP_{u=l_{i,(m)}})\alpha_{11}]i}_{\textit{surge force component}}$$

$$\underbrace{+ [FP_{w_{i,(m)}} \alpha_{23} + FP_{v_{i,(m)}} \alpha_{22} + (FP_{u=0_{i,(m)}} - FP_{u=l_{i,(m)}})\alpha_{21}]j}_{\textit{heave force component}}$$

$$\underbrace{+ [FP_{w_{i,(m)}} \alpha_{33} + FP_{v_{i,(m)}} \alpha_{32} + (FP_{u=0_{i,(m)}} - FP_{u=l_{i,(m)}})\alpha_{31}]k}_{\textit{sway force component}}$$

(3.39)

The total force components are transferred to the fixed wave reference system to obtain heave, surge and sway force components with the following equation:

$$FP_{i,(w)} = (FP_{i,(w)} i')i' + (FP_{i,(s)} j')j' + (FP_{i,(s)} k')k' \tag{3.40}$$

or

$$FP_{i,(w)} = \left.\begin{aligned} &[FP_{w_{i,(m)}}\alpha_{13} + FP_{v_{i,(m)}}\alpha_{12} + (FP_{u=0_{i,(m)}} - FP_{u=l_{i,(m)}})\alpha_{11}]\beta_{11} \\ &+ [FP_{w_{i,(m)}}\alpha_{23} + FP_{v_{i,(m)}}\alpha_{22} + (FP_{u=0_{i,(m)}} - FP_{u=l_{i,(m)}})\alpha_{21}]\beta_{12} \\ &+ [FP_{w_{i,(m)}}\alpha_{33} + FP_{v_{i,(m)}}\alpha_{32} + (FP_{u=0_{i,(m)}} - FP_{u=l_{i,(m)}})\alpha_{31}]\beta_{13} \end{aligned}\right\} \text{surge}$$

$$\left.\begin{aligned} &+ [FP_{w_{i,(m)}}\alpha_{13} + FP_{v_{i,(m)}}\alpha_{12} + (FP_{u=0_{i,(m)}} - FP_{u=l_{i,(m)}})\alpha_{11}]\beta_{21} \\ &+ [FP_{w_{i,(m)}}\alpha_{23} + FP_{v_{i,(m)}}\alpha_{22} + (FP_{u=0_{i,(m)}} - FP_{u=l_{i,(m)}})\alpha_{21}]\beta_{22} \\ &+ [FP_{w_{i,(m)}}\alpha_{33} + FP_{v_{i,(m)}}\alpha_{32} + (FP_{u=0_{i,(m)}} - FP_{u=l_{i,(m)}})\alpha_{31}]\beta_{23} \end{aligned}\right\} \text{heave}$$

$$\left.\begin{aligned} &+ [FP_{w_{i,(m)}}\alpha_{13} + FP_{v_{i,(m)}}\alpha_{12} + (FP_{u=0_{i,(m)}} - FP_{u=l_{i,(m)}})\alpha_{11}]\beta_{31} \\ &+ [FP_{w_{i,(m)}}\alpha_{23} + FP_{v_{i,(m)}}\alpha_{22} + (FP_{u=0_{i,(m)}} - FP_{u=l_{i,(m)}})\alpha_{21}]\beta_{32} \\ &+ [FP_{w_{i,(m)}}\alpha_{33} + FP_{v_{i,(m)}}\alpha_{32} + (FP_{u=0_{i,(m)}} - FP_{u=l_{i,(m)}})\alpha_{31}]\beta_{33} \end{aligned}\right\} \text{sway}$$

(3.41)

3.2.4 THE CALCULATION OF ACCELERATION FORCES

The horizontal and vertical components of wave particle acceleration in the structure reference system have been given in Eqs.(3.5-6) in the following form:

$$\dot{u}_{x,(s)} = 0.5H_w\,\omega^2 e^{k(\beta_{21}X + \beta_{22}Y + \beta_{23}Z + Y_G)}$$

$$\sin[k(\beta_{11}X + \beta_{12}Y + \beta_{13}Z + X_G) - \omega t]$$

$$\dot{u}_{y,(s)} = -0.5H_w\,\omega^2 e^{k(\beta_{21}X + \beta_{22}Y + \beta_{23}Z + Y_G)}$$

$$\cos[k(\beta_{11}X + \beta_{12}Y + \beta_{13}Z + X_G) - \omega t]$$

Assuming that the change of wave particle accelerations across the diameter of a cylinder can be neglected for small diameter cylinders, the following equations are obtained for the acceleration components in the member reference system:

$$\dot{u}_{x,(m)} = 0.5 H_w \omega^2 e^{kE} \sin(kF - \omega t) \tag{3.42}$$

$$\dot{u}_{y,(m)} = 0.5 H_w \omega^2 e^{kE} \cos(kF - \omega t) \tag{3.43}$$

The above expressions have been written in the member reference system but they are along lines which are parallel to the wave propagation. If one resolves them along the structure reference system's axes the following equations are obtained

$$\dot{u}^{x}_{X,(m)} = \dot{u}_{x,(m)} \cos(x, X) \qquad \cos(x, X) = \beta_{11}$$

$$\dot{u}^{y}_{X,(m)} = \dot{u}_{y,(m)} \cos(y, X) \qquad \cos(y, X) = \beta_{21}$$

$$\dot{u}^{x}_{Y,(m)} = \dot{u}_{x,(m)} \cos(x, Y) \qquad \cos(x, Y) = \beta_{12}$$

$$\dot{u}^{y}_{Y,(m)} = \dot{u}_{y,(m)} \cos(y, Y) \qquad \cos(y, Y) = \beta_{22}$$

$$\dot{u}^{x}_{Z,(m)} = \dot{u}_{x,(m)} \cos(x, Z) \qquad \cos(x, Z) = \beta_{13}$$

$$\dot{u}^{y}_{Z,(m)} = \dot{u}_{y,(m)} \cos(y, Z) \qquad \cos(y, Z) = \beta_{23} \tag{3.44}$$

Now one can write the wave acceleration forces in the member reference system along the w and v axes

$$\begin{aligned} FA_{w_{i,(m)}} = k_{33}\rho \Big[& \iiint_V (\dot{u}^{x}_{X,(m)} + \dot{u}^{y}_{X,(m)}) \cos(w, X)\, dV \\ & + \iiint_V (\dot{u}^{x}_{Y,(m)} + \dot{u}^{y}_{Y,(m)}) \cos(w, Y)\, dV \\ & + \iiint_V (\dot{u}^{x}_{Z,(m)} + \dot{u}^{y}_{Z,(m)}) \cos(w, Z)\, dV \Big] e_3 \end{aligned} \tag{3.45}$$

Substituting k_{33}=1 (since the acceleration force is calculated along the w axis on circular cylinders), the values of $\dot{u}_{X,(m)}, \dot{u}_{Y,(m)}, \dot{u}_{Z,(m)}$ from Eq.(3.44) and $dV = \pi R^2 du$ into Eq.(3.45) the wave acceleration force becomes:

$$FA_{w_{i,(m)}} = \rho \pi R^2 \int_{u=0}^{l} [(\dot{u}_{x,(m)}\beta_{11} + \dot{u}_{y,(m)}\beta_{21})\alpha_{13} + (\dot{u}_{x,(m)}\beta_{12} + \dot{u}_{y,(m)}\beta_{22})\alpha_{23} + (\dot{u}_{x,(m)}\beta_{13} + \dot{u}_{y,(m)}\beta_{23})\alpha_{33}]du\, e_3 \quad (3.46)$$

If $\dot{u}_{x,(m)}$ and $\dot{u}_{y,(m)}$ given in Eqs.(3.42-43) are substituted in Eq.(3.46), the wave acceleration force on the circular cylindrical member along the w axis can also be written as:

$$FA_{w_{i,(m)}} = \rho \pi R^2 0.5 H_w \omega^2 \int_{u=0}^{l} e^{kE} \{[\sin(kF - \omega t)\beta_{11} - \cos(kF - \omega t)\beta_{21}]\alpha_{13} + [\sin(kF - \omega t)\beta_{12} - \cos(kF - \omega t)\beta_{22}]\alpha_{23} + [\sin(kF - \omega t)\beta_{13} - \cos(kF - \omega t)\beta_{23}]\alpha_{33}\} du\, e_3 \quad (3.47)$$

A similar expression to that in Eq.(3.45) can be written to obtain $FA_{v_{i,(m)}}$.

$$FA_{v_{i,(m)}} = k_{22}\rho [\iiint_V (u^x_{X,(m)} + u^y_{X,(m)}) \cos(v, X) dV + \iiint_V (u^x_{Y,(m)} + u^y_{Y,(m)}) \cos(v, Y) dV + \iiint_V (u^x_{Z,(m)} + u^y_{Z,(m)}) \cos(v, Z) dV\ ] e_2 \quad (3.48)$$

Substituting k_{33}=1 (since the acceleration force is calculated along the w axis on circular cylinders), the values of $\dot{u}_{X,(m)}, \dot{u}_{Y,(m)}, \dot{u}_{Z,(m)}$ from Eq.(3.44) and $dV = \pi R^2 du$ into Eq.(3.48) the wave acceleration force along v direction becomes:

$$FA_{v_{i,(m)}} = \rho \pi R^2 \int_{u=0}^{l} [(\dot{u}_{x,(m)}\beta_{11} + \dot{u}_{y,(m)}\beta_{21})\alpha_{12} + (\dot{u}_{x,(m)}\beta_{12} + \dot{u}_{y,(m)}\beta_{22})\alpha_{22} + (\dot{u}_{x,(m)}\beta_{13} + \dot{u}_{y,(m)}\beta_{23})\alpha_{32}]du\, e_2 \tag{3.49}$$

If $\dot{u}_{x,(m)}$ and $\dot{u}_{y,(m)}$ given in Eqs.(3.42-43) are substituted in Eq.(3.49) the wave acceleration force on the circular cylindrical member along the v axis can also be written as:

$$FA_{v_{i,(m)}} = \rho \pi R^2 0.5 H_w \omega^2 \int_{u=0}^{l} e^{kE} \{[\sin(kF - \omega t)\beta_{11} - \cos(kF - \omega t)\beta_{21}]\alpha_{12} + [\sin(kF - \omega t)\beta_{12} - \cos(kF - \omega t)\beta_{22}]\alpha_{22} + [\sin(kF - \omega t)\beta_{13} - \cos(kF - \omega t)\beta_{23}]\alpha_{32}\}du\, e_2 \tag{3.50}$$

Finally the acceleration forces on the end surfaces of a cylindrical member can be calculated as follows:

$$FA_{u=0_{i,(m)}} = m_{11}[(u^{x}_{X,(m)} + u^{.y}_{X,(m)})\cos(u, X) + (u^{x}_{Y,(m)} + u^{.y}_{Y,(m)})\cos(u, Y) + (u^{x}_{Z,(m)} + u^{.y}_{Z,(m)})\cos(u, Z)]e_1 \tag{3.51}$$

If $\dot{u}_{x,(m)}$ and $\dot{u}_{y,(m)}$ are replaced with Eqs.(3.42-43) respectively, Eq.(3.51) takes the following form:

$$FA_{u=0_{i,(m)}} = k_{22} 0.5 H_w \omega^2 e^{kI}$$

$$\{[\beta_{11}\sin(kJ - \omega t) - \beta_{21}\cos(kJ - \omega t)]\alpha_{11}$$

$$+ [\beta_{12}\sin(kJ - \omega t) - \beta_{22}\cos(kJ - \omega t)]\alpha_{21}$$

$$+ [\beta_{13}\sin(kJ - \omega t) - \beta_{23}\cos(kJ - \omega t)]\alpha_{31}\}e_1 \tag{3.52}$$

$$FA_{u=l_{i,(m)}} = k_{22} 0.5 H_w \omega^2 e^{kK}$$

$$\{[\beta_{11}\sin(kL - \omega t) - \beta_{21}\cos(kL - \omega t)]\alpha_{11}$$

$$+ [\beta_{12}\sin(kL - \omega t) - \beta_{22}\cos(kL - \omega t)]\alpha_{21}$$

$$+ [\beta_{13}\sin(kL - \omega t) - \beta_{23}\cos(kL - \omega t)]\alpha_{31}\}e_1 \tag{3.53}$$

where

$$k_{22} = \frac{4}{3}\rho R^3 \tag{3.54}$$

3.2.5 THE CALCULATION OF VELOCITY FORCES

As with the acceleration force calculations, if one neglects the velocity variation along the diameter of the cylinder, and assuming that wave particles move along the diameter of the cylinder with a velocity equal to that at the centre of the cylinder cross-section, the following equations can be written to calculate the velocity forces.

The horizontal and vertical components of the wave particle velocity given in the structure reference system by Eqs.(3.3-4) can be transferred into the member reference

system as follows:

$$u_{x,(m)} = 0.5 H_w \, \omega \, e^{k E} \cos(k F - \omega t) \tag{3.55}$$

$$u_{y,(m)} = 0.5 H_w \, \omega \, e^{k E} \sin(k F - \omega t) \tag{3.56}$$

The above expressions for the water particle velocity are written in the member reference system but they are parallel to the direction of wave propagation. If one resolves them along lines which are parallel to the structure reference system's axes the following equations are obtained:

$$\begin{aligned}
u^{x}_{X,(m)} &= u_{x,(m)} \cos(x, X) & \cos(x, X) &= \beta_{11} \\
u^{y}_{X,(m)} &= u_{y,(m)} \cos(y, X) & \cos(y, X) &= \beta_{21} \\
u^{x}_{Y,(m)} &= u_{x,(m)} \cos(x, Y) & \cos(x, Y) &= \beta_{12} \\
u^{y}_{Y,(m)} &= u_{y,(m)} \cos(y, Y) & \cos(y, Y) &= \beta_{22} \\
u^{x}_{Z,(m)} &= u_{x,(m)} \cos(x, Z) & \cos(x, Z) &= \beta_{13} \\
u^{y}_{Z,(m)} &= u_{y,(m)} \cos(y, Z) & \cos(y, Z) &= \beta_{23}
\end{aligned} \tag{3.57}$$

Now one can obtain the velocity forces in the member reference system along the w and v axes:

$$FV_{w_{i,(m)}} = \frac{1}{2}\rho C_D D \int_{u=0}^{l} [(u^x_{X,(m)} + u^y_{X,(m)})\cos(w, X)$$

$$+ (u^x_{Y,(m)} + u^y_{Y,(m)})\cos(w, Y)$$

$$+ (u^x_{Z,(m)} + u^y_{Z,(m)})\cos(w, Z)]$$

$$|[(u^x_{X,(m)} + u^y_{X,(m)})\cos(w, X)$$

$$+ (u^x_{Y,(m)} + u^y_{Y,(m)})\cos(w, Y)$$

$$+ (u^x_{Z,(m)} + u^y_{Z,(m)})\cos(w, Z)]|du\, e_3 \qquad (3.58)$$

where

C_D	Drag coefficient
D	Diameter of the members

or substituting Eq.(3.57) into Eq.(3.58) the drag force along w axes on each member may also be written as follows

$$FV_{w_{i,(m)}} = \frac{1}{2}C_D \rho D\ (0.5H_w \omega)^2$$

$$\int_{u=0}^{l} e^{2kE} \{[\cos(kF - \omega t)\beta_{11} + \sin(kF - \omega t)\beta_{21}]\alpha_{13}$$

$$+ [\cos(kF - \omega t)\beta_{12} + \sin(kF - \omega t)\beta_{22}]\alpha_{23}$$

$$+ [\cos(kF - \omega t)\beta_{13} + \sin(kF - \omega t)\beta_{23}]\alpha_{33}\}$$

$$|\{[\cos(kF - \omega t)\beta_{11} + \sin(kF - \omega t)\beta_{21}]\alpha_{13}$$

$$+ [\cos(kF - \omega t)\beta_{12} + \sin(kF - \omega t)\beta_{22}]\alpha_{23}$$

$$+ [\cos(kF - \omega t)\beta_{13} + \sin(kF - \omega t)\beta_{23}]\alpha_{33}\}|du\, e_3$$

(3.59)

Similarly the velocity force along the v axis will be

$$FV_{v_{i,(m)}} = \frac{1}{2}\rho C_D D \int_{u=0}^{l} [(u^x_{X,(m)} + u^y_{X,(m)})\cos(v, X)$$

$$+ (u^x_{Y,(m)} + u^y_{Y,(m)})\cos(v, Y)$$

$$+ (u^x_{Z,(m)} + u^y_{Z,(m)})\cos(v, Z)]$$

$$|[(u^x_{X,(m)} + u^y_{X,(m)})\cos(v, X)$$

$$+ (u^x_{Y,(m)} + u^y_{Y,(m)})\cos(v, Y)$$

$$+ (u^x_{Z,(m)} + u^y_{Z,(m)})\cos(v, Z)]|du\, e_2 \qquad (3.60)$$

By substituting Eq.(3.57) into Eq.(3.60) the drag force along v axes on each member may also be written as follows:

$$FV_{v_{i,(m)}} = \frac{1}{2}\rho C_D D\,(0.5H_w\,\omega)^2$$

$$\int_{u=0}^{l} e^{2kE}\{[\cos(kF - \omega t)\beta_{11} + \sin(kF - \omega t)\beta_{21}]\alpha_{12}$$

$$+ [\cos(kF - \omega t)\beta_{12} + \sin(kF - \omega t)\beta_{22}]\alpha_{22}$$

$$+ [\cos(kF - \omega t)\beta_{13} + \sin(kF - \omega t)\beta_{23}]\alpha_{32}\}$$

$$|\{[\cos(kF - \omega t)\beta_{11} + \sin(kF - \omega t)\beta_{21}]\alpha_{12}$$

$$+ [\cos(kF - \omega t)\beta_{12} + \sin(kF - \omega t)\beta_{22}]\alpha_{22}$$

$$+ [\cos(kF - \omega t)\beta_{13} + \sin(kF - \omega t)\beta_{23}]\alpha_{32}\}|du\, e_2$$

(3.61)

3.2.6 CALCULATION OF CURRENT FORCES

Currents have a velocity profile which decays very slowly with depth if a pure tidal current arises from the propagation of very long tidal waves. In such a wave, the water particle motion is nearly horizontal and the decay with depth may be given by a factor of $exp(ky)$ where the wave number $k=2\pi/\lambda$ and, y is the negative downward. For long waves k is very small, thus the decay is very slow. Therefore, the current can be expected to have an influence over the whole immersed part of the structure.

Brebbia and Walker (1979) reported that the presence of the current implies four main effects in the force calculation as follows:

i) The water particle velocities of the surface waves are affected by the current. A moderately small current may have a significant effect because the drag force is proportional the square of the velocity.

ii) Some modification may also be necessary to the surface field. For example, surface wave amplitude may be changed and wave steepening may occur as given by Longuet-Higgins and Stewart, (1961). The velocity of propagation and length of the waves can be altered. Taylor (1955) showed that a potentially dangerous concentration of wave energy may be cancelled due to currents which can stop the waves. Waves travelling obliquely over a current will also be refracted (Muir Wood (1969)).

iii) A current acting on a fixed body gives a rise to a standing wave pattern behind the body which is analogous to the waves generated by a ship travelling in calm water. Methods using Green's function are available to solve for this type of problems but they are very complex and the effort required for the calculation would not be justified except for large diameter members.

iv) Vortex shedding is the fourth effect of a current for slender members. A lift force perpendicular to the current direction is created due to vortex shedding.

The equations for velocity forces given in Section 3.2.5. are modified to take into account the effect of steady current forces. The current is assumed to have a constant velocity with depth. In the calculation procedure only the first two effects mentioned above are taken into account. However, no modification is made to the surface wave amplitude.

Wave Modification

In order to calculate the current forces, wave modifications given by Brebbia and Walker (1979) are adopted in the drag force calculations. When the current velocity is incorporated into the water particle velocity equation, only the component of water particle velocity in the wave propagation direction is assumed to be effected.

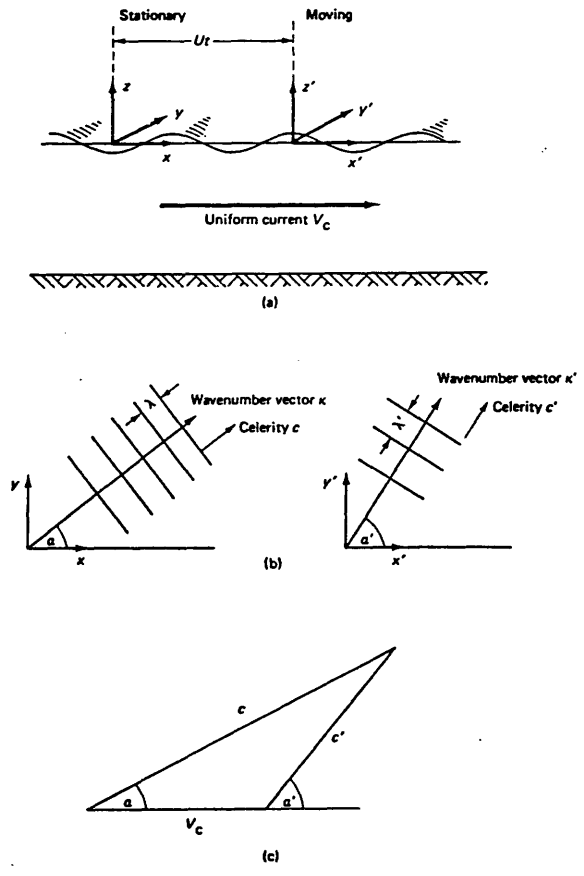

Fig.3.3 Wave modification a) coordinate systems; b) wave crest; c) wave and current speeds (Brebbia and Walker, 1979)

The dispersion relation in the moving coordinate system $k' = \omega'^2 / g$ is given in the following form:

$$k' = \frac{1}{g}(\omega - V_c\, \boldsymbol{k})^2 \tag{3.62}$$

Modified wave frequency can be expressed after some manipulations to the equation above as follows:

$$\begin{aligned}\omega' &= \omega - V_c\, \boldsymbol{k} \\ &= \omega - V_c\, k \cos\ \alpha\end{aligned}$$

or the above equation can be written in terms of the x component of the current velocity V_x:

$$\omega' = \omega - k V_x$$

If similar manipulations are done to Eq.(3.62), the following expression is obtained:

$$k' = \frac{1}{g}(\omega - k V_x)^2$$

In order to include the effect of current forces in the drag force calculations, the component of the current in the wave propagation direction is added to the water particle velocity expression in the member reference system which is given in Chapter 3, Eq.(3.55).

$$u_{x,(m)} = 0.5 H_w\ \omega\, e^{kE} \cos(k\ F\ -\ \omega\, t) +\ V_x$$

Hence, the velocity force in direction w given in Chapter 3 may be re-written in terms of both wave and current velocity:

$$FV_{w_{i,(m)}} = \frac{1}{2}\rho C_D D \int_{u=0}^{l} \{[(u_{x,(m)} + V_x)\beta_{11} + u_{y,(m)}\beta_{21})]\alpha_{13}$$

$$+ [(u_{x,(m)} + V_x)\beta_{12} + u_{y,(m)}\beta_{22}]\alpha_{23}$$

$$+ [(u_{x,(m)} + V_x)\beta_{13} + u_{y,(m)}\beta_{23})]\alpha_{33}\}$$

$$|\{[(u_{x,(m)} + V_x)\beta_{11} + u_{y,(m)}\beta_{21})]\alpha_{13}$$

$$+ [(u_{x,(m)} + V_x)\beta_{12} + u_{y,(m)}\beta_{22}]\alpha_{23}$$

$$+ [(u_{x,(m)} + V_x)\beta_{13} + u_{y,(m)}\beta_{23})]\alpha_{33}\}|du\, e_3$$

Similarly the velocity force in direction v can be given as follows:

$$FV_{v_{i,(m)}} = \frac{1}{2}\rho C_D D \int_{u=0}^{l} \{[(u_{x,(m)} + V_x)\beta_{11} + u_{y,(m)}\beta_{21})]\alpha_{12}$$

$$+ [(u_{x,(m)} + V_x)\beta_{12} + u_{y,(m)}\beta_{22}]\alpha_{22}$$

$$+ [(u_{x,(m)} + V_x)\beta_{13} + u_{y,(m)}\beta_{23})]\alpha_{32}\}$$

$$|\{[(u_{x,(m)} + V_x)\beta_{11} + u_{y,(m)}\beta_{21})]\alpha_{12}$$

$$+ [(u_{x,(m)} + V_x)\beta_{12} + u_{y,(m)}\beta_{22}]\alpha_{22}$$

$$+ [(u_{x,(m)} + V_x)\beta_{13} + u_{y,(m)}\beta_{23})]\alpha_{32}\}|du\, e_2$$

3.2.7 CALCULATION OF THE TOTAL WAVE FORCE

The total wave force which consists of the dynamic pressure force, acceleration force and velocity force can be written in the structure's reference system in the following form:

$$FT_{i,(s)} = \sum_{i=1}^{m} \underbrace{[FTw_{i,(m)}\alpha_{13} + FTv_{i,(m)}\alpha_{12} + FTu_{i,(m)}\alpha_{11}]i}_{surge\,force\,component}$$

$$+ \sum_{i=1}^{m} \underbrace{[FTw_{i,(m)}\alpha_{23} + FTv_{i,(m)}\alpha_{22} + FTu_{i,(m)}\alpha_{21}]j}_{heave\,force\,component}$$

$$+ \sum_{i=1}^{m} \underbrace{[FTw_{i,(m)}\alpha_{33} + FTv_{i,(m)}\alpha_{32} + FTu_{i,(m)}\alpha_{31}]k}_{sway\,force\,component} \qquad (3.63)$$

When Eq.(3.63) is transferred to the wave reference system the following equation is obtained to calculate the total wave force acting on a floating structure.

$$FT_{(w)} = \underbrace{(FT_{(s)}i')i'}_{surge} + \underbrace{(FT_{(s)}j')j'}_{heave} + \underbrace{(FT_{(s)}k')k'}_{sway} \qquad (3.64)$$

or the total force can be written in the wave reference system in the following form:

$$\begin{aligned} FT_{i,(w)} = \sum_{i=1}^{m} \Big\langle & \Big\{ \Big\} surge \\ & \{[FTw_{i,(m)}\alpha_{13} + FTv_{i,(m)}\alpha_{12} + FTu_{i,(m)}\alpha_{11}]\ \beta_{11} \\ & + [FTw_{i,(m)}\alpha_{23} + FTv_{i,(m)}\alpha_{22} + FTu_{i,(m)}\alpha_{21}]\ \beta_{12} \\ & + [FTw_{i,(m)}\alpha_{33} + FTv_{i,(m)}\alpha_{32} + FTu_{i,(m)}\alpha_{31}]\beta_{13}\}i' \\ & \Big\} \\ & \Big\{ \Big\} heave \\ & + \{[FTw_{i,(m)}\alpha_{13} + FTv_{i,(m)}\alpha_{12} + FTu_{i,(m)}\alpha_{11}]\ \beta_{21} \\ & + [FTw_{i,(m)}\alpha_{23} + FTv_{i,(m)}\alpha_{22} + FTu_{i,(m)}\alpha_{21}]\ \beta_{22} \\ & + [FTw_{i,(m)}\alpha_{33} + FTv_{i,(m)}\alpha_{32} + FTu_{i,(m)}\alpha_{31}]\beta_{23}\}j' \\ & \Big\} \\ & \Big\{ \Big\} sway \\ & + \{[FTw_{i,(m)}\alpha_{13} + FTv_{i,(m)}\alpha_{12} + FTu_{i,(m)}\alpha_{11}]\ \beta_{31} \\ & + [FTw_{i,(m)}\alpha_{23} + FTv_{i,(m)}\alpha_{22} + FTu_{i,(m)}\alpha_{21}]\ \beta_{32} \\ & + [FTw_{i,(m)}\alpha_{33} + FTv_{i,(m)}\alpha_{32} + FTu_{i,(m)}\alpha_{31}]\beta_{33}\}k' \Big\rangle \\ & \Big\} \end{aligned} \qquad (3.65)$$

where

$$FT_{w_{i,(m)}} = FP_{w_{i,(m)}} + FA_{w_{i,(m)}} + FV_{w_{i,(m)}}$$

$$FT_{v_{i,(m)}} = FP_{v_{i,(m)}} + FA_{v_{i,(m)}} + FV_{v_{i,(m)}}$$

$$FT_{u_{i,(m)}} = FP_{u=0_{i,(m)}} + FP_{u=l_{i,(m)}} + FA_{u=0_{i,(m)}} + FA_{u=l_{i,(m)}} \tag{3.66}$$

The terms in the last expression in Eq.(3.66) are to be determined according to the ends of the cylindrical members exposed to the wave loading, i.e. if the member is inter-costal these terms will vanish.

3.2.8 CALCULATION OF THE TOTAL WAVE MOMENT

If an individual member is considered in a member reference system, the moments due to the wave forces about the member reference system's origin, A, can be written as follows:

$$m_{A_i} = \int_{u=0}^{l} [u\, e_1 \wedge \frac{d}{du}(FT_{w_{i,(m)}} e_3 + FT_{v_{i,(m)}} e_2)]du \tag{3.67}$$

$$\begin{vmatrix} e_1 & e_2 & e_3 \\ u & 0 & 0 \\ 0 & 0 & \frac{d}{du}(FT_{w_{i,(m)}}) \end{vmatrix} = -(\frac{d}{du}FT_{w_{i,(m)}})u\, e_2 \tag{3.68}$$

$$\begin{vmatrix} e_1 & e_2 & e_3 \\ u & 0 & 0 \\ 0 & \frac{d}{du}(FT_{v_{i,(m)}}) & 0 \end{vmatrix} = -(\frac{d}{du}FT_{v_{i,(m)}})u\, e_3 \tag{3.69}$$

Eq.(3.67) becomes:

$$m_{A_i} = -\int_{u=0}^{l} \frac{d}{du}(FT_{w_{i,(m)}})u\,du\,e_2 + \int_{u=0}^{l} \frac{d}{du}(FT_{v_{i,(m)}})u\,du\,e_3 \tag{3.70}$$

The total moment about the structure reference system's origin can easily be obtained by using the moment transformation rule as follows:

$$m_{G_i} = m_{A_i} + r \wedge (FT_{w_{i,(m)}} e_3 + FT_{v_{i,(m)}} e_2 + FT_{u_{i,(m)}} e_1) \tag{3.71}$$

where

$$r = GA = X_1 i + Y_1 j + Z_1 k \tag{3.72}$$

and, e_1 and e_2 are defined in Eq.(3.9).

The total moment acting on the structure:

$$M = \sum_{i=1}^{m} m_{G_i} \tag{3.73}$$

The total moment vector can also be expressed in terms of principal components as follows:

$$M = \underbrace{ai}_{\text{roll moment}} + \underbrace{bj}_{\text{yaw moment}} + \underbrace{ck}_{\text{pitch moment}} \tag{3.74}$$

If the second term of Eq.(3.71) is calculated as follows:

$$r \wedge FT = \begin{vmatrix} i & j & k \\ X_1 & Y_1 & Z_1 \\ FT_{w_{i,(m)}}\alpha_{13} & FT_{w_{i,(m)}}\alpha_{23} & FT_{w_{i,(m)}}\alpha_{33} \\ +FT_{v_{i,(m)}}\alpha_{12} & +FT_{v_{i,(m)}}\alpha_{22} & +FT_{v_{i,(m)}}\alpha_{32} \\ +FT_{u_{i,(m)}}\alpha_{11} & +FT_{u_{i,(m)}}\alpha_{21} & +FT_{u_{i,(m)}}\alpha_{31} \end{vmatrix} \tag{3.75}$$

Each component of the roll moment can be written as follows:

Roll moment component:

$$a = \sum_{i=1}^{m} \left[\int_{u=0}^{l} \frac{d}{du}(\alpha_{13} FT_{v_{i,(m)}} - \alpha_{12} FT_{w_{i,(m)}}) u \, du \right.$$
$$+ FT_{u_{i,(m)}}(Y_1 \alpha_{31} - Z_1 \alpha_{21})$$
$$+ FT_{v_{i,(m)}}(Y_1 \alpha_{32} - Z_1 \alpha_{22})$$
$$\left. + FT_{w_{i,(m)}}(Y_1 \alpha_{33} - Z_1 \alpha_{23}) \right] \tag{3.76}$$

Yaw moment component:

$$b = \sum_{i=1}^{m} \left[\int_{u=0}^{l} \frac{d}{du}(\alpha_{23} FT_{v_{i,(m)}} - \alpha_{22} FT_{w_{i,(m)}}) u \, du \right.$$
$$+ FT_{u_{i,(m)}}(Z_1 \alpha_{11} - X_1 \alpha_{31})$$
$$+ FT_{v_{i,(m)}}(Z_1 \alpha_{12} - X_1 \alpha_{32})$$
$$\left. + FT_{w_{i,(m)}}(Z_1 \alpha_{13} - X_1 \alpha_{33}) \right] \tag{3.77}$$

Pitch moment component:

$$c = \sum_{i=1}^{m} \left[\int_{u=0}^{l} \frac{d}{du}(\alpha_{33} FT_{v_{i,(m)}} - \alpha_{32} FT_{w_{i,(m)}}) u \, du \right.$$
$$+ FT_{u_{i,(m)}}(X_1 \alpha_{21} - Y_1 \alpha_{11})$$
$$+ FT_{v_{i,(m)}}(X_1 \alpha_{22} - Y_1 \alpha_{12})$$
$$\left. + FT_{w_{i,(m)}}(X_1 \alpha_{23} - Y_1 \alpha_{13}) \right] \tag{3.78}$$

CHAPTER 4

MOTION RESPONSE SIMULATION

4.1 INTRODUCTION

In this chapter, hydrodynamic and restoring forces due to the motions of a floating structure composed of circular cylindrical members are discussed. A general method to calculate the hydrodynamic loading on the circular cylindrical members of offshore structures is derived. A general calculation procedure for rigid-body induced inertia forces are presented. The motion equations are obtained using Newton's second law and the numerical solution technique of non-linear motion equations is explained for intact and damaged cases. The computer program developed for the time-domain simulation is introduced.

4.2 DERIVATION OF A GENERAL METHOD TO CALCULATE HYDRODYNAMIC LOADING ON THE CIRCULAR CYLINDRICAL MEMBERS OF OFFSHORE STRUCTURES

In this section, a general method is described to calculate the hydrodynamic loading due to the rigid body motions of a platform with circular cylindrical members. The general method used in deriving the formulations given in this section is based on the theory given by Incecik (1982). The hydrodynamic loading is calculated on each individual member of the structure in terms of the velocities and accelerations of the structure in its translational and rotational modes. The total hydrodynamic loading is obtained by summing up these forces along the members and then transferring them to the principal axes of the structure reference system (G,X,Y,Z). The velocities and the accelerations of the structure are determined from the numerical solutions of the motion equations in the time-domain.

During derivation of the equations, it is assumed that the centre of rotation is at the origin of the structure reference system of the floating platform. Therefore, velocity and acceleration at any point on an individual member can be defined in terms of the structure's velocities and accelerations in translational and in rotational modes as follows

(see Fig.(4.1)).

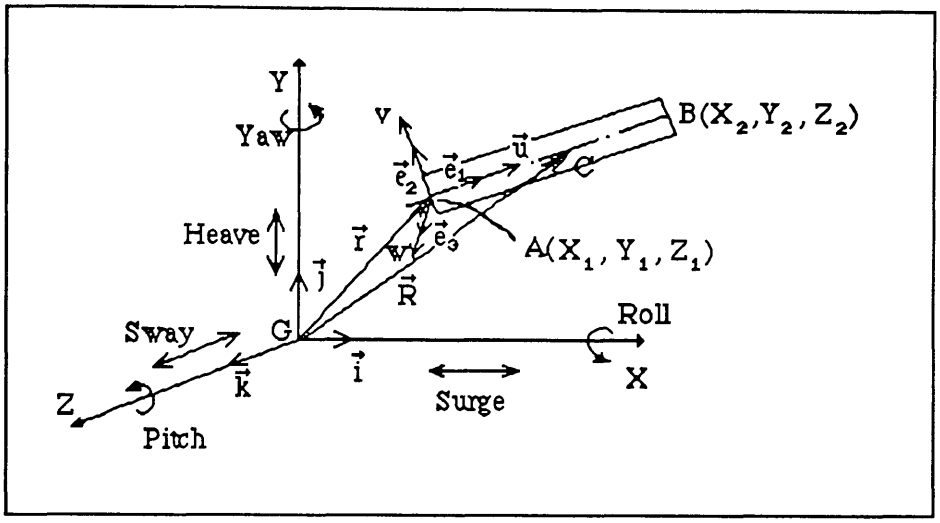

Fig.4.1 Co-ordinate system used in hydrodynamic force calculation

The expressions of velocities and accelerations of a point on an individual member in this member's reference system will be as follows:

$$U_{M_{T,S}} = U_{S_T} + U_{S_R} \wedge R = U_{S_T} + U_{S_R} \wedge (r + AC) \tag{4.1}$$

where

$U_{M_{T,S}}$	Velocity of point C relative to structural reference system
U_{S_T}	Translational velocity of point C relative to member reference system,
U_{S_R}	Rotational or angular velocity of point C relative to member reference system

In the following equation the Coriolis acceleration is neglected.

$$\dot{U}_{M_{T,S}} = \dot{U}_{S_T} + \underbrace{U_{S_R} \wedge (U_{S_R} \wedge R)}_{centripetal\,acceleration} + \underbrace{\dot{U}_{S_R} \wedge R}_{linear\,acceleration} \tag{4.2}$$

where

$\dot{U}_{M_{T,S}}$ Acceleration of point C relative to structural reference system

$\dot{U}_{S_T}$ Translational acceleration of point C relative to member reference system

$\dot{U}_{S_R}$ Rotational or angular acceleration of point C relative to member reference system

or

$$\dot{U}_{M_{T,S}} = \dot{U}_{S_T} + U_{S_R} \wedge [U_{S_R} \wedge (r + AC)] + \dot{U}_{S_R} \wedge (r + AC) \tag{4.3}$$

where

$$U_{S_T} = U_{1_{(S)}} i + U_{2_{(S)}} j + U_{3_{(S)}} k \tag{4.4}$$

$$U_{S_R} = U_{4_{(S)}} i + U_{5_{(S)}} j + U_{6_{(S)}} k \tag{4.5}$$

$$\dot{U}_{S_T} = \dot{U}_{1_{(S)}} i + \dot{U}_{2_{(S)}} j + \dot{U}_{3_{(S)}} k \tag{4.6}$$

$$\dot{U}_{S_R} = \dot{U}_{4_{(S)}} i + \dot{U}_{5_{(S)}} j + \dot{U}_{6_{(S)}} k \tag{4.7}$$

$$AC = ue_1 = u[\underbrace{(e_1 \cdot i)}_{\alpha_{11}} . i + \underbrace{(e_1 \cdot j)}_{\alpha_{21}} . j + \underbrace{(e_1 \cdot k)}_{\alpha_{31}} . k] \tag{4.8}$$

$$AC = u(\alpha_{11}i + \alpha_{21}j + \alpha_{31}k) \tag{4.9}$$

α_{ij} is the transformation matrix to transfer the co-ordinates from (G,X,Y,Z) structure's reference system to (A,u,v,w) member's reference system. The second term in Eqs.(4.2-3) can be omitted since the centripetal acceleration of the structure due to the rigid body motion is of a small magnitude.

Eqs.(4.1-3) define vectors in the member reference system whose principal components are along lines parallel to the structure's reference system. These velocity and acceleration vectors can also be written with reference to lines parallel to the member reference system's axes using the following transformation matrix:

$$U_{M_{T,M}} = [T]^T U_{M_{T,S}} \tag{4.10}$$

$$\dot{U}_{M_{T,M}} = [T]^T \dot{U}_{M_{T,S}} \tag{4.11}$$

where

$$[T]^T = \begin{bmatrix} \alpha_{11} & \alpha_{21} & \alpha_{31} \\ \alpha_{12} & \alpha_{22} & \alpha_{32} \\ \alpha_{13} & \alpha_{23} & \alpha_{33} \end{bmatrix} \tag{4.12}$$

The $U_{M_{T,S}}$, $\dot{U}_{M_{T,S}}$, $U_{M_{T,M}}$, $\dot{U}_{M_{T,M}}$ vectors can be written explicitly with reference to the chosen axes system of a member. The rigid body velocities of the structure and the member co-ordinate u are as follows:

$$r = X_1 i + Y_1 j + Z_1 k \tag{4.13}$$

$$U_{M_{T,S}} = U_1 i + U_2 j + U_3 k + \begin{vmatrix} i & j & k \\ U_4 & U_5 & U_6 \\ X_1 + u\alpha_{11} & Y_1 + u\alpha_{21} & Z_1 + u\alpha_{31} \end{vmatrix} \tag{4.14}$$

$$\boldsymbol{U}_{M_T,S} = [U_1 + U_5(Z_1 + u\alpha_{31}) - U_6(Y_1 + u\alpha_{21})]\boldsymbol{i}$$
$$+ [U_2 + U_6(X_1 + u\alpha_{11}) - U_4(Z_1 + u\alpha_{31})]\boldsymbol{j}$$
$$+ [U_3 + U_4(Y_1 + u\alpha_{21}) - U_5(X_1 + u\alpha_{11})]\boldsymbol{k} \tag{4.15}$$

$$\dot{\boldsymbol{U}}_{M_T,S} = [\dot{U}_1 + \dot{U}_5(Z_1 + u\alpha_{31}) - \dot{U}_6(Y_1 + u\alpha_{21})]\boldsymbol{i}$$
$$+ [\dot{U}_2 + \dot{U}_6(X_1 + u\alpha_{11}) - U_4(Z_1 + u\alpha_{31})]\boldsymbol{j}$$
$$+ [\dot{U}_3 + \dot{U}_4(Y_1 + u\alpha_{21}) - \dot{U}_5(X_1 + u\alpha_{11})]\boldsymbol{k} \tag{4.16}$$

$$\boldsymbol{U}_{M_T,S} = A(u)\boldsymbol{e}_1 + B(u)\boldsymbol{e}_2 + C(u)\boldsymbol{e}_3 \tag{4.17}$$

where

$$\left.\begin{aligned} A(u) &= A1(u)\alpha_{11} + B1(u)\alpha_{21} + C1(u)\alpha_{31} \\ B(u) &= A1(u)\alpha_{12} + B1(u)\alpha_{22} + C1(u)\alpha_{32} \\ C(u) &= A1(u)\alpha_{13} + B1(u)\alpha_{23} + C1(u)\alpha_{33} \end{aligned}\right\} \tag{4.18}$$

$$\left.\begin{aligned} A1(u) &= U_1 + U_5(Z_1 + u\alpha_{31}) - U_6(Y_1 + u\alpha_{21}) \\ B1(u) &= U_2 + U_6(X_1 + u\alpha_{11}) - U_4(Z_1 + u\alpha_{31}) \\ C1(u) &= U_3 + U_4(Y_1 + u\alpha_{21}) - U_5(X_1 + u\alpha_{11}) \end{aligned}\right\} \tag{4.19}$$

Similarly,

$$\dot{\boldsymbol{U}}_{M_T,S} = \dot{A}(u)\boldsymbol{e}_1 + \dot{B}(u)\boldsymbol{e}_2 + \dot{C}(u)\boldsymbol{e}_3 \tag{4.20}$$

where

$$\left.\begin{aligned} \dot{A}(u) &= \dot{A}1(u)\alpha_{11} + \dot{B}1(u)\alpha_{21} + \dot{C}1(u)\alpha_{31} \\ \dot{B}(u) &= \dot{A}1(u)\alpha_{12} + \dot{B}1(u)\alpha_{22} + \dot{C}1(u)\alpha_{32} \\ \dot{C}(u) &= \dot{A}1(u)\alpha_{13} + \dot{B}1(u)\alpha_{23} + \dot{C}1(u)\alpha_{33} \end{aligned}\right\} \tag{4.21}$$

and

$$\left.\begin{aligned} \dot{A}1(u) &= \dot{U}_1 + \dot{U}_5(Z_1 + u\alpha_{31}) - \dot{U}_6(Y_1 + u\alpha_{21}) \\ \dot{B}1(u) &= \dot{U}_2 + \dot{U}_6(X_1 + u\alpha_{11}) - \dot{U}_4(Z_1 + u\alpha_{31}) \\ \dot{C}1(u) &= \dot{U}_3 + \dot{U}_4(Y_1 + u\alpha_{21}) - \dot{U}_5(X_1 + u\alpha_{11}) \end{aligned}\right\} \tag{4.22}$$

The total hydrodynamic forces and moments on an individual member can be written in this member's reference system as follows:

$$\begin{aligned} \boldsymbol{F}_{i,(m)} = \{ & [a_{11}\dot{A}(u) + b_{11}A(u)|A(u)|]_{u=0} \\ & + [a_{11}\dot{A}(u) + b_{11}A(u)|A(u)|]_{u=l} \}\boldsymbol{e}_1 \\ & + \int_{u=0}^{l} [a_{22}\dot{B}(u) + b_{22}B(u)|B(u)|]du\,\boldsymbol{e}_2 \\ & + \int_{u=0}^{l} [a_{33}\dot{C}(u) + b_{33}C(u)|C(u)|]du\,\boldsymbol{e}_3 \end{aligned} \tag{4.23}$$

where

$$\left.\begin{aligned} a_{11} &= \tfrac{4}{3}\rho R^3 & b_{11} &= \tfrac{1}{2}\rho C_D A_P \\ a_{22} &= 1 & b_{22} &= \tfrac{1}{2}\rho C_D A_P \\ a_{33} &= 1 & b_{33} &= \tfrac{1}{2}\rho C_D A_P \end{aligned}\right\} \tag{4.24}$$

a_{11}, a_{22}, a_{33}	Added mass coefficients in heave, surge and sway modes respectively
b_{11}, b_{22}, b_{33}	Damping force coefficients in heave, surge and sway modes respectively

where

ρ	Water density
C_D	Drag coefficient
A_P	Projection area of the member
R	Radius of the member
l	Member length

$$M_{i,(m)} = \int_{u=0}^{l} \{e_1 \wedge [(a_{22}\dot{B}(u) + b_{22}B(u)|B(u)|)e_2 + (a_{33}\dot{C}(u) + b_{33}C(u)|C(u)|)e_3]u\,du \tag{4.25}$$

The first component of the force vector given in Eq.(4.23) is to be determined according to the cylindrical member's ends exposed to wave loading, i.e. if the member is inter-costal this component will vanish.

The moment due to the hydrodynamic loading about the origin of the structure's reference system can be expressed as follows:

$$M_{i_S} = M_{i_M} + r \wedge F_{i_M} \tag{4.26}$$

The total hydrodynamic forces and moments are calculated to obtain the principal components as follows:

$$F = -(\underbrace{ai}_{surge} + \underbrace{bj}_{heave} + \underbrace{ck}_{sway}) \tag{4.27}$$

$$M = -(\underbrace{d\,i}_{roll} + \underbrace{e\,j}_{yaw} + \underbrace{f\,k}_{pitch}) \tag{4.28}$$

where

$$a = \sum_{i=1}^{m} [\alpha_{11} F1_{i,(m)} + \alpha_{12} F2_{i,(m)} + \alpha_{13} F3_{i,(m)}] \tag{4.29}$$

$$b = \sum_{i=1}^{m} [\alpha_{21} F1_{i,(m)} + \alpha_{22} F2_{i,(m)} + \alpha_{23} F3_{i,(m)}] \tag{4.30}$$

$$c = \sum_{i=1}^{m} [\alpha_{31} F1_{i,(m)} + \alpha_{32} F2_{i,(m)} + \alpha_{33} F3_{i,(m)}] \tag{4.31}$$

where

$$F1_{i,(m)} = [a_{11} \dot{A}(u) + b_{11} A(u) |A(u)|]_{u=0} + [a_{11} \dot{A}(u) + b_{11} A(u) |A(u)|]_{u=l} \tag{4.32}$$

$$F2_{i,(m)} = \int_{u=0}^{l} [a_{22} \dot{B}(u) + b_{22} B(u) |B(u)|] du \tag{4.33}$$

$$F3_{i,(m)} = \int_{u=0}^{l} [a_{33} \dot{C}(u) + b_{33} C(u) |C(u)|] du \tag{4.34}$$

Using Eqs.(4.25-26) the principal components of the hydrodynamic moment vector can be written as follows:

$$M_{i,(m)} = \int_{u=0}^{l} [\underbrace{(a_{22} \dot{B}(u) + b_{22} B(u) |B(u)|) e_3}_{M2_{i,(m)}} - \underbrace{(a_{33} \dot{C}(u) + b_{33} C(u) |C(u)|) e_2}_{M3_{i,(m)}}] u\, du \tag{4.35}$$

$$d = \sum_{i=1}^{m} [\alpha_{13} M_{2_{i,(m)}} - \alpha_{12} M_{3_{i,(m)}} + Y_1 c'_i - Z_1 b'_i] \tag{4.36}$$

$$e = \sum_{i=1}^{m} [\alpha_{23} M_{2_{i,(m)}} - \alpha_{22} M_{3_{i,(m)}} + Z_1 a'_i - X_1 c'_i] \tag{4.37}$$

$$f = \sum_{i=1}^{m} [\alpha_{33} M_{2_{i,(m)}} - \alpha_{32} M_{3_{i,(m)}} + X_1 b'_i - Y_1 a'_i] \tag{4.38}$$

where

$$a'_i = \alpha_{11} F_{1_{i,(m)}} + \alpha_{12} F_{2_{i,(m)}} + \alpha_{13} F_{3_{i,(m)}} \tag{4.39}$$

$$b'_i = \alpha_{21} F_{1_{i,(m)}} + \alpha_{22} F_{2_{i,(m)}} + \alpha_{23} F_{3_{i,(m)}} \tag{4.40}$$

$$c'_i = \alpha_{31} F_{1_{i,(m)}} + \alpha_{32} F_{2_{i,(m)}} + \alpha_{33} F_{3_{i,(m)}} \tag{4.41}$$

$$M_{2_{i,(m)}} = \int_{u=0}^{l} (a_{22} B'(u) + b_{22} B(u)) u \, du \tag{4.42}$$

$$M_{3_{i,(m)}} = \int_{u=0}^{l} (a_{33} C'(u) + b_{33} C(u)) u \, du \tag{4.43}$$

4.3 CALCULATION OF NON-LINEAR RESTORING FORCES AND MOMENTS

In this section, the restoring forces and moments which are introduced by an excursion of the platform from its equilibrium position are discussed. The main components of restoring forces can be classified as buoyancy forces due to change in the structure's underwater geometry and mooring forces due to the weight of its mooring lines. In addition to these main components, restoring force can also be generated by

dynamic positioning systems.

In the following, only restoring forces due to hydrostatic and mooring effects will be discussed only.

For floating structures, the hydrostatic restoring forces and moments can be related to the translational and/or rotational displacements with the following equation by making use of standard naval architectural formulae (see Rawson and Tupper (1968)).

$$\sum_{k=1}^{6} (K_{jk}(\aleph) + R_{jk}(\aleph))x_k = F_{j_{HYD}} \qquad j = 1, 2,.., 6 \tag{4.44}$$

where

$K_{jk}(\aleph)$: Mooring stiffness coefficient

$R_{jk}(\aleph)$: Hydrostatic Restoring coefficient

$F_{j_{HYD}}$: Total restoring force

$R_{jk}(\aleph)$ can be given in the following equations:

$$\left.\begin{aligned} R_{jk}(\aleph) &= \rho\ g\ A_{WP}(\aleph) && j = k = 3 \\ R_{jk}(\aleph) &= \rho\ g \nabla\ (t)GZ_T(\aleph) && j = k = 4 \\ R_{jk}(\aleph) &= \rho\ g \nabla\ (t)GZ_L(\aleph) && j = k = 6 \end{aligned}\right\} \tag{4.45}$$

where

A_{WP} Total water plane area of surface piercing members

∇ Displacement of the floating structure

$GZ_T(\aleph)$, $GZ_L(\aleph)$ Transverse and longitudinal righting lever respectively

The calculation procedure for restoring forces due to heave, roll and pitch motions and a flow chart of computer subroutines to calculate these forces are given in

Appendix C. The calculation of mooring forces for surge, sway and yaw motions is presented in Appendix B.

The non-linear stiffness characteristics are taken into account by calculating the $GZ(\aleph)$ value corresponding to an instantaneous displacement and the heel or list angle at every time step from a data block generated from the cross curves of stability. The details of the program for the calculation of stability curves and the interpolation and extrapolation programs are explained in Appendix C. The non-linear restoring moment can be given in the following form for roll and pitch motions.

$$F_R = \rho\ g\ GZ(\aleph)\nabla(t) \tag{4.46}$$

where

ρ	Water density
g	Gravitational constant
$GZ(\aleph)$	Instantaneous righting moment lever
$\nabla(t)$	Instantaneous displacement of the structure.

REST and PREST are the subroutines which calculate the non-linear restoring moment for roll and pitch motions respectively by using the $GZ(\aleph)$ value calculated by subroutines SINT and PSINT.

The non-linear heave restoring force is calculated in subroutine HSTIFF. The heave restoring force formulation was carried out taking into account the pitch and roll motions in calculating the water plane areas of the columns. Heave restoring force is formulated as follows:

$$F_H = \rho\ g\ A_{WP} X_2 \tag{4.47}$$

where

$$A_{WP} = \frac{1}{\cos X_4 \cos X_6} \sum_{i=1}^{m} \pi\ R_{i_s}^2$$

where

R_{i_S} Radius of surface piercing members

4.4 CALCULATION OF BODY FORCES

The inertia forces and moments defined from Newton's second law as the multiplication of actual mass of a cylinder element $\rho_M \, dV$ and the absolute body acceleration of the structure can be calculated as follows (see Fig.4.2.):

$$\boldsymbol{F} = M \dot{\boldsymbol{U}}_G \tag{4.48}$$

$$\boldsymbol{M} = \rho_M \iiint_V \boldsymbol{r}_A \wedge \dot{\boldsymbol{U}}_i \, dV \tag{4.49}$$

where

M Total mass of the floating structure

$\dot{\boldsymbol{U}}_G$ Acceleration vector at the gravity centre of the platform

$\dot{\boldsymbol{U}}_i$ Acceleration vector at the centre of the mass element i

$\boldsymbol{r}_A$ $= \boldsymbol{r}_G + \boldsymbol{r}_i$

$\boldsymbol{r}_G$ Position vector of the centre of rotation from the centre of gravity

$\boldsymbol{r}_i$ Position vector of the mass element i from the centre of rotation

ρ_M Mass density

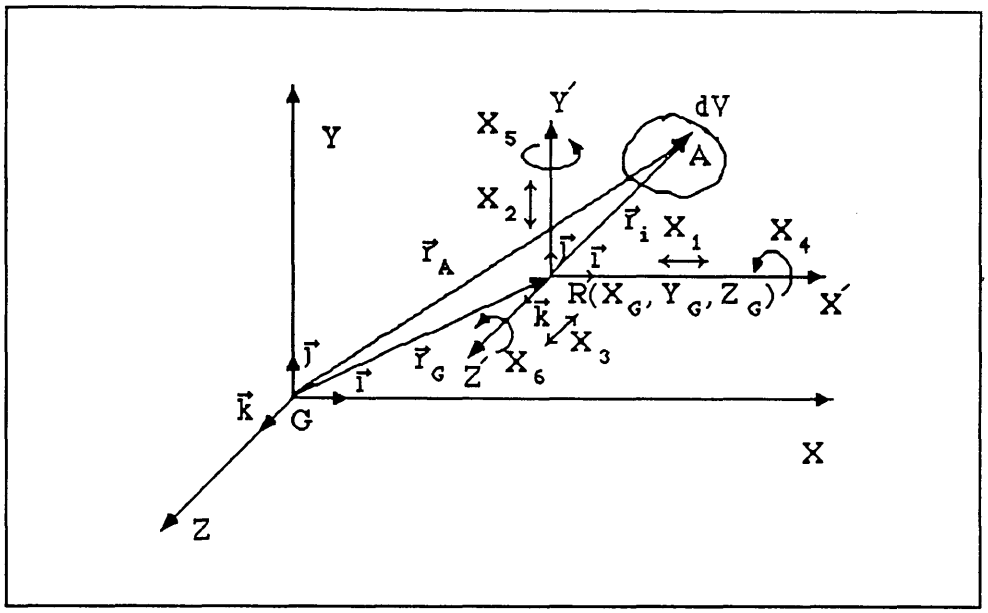

Fig.4.2 Co-ordinate systems used in inertia force calculations

The total force vector can be calculated in terms of translational and rotational acceleration and the total mass as follows.

$$\dot{U}_G = \dot{U}_{S_T} + \dot{U}_{S_R} \wedge r_G \tag{4.50}$$

where

$$\dot{U}_{S_T} = \dot{U}_1 i + \dot{U}_2 j + \dot{U}_3 k \tag{4.51}$$

$$\dot{U}_{S_R} = \dot{U}_4 i + \dot{U}_5 j + \dot{U}_6 k \tag{4.52}$$

$$r_G = X_G\, i + Y_G\, j + Z_G\, k \tag{4.53}$$

If Eq.(4.50) is substituted in Eq.(4.48) the total force vector becomes:

$$F = M\,(\dot{U}_1 + \dot{U}_5 Z_G - \dot{U}_6 Y_G)\,i$$

$$+ M\,(\dot{U}_2 + \dot{U}_6 X_G - \dot{U}_4 Z_G)\,j$$

$$+ M\,(\dot{U}_3 + \dot{U}_4 Y_G - \dot{U}_5 X_G)\,k \tag{4.54}$$

If we replace r_A with $r_G + r_i$ and $\dot{U}_i$ with $U_{S_T} + \dot{U}_{S_R} \wedge r_i$ in Eq.(4.49), the following equation is obtained to calculate moments due to the structure's rigid body acceleration:

$$M = \rho \iiint_V \{[- Z_G \dot{U}_2 + Y_G \dot{U}_3 + \dot{U}_4 (Y_i^2 + Z_i^2) - X_i Y_i \dot{U}_5 - X_i Z_i \dot{U}_6]\,i$$

$$+ [Z_G \dot{U}_1 - X_G \dot{U}_3 - X_i Y_i \dot{U}_4 + \dot{U}_5 (X_i^2 + Z_i^2) - Y_i Z_i \dot{U}_6]\,j$$

$$+ [- Y_G \dot{U}_1 + X_G \dot{U}_2 - X_i Z_i \dot{U}_4 - Y_i Z_i \dot{U}_5 + \dot{U}_6 (X_i^2 + Y_i^2)]\,k \}\,dV \tag{4.55}$$

The basic definitions to find the mass and mass moments of inertia can be written as follows:

$$M = \rho_M \iiint_V dV \tag{4.56}$$

$$I_{XX} = \rho_M \iiint_V (Y_i^2 + Z_i^2)dV \tag{4.57}$$

$$I_{YY} = \rho_M \iiint_V (X_i^2 + Z_i^2)dV \tag{4.58}$$

$$I_{ZZ} = \rho_M \iiint_V (X_i^2 + Y_i^2)dV \tag{4.59}$$

$$I_{XY} = I_{YX} = - \rho_M \iiint_V X_i Y_i\,dV \tag{4.60}$$

$$I_{XZ} = I_{ZX} = -\rho_M \iiint_V X_i \, Z_i \, dV \tag{4.61}$$

$$I_{YZ} = I_{ZY} = -\rho_M \iiint_V Y_i \, Z_i \, dV \tag{4.62}$$

Eqs.(4.54-55) can be summarised with the following matrix equation using Eqs.(4.56-62):

$$\begin{Bmatrix} F_1 \\ F_2 \\ F_3 \\ F_4 \\ F_5 \\ F_6 \end{Bmatrix} = \begin{bmatrix} M & 0 & 0 & 0 & MZ_G & -MY_G \\ 0 & M & 0 & -MZ_G & 0 & MX_G \\ 0 & 0 & M & MY_G & -MX_G & 0 \\ 0 & -MZ_G & MY_G & I_{XX} & I_{XY} & I_{XZ} \\ MZ_G & 0 & -MX_G & I_{YX} & I_{YY} & I_{YZ} \\ -MY_G & MX_G & 0 & I_{ZX} & I_{ZY} & I_{ZZ} \end{bmatrix} \begin{Bmatrix} \dot{U}_1 \\ \dot{U}_2 \\ \dot{U}_3 \\ \dot{U}_4 \\ \dot{U}_5 \\ \dot{U}_6 \end{Bmatrix} \tag{4.63}$$

For structures having cylindrical members, the mass moment of inertia values can be predicted for each member. It will be assumed that the mass of each volume element can be concentrated at the centre of this volume. Since the diameter over length ratio is generally small this assumption may be acceptable and can be formulated as follows:

$$\rho_M \iiint_V dV = \rho_M \int_{u=0}^{l} \pi \, R^2 du \tag{4.64}$$

Following the above statement the X_i, Y_i, Z_i co-ordinates can be written in the individual member's reference system as:

$$\left.\begin{aligned} X_i &= u\,\alpha_{11} + X_1 \\ Y_i &= u\,\alpha_{21} + Y_1 \\ Z_i &= u\,\alpha_{31} + Z_1 \end{aligned}\right\} \tag{4.65}$$

If we substitute Eq.(4.65) into Eqs.(4.57-62) the following mass moment of inertia values are obtained for an individual member:

$$i_{XX_i} = m_i \left[\tfrac{1}{3} l^2 (\alpha_{21}^2 + \alpha_{31}^2) + l\,(Y_1 \alpha_{21} + Z_1 \alpha_{31}) + Y_1^2 + Z_1^2\right] \tag{4.66}$$

$$i_{YY_i} = m_i \left[\tfrac{1}{3} l^2 (\alpha_{11}^2 + \alpha_{31}^2) + l\,(X_1 \alpha_{11} + Z_1 \alpha_{31}) + X_1^2 + Z_1^2\right] \tag{4.67}$$

$$i_{ZZ_i} = m_i \left[\tfrac{1}{3} l^2 (\alpha_{11}^2 + \alpha_{21}^2) + l\,(X_1 \alpha_{11} + Y_1 \alpha_{21}) + X_1^2 + Y_1^2\right] \tag{4.68}$$

$$i_{XY_i} = m_i \left[\tfrac{1}{3} l^2 \alpha_{11} \alpha_{21} + \tfrac{l}{2} (Y_1 \alpha_{11} + X_1 \alpha_{21}) + X_1 Y_1\right] \tag{4.69}$$

$$i_{XZ_i} = m_i \left[\tfrac{1}{3} l^2 \alpha_{11} \alpha_{31} + \tfrac{l}{2} (Z_1 \alpha_{11} + X_1 \alpha_{31}) + X_1 Z_1\right] \tag{4.70}$$

$$i_{YZ_i} = m_i \left[\tfrac{1}{3} l^2 \alpha_{21} \alpha_{31} + \tfrac{l}{2} (Z_1 \alpha_{21} + Y_1 \alpha_{31}) + Y_1 Z_1\right] \tag{4.71}$$

The total moment of inertia of mass can be calculated by summing Eqs.(4.66-71) as follows:

$$I_{XX} = \sum_{i=1}^{m} i_{XX_i} \tag{4.72}$$

$$I_{YY} = \sum_{i=1}^{m} i_{YY_i} \tag{4.73}$$

$$I_{ZZ} = \sum_{i=1}^{m} i_{ZZ_i} \tag{4.74}$$

$$I_{XY} = \sum_{i=1}^{m} i_{XY_i} \tag{4.75}$$

$$I_{XZ} = \sum_{i=1}^{m} i_{XZ_i} \tag{4.76}$$

$$I_{YZ} = \sum_{i=1}^{m} i_{YZ_i} \tag{4.77}$$

4.5 SOLUTION OF NON-LINEAR MOTION EQUATIONS IN THE TIME-DOMAIN

In this section, a method to solve the motion equations which take into account the non-linearities in wave and motion induced forces is discussed.

The wave excitation, hydrodynamic, steady wind and current and restoring forces on the floating structure are calculated at each time step taking into account the exact instantaneous position of the floating structure in the waves.

The following non-linear differential equation system is solved to obtain the motion responses in six degrees of freedom.

$$[M + A]\{\ddot{\aleph}\} + [B]\{\dot{\aleph}\,|\dot{\aleph}|\} + [R + K]\{\aleph\} = \{F\} \tag{4.78}$$

where

$[M]$	Mass and mass moment of inertia matrix of the structure
$[A]$	Added mass and added mass moment of inertia matrix of the structure
$[B]$	Damping coefficient matrix
$[R]$	Hydrostatic restoring coefficient matrix
$[K]$	Mooring stiffness coefficient matrix
$\{F\}$	Total external force

$\{\ddot{X}\}, \{\dot{X}\}, \{X\}$ Acceleration, velocity and displacement vectors respectively in six degrees of freedom

$$\{X\} = \begin{Bmatrix} X_1 \\ X_2 \\ X_3 \\ X_4 \\ X_5 \\ X_6 \end{Bmatrix} \qquad \{\dot{X}\} = \begin{Bmatrix} \dot{X}_1 \\ \dot{X}_2 \\ \dot{X}_3 \\ \dot{X}_4 \\ \dot{X}_5 \\ \dot{X}_6 \end{Bmatrix} \qquad \{\ddot{X}\} = \begin{Bmatrix} \ddot{X}_1 \\ \ddot{X}_2 \\ \ddot{X}_3 \\ \ddot{X}_4 \\ \ddot{X}_5 \\ \ddot{X}_6 \end{Bmatrix} \tag{4.79}$$

This system of second order non-linear differential equations in six degrees of freedom is solved using a numerical step-by-step integration technique. The NAG Library Routines (1978) provide several different numerical methods for solving non-linear differential equations. In order to solve a non-linear second order (or higher order) ordinary differential equation system, a system of ordinary differential equations has to be written in first-order form as follows:

$$\begin{aligned} y_1' &= f_1(x, y_1, y_2, \ldots, y_N) \\ y_2' &= f_2(x, y_1, y_2, \ldots, y_N) \\ &\cdots\cdots\cdots \\ y_N' &= f_N(x, y_1, y_2, \ldots, y_N) \end{aligned} \tag{4.80}$$

The N dependent variables which are the solutions of the system of differential equations $y_1, y_2, \ldots, y_N$ are functions of the independent variable x. The above differential equations written in first-order form give the expressions for the first derivatives $y_i' = dy_i / dx$ in terms of an independent x and dependent variables $y_1, y_2, \ldots, y_N$. For a system of N first-order differential equations, N associated boundary conditions are required to obtain the solutions.

Using the general mathematical methodology given above, Eq.(4.78) can be written as a system of first order non-linear differential equations. Hence the number of equations is doubled. If one writes $\{\Re_1\} = \{\aleph\}$ and $\{\Re_2\} = \{\dot{\aleph}\}$, then Eq.(4.78) can be expressed in the form of a first order non-linear differential equation system:

$$\{\dot{\Re}_1\} = \{\Re_2\} \tag{4.81}$$

$$\{\dot{\Re}_2\} = \frac{1}{[M + A]}\left(\{F\} - [B]\{\Re_2|\Re_2|\} - [R + K]\{\Re_1\}\right) \tag{4.82}$$

Hence, a system of first order non-linear differential equations is obtained and the number of boundary conditions required in order to define the solution is equal to the number of equations in the system of first order non-linear differential equations. This is so called an initial value problem because these boundary conditions are specified values at certain points given below:

$$\left.\begin{aligned} \{\Re_1\} &= 0 \qquad at \quad t = 0 \\ \{\Re_2\} &= 0 \qquad at \quad t = 0 \end{aligned}\right\} \tag{4.83}$$

These conditions would enable the solution technique to integrate the equations numerically from the point t=0 to some specified end-point.

4.6 DEVELOPMENT OF THE TIME-DOMAIN SIMULATION

In linear theory, it is assumed that the motions of the platform are small and member configurations are symmetrical. Based on these assumptions, the motion equations can be written in terms of constant hydrodynamic and hydrostatic coefficients, and the wave excitation forces are calculated at the mean draft level of the vessel.

In order to simulate the damaged behaviour of a platform in extreme conditions, one has to consider that the mass of the platform will increase due to flooding. The hydrodynamic, hydrostatic and wave excitation forces will vary either linearly or non-linearly as the platform experiences large amplitude oscillations. Since all hydrodynamic and hydrostatic coefficients tend to be non-linear as well as time-dependant, it is almost impossible to find a closed-form solution. In order to avoid the risk of obtaining inaccurate results associated with a simplified non-linear mathematical model for which a closed form solution can be found, it becomes necessary to use a numerical technique based on the integration of differential equations in a step-wise manner as described in the previous section.

The non-linear large amplitude motion equations in six degrees of freedom as a function of time and position are given in the following to show the three stages of motion simulation of a semi-submersible platform:

1) When the platform is in intact condition:

$$[M + A]\{\ddot{\aleph}\} + [B]\{\dot{\aleph}\,|\dot{\aleph}|\} + [R + K]\{\aleph\} = \{F\} \tag{4.84}$$

2) When the platform is in progressive flooding condition:

$$[M(t) + A]\{\ddot{\aleph}\} + [B]\{\dot{\aleph}\,|\dot{\aleph}|\} + [R + K]\{\aleph\} = \{F\} \tag{4.85}$$

where

$$M(t) = M + R\,t \qquad \text{for } t_{SF} < t < t_{EF} \tag{4.86}$$

R flooding rate and is given in the following expression by Moncarz et al. (1985):

$$R = c\,A\,\sqrt{2\,g\,h} \tag{4.87}$$

where

c	Coefficient of contraction for flow through an opening
A	Contraction area
g	Acceleration of gravity
h	Average water head

3) When the platform is in the post-flooding condition:

$$[M_{PF} + A]\{\ddot{\aleph}\} + [B]\{\dot{\aleph}\,|\dot{\aleph}|\} + [R + K]\{\aleph\} = \{F\} \tag{4.88}$$

where

$$M_{PF} = M + R\,(t_{EF} - t_{SF}) \tag{4.89}$$

The non-linear motion equations given above are solved in the time-domain using the Runge-Kutta-Merson numerical integration technique. The right hand side of the equations is re-calculated at each time step following the procedure described in Chapter 3 as a function of both time and the structure's location with respect to the wave reference system. The non-linear stiffness co-efficients are obtained at each time step from pre-calculated stiffness values as a function of the instantaneous displacement and the position of the floating structure. A method to calculate A and B given in Eqs.(4.84)-(4.88) is described at the beginning of this chapter. This method is utilised in the numerical calculations.

In order to achieve fast steady-state solutions of the non-linear motion equations, and thereby to save computing time various types of ramp functions are introduced to the excitation forces. In the solution of the motion equations variable integration steps are selected to improve the accuracy of the solutions. The integration steps are varied automatically by the NAG routine for a fast stable convergence.

4.7 DEVELOPMENT STAGES FOR THE TIME-DOMAIN SIMULATION PROGRAMS

In this section a brief summary of the development stages for the time-domain motion simulation programs is given to highlight the problems such as slow convergence, large CPU time, etc. encountered during the study.

Development of the time domain simulation programs was started by solving a non-linear second order differential equation which represents uncoupled heave motions of the semi-submersible platform. Having obtained the heave displacements in the time-domain, the amplitudes of heave oscillations were verified with those obtained from the frequency-domain analysis (see Söylemez (1986)). In solving the heave motion equation, NAG routines based on the Runge-Kutta-Merson method were employed.

During the development of the time-domain programs for the simulation of large amplitude uncoupled roll motions, a large CPU time was required due to slow convergence of non-linear roll motion equations. In order to overcome this problem the following steps were taken: Firstly, different differential equation solvers within the NAG library were tried. This attempt did not yield any improvement on CPU time. Secondly, the parametric studies involving the variation of different damping co-efficients were tested. However, a typical computer run on VAX 11/730 for a converged solution required 1 hr 30 min 3.34 sec CPU time. Thirdly, it was decided to introduce ramp functions to the excitation moment. Two different types of ramp function i.e. sinusoidal and exponential were tested. It was found that the introduction of exponential ramp function yielded a significant reduction in CPU time. A typical CPU time required for the

solution of uncoupled roll motion equation reduced to 40.15 sec. Details of ramp functions are given in Section 4.8.3.

Having improved the computational time, the non-linear roll restoring co-efficient was included in the large amplitude roll equation and it was found that this increased the required CPU time by a factor of 2. At this stage the programs were transferred from VAX 11/730 to ICL 3980. The CPU time was reduced by a factor of about 7 when the programs were mounted and run on ICL 3980 for solving the motion equations representing a 3 degrees of freedom system (heave, roll and pitch). However, it was anticipated that solutions of the coupled motion equations to simulate large amplitude oscillations of an intact or a damaged platform would require a considerably faster computer for the efficient development of the time-domain simulation package. Fortunately, the arrival of an IBM 3090 computer at the University was very timely for the smooth progress of this study.

The remaining major development work was carried out on IBM 3090 utilising the vectorisation and optimisation features of the machine.

The following figures are given as a typical example to indicate the CPU time efficiency achieved when the IBM 3090 was used. For the same input conditions, coupled large amplitude motion simulations of the semi-submersible in three degrees of freedom required $2^1/_4$ hours CPU time on VAX 11/730 whereas they required about $1^1/_2$ minutes on IBM 3090. Morover this figure could further be improved with the introduction of new vectorised NAG routines. The CPU time required on IBM 3090 to simulate large amplitude non-linear motions of an intact and damaged platform in six degrees of freedom is about 4 minutes for a 120 second real time simulation on model scale which corresponds to 20 minutes in full scale.

Another important aspect in using the differential equation solvers in the NAG library is the correct choice of tolerance. Tolerance must be set to a positive value to control the error in the integration. The user of NAG routines is recommended to call the time-solver routine with more than one value of TOL and to compare the results obtained

to estimate their accuracy.

In order to decide on the tolerance range, a few tests were carried out. The highest tolerance range was taken as 10^{-3} which yielded converging solutions over a long period of simulation time whereas when the tolerance range was decreased to 10^{-6} it was found that convergence was quicker and therefore 10^{-6} was chosen which also gave appropriate simulation period for comparing the physical simulation with numerical ones.

4.8 BRIEF DESCRIPTION OF THE COMPUTER PROGRAM

In this section, a brief description of the computer program MOTION which was developed for the motion simulation of a semi-submersible in the time-domain is given. The program MOTION has twenty one subroutines which were written to implement different types of calculation required to simulate non-linear, large motions of a floating structure in intact and damaged conditions. A flow chart of the program MOTION is shown in Fig.4.3.

4.8.1 NON-LINEAR FORCING FUNCTION

The general method described in Chapter 3 to calculate wave loading on the circular cylindrical members of floating structures forms the basis for the subroutine FORCE. Three components of the wave exciting force are calculated on each member of the structure every time step by taking into account the position of each member and the instantaneous wave profile. In order to take into account the instantaneous position of the structure in the wave reference system subroutine BETDIR was written. This subroutine calculates the direction cosines which relate the co-ordinates defined in the wave reference system to those in the structure reference system. Subroutine DIRCOS was written to relate the co-ordinates defined in the member reference system to those in the structure reference system (see also Chapter 3).

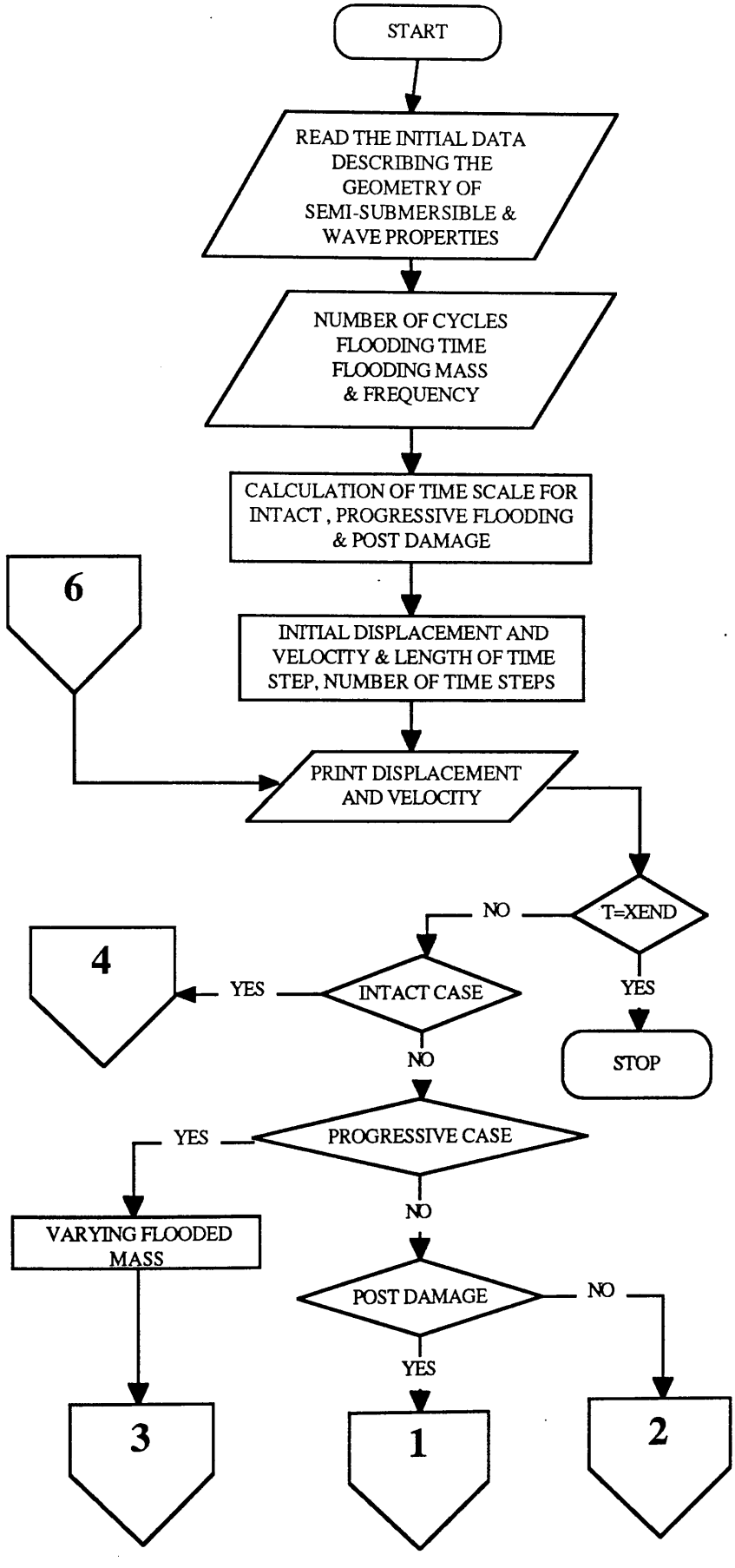

Fig.4.3 Flow -chart of program MOTION

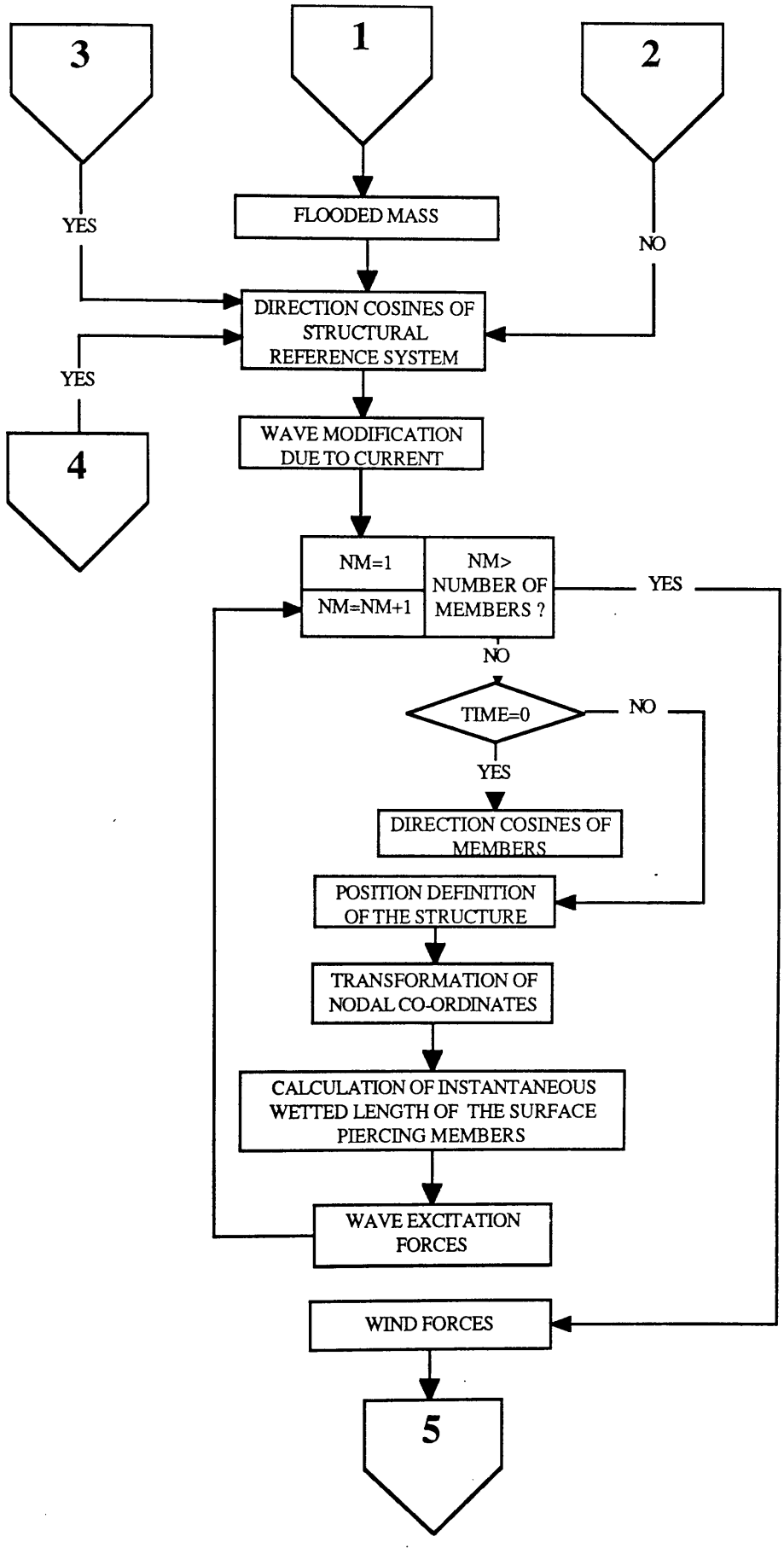

Fig.4.3 Flow -chart of program MOTION

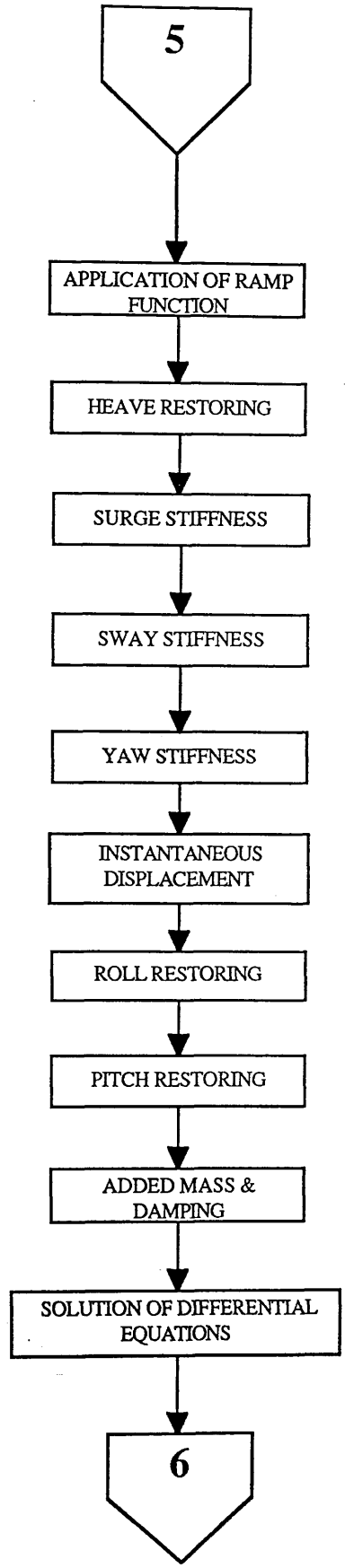

Fig.4.3 Flow -chart of program MOTION

4.8.2 POSITION DEFINITION OF THE STRUCTURE

In order to calculate the wetted length of surface piercing members by either assuming that the surface piercing members intersect with calm water or with waves, a number of subroutines were written. Subroutines POSW and TRANS calculate the co-ordinates of an intersecting point between a surface piercing member and water level by allowing rigid-body motions of the structure. The co-ordinates of the intersecting point between the surface piercing member and the water level together with the co-ordinates of the starting point of the member are used to determine the wetted length of the member. The wetted length which is calculated at each time step determines the integration limits during the calculation of wave forces and moments on surface piercing members.

Subroutine ITRW which is called by POSW was written to calculate the co-ordinates of the intersecting point berween the surface piercing member and the wave profile.

Derivation of the function to calculate the intersection point of a surface piercing member with a propagating wave profile is based on the assumption that the cylindrical member of the structure is represented as a straight line in space. The calculation of the intersection points of the straight line with a sinusoidal surface representing wave elevation is carried out in following (see Sommerville (1939)).

The Equation of a Straight Line

If let the straight line is allowed to pass through the point $A \equiv [x_1, y_1, z_1]$ and to have direction-cosines (or ratios) $[l, m, n]$, then if $P \equiv [x, y, z]$ is any point on the line, and $AP = r$, we have

$$\left.\begin{aligned} x &= x_1 + l\,r \\ y &= y_1 + m\,r \\ z &= z_1 + n\,r \end{aligned}\right\} \qquad (4.90)$$

Eliminating r, the following equation is obtained,

$$\frac{x - x_1}{l} = \frac{y - y_1}{m} = \frac{z - z_1}{n} = r \tag{4.91}$$

Eq.(4.91) is adopted as the standard form for the equations of a straight line. Eq.(4.90) is called the *freedom-equation* of the line in terms of the parameter r. $[x_1, y_1, z_1]$ which are the beginning co-ordinates of the surface piercing members. The co-ordinates of any point on the joint of $[x_1, y_1, z_1]$ and $[x_2, y_2, z_2]$ which are the end co-ordinates of the member can be written as follows:

$$\left.\begin{aligned} x &= x_1 + r\,(x_2 - x_1) \\ y &= y_1 + r\,(y_2 - y_1) \\ z &= z_1 + r\,(z_2 - z_1) \end{aligned}\right\} \tag{4.92}$$

These are the freedom equations in terms of the parameter t.

Intersection of a Column and Water Surface

Instantaneous water surface is defined as a function of y and t along x direction as it does not vary along the z axis.

$$y = a\cos(k\,x - \omega\,t) \tag{4.93}$$

Substituting for x, y, z in the Eq.(4.93) of the plane the following equation is obtained.

$$y_1 + m\,r - a\,\cos[k\,(x_1 + l\,r) - \omega\,t\,] = 0 \tag{4.94}$$

where

x_1, y_1	Beginning co-ordinates of the member
m, l	Direction cosines of the member
r	Wetted length
k	Wave number
ω	Wave frequency
t	Time

If r is obtained by iterating the above equation, the co-ordinates of the intersection point can be calculated. However, direction-cosines of the straight line are needed in order to start iteration. In order to calculate the direction-cosines the co-ordinates of two points (which are the beginning and the end co-ordinates of the member) on the straight line are provided by subroutine TRANS.

Eq.(4.94) is solved by the Newton-Raphson iteration method, thus the wetted length of the member is calculated taking into account the relative wave elevation at each time step.

4.8.3 RAMP FUNCTIONS

In order to avoid slowly decaying transient motions of the structure due to wave excitation forces an exponantial ramp function is used. A ramp function is multiplied with the external force for a certain period at the beginning of the simulation. By means of this ramp function, the external force is increased gradually for a certain period to avoid slowly decaying transient motions due to suddenly applied environmental forces. The application of a ramp function enables a quick convergance in the time-domain solution of motion equations.

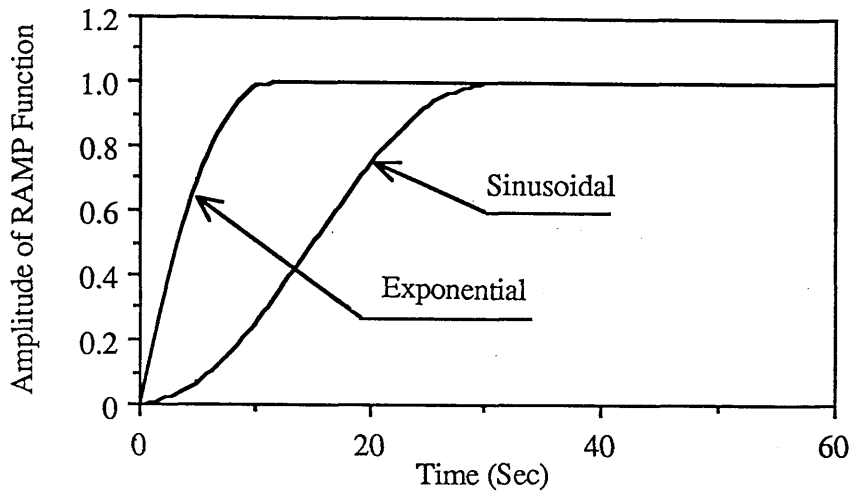

Fig.4.4 Sinusoidal and Exponential ramp functions

The ramp(slope) function can be any function which increase gradually and reaches 1 after a certain period. Two of the ramp functions which are shown in Fig.(4.4) are given in the following expressions:

Sinusoidal Ramp Function:

$$RAMP = \begin{cases} -\frac{1}{2}\cos(\frac{2\pi}{T})t + \frac{1}{2} & t \le \frac{T}{2} \\ 1 & t > \frac{T}{2} \end{cases} \tag{4.95}$$

This ramp function reaches 1 at the half period. However, this function can be set to reach at time segment to be 1. An exponential ramp function which is given in the following is more flexible than Eq.(4.95).

Exponential Ramp Function:

$$RAMP = 1 - e^{-at^2} \tag{4.96}$$

where

a was calculated in the following form so that e^{-at^2} approaches zero as t approaches t_{hend} .

$$a = \ln(1000)\frac{1}{t_{hend}^2} \tag{4.97}$$

where

$$t_{hend} = \frac{1}{n} t_{end} \tag{4.98}$$

where

t_{end}	End of simulation
n	An integer to divide t_{end}
t_{hend}	A certain beginning part of simulation in which the ramp function is applied

One important point in applying a ramp function to a numerical solution is that the derivative of the function should be zero at time $t=0$ and at the end of the application of the function in order to avoid any discontinuity in the function on which the ramp function is applied. Thus, numerical instability during a solution procedure is avoided.

The results of a sample run are shown in Figs.4.5-6 to demonstrate the effect of a ramp function on the numerical solution. Fig.4.5(a.b.c) and Fig.4.6(a-b) show the last 20 second time intervals of 1000, 1500, 3000, 4000 and 6000 cyle of roll simulation. As shown in these figures, if no ramp function is employed, the more the number of cyles for the simulation the better the convergence obtained for the solution. During the study, various ramp functions were applied in order to achieve quicker convergence of solutions of non-linear differential equations. The ramp functions used were various forms of sinusoidal and hyperbolic function. It was concluded the exponential function given in Eq.4.96) was the most effective one in yielding the quickest convergence. As can be seen

from Fig.4.6.c when the exponential function was applied to the roll motion equation. The steady solution was reached in 10 seconds.

Finally it should also be noted that when a ramp function is not applied to a function describing the wave excitation on a platform at the initial stages of simulation, the rigid body oscillations of the platform comprise slowly varying oscillations at the rigid-body natural frequencies and oscillations at the frequency of wave excitation. As the simulation proceeds the slowly varying oscillations disappear. This phenomenon is illustrated in Figs.4.7 and 4.8. Fig.4.8 was obtained by applying a Fast Fourier Transform to the time-series data shown in Fig.4.7.

It was also noted that increased damping in the transient region yields quick convergence in the solution of motion equations. However, the application of a ramp function yields a much faster convergence.

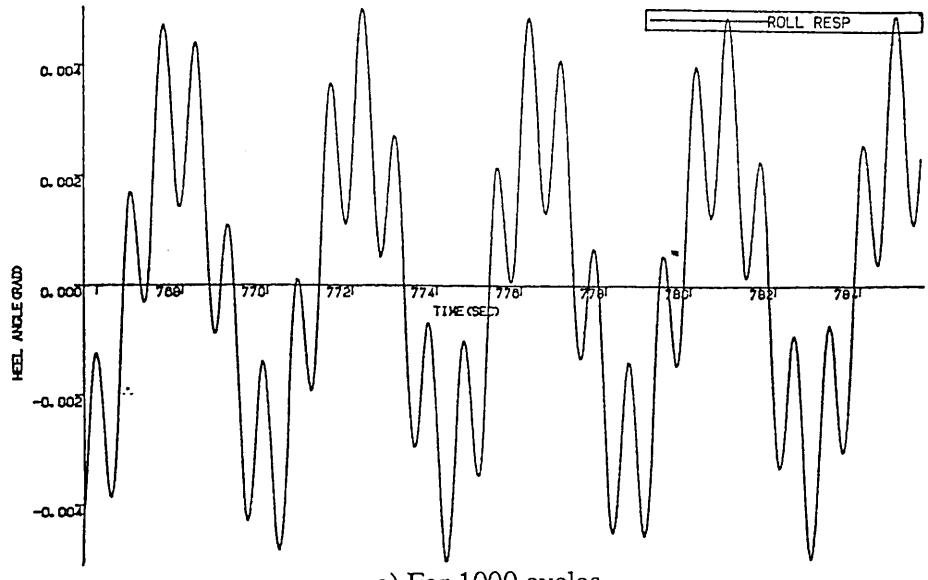

a) For 1000 cycles

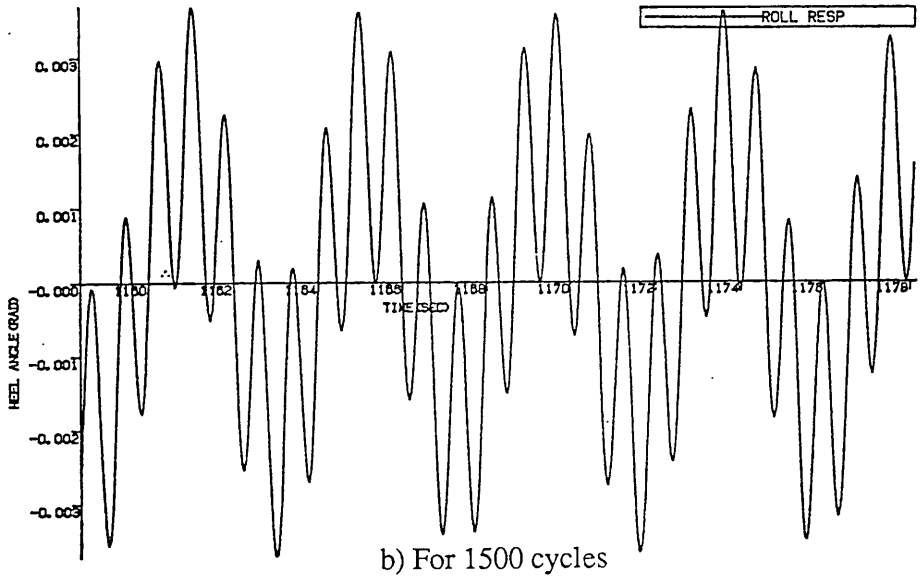

b) For 1500 cycles

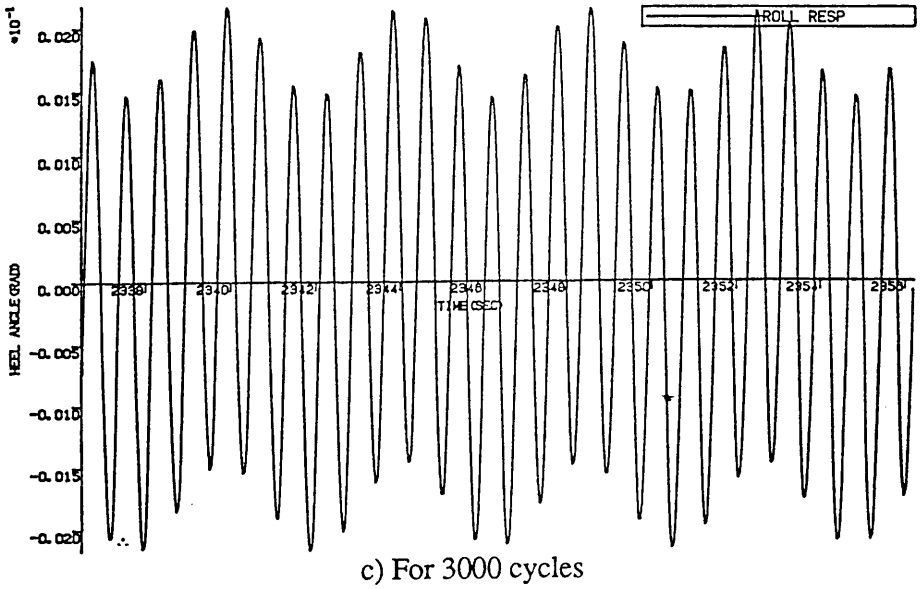

c) For 3000 cycles

Fig.4.5 Roll motion simulation for intact case, ω=8 rad/s
Wave Height=0.1 m

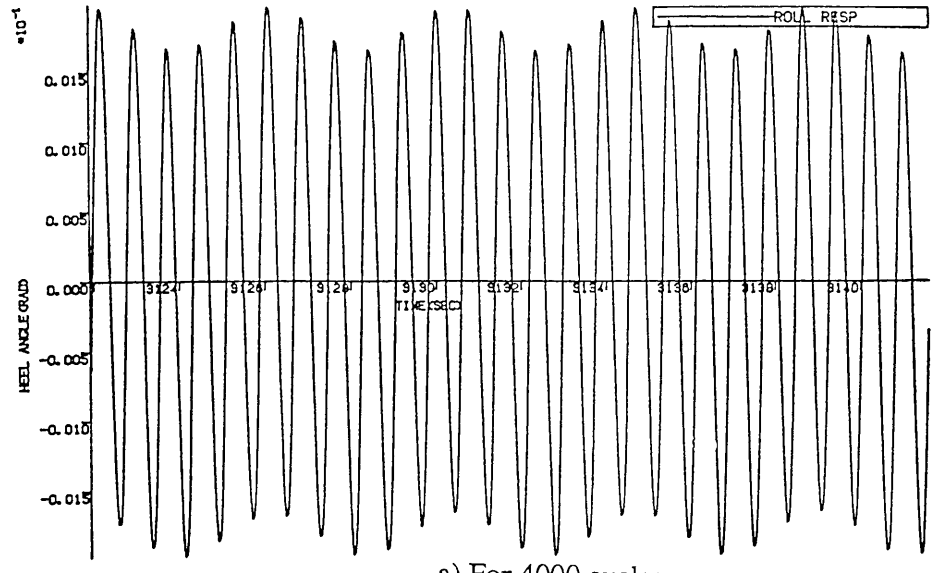

a) For 4000 cycles

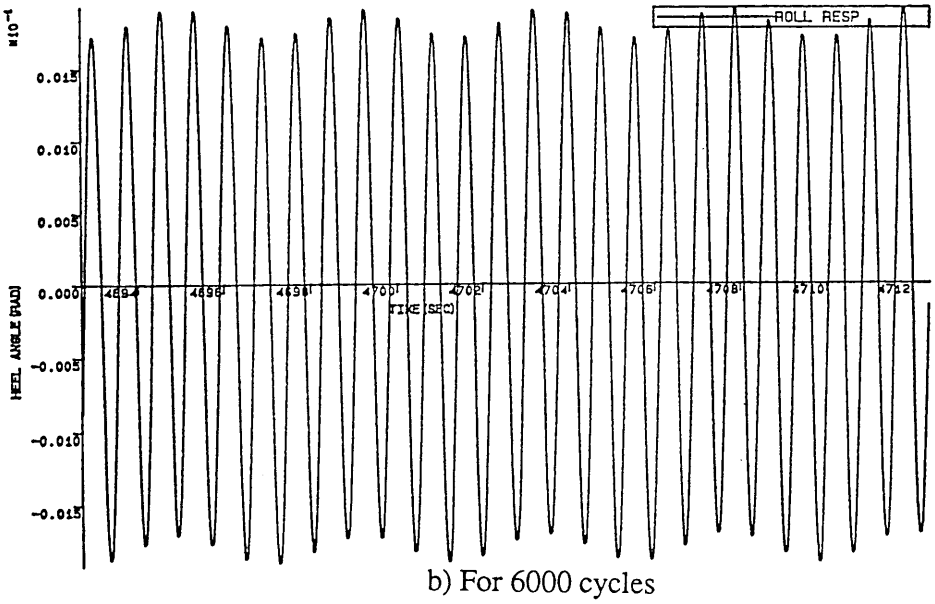

b) For 6000 cycles

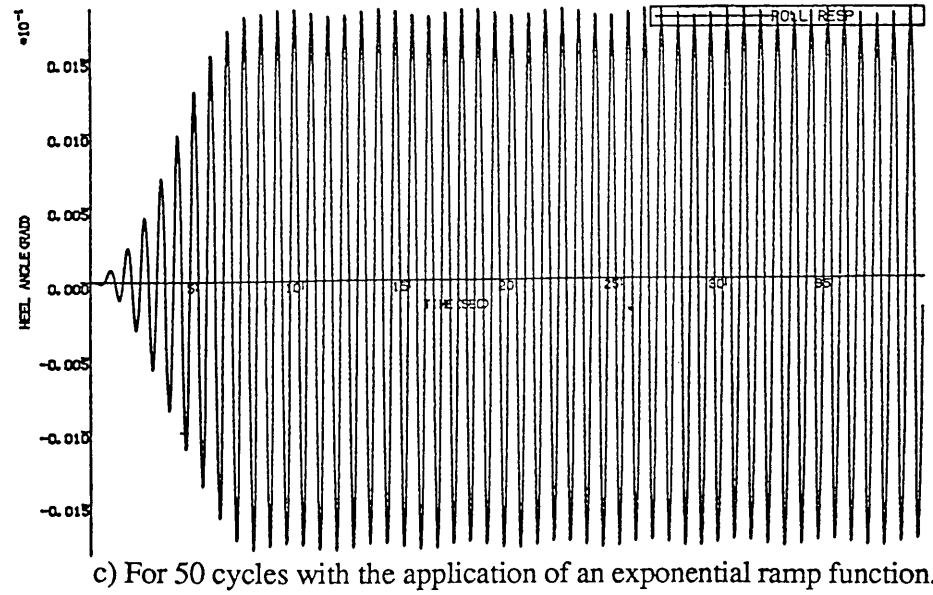

c) For 50 cycles with the application of an exponential ramp function.

Fig.4.6 Roll motion simulation for intact case, ω=8 rad/s
Wave Height=0.1 m

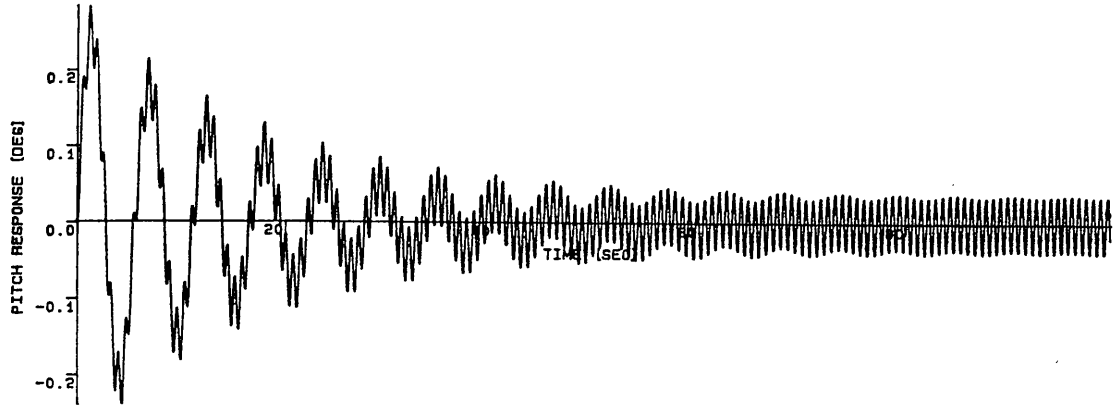

Fig.4.7 Time-domain history of roll motion simulation

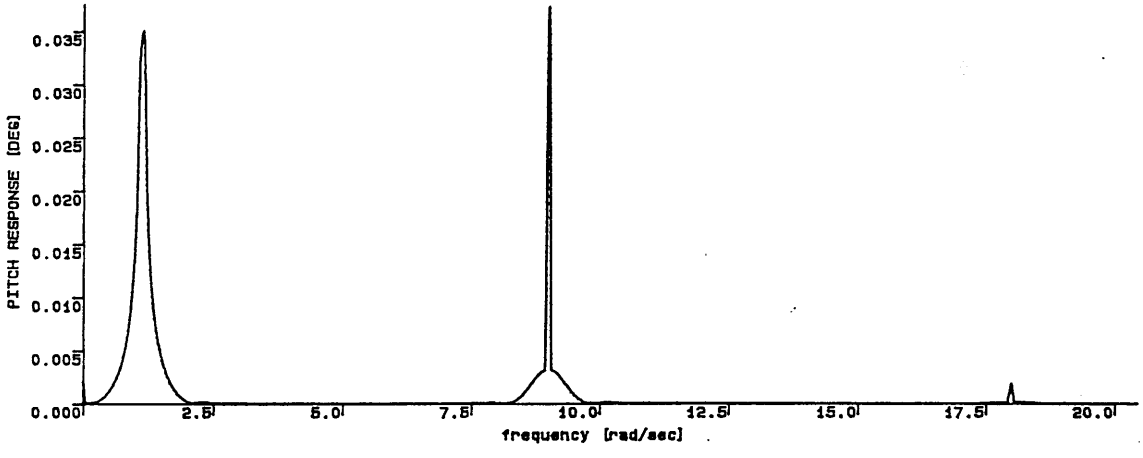

Fig.4.8 Spectral analysis of time-domain simulation for roll motion

CHAPTER 5

NUMERICAL AND PHYSICAL SIMULATION STUDIES

5.1 INTRODUCTION

This chapter presents the results of model tests carried out to measure the motions of the model platform under intact, progressive flooding and post flooding conditions and the results of numerical simulation studies representing the model test conditions.

There have been two main objectives in carrying out this test series:

1) To study the motions of the model semi-submersible in a range of wave frequencies and heights varying from 2.5 to 8.8 rad/s (0.3 to 1.05 rad/s in full scale) and 6.7 to 12.3 cm (4.69 m to 8.61 m in full scale) respectively during intact, progressive flooding and post flooding conditions.

2) To verify the computer generated simulations obtained by means of the method developed in the previous chapters with the experimental measurements.

A twin-hulled 1:70 scale semi-submersible model shown in Fig.2.1 was tested for one draught (36 cm), two heading angles (head and beam seas) and two different GMs (7.8 cm and 2.29 cm) in the 77 m x4.6 m x2.4 m towing tank of Glasgow University.

The results of the motion response analyses for six degrees of freedom and the wave elevation are given in the form of time histories at the end of this chapter.

Intact, progressive flooding and post-flooding conditions were simulated during each experiment. The progressive flooding condition was initiated by filling one or two of the inner columns (symmetrical or asymmetrical damage) on seaward side and a variety of flooding time and flooding mass (or the size of the compartment) were adopted in simulating the progressive flooding condition. About 110 individual experimental runs were carried out, including inclining tests and natural frequency tests to determine the dynamic particulars of the model. Tests were performed in order to measure heave, sway, surge, roll, pitch and yaw motions as well as the flooding mass versus flooding time.

5.2 NUMERICAL SIMULATION

As the second objective of the experimental study was to verify the theoretical formulation and the computer software developed, numerical simulations were carried out for the model test conditions.

The non-linear, large amplitude coupled motion equations introduced in Section 4.5 were applied to the semi-submersible geometry shown in Fig. 2.1. The results of surge, sway, heave, roll, pitch and yaw motion simulations in intact, progressive flooding and post-flooding conditions are presented in this chapter in order to make comparisons between experimental measurements and numerical simulations.

The initial conditions for each simulation run were set to zero for initial velocity and displacement of the model. The ramp function was applied to the external forces for one fifth of the total simulation time. This time-scale was long enough for the wave form to develop to its required amplitude at a point where the model semi-submersible was moored.

In simulating the test conditions, the flooding mass measured and the flooding time during experiments were used as input in the numerical motion simulation program.

In order to reduce the computation time, constant added mass and non-linear damping force for the entire structure rather than those for each segment of each member of the structure were taken into account in the motion equations.

5.3 PHYSICAL SIMULATION

5.3.1 DESCRIPTION OF THE MODEL

A twin hulled semi-submersible model was built to the scale of 1:70 in accordance with the drawings shown in Fig.2.1. The semi-submersible model consists of two circular pontoons each with four circular columns (see Figs.5.1-5.2). The reason for choosing this particular geometry for the semi-submersible model was because it was already available in the department's hydrodynamics laboratory.

5.3.2 MODEL PARTICULARS

The principal dimensions for the prototype and the model are given in Table 5.1.

The twin circular hulled semi-submersible model consists of members which are made of P.V.C., aluminium sheets and bolts. P.V.C. welding was the means of connecting the P.V.C. parts. Special ballast containers were placed in the corner columns to ballast the model to the desired draught level. These ballast containers could be moved vertically so as to adjust the centre of gravity of the model for the desired GMs. The ballast material was made of leadshot and arrangements were made so that any movement of the ballast due to model motion was prevented.

Harnesses were used as soft moorings in order to stop the model from drifting along the tank.

The mass distribution and geometrical properties of the model are given in Table 5.2a-2b. The mass moment of inertia of each member of the model is calculated in Table 5.2a-2b according to the formulation given in Section 4.4 for roll, pitch and yaw motions. The total mass moments of inertia of the semi-submersible are listed in Table 5–3.

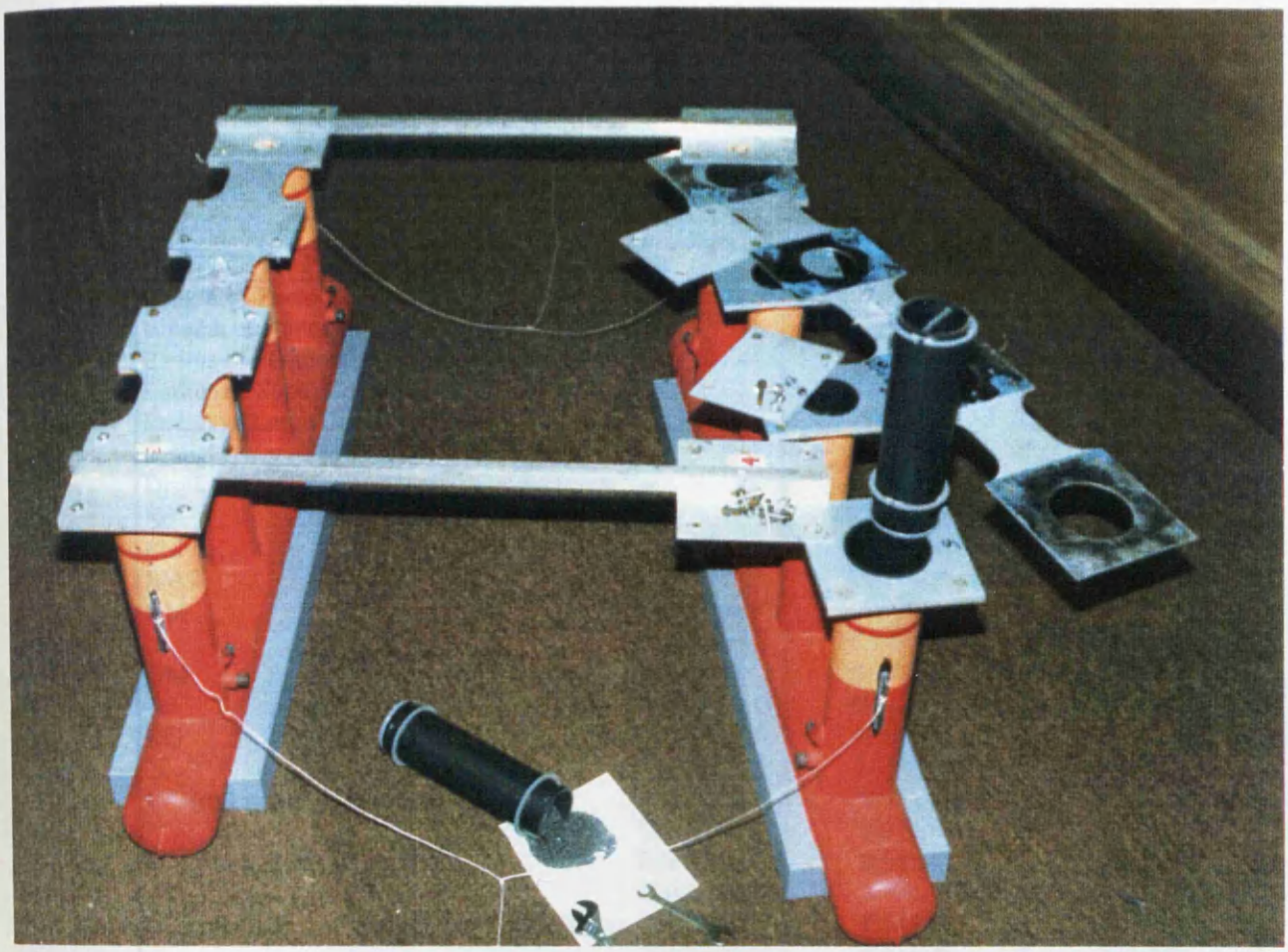

Fig.5.1 Disassembled view of the semi-submersible model

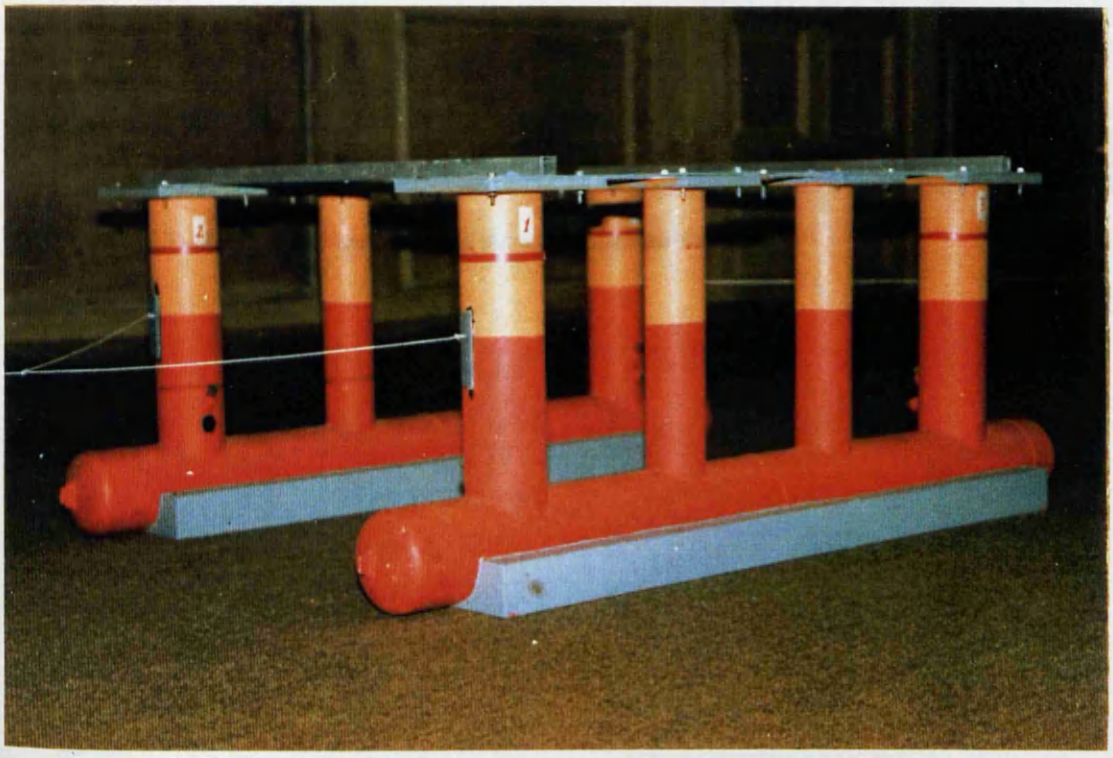

Fig.5.2 Side view of the semi-submersible model

Particulars of the Model		1/70 Model			Prototype		
Length of Pontoon		1.446 m			101.22 m		
Breadth of Pontoons		0.834 m			58.38 m		
Radius of Pontoon		0.070 m			4.90 m		
Radius of Small Column		0.0415 m			2.905 m		
Radius of Large Column		0.057 m			3.99 m		
Draught		0.360 m			25.20 m		
Displacement		58.400 kg			20031.2 t		
KB		0.1134 m			7.935 m		
BM		0.1867 m			13.069 m		
BM		0.1814 m			12.698 m		
GM	Test Series 1	0.0781 m			5.467 m		
	Test Series 2	0.0229 m			1.603 m		
GM	Test Series 1	0.0712 m			4.984 m		
	Test Series 2	0.0154 m			1.078 m		
KG	Test Series 1	0.2224 m			15.568 m		
	Test Series 2	0.2781 m			19.467 m		
k (roll radius of gyration)	Test Series 1	0.463 m			32.41 m		
	Test Series 2	0.454 m			31.78 m		
k (pitch radius of gyration)	Test Series 1	0.489 m			34.23 m		
	Test Series 2	0.481 m			33.67 m		
k (yaw radius of gyration from calculation)	Test Series 1	0.617 m			43.19 m		
	Test Series 2	0.614 m			42.98 m		
Natural (Period-Charac. Freq.-Radian Freq.)		S	Hz	rad/s	S	Hz	rad/s
Heave		2.44	0.41	2.57	20.45	0.049	0.31
Surge (calc.)		29.8	0.034	0.21	249.3	0.004	0.025
Sway (calc.)		36	0.028	0.174	301.2	0.003	0.021
Roll	Test Series 1	4.19	0.24	1.5	35.05	0.029	0.18
	Test Series 2	9	0.11	0.69	75.3	0.013	0.08
Pitch	Test Series 1	4.3	0.23	1.46	36.01	0.03	0.17
	Test Series 2	8.56	0.117	0.734	71.62	0.014	0.088
Yaw (calc.)		206	0.005	0.031	1723	6E-04	0.004

Table 5.1 Main particulars of the semi-submersible model

	Hull (2)	Small Columns (4)	Large Columns (4)	Ballast Cont. DS (2)	Ballast Cont. IS (2)	Alluminium Deck (2)	Ballast on Damage Side (2)
M	6.55	1.05	0.95	0.632	0.632	1.5	6.55
L	1.446	0.544	0.525	0.31	0.31	1.192	0.165
A11	0	0	0	0	0	0	0
A21	0	1	1	1	1	0	1
A31	-1	0	0	0	0	-1	0
X1/GM1	0.4175	0.4175	0.4175	-0.4175	0.4175	0.4175	-0.4175
Y1/GM1	-0.15	-0.198	-0.179	-0.162	-0.194	0.345	-0.162
Z1/GM1	0.723	0.165	0.495	0.495	0.495	0.596	0.495
X1/GM2	0.4175	0.4175	0.4175	-0.4175	0.4175	0.4175	-0.4175
Y1/GM2	-0.21	-0.258	-0.239	-0.105	-0.105	0.285	-0.105
Z1/GM2	0.723	0.165	0.495	0.495	0.495	0.596	0.495
IXX (PITCH) GM1	1.289	0.060	0.261	0.160	0.161	0.356	1.661
IXX (PITCH) GM2	1.430	0.055	0.255	0.161	0.161	0.299	1.623
IYY (YAW) GM1	2.283	0.212	0.398	0.265	0.265	0.439	2.747
IYY (YAW) GM2	2.283	0.212	0.398	0.265	0.265	0.439	2.747
IZZ (ROLL) GM1	1.289	0.215	0.194	0.115	0.116	0.440	1.198
IZZ (ROLL) GM2	1.431	0.209	0.188	0.117	0.117	0.383	1.160

Table 5-2a Calculation of the mass moment of inertia

	Ballast on Intact Side (2)	Alluminium Covers/L (4)	PVC Deck/L (4)	PVC Deck/S (6)	Alluminium Bar (2)	Water Containers (2)
M	6	0.354	0.525	0.43	0.806	0.62
L	0.182	0.203	0.204	0.152	0.835	0.546
A11	0	0	0	0	-1	0
A21	1	0	0	0	0	1
A31	0	-1	-1	-1	0	0
X1/GM1	0.4175	0.4175	0.4175	0.4175	0.4175	-0.4175
Y1/GM1	-0.194	0.347	0.34	0.34	0.36	-0.195
Z1/GM1	0.495	0.596	0.596	0.241	0.495	0.165
X1/GM2	0.4175	0.4175	0.4175	0.4175	0.4175	-0.4175
Y1/GM2	-0.105	0.287	0.28	0.28	0.3	-0.255
Z1/GM2	0.495	0.596	0.596	0.241	0.495	0.165
IXX (PITCH) GM1	1.550	0.130	0.191	0.062	0.302	0.036
IXX (PITCH) GM2	1.488	0.117	0.171	0.046	0.270	0.032
IYY (YAW) GM1	2.516	0.149	0.221	0.087	0.244	0.125
IYY (YAW) GM2	2.516	0.149	0.221	0.087	0.244	0.125
IZZ (ROLL) GM1	1.126	0.104	0.152	0.125	0.151	0.127
IZZ (ROLL) GM2	1.064	0.091	0.133	0.109	0.119	0.124

Table 5-2b Calculation of the mass moment of inertia

Figures in brackets indicate the number of members.

M	Mass of the member
L	Length of the member
A11, A21, A31	Direction cosines of members defined in Chapter 3.
X1,Y1,Z1	Beginning co-ordinates of members
Ixx	Rolling mass moment of inertia
Iyy	Yawing mass moment of inertia
Izz	Pitching mass moment of inertia

GM (cm)	KG (cm)	Ixx (kgm2)	Iyy (kgm2)	Izz (kgm2)
2.29	27.81	13.601	22.216	12.162
7.81	22.43	13.974	22.216	12.535

Table 5-3 Total mass moment of inertia for roll, yaw and pitch

5.3.3 INCLINATION TESTS

The basic purpose of the inclination tests was to identify the actual GM of the model before the each test series was carried out. The instrumentation of the inclination test was the same as for motion tests (see Section 5.3.5). An analysis method for these test series is given by Atlar (1986), therefore the method is not included in this section. Briefly, during the inclination test procedure, a group of known test weights was placed at the longitudinal or transverse symmetry of the deck in a row and symmetrical to both the longitudinal and transverse axes of the model for pitch and roll inclination tests respectively. Therefore, no heel or trim was recorded. The deflection corresponding to zero level due to the addition of test weights was marked on the chart recorder. Progressively the weights on the centre line were removed to an equal distance and the resultant heel or trim angle was recorded. Then the weights were returned to their original position at the centre. The same procedure was repeated by transferring the weights to the other side of the model. The results of these tests are given in Table 5.4a-4d.

i	w_i (grs)	d_i (cms)	Y_i (cms)	ϕ_i (deg)	m_i (gr*cm)	GM_i (cms)	Δ_c=58400 gr Σw_i=600 gr Δ =59000 grs
							GM=7.85 cm KB=11.60 cm
1	200	41.75	1.56	1.07	8350	7.63	BM=18.51 cm
2	400	41.75	3.04	2.09	16700	7.80	KG=22.26 cm
3	600	41.75	4.75	3.26	25050	7.46	KG_c=22.24 cm
4	200	-41.75	1.42	0.97	-8350	8.38	KB_c=11.34 cm
5	400	-41.75	3	2.06	-16700	7.91	BM_c=18.71 cm
6	600	-41.75	4.49	3.08	-25050	7.90	GM_c=7.81 cm

Table 5-4a Inclination test data for bigger GM in Roll

i	w_i (grs)	d_i (cms)	Y_i (cms)	ϕ_i (deg)	m_i (gr*cm)	GM_i (cms)	Δ_c=58400 gr Σw_i=600 gr Δ =59000 grs
							GM=6.72 cm KB=11.60 cm
1	200	49.5	2.07	1.40	9900	6.94	BM=18.03 cm
2	400	49.5	4.29	2.89	19800	6.67	KG=22.91 cm
3	600	49.5	6.3	4.24	29700	6.79	KG_c=22.43 cm
4	200	-49.5	2.18	1.47	9900	6.59	KB_c=11.34 cm
5	400	-49.5	4.16	2.80	19800	6.88	BM_c=18.21 cm
6	600	-49.5	6.64	4.47	29700	6.44	GM_c=7.12 cm

Table 5-4b Inclination test data for bigger GM in Pitch

i	w_i (grs)	d_i (cms)	Y_i (cms)	ϕ_i (deg)	m_i (gr*cm)	GM_i (cms)	Δ_c=58900 gr Σw_i=345 gr Δ =59245 grs
							GM=2.16 cm KB=11.70 cm
1	111	41.75	4.48	3.07	4634	1.46	BM=18.53 cm
2	234	41.75	6.03	4.13	9770	2.29	KG=28.07 cm
3	345	41.75	9.12	6.23	14404	2.23	KG_c=27.81 cm
-4	111	-41.75	2.6	1.78	4634	2.52	KB_c=11.55 cm
5	234	-41.75	6.29	4.31	9770	2.19	BM_c=18.55 cm
6	345	-41.75	8.93	6.10	14404	2.27	GM_c=2.29 cm

Table 5-4c Inclination test data for smaller GM in Roll

i	w_i (grs)	d_i (cms)	Y_i (cms)	ϕ_i (deg)	m_i (gr*cm)	GM_i (cms)	Δ_c=58900 gr Σw_i=345 gr Δ =59245 grs
							GM=1.20 cm KB=11.70 cm
1	111	49.5	6.9	4.64	5495	1.15	BM=18.10 cm
2	234	49.5	14.9	9.94	11583	1.12	KG=28.60 cm
3	345	49.5	17.58	11.69	17078	1.39	KG_c=28.22 cm
4	111	-49.5	7.68	5.16	5495	1.03	KB_c=11.55 cm
5	234	-49.5	14.21	9.49	11583	1.17	BM_c=18.21 cm
6	345	-49.5	17.97	11.94	17078	1.36	GM_c=1.54 cm

Table 5-4d Inclination test data for smaller GM in Pitch

i Number of shifts carried out.

w_i The sum of the weights transferred each time.

d_i Horizontal shift of the weights. A plus sign (+) indicates a shift from the centre line to leeward, a negative sign (-) indicates a shift from the centre line to seaward.

Y_i Total heel on the model

ϕ_i Total heel angle calculated by:

$$\phi_i = \arctan\ (Y_i / l)$$

where l is the distance between the vertical axes of the transducers and its value is 83.5 cm for roll and 99 cm for pitch tests

m_i static moments of the test weights calculated by:

$$m_i = w_i\, d_i$$

GM_i Metacentric height, which includes the effect of test weights, after each shift calculated by:

$$GM_i = m_i / (\Delta + w_i) \tan\ \phi_i$$

where Δ is model displacement

GM Mean metacentric height calculated by:

$$GM = \sum_{i=1}^{N} GM_i / N$$

where GM includes the effect of test weights which should be corrected to have the model's actual GM.

Subscript c indicates the actual values of the geometrical properties.

5.3.4 NATURAL PERIOD TEST

Free motion tests were carried out in order to measure the natural heave, roll and pitch periods of the model. The yaw period was not measured because the model was not moored by catenary moorings. However, the calculated value of the yaw period is given in Table 5.1.

The model was pushed down symmetrically at a certain draught and then released to perform the free oscillations. Therefore, the heave free oscillations were recorded on the chart recorder. The natural heave period was determined by taking the average period over a number of cycles.

For the natural roll and pitch periods, the model was heeled or listed to one side symmetrically by applying a moment and then released to perform free oscillations in roll or pitch mode. Recordings were taken as for the free heave oscillation test. The same calculation method was applied to determine the natural periods of roll and pitch as explained for heave.

The measured and calculated natural periods and frequencies for each mode are presented in Table 5.1. Figs.5.3-5 show the recordings of natural pitch period test, the numerical simulation of free pitch oscillation test and the results of FFT analysis of the numerical simulation in order to obtain the natural pitch frequency. The natural pitch frequency obtained from the model test is 1.46 rad/s whereas it was calculated by FFT analysis of numerical simulation as 1.2 rad/s.

5.3.5 INSTRUMENTATION FOR MOTION RESPONSE EXPERIMENTS

The instrumentation was organised so that the amplitudes of the regular wave trains, heave, surge, sway, roll, pitch and yaw motions of the model and also the amount of flooding water could be measured. Tests were carried out for two different GMs. The model was moored beam and head onto waves on the centre line of the tank. The mooring lines were attached at the level of the CG of the model and to the walls of the tank in order to give a soft spring effect (see Fig.5.6).

Regular waves were created by a plunger type wave-maker driven by an electronically controlled hydraulic pump.

Three resistance type wave probes were installed across the tank width. These probes induce electrical signals whose strength is changed by the varying wave height. These electrical signals were amplified and recorded by the chart recorder and on the computer as well.

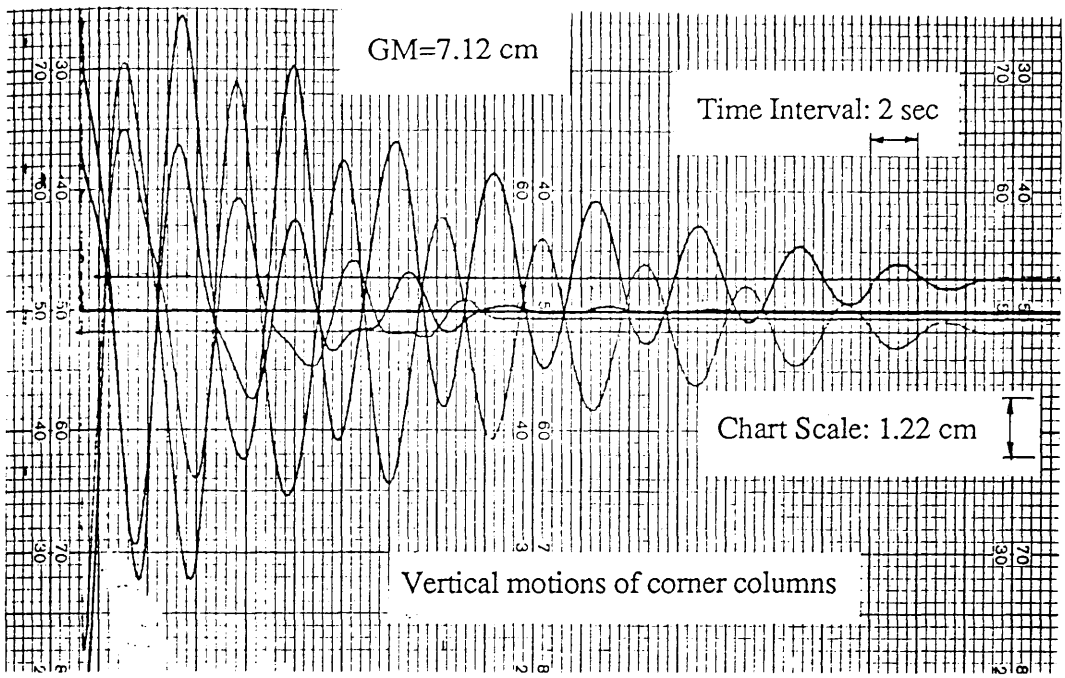

Fig.5.3 Chart records for the natural pitch period test

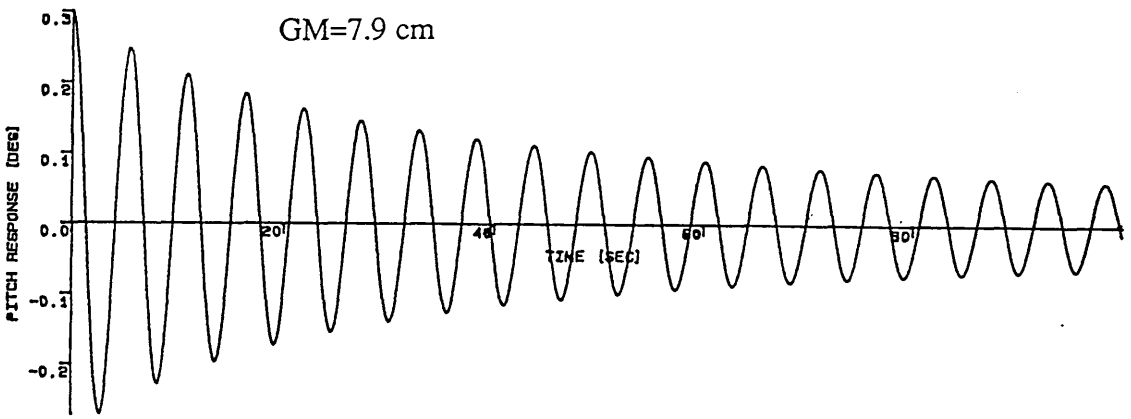

Fig.5.4 Numerical simulation of free pitch oscillation test

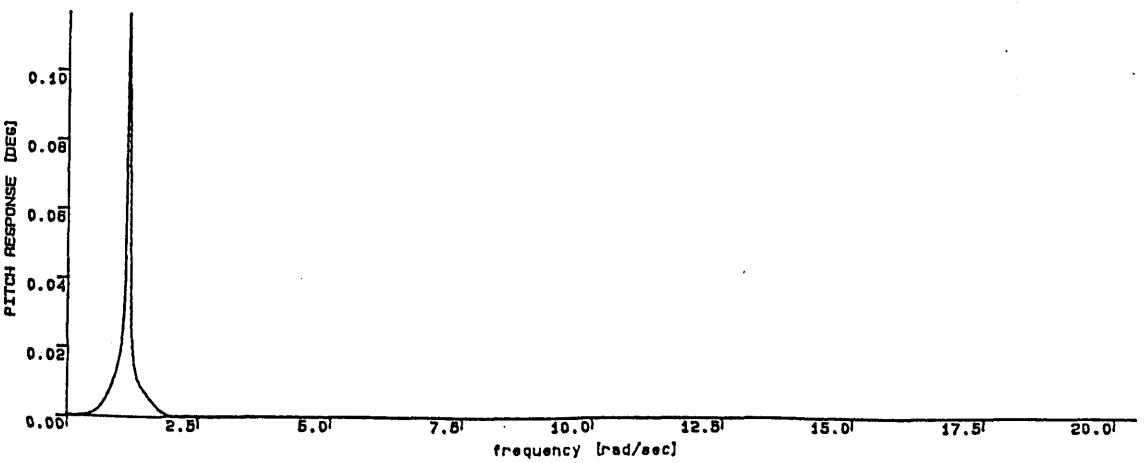

Fig.5.5 FFT analysis of numerical simulation of free pitch oscillation test

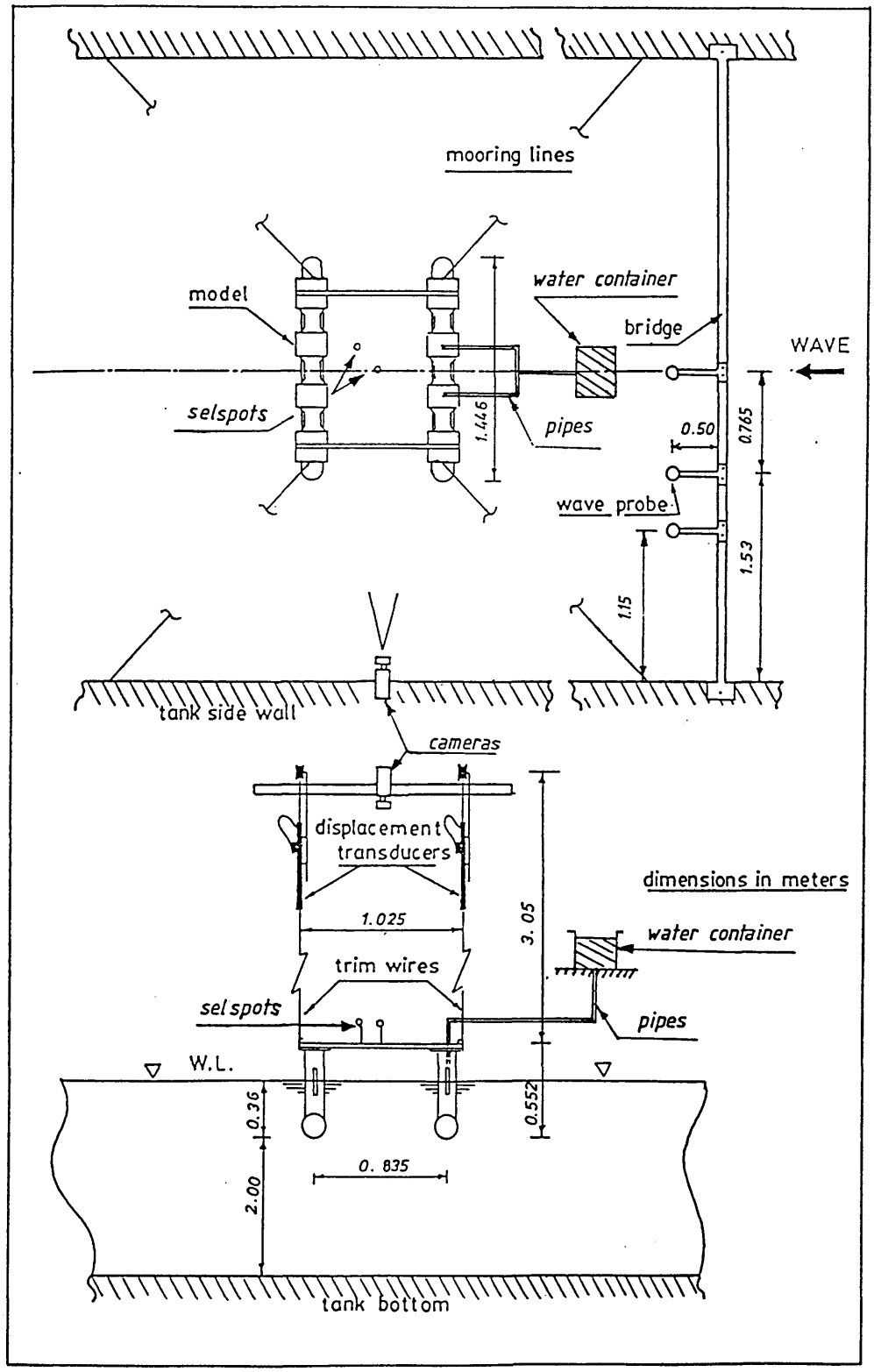

Fig.5.6 Experimental setup for the inclining test and the motion test

The heave, roll and pitch motions of the model platform were recorded with two pairs of gravity type Linear Vertical Displacement Transducers (LVDT). They were connected to a sub-carriage and attached to the deck of the model with piano wires suspended over a pair of pulleys. The weight of the LVDTs were balanced in order to avoid any possible acceleration being induced on the transducers during the motion of the model.

Electronic signals were sent to the chart recorder via an amplifier to record the vertical displacements of LVDTs versus real time.

The surge, sway and yaw motions of the model were recorded with two Light Emitting Diodes (LEDs or selspots) and two cameras. The displacements of LEDs were also recorded on the pen recorder chart. Program DATAGRAPHMOD was written to analyse the experimental data stored in digital form on the computer the experimental data were analysed and converted to real physical magnitudes.

In order to flood one or two of the inner columns, a water container was placed on the carriage. Fig.5.7 shows the set up of the water container and the pipe connections and stop valves which were used to flood the compartments through the pipes. Either or both of the two inner columns on the seaward side were flooded in order to simulate symmetrical or asymmetrical damage conditions. Flooded compartments were emptied by sucking the water from the compartments using a water pump.

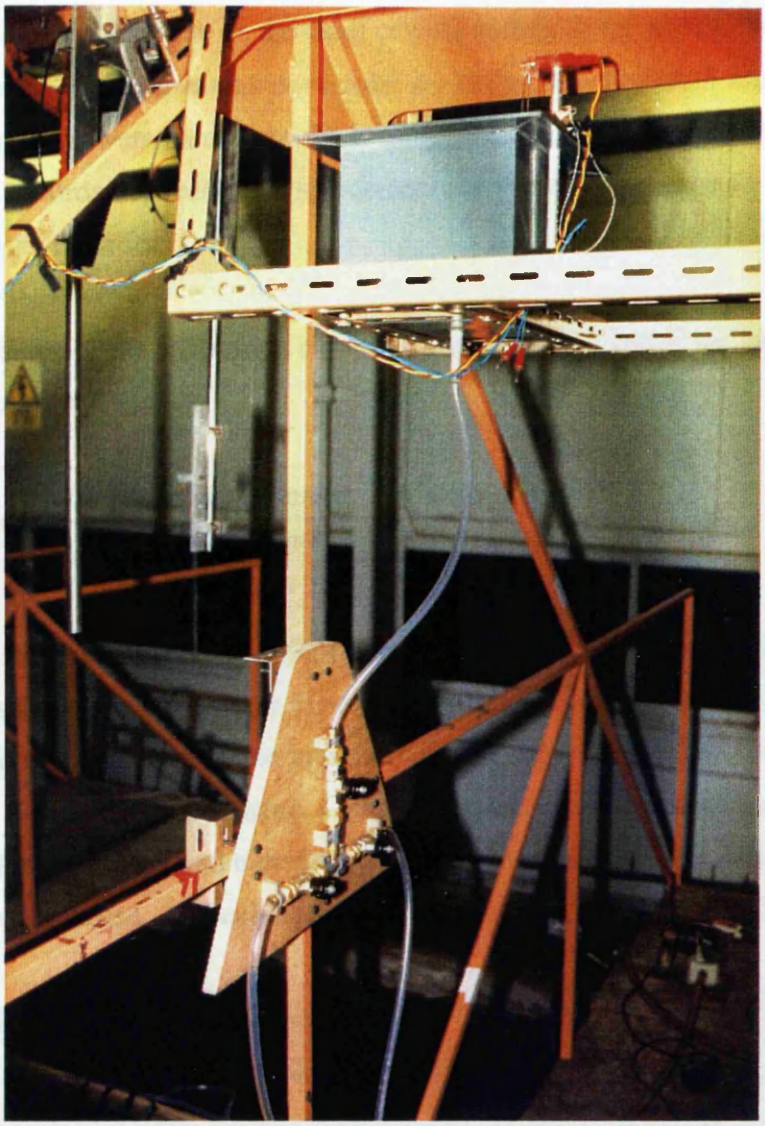

Fig.5.7 Experimental setup for the water container and the stop-valves to flood the compartments of the model

5.3.6 DESCRIPTION OF CALIBRATION PROCEDURES

All wave probes were calibrated when they were submerged 5 cm into the tank while the water was calm and zero readings on the wave probe amplifiers were taken by marking the pens' positions on the chart corresponding to the zero wave elevation. Then the calibration procedure was continued by lifting the probes 5 cm up and the new positions of pens were marked on the recorder. A linear relationship was found from the calibration records between the displacements of the wave probes and the displacements of pens on the recorder.

The slope of the calibration curves or the calibration factor for the wave height was given as follows:

$$K = \frac{Wave\ \ probe\ displacement\ \ (=\ wave\ elevation\ )}{Pen\ displacement\ \ (or\ voltage\ )} \tag{5.1}$$

The calibration of the LVDTs was similar to that of the wave probes. While the model was floated in calm water, zero deflections were recorded by the pen recorder from four transducers attached to the upper corners of the model. Then each transducer was displaced 5 cm downward using a vertical vernier attached to the piano wires which connected to the model and transducers. At that moment, the pen deflection on the chart recorder was marked. The calibration factor was evaluated using Eq.(5.1).

Calibration of LEDs was done by moving the cameras 5 cms towards the wave maker. Calibration factors of LEDs were also calculated by Eq.(5.1).

5.3.7 DESCRIPTION OF MOTION RECORDS

Typical time history records of the motion responses drawn by the multi-channel pen recorder are shown in Fig.5.8.

As shown in Fig.5.8, the records indicate the displacements versus real time which was scaled by the chart feeder speed. Four records at the centre of the chart show the displacements received from LVDTs due to the vertical motion of the corner columns. The other three records at the top of the chart show the wave displacements while the

record at the bottom of the chart shows the amount of water flooding into the column.

Time history records of the motion test were produced from the stored data on the computer and each run was also simulated on the computer in order to make comparisons between theoretical results and experimental measurements which are given at the end of this chapter.

As evidenced by some of the test recordings, at the beginning of the test a large steady displacement developed following the first impact of the wave on the model and then the displacements settled down to steady values. In order to avoid this, the wavemaker was operated in such a way that regular wave trains gradually reached their required amplitudes. Therefore, the motion of the model semi-submersible was also built up gradually as seen in Fig.5.8.

5.3.8 MOTION TEST PROCEDURE

During the motion experiments, signals from 14 channels (4 from wave probes, 4 from LVDTs, 6 from, LEDs) were recorded and stored by the multi-channel pen recorder and the computer simultaneously.

Each test was preceded and followed by zero measurements in calm water. Before recording of the test signals started, the wavemaker was started and a period of time was allowed for the waves to arrive at the wave probes. The duration of tests varied from 55 s to 120 s (9 m to 17 m in full scale) depending on the wave frequency and duration of flooding. In the first stage of each run, the model was tested in the intact condition and then one or two of the compartments were flooded for 10 or 5 seconds. For the remaining time of the run, the model test was continued for the post-damage simulation.

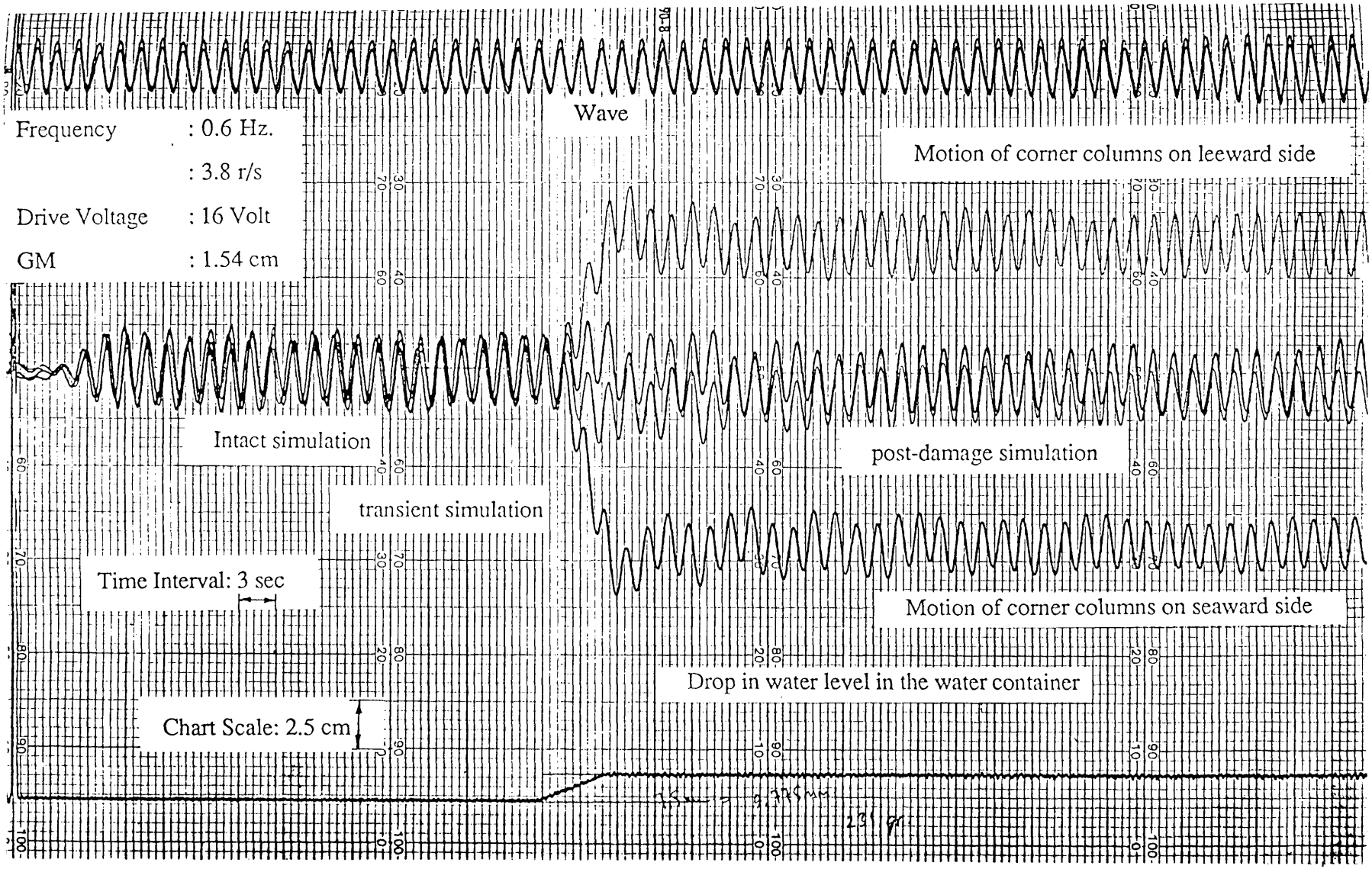

Fig.5.8 Chart record for the motions of the model from multi-channel pen recorder

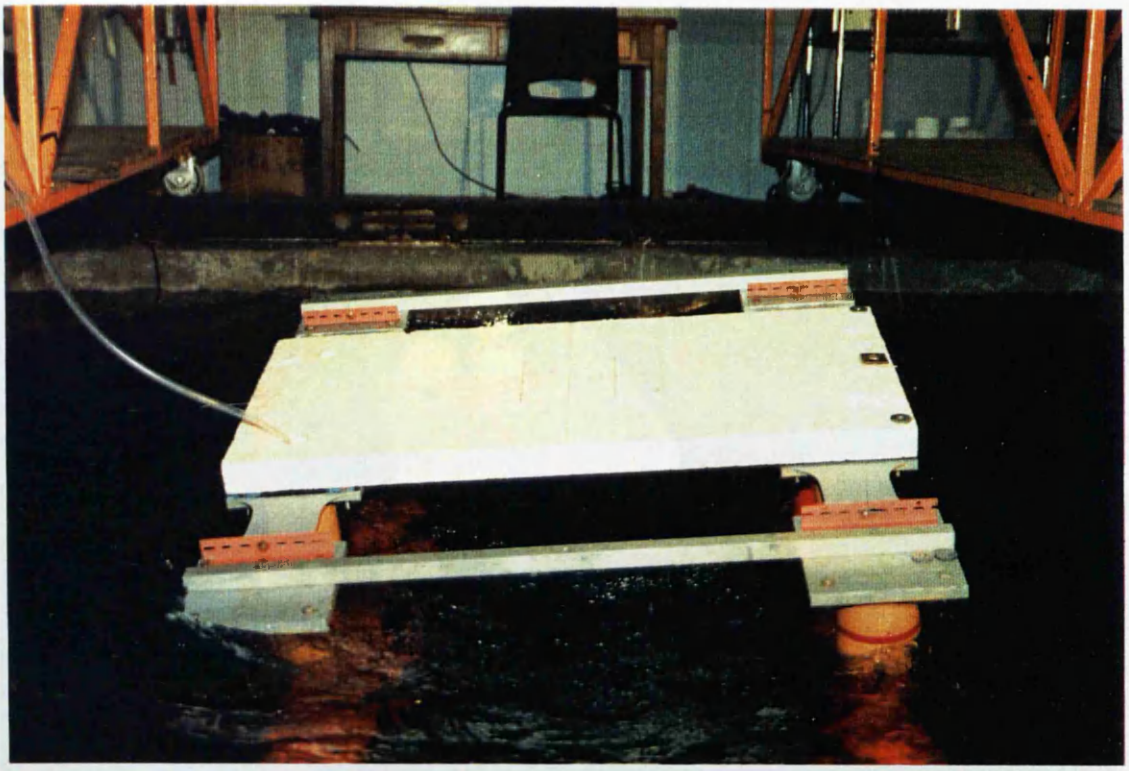

Fig 5.9 Motion response experiment (Beam sea condition-asymmetrical flooding)
WH=9.8 cm Flooding Mass=0.9 kg Flooding Time=20 s
GM=2.29 cm ω=6.3 r/s (1.0 hertz)

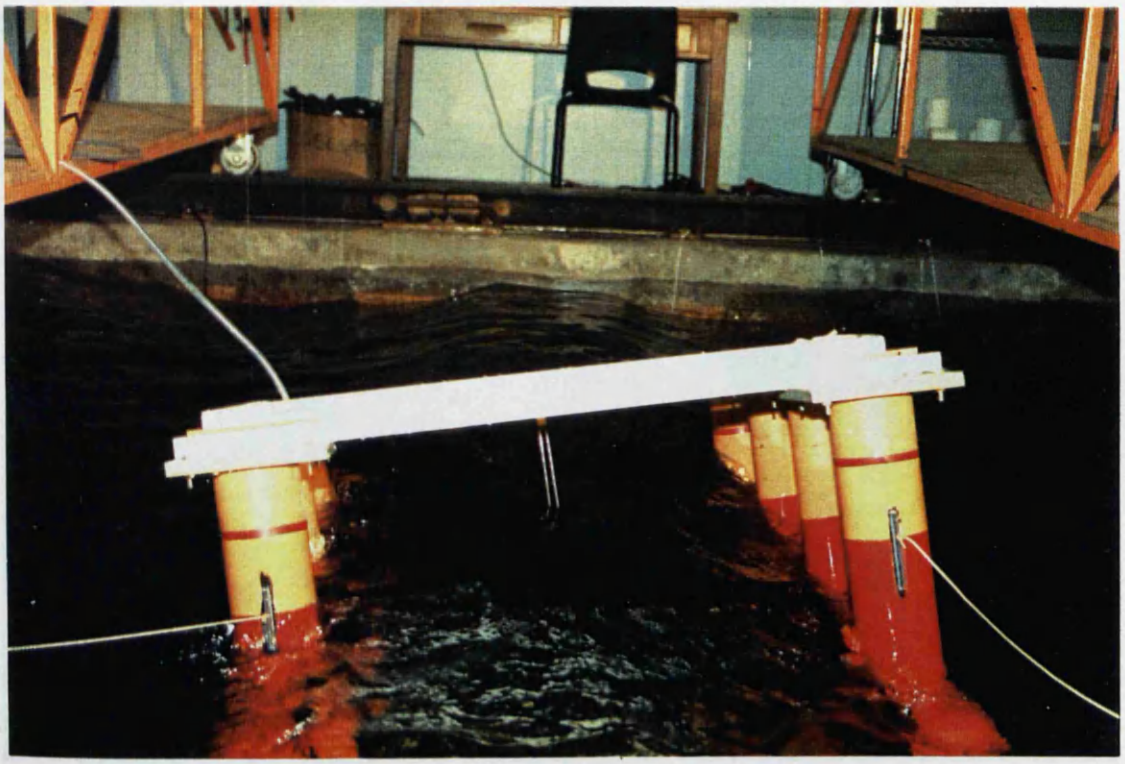

Fig 5.10 Motion response experiment (Beam sea condition-asymmetrical flooding)
WH=9.8 cm Flooding Mass=0.5 kg Flooding Time=10 s
GM=2.29 cm ω=6.3 r/s (1.0 hertz)

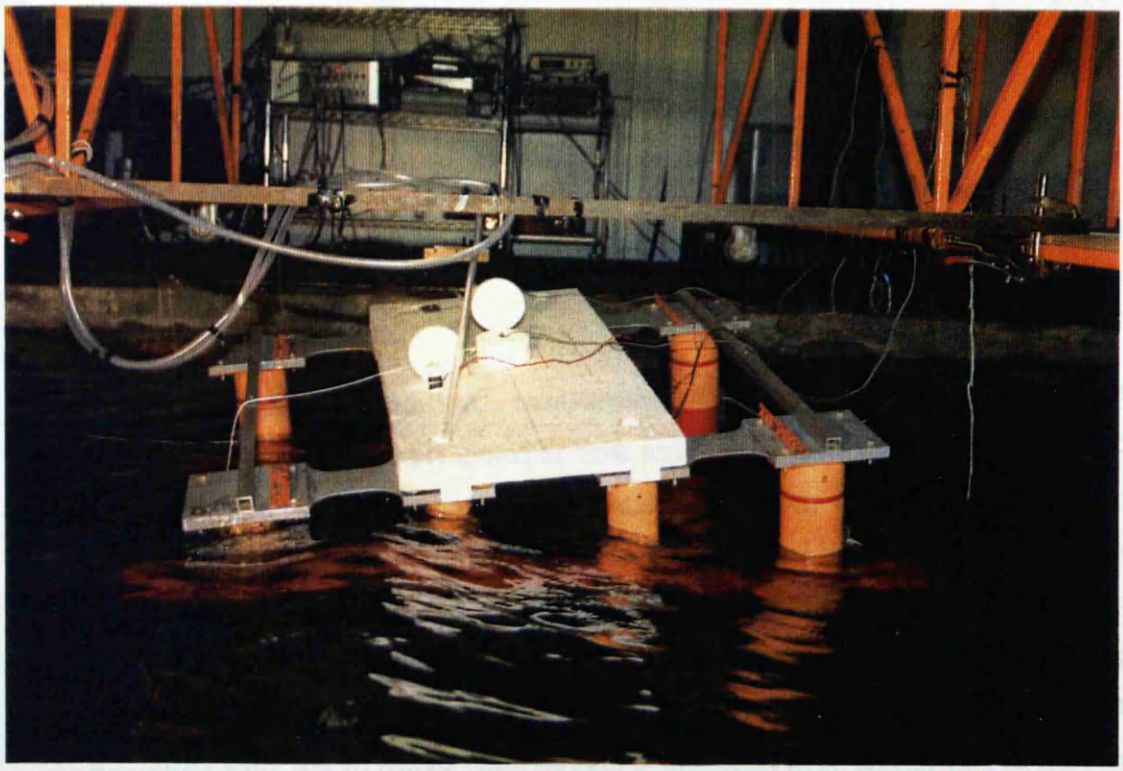

Fig 5.11 Motion response experiment (Head sea condition-asymmetrical flooding)
WH=9.8 cm Flooding Mass=0.5 kg Flooding Time=10 s
GM=2.29 cm ω=6.3 r/s (1.0 hertz)

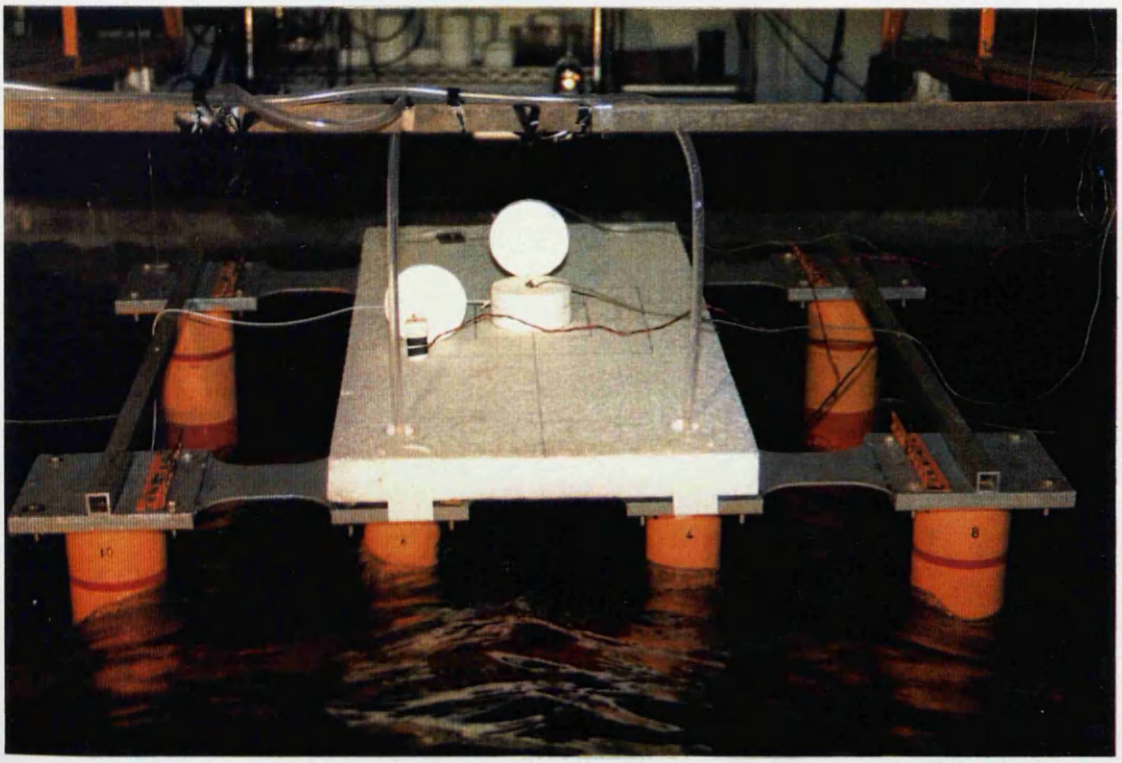

Fig 5.12 Motion response experiment (Head sea condition-asymmetrical flooding)
WH=7.3 cm Flooding Mass=0.5 kg Flooding Time=10 s
GM=2.29 cm ω=7.5 r/s (1.2 hertz)

5.4 PRESENTATION AND DISCUSSION OF RESULTS

Results of motion experiments and their numerical simulations are presented in Figs.5.13-101. Experimental results were obtained in head and beam sea conditions for two different GMs.

For the head sea condition, measurements of surge, heave, roll, yaw, pitch motions and wave height are presented as time series data. Sway motion is not included in the presentation of numerical and physical simulations carried out for head sea condition. Similarly, surge motion response is not presented for the beam sea condition. Roll motion responses in head sea condition or pitch motion responses in beam sea condition are presented because they are affected by asymmetrical damage to the platform. Although the test was initiated in an intact condition in each experiment, changes in model configuration gave rise to roll or pitch motion response in head and beam sea conditions respectively.

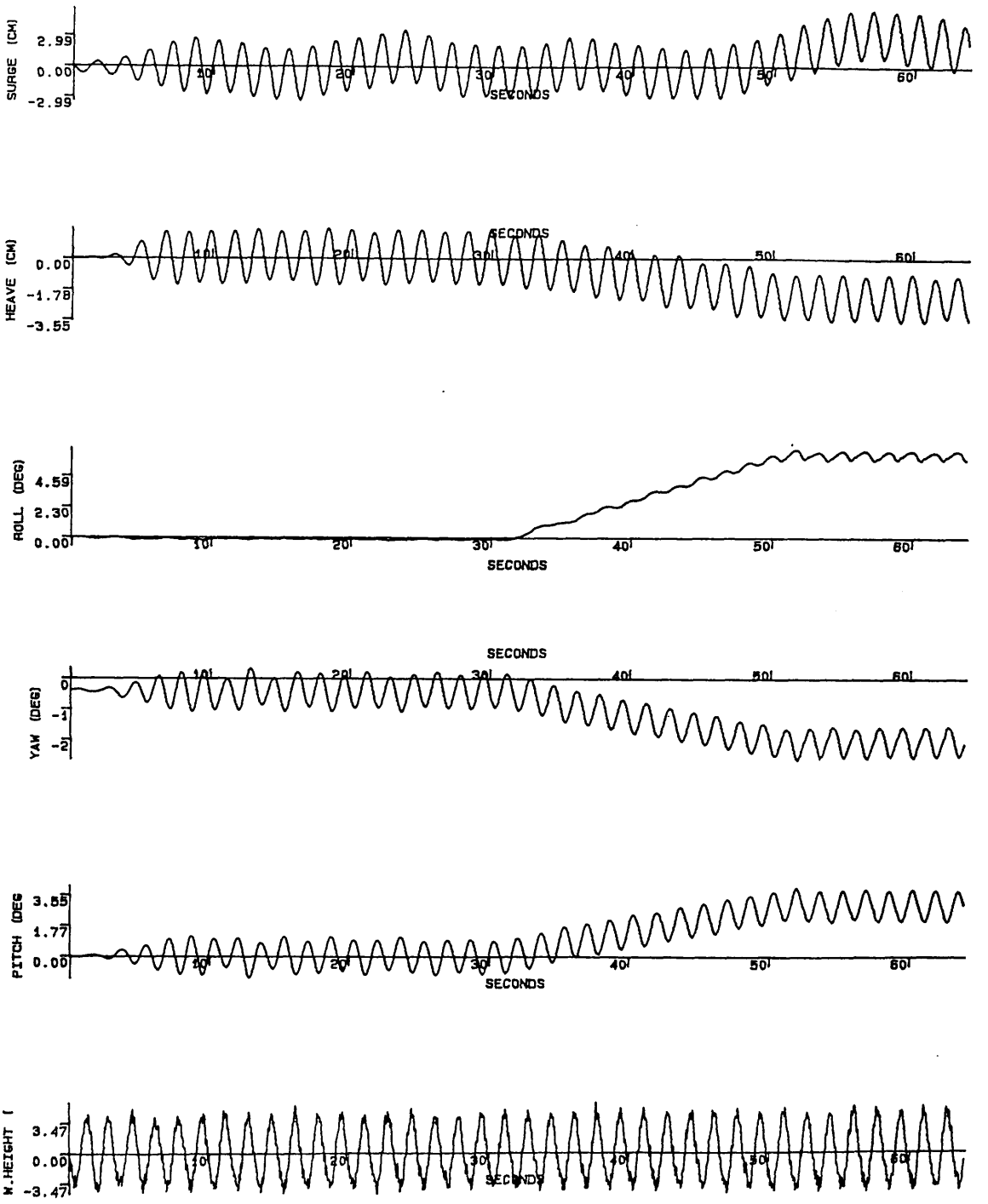

Fig.5.13 Motion response experiment (Head sea condition-asymmetrical flooding)
WH=8.8 cm Flooding Mass=1.5 kg Flooding Time=20 s
GM=7.81 cm ω=3.8 r/s (0.6 hertz) TS2916S.DAT

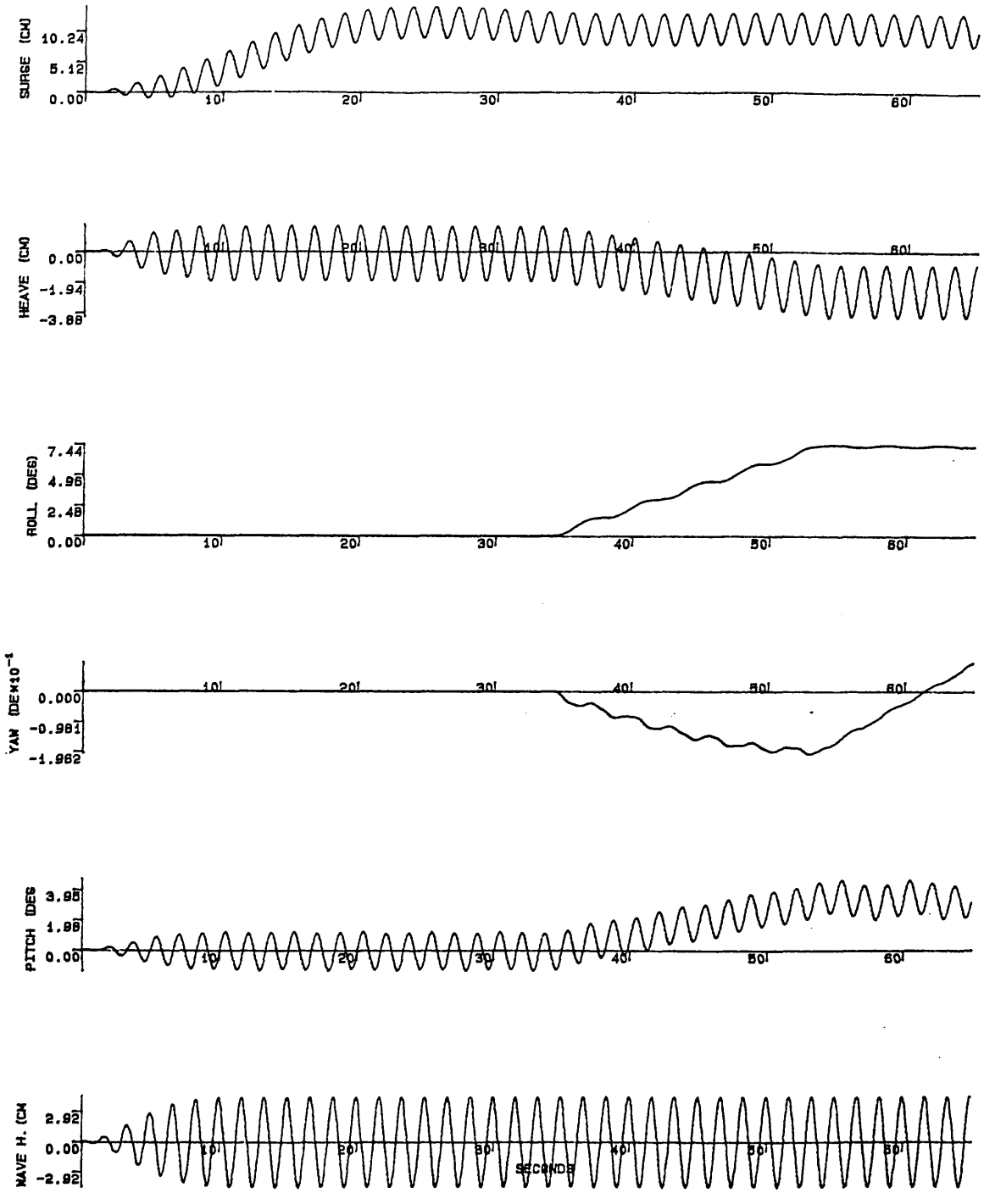

Fig.5.14 Motion response simulation (Head sea condition-asymmetrical flooding)
WH=8.8 cm Flooding Mass=1.5 kg Flooding Time=20 s
GM=7.81 cm ω=3.8 r/s (0.6 hertz)

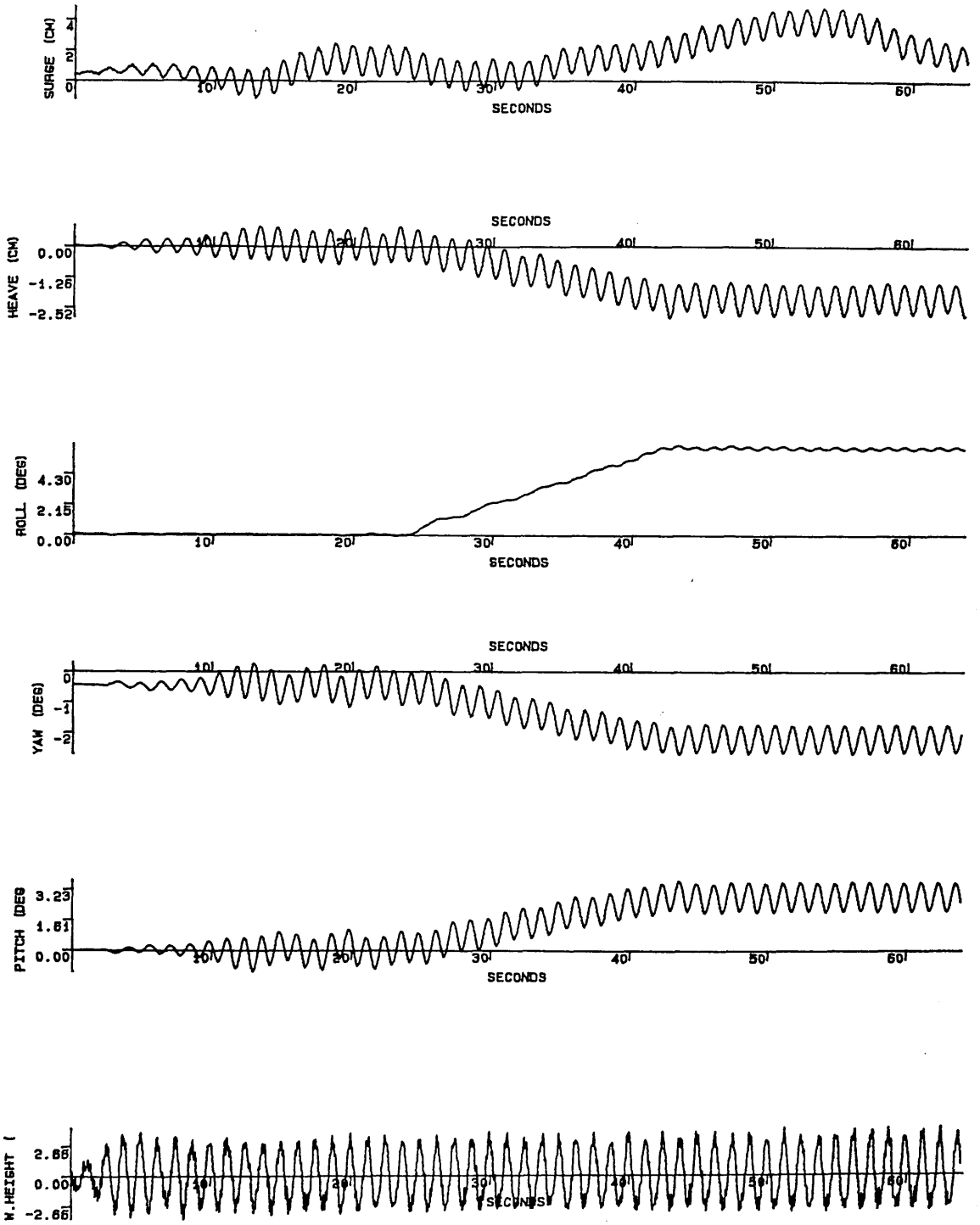

Fig.5.15 Motion response experiment (Head sea condition-asymmetrical flooding)

WH=6.7 cm	Flooding Mass=1.4 kg	Flooding Time=20 s
GM=7.81 cm	ω=5.0 r/s (0.8 hertz)	TS2917S.DAT

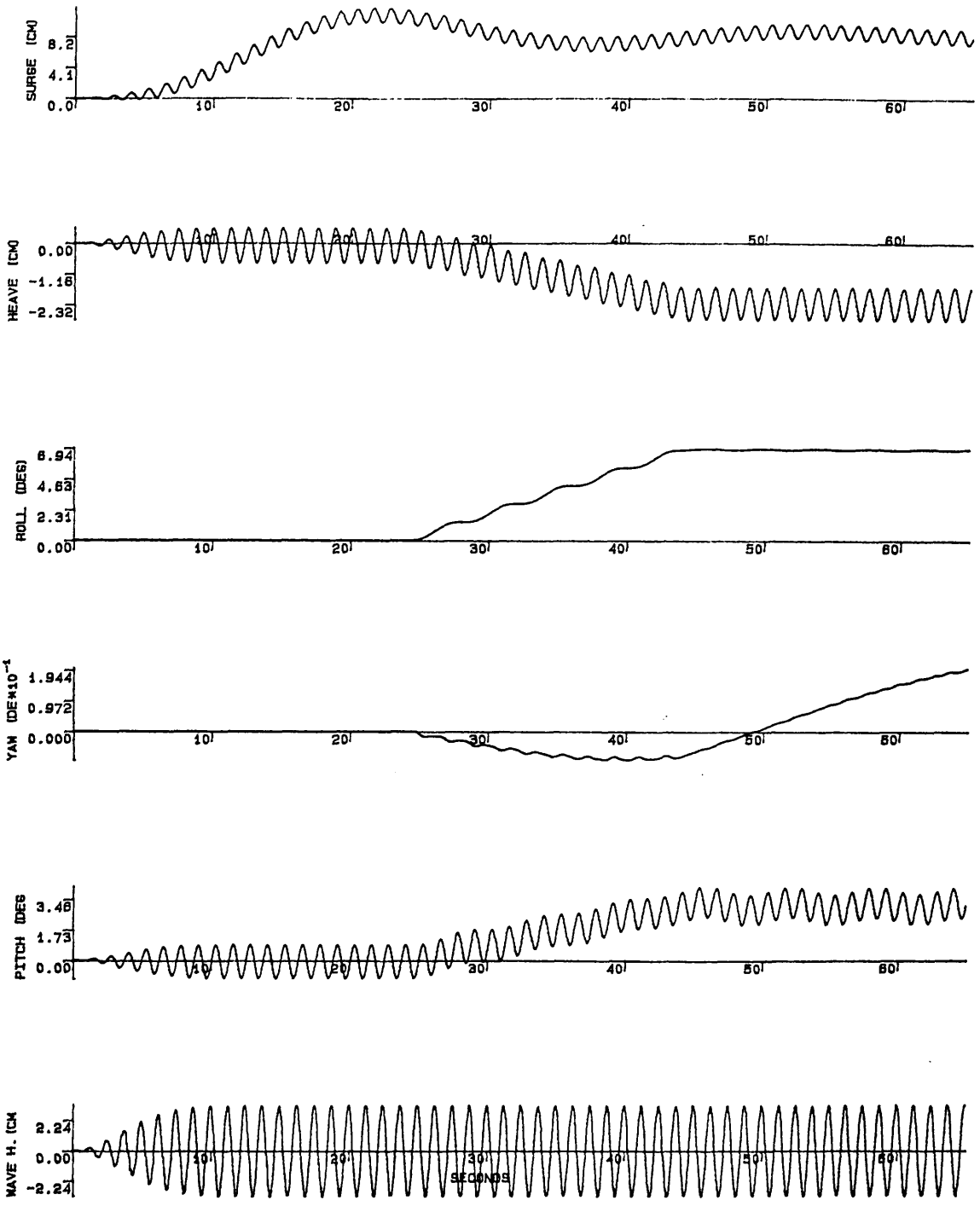

Fig.5.16 Motion response simulation (Head sea condition-asymmetrical flooding)
WH=6.7 cm Flooding Mass=1.4 kg Flooding Time=20 s
GM=7.81 cm ω=5.0 r/s (0.8 hertz)

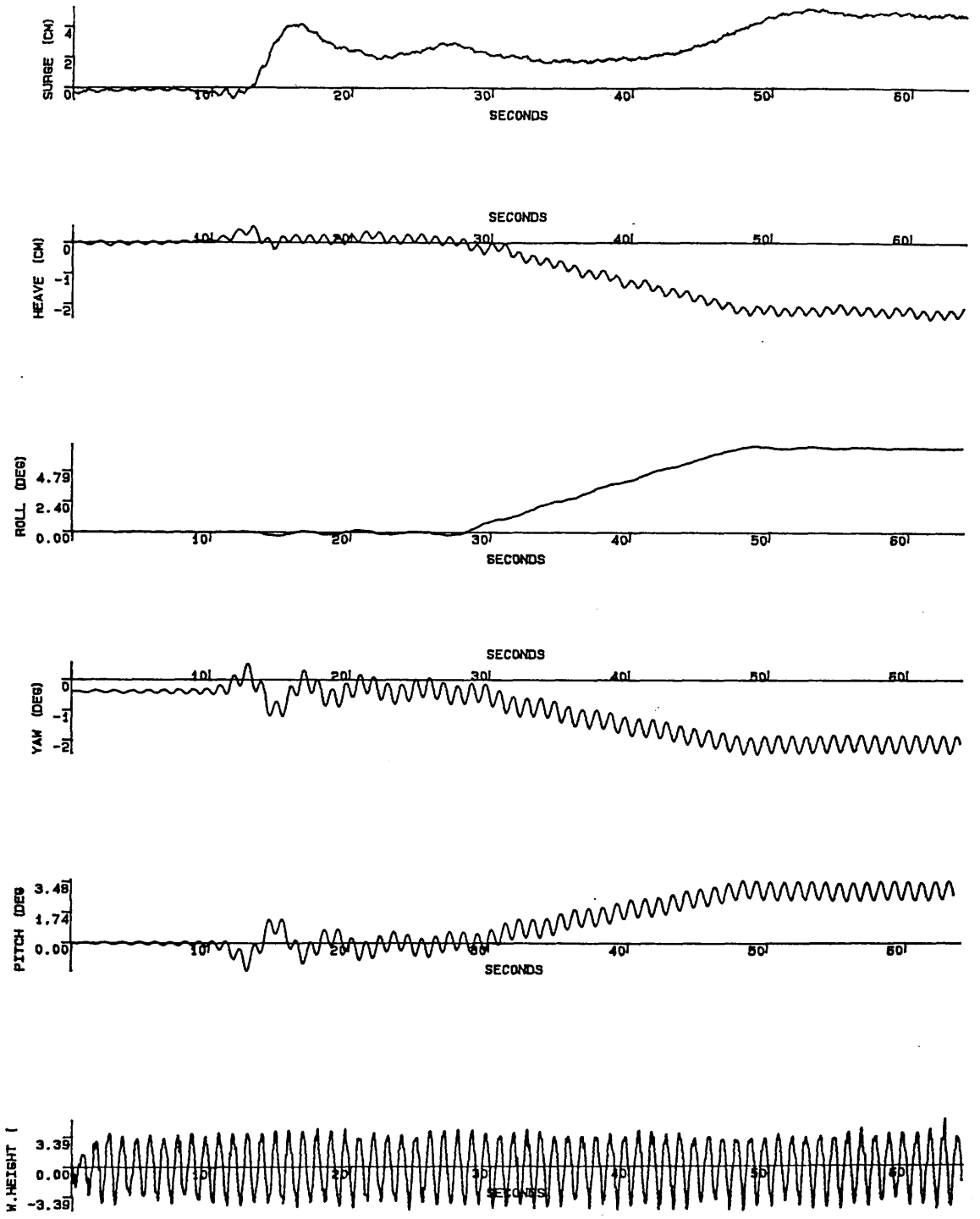

Fig.5.17 Motion response experiment (Head sea condition-asymmetrical flooding)
WH=8.6 cm Flooding Mass=1.4 kg Flooding Time=20 s
GM=7.81 cm ω=6.3 r/s (1.0 hertz) TS2918S.DAT

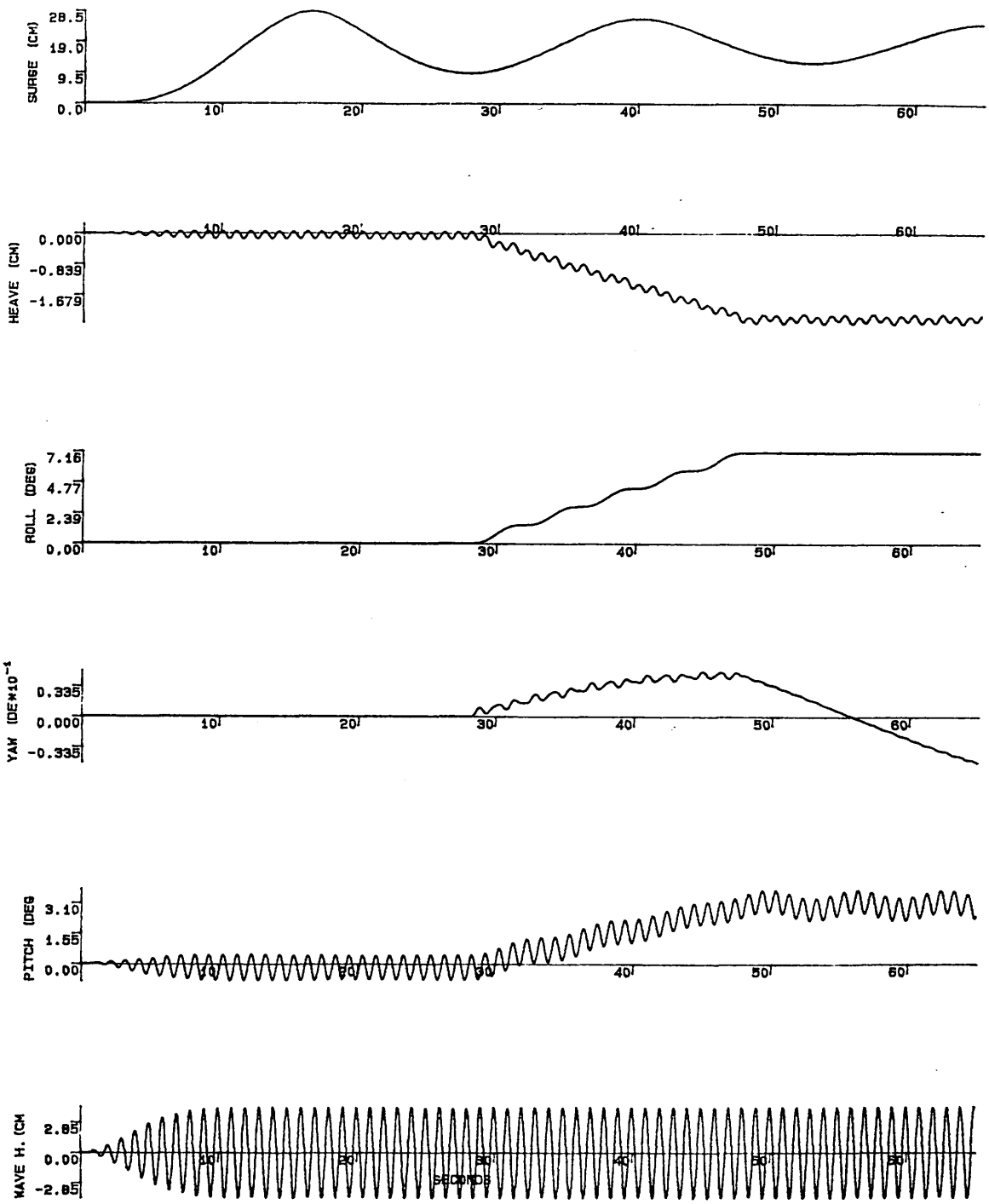

Fig.5.18 Motion response simulation (Head sea condition-asymmetrical flooding)
WH=8.6 cm Flooding Mass=1.4 kg Flooding Time=20 s
GM=7.81 cm ω=6.3 r/s (1.0 hertz)

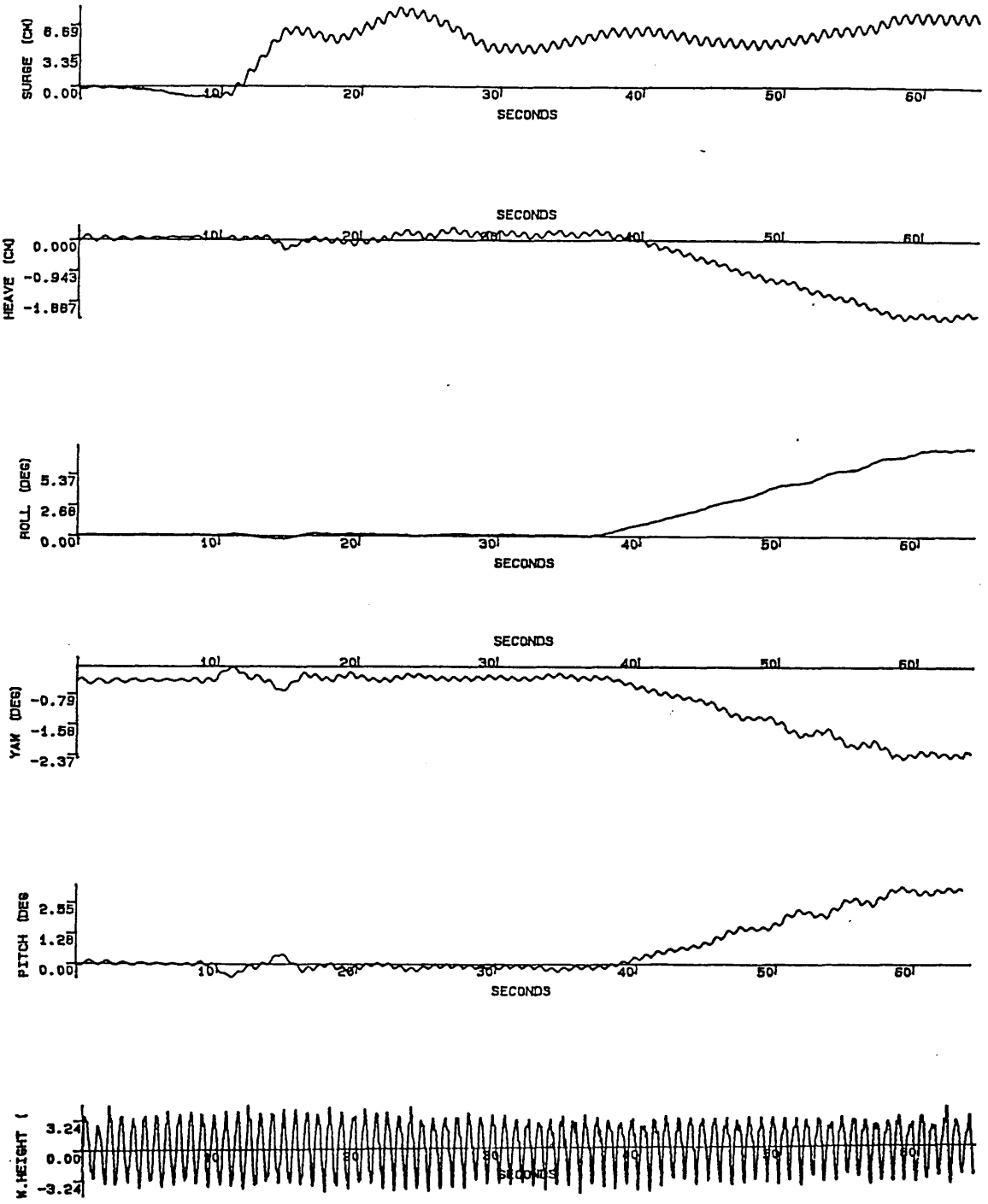

Fig.5.19 Motion response experiment (Head sea condition-asymmetrical flooding)

WH=8.2 cm	Flooding Mass=1.7 kg	Flooding Time=20 s
GM=7.81 cm	ω=7.5 r/s (1.2 hertz)	TS2919S.DAT

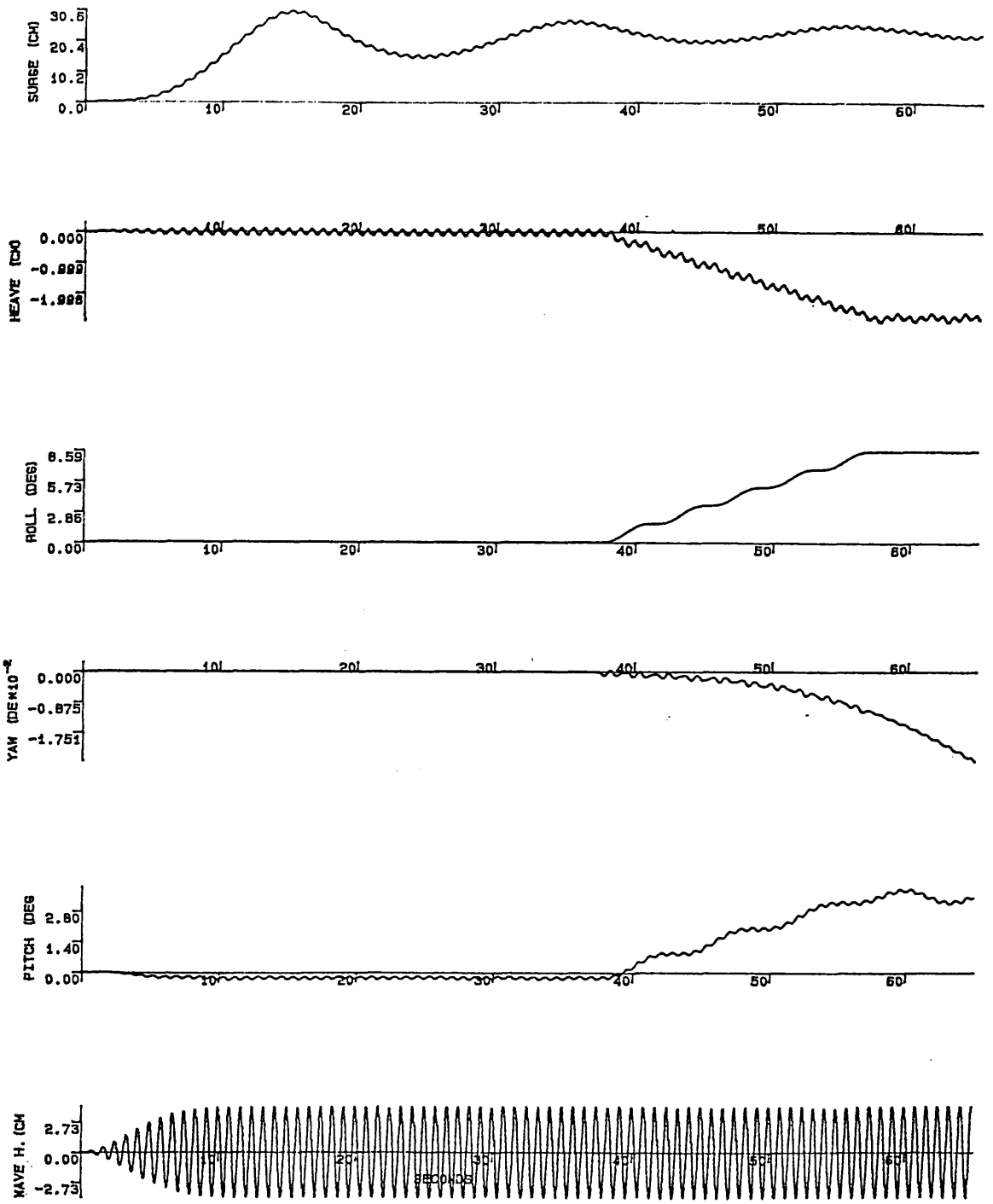

Fig.5.20 Motion response simulation (Head sea condition-asymmetrical flooding)
WH=8.2 cm Flooding Mass=1.7 kg Flooding Time=20 s
GM=7.81 cm ω=7.5 r/s (1.2 hertz)

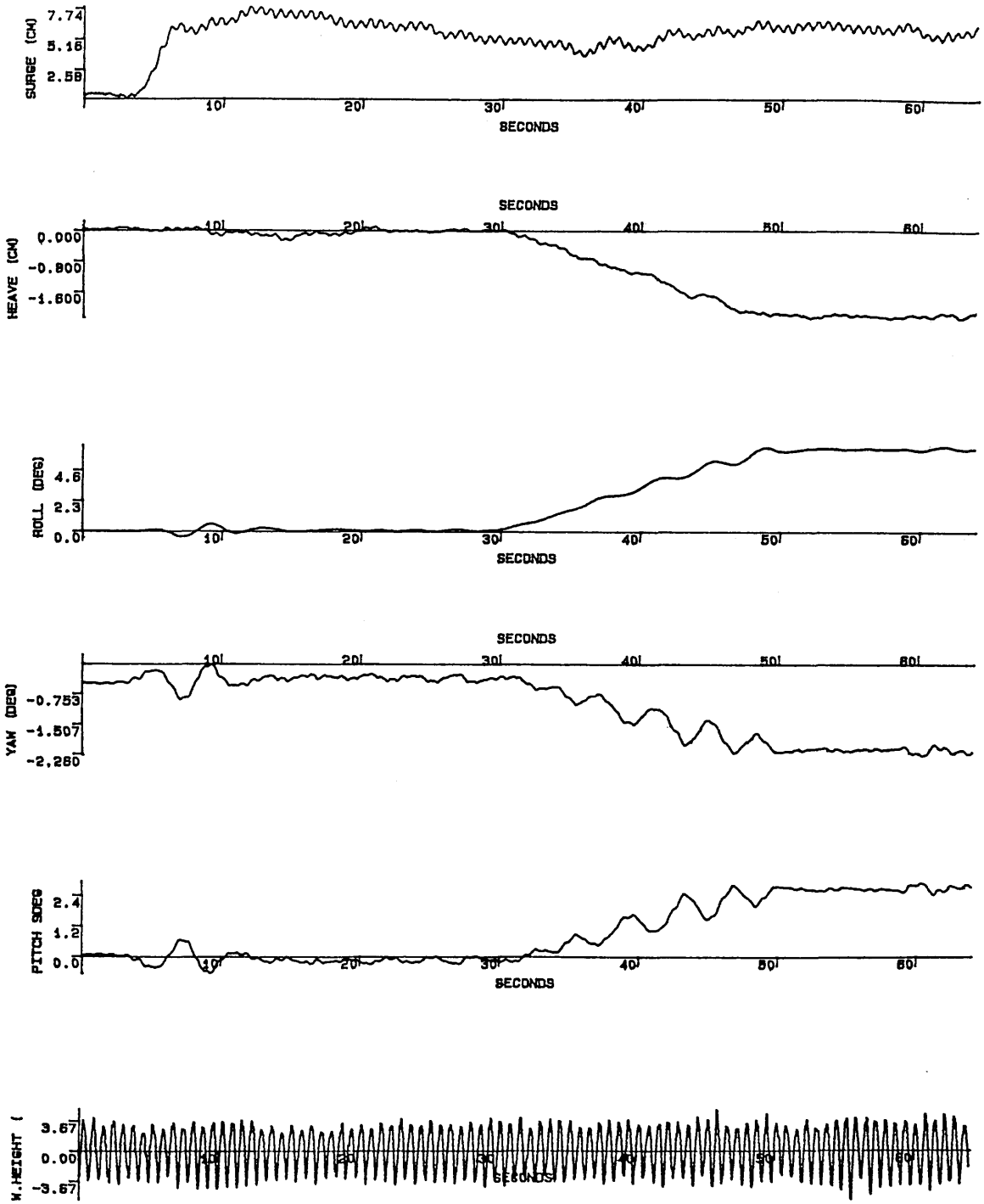

Fig.5.21 Motion response experiment (Head sea condition-asymmetrical flooding)

WH=7.7 cm	Flooding Mass=1.4 kg	Flooding Time=20 s
GM=7.81 cm	ω=8.8 r/s (1.4 hertz)	TS2920S.DAT

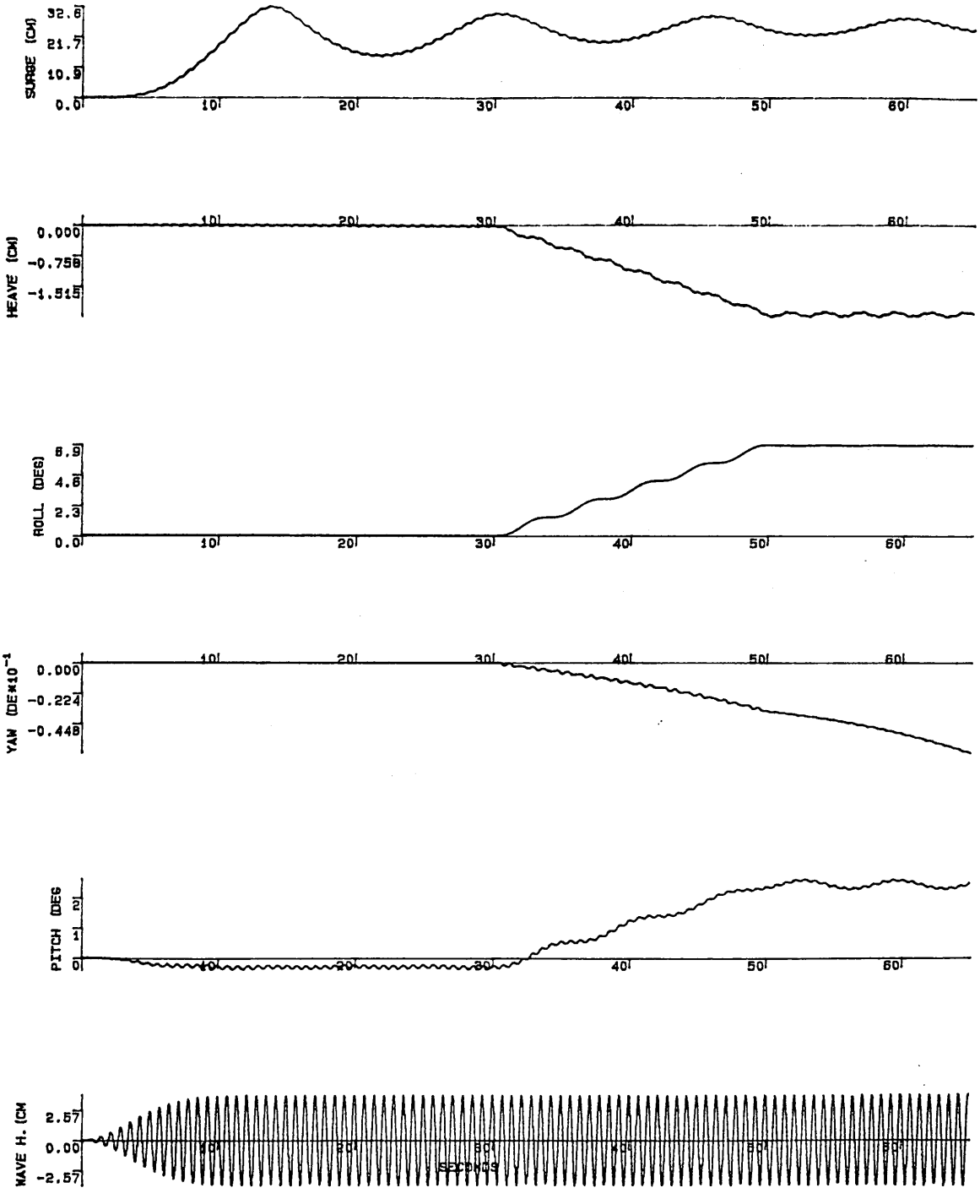

Fig.5.22 Motion response simulation (Head sea condition-asymmetrical flooding)
WH=7.7 cm Flooding Mass=1.4 kg Flooding Time=20 s
GM=7.81 cm ω=8.8 r/s (1.4 hertz)

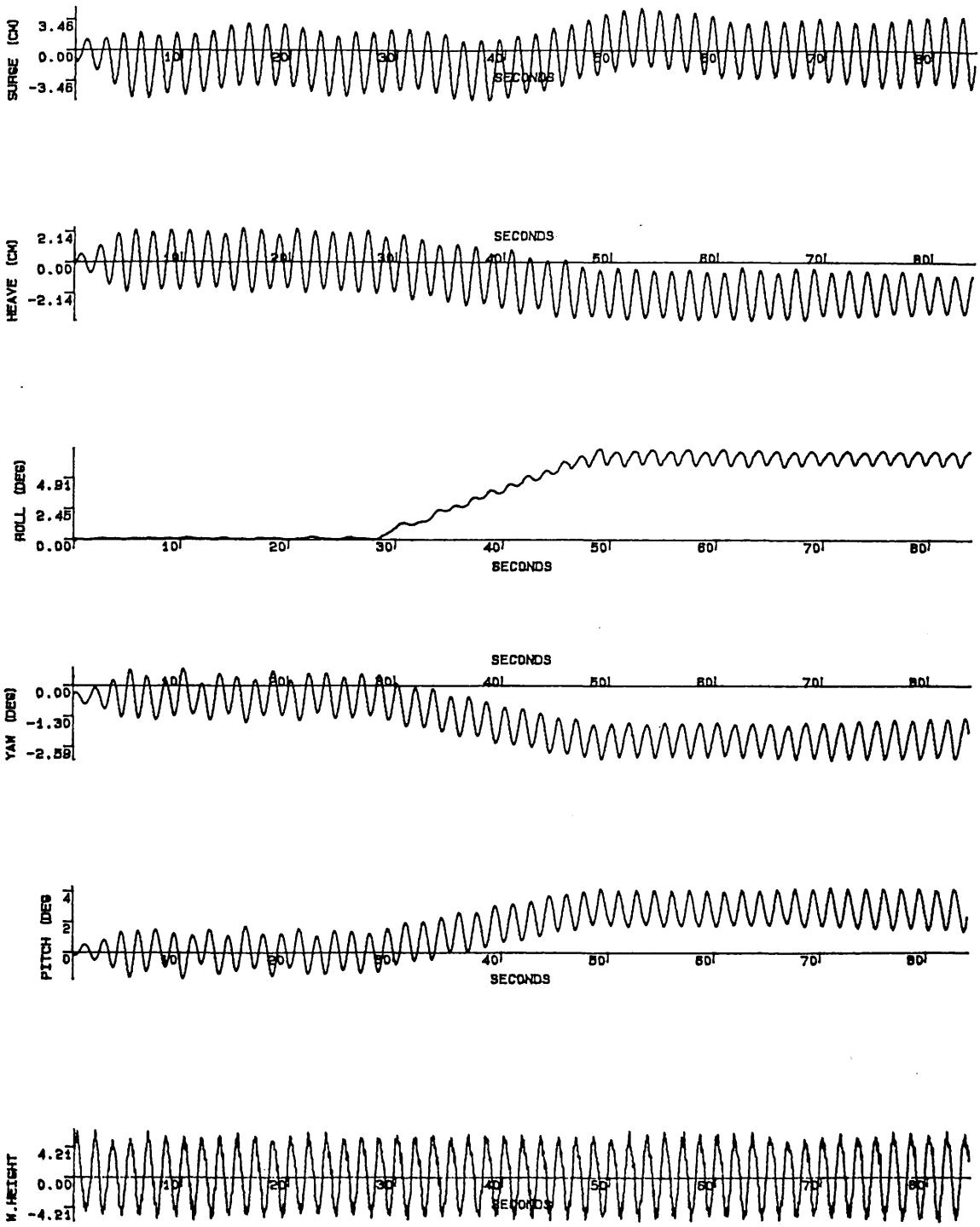

Fig.5.23 Motion response experiment (Head sea condition-asymmetrical flooding)
WH=11.5 cm Flooding Mass=1.7 kg Flooding Time=20 s
GM=7.81 cm ω=3.8 r/s (0.6 hertz) TS2922S.DAT

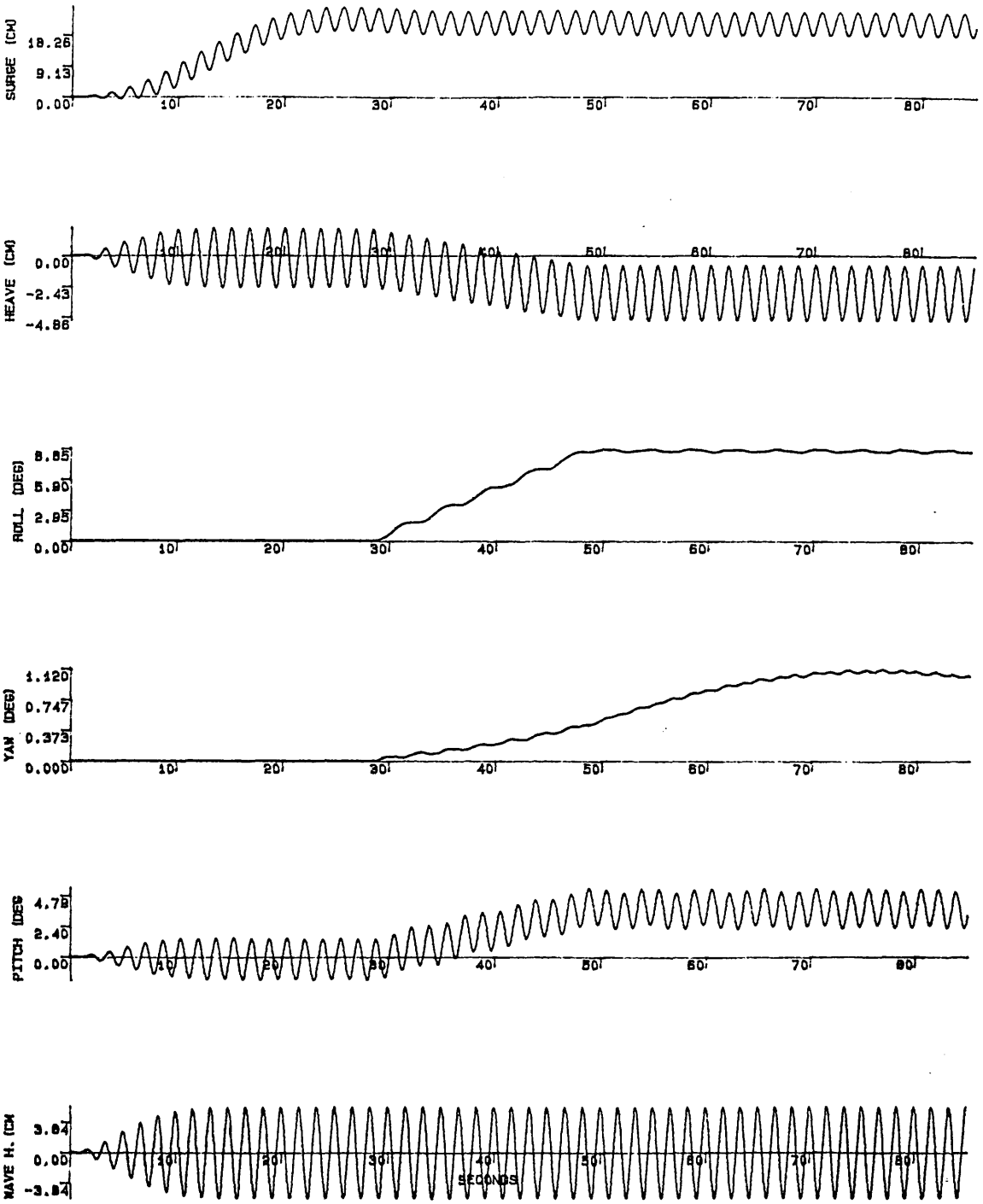

Fig.5.24 Motion response simulation (Head sea condition-asymmetrical flooding)
WH=11.5 cm Flooding Mass=1.7 kg Flooding Time=20 s
GM=7.81 cm ω=3.8 r/s (0.6 hertz)

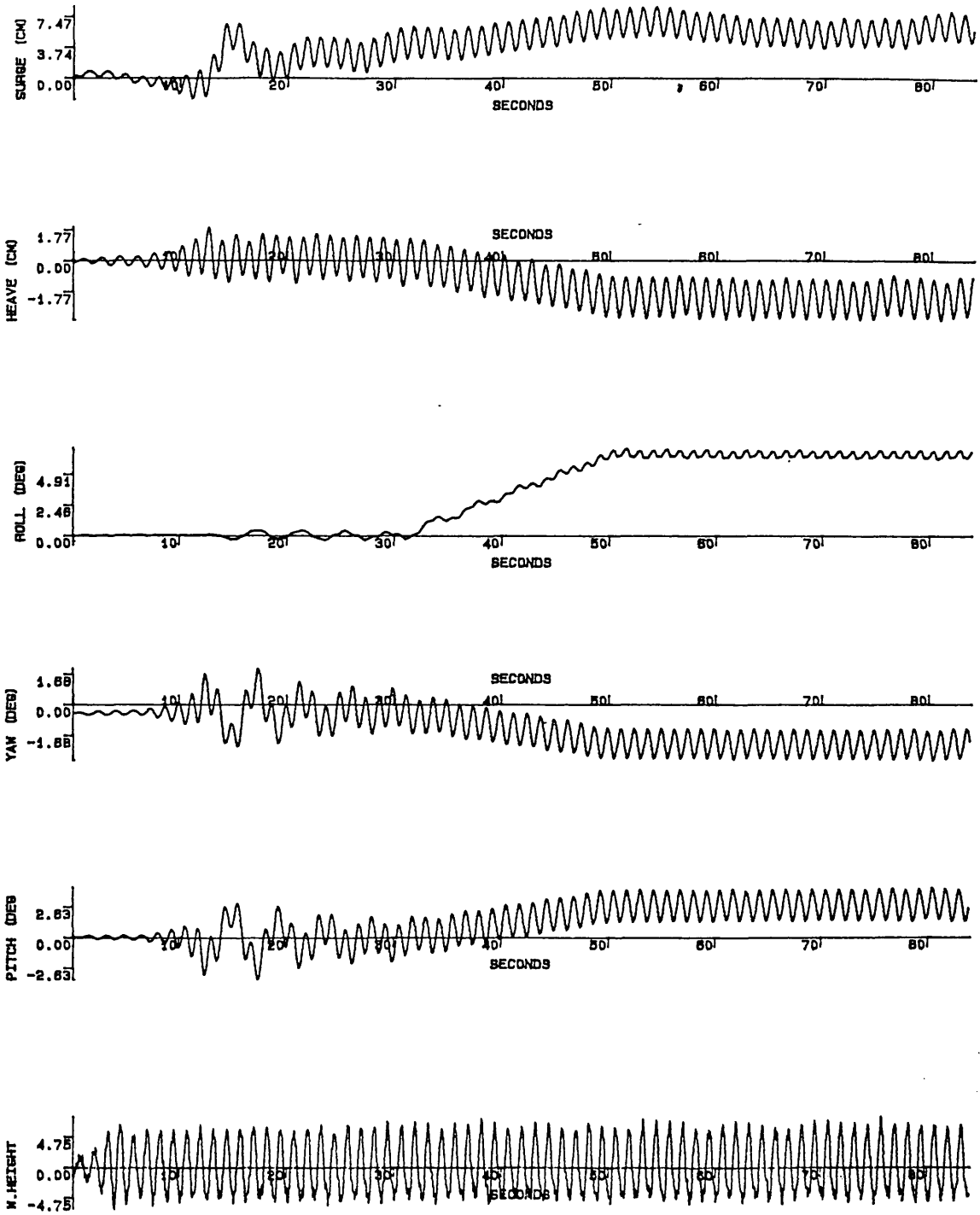

Fig.5.25 Motion response experiment (Head sea condition-asymmetrical flooding)
WH=12.0 cm Flooding Mass=1.6 kg Flooding Time=20 s
GM=7.81 cm ω=5.0 r/s (0.8 hertz) TS2923S.DAT

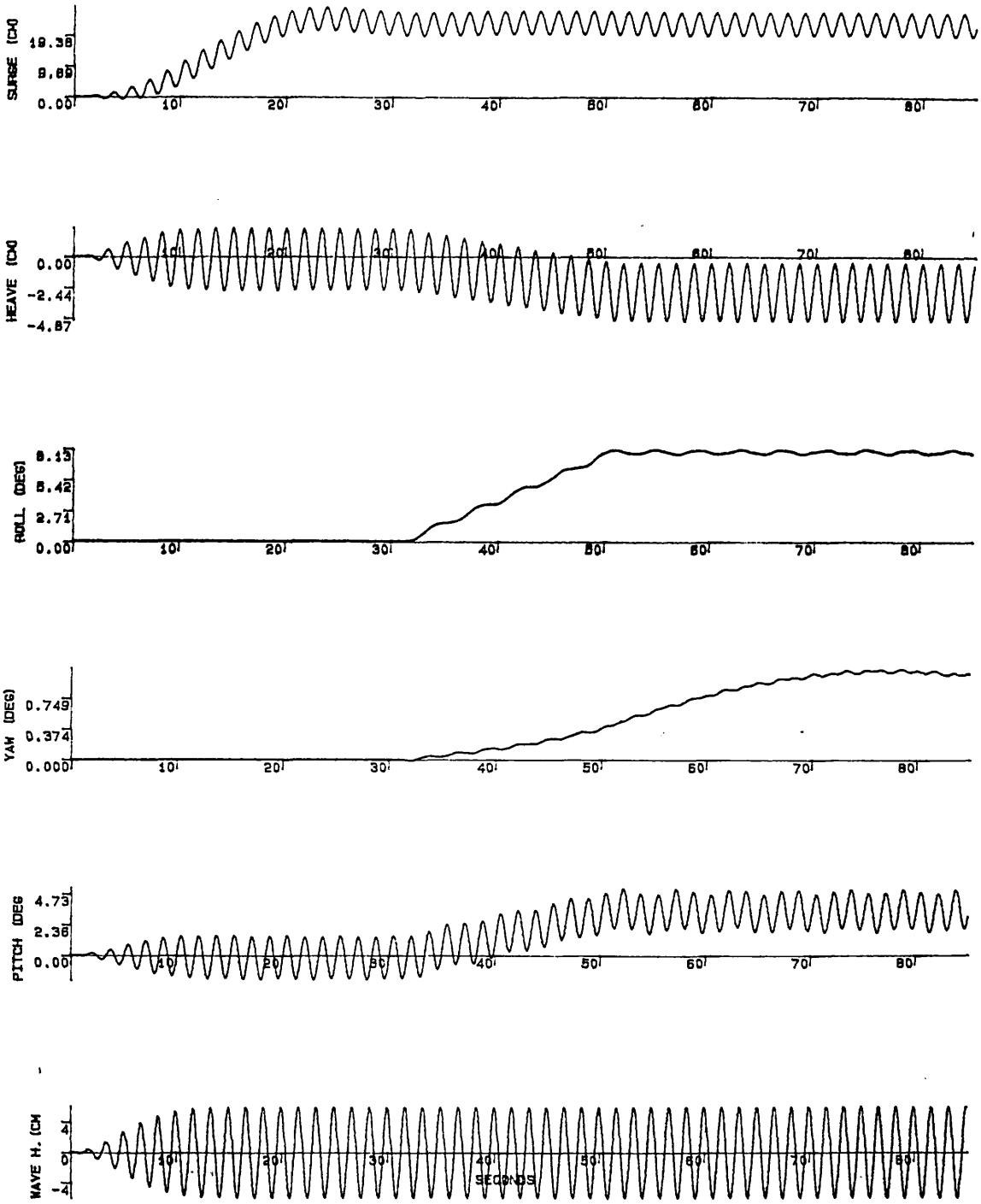

Fig.5.26 Motion response simulation (Head sea condition-asymmetrical flooding)
WH=12.0 cm Flooding Mass=1.6 kg Flooding Time=20 s
GM=7.81 cm ω=5.0 r/s (0.8 hertz)

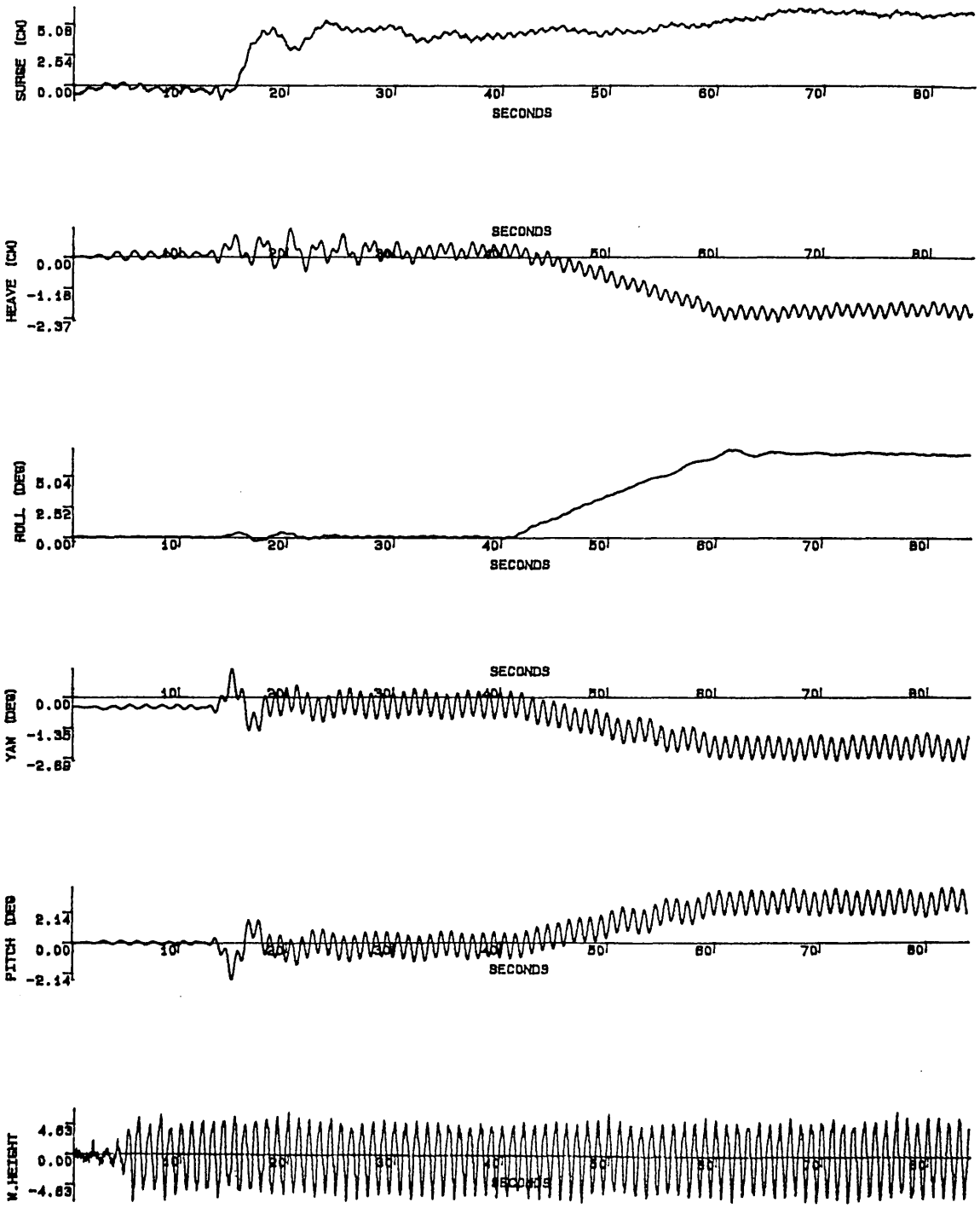

Fig.5.27 Motion response experiment (Head sea condition-asymmetrical flooding)
WH=11.7 cm Flooding Mass=1.5 kg Flooding Time=20 s
GM=7.81 cm ω=6.3 r/s (1.0 hertz) TS2924S.DAT

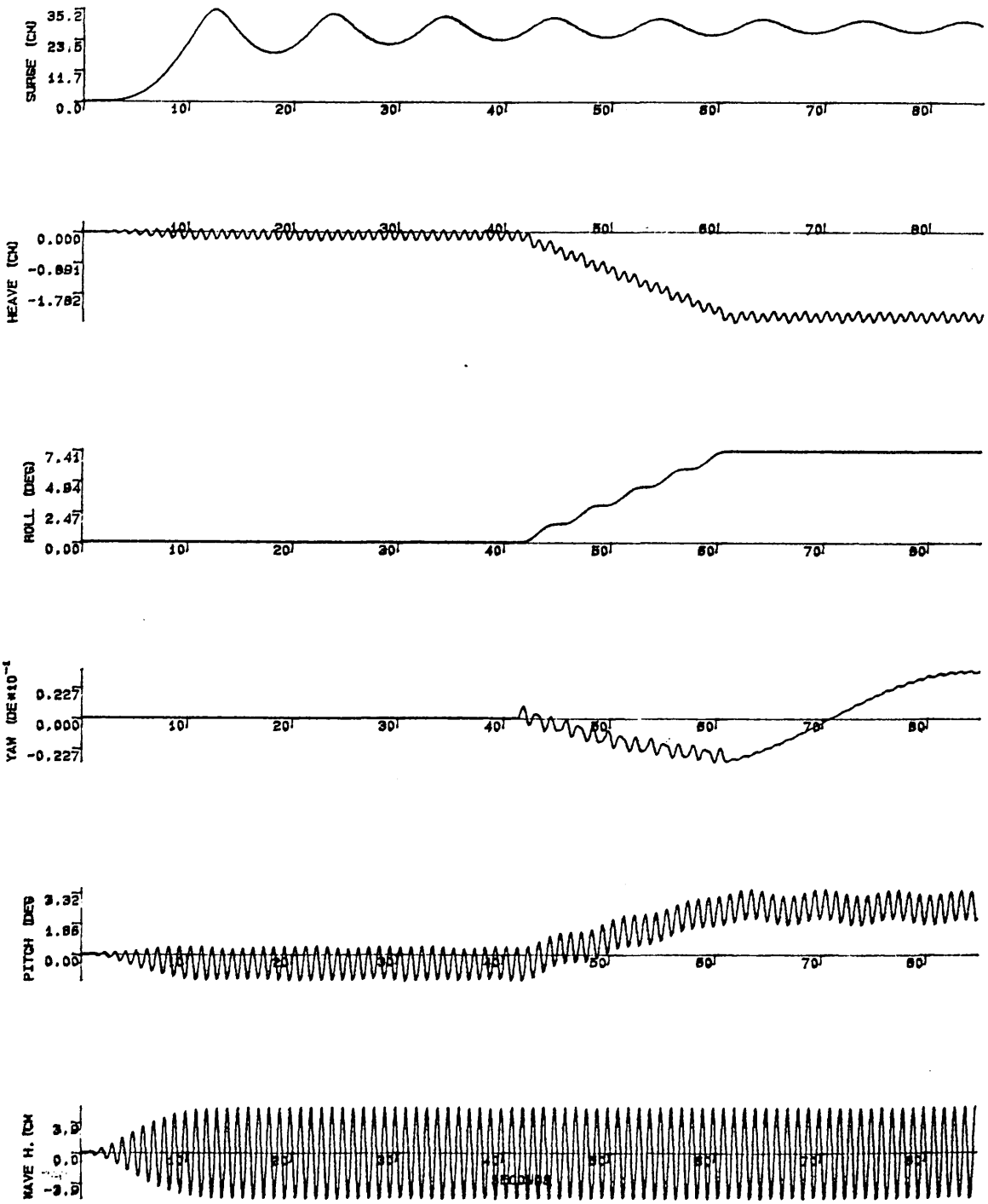

Fig.5.28 Motion response simulation (Head sea condition-asymmetrical flooding)
WH=11.7 cm Flooding Mass=1.6 kg Flooding Time=20 s
GM=7.81 cm ω=6.3 r/s (1.0 hertz)

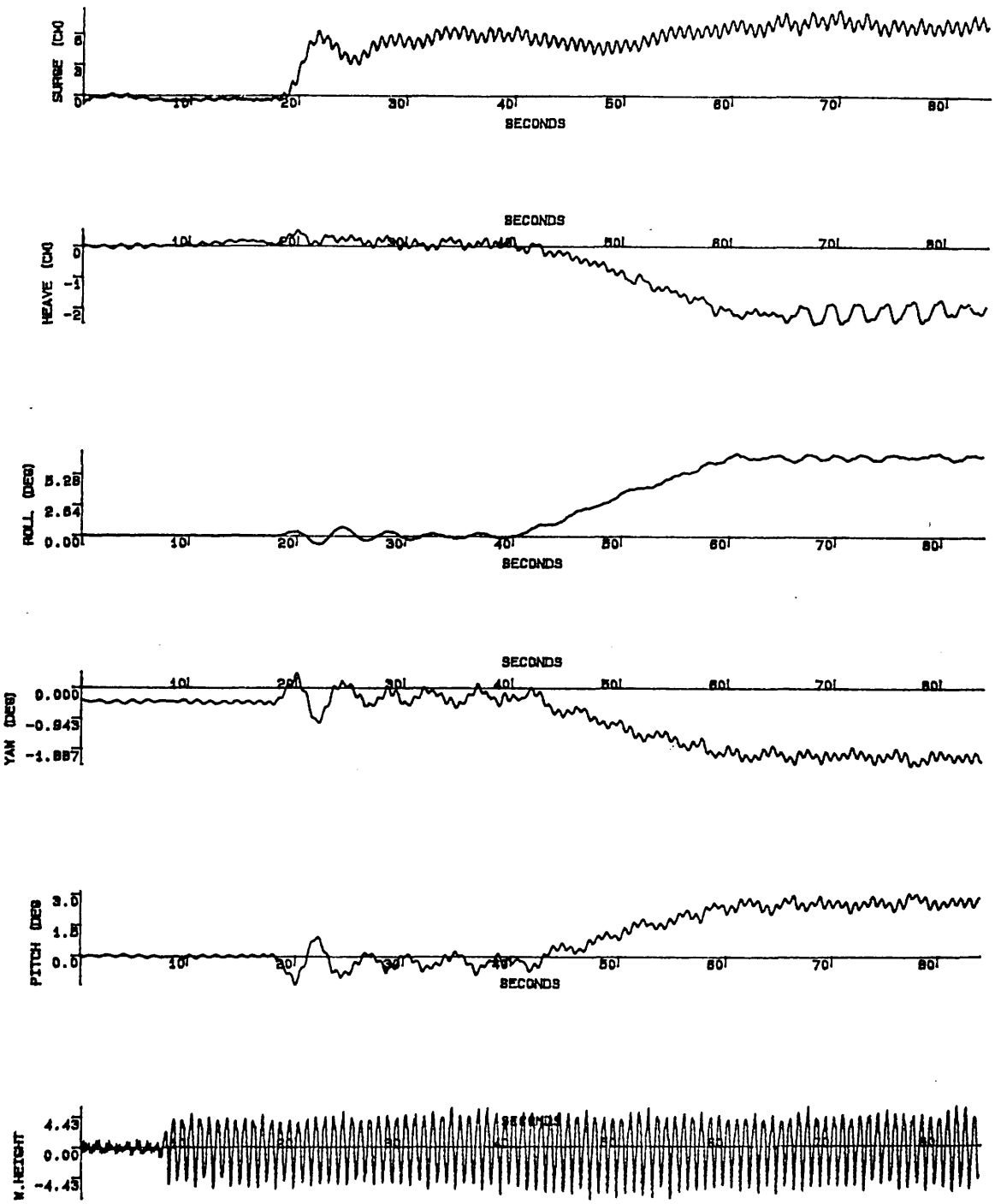

Fig.5.29 Motion response experiment (Head sea condition-asymmetrical flooding)

WH=11.2 cm	Flooding Mass=1.5 kg	Flooding Time=20 s
GM=7.81 cm	ω=7.5 r/s (1.2 hertz)	TS2925S.DAT

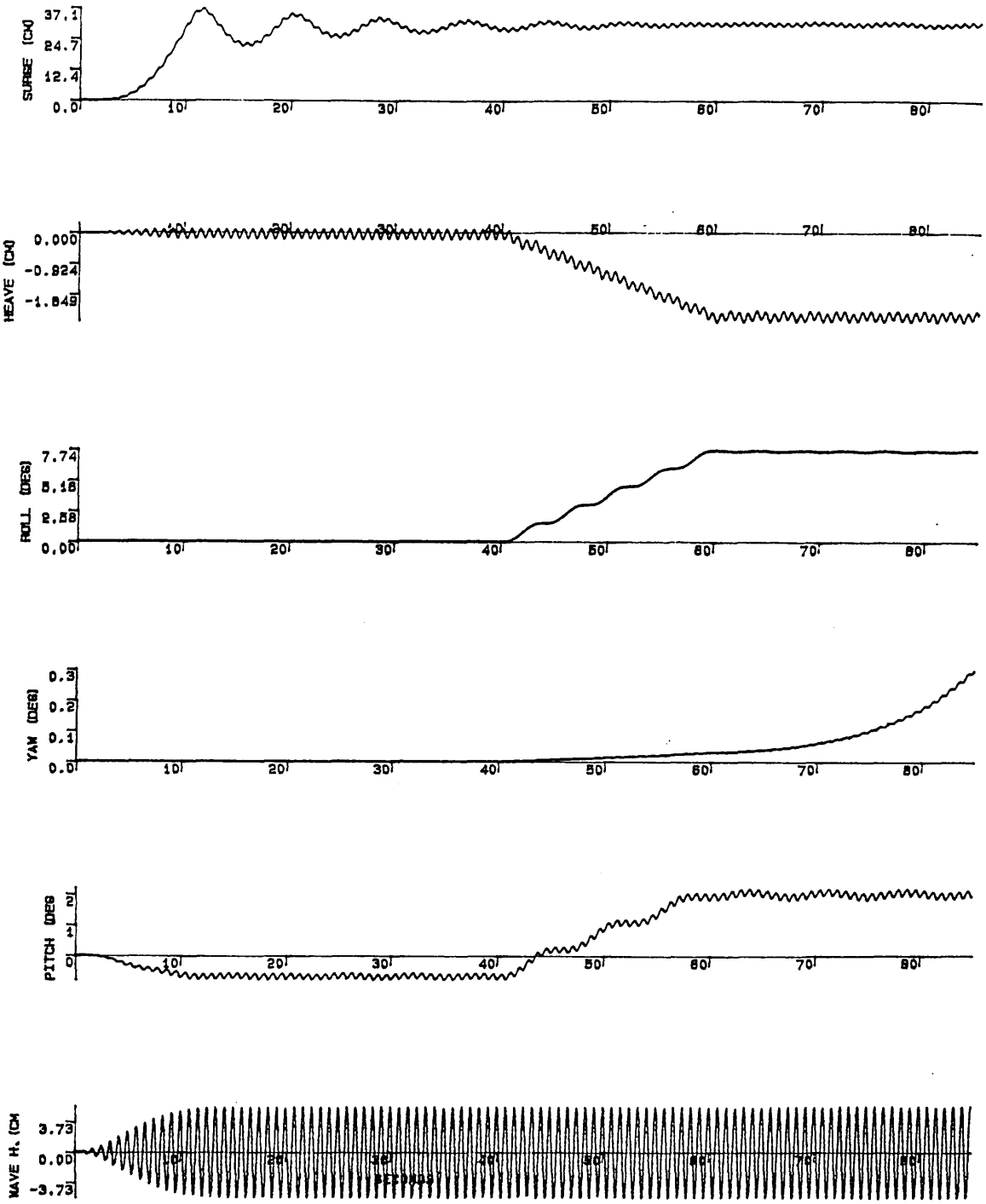

Fig.5.30 Motion response simulation (Head sea condition-asymmetrical flooding)
WH=11.2 cm Flooding Mass=1.5 kg Flooding Time=20 s
GM=7.81 cm ω=7.5 r/s (1.2 hertz)

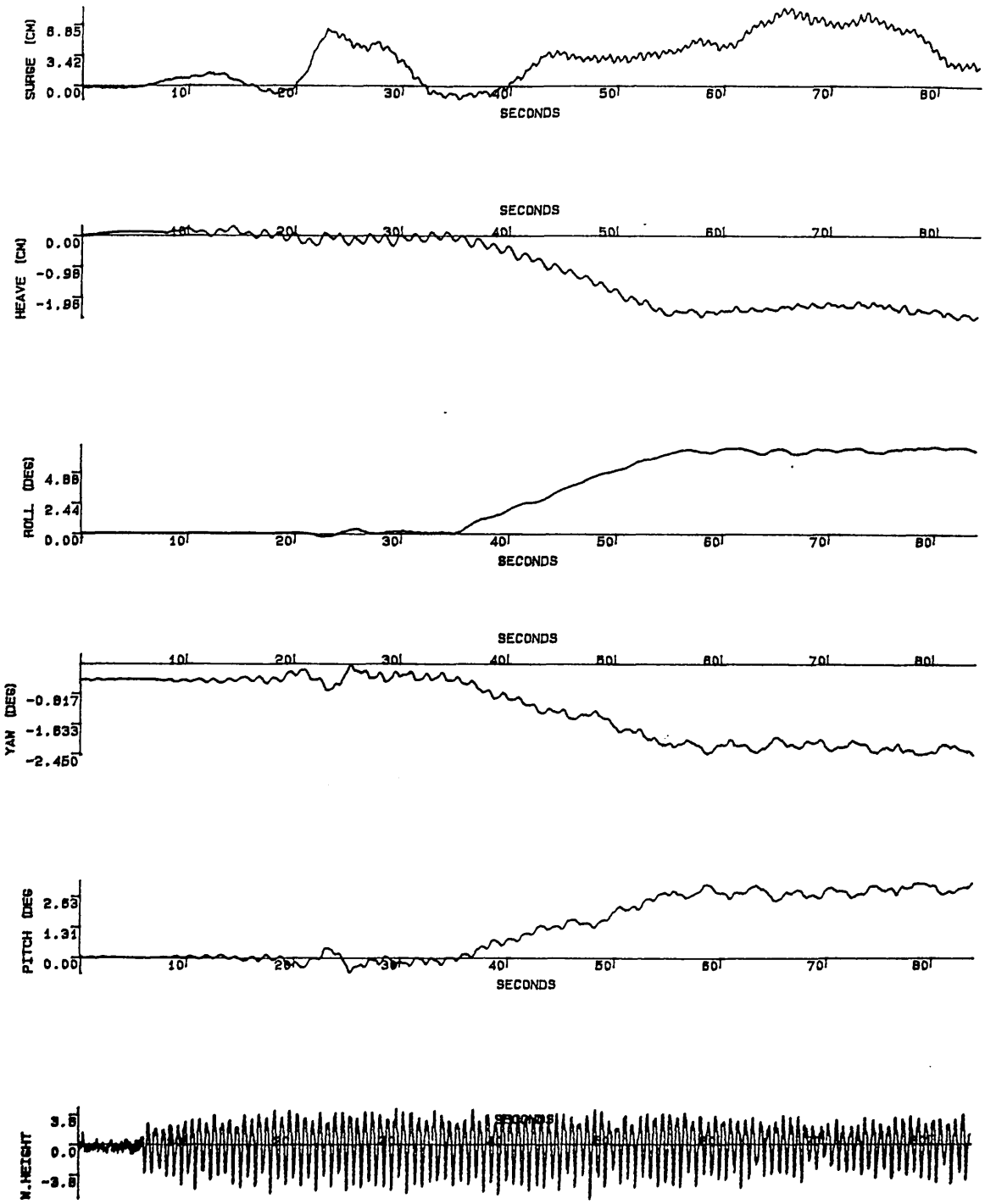

Fig.5.31 Motion response experiment (Head sea condition-asymmetrical flooding)

WH=8.8 cm Flooding Mass=1.7 kg Flooding Time=20 s

GM=7.81 cm ω=8.8 r/s (1.4 hertz) TS2927S.DAT

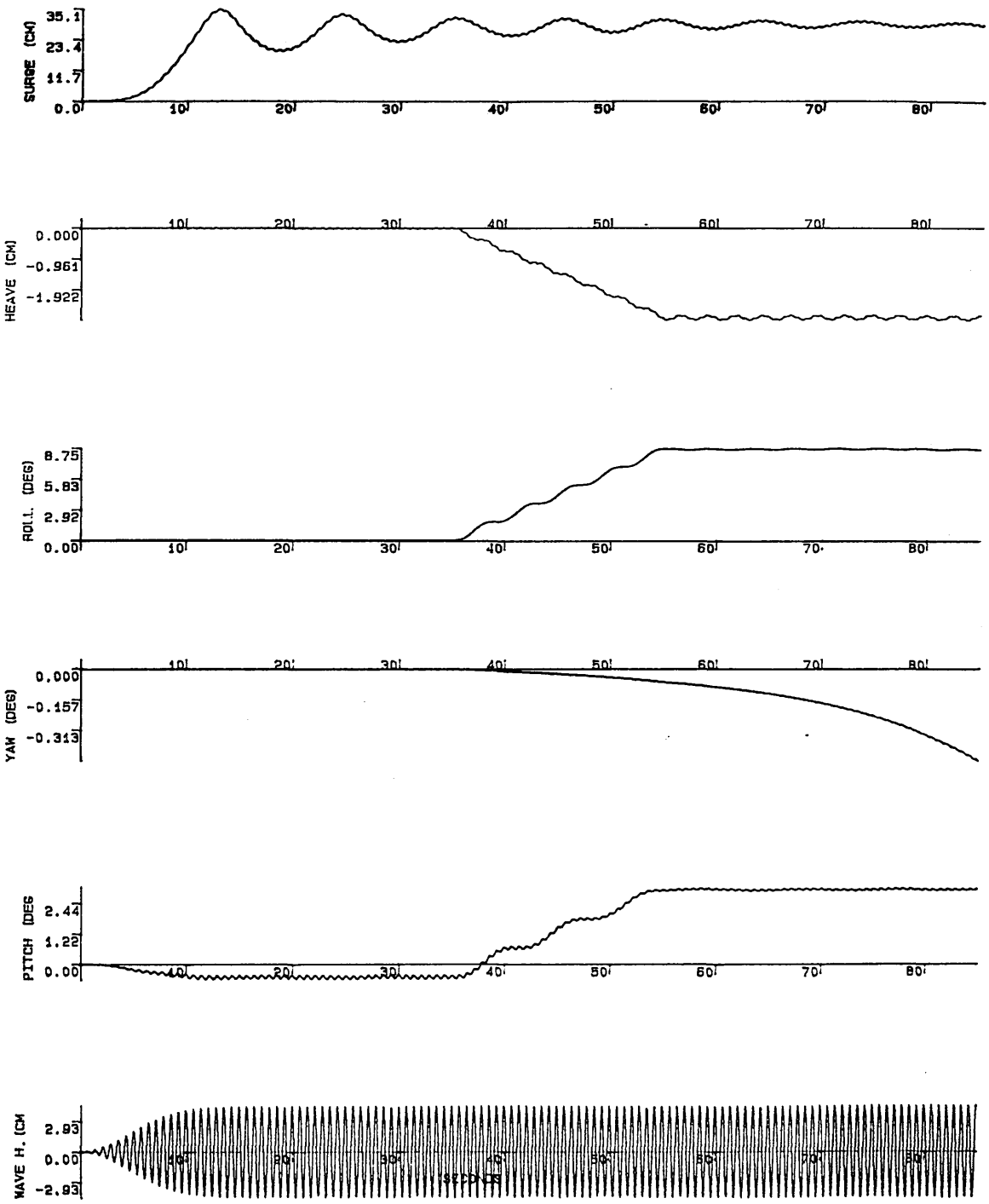

Fig.5.32 Motion response simulation (Head sea condition-asymmetrical flooding)
WH=8.8 cm Flooding Mass=1.7 kg Flooding Time=20 s
GM=7.81 cm ω=8.8 r/s (1.4 hertz)

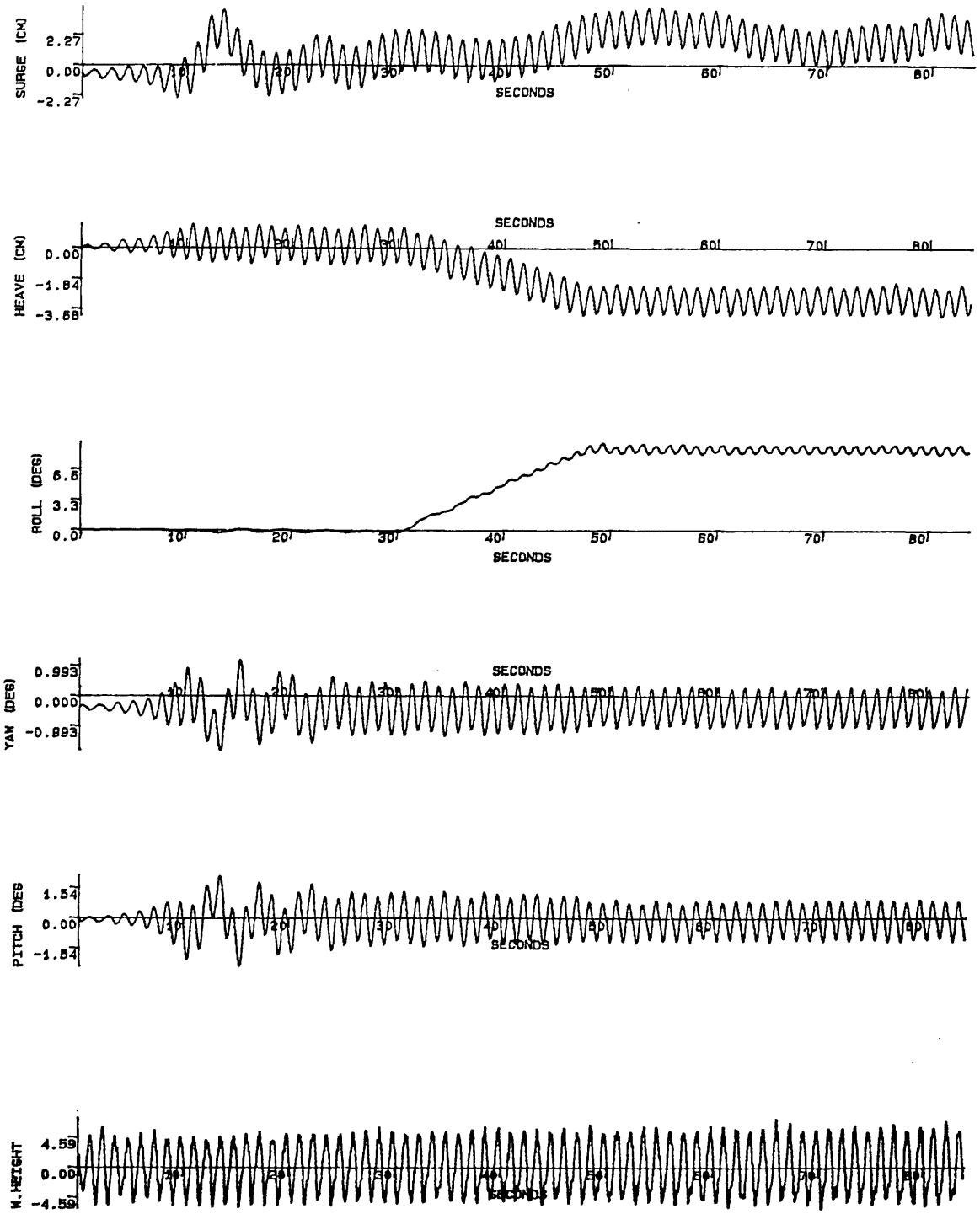

Fig.5.33 Motion response experiment (Head sea condition-symmetrical flooding)
WH=11.6 cm Flooding Mass=2.2 kg Flooding Time=20 s
GM=7.81 cm ω=5.0 r/s (0.8 hertz) TS2928S.DAT

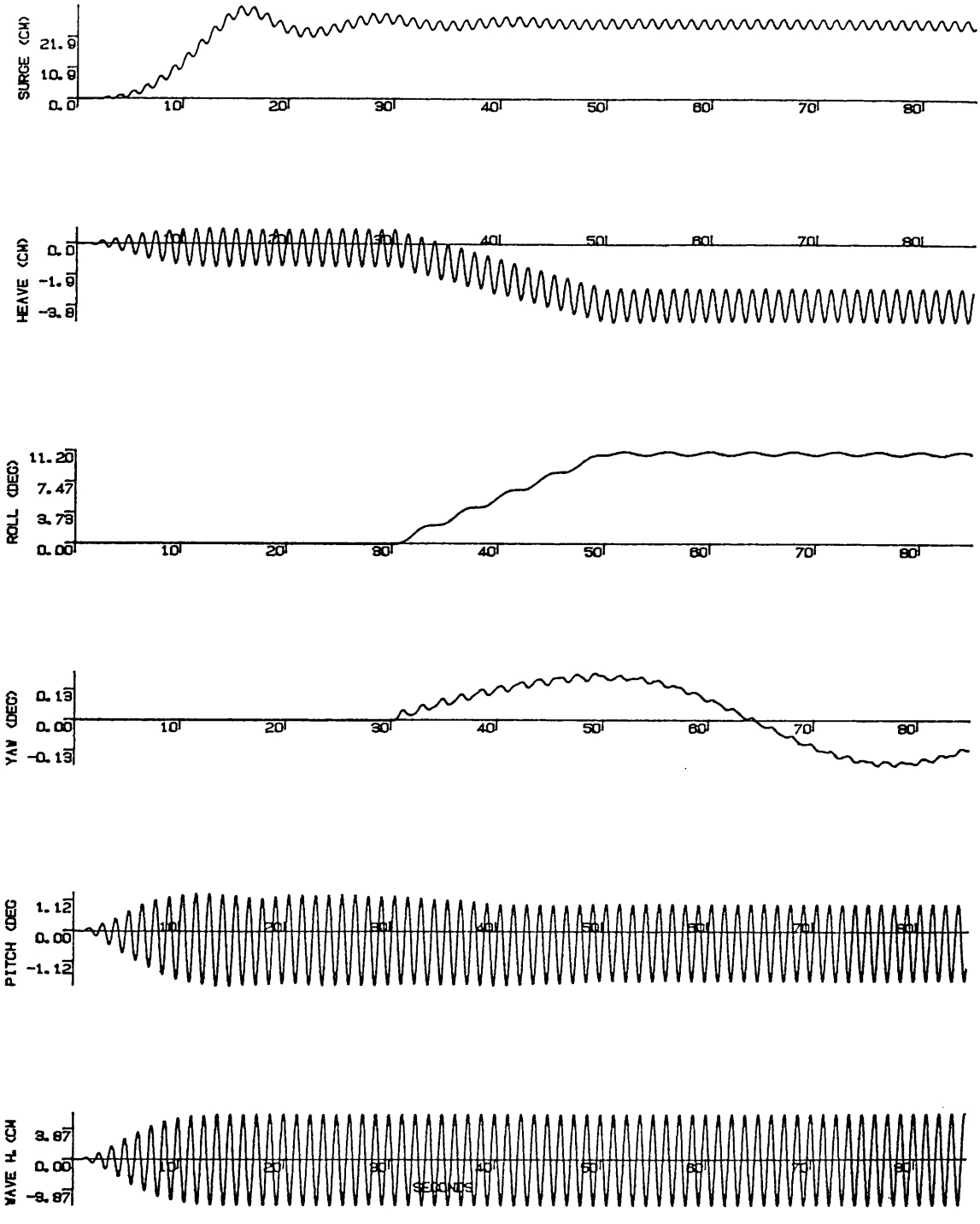

Fig.5.34 Motion response simulation (Head sea condition-symmetrical flooding)
WH=11.6 cm Flooding Mass=2.2 kg Flooding Time=20 s
GM=7.81 cm ω=5.0 r/s (0.8 hertz)

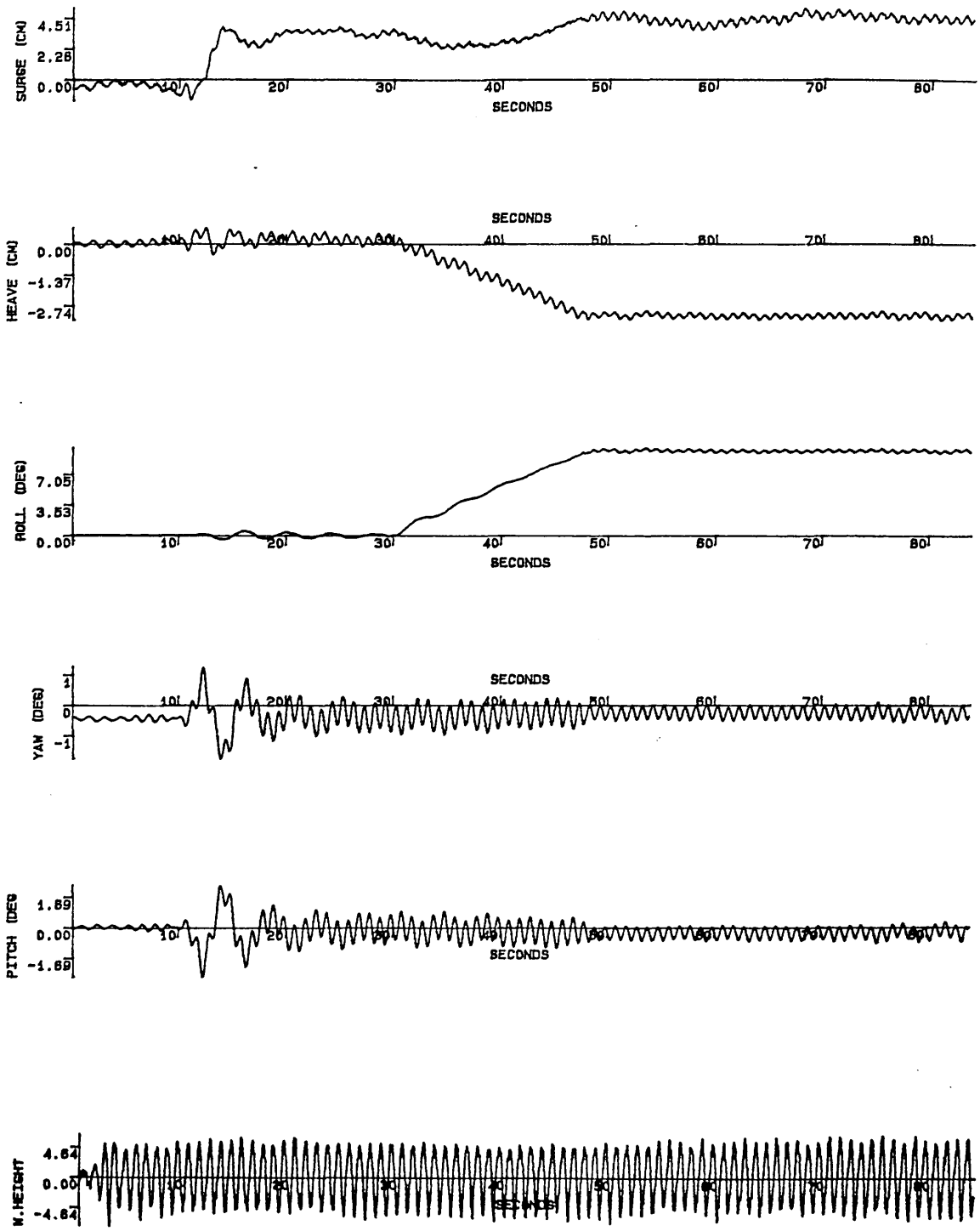

Fig.5.35 Motion response experiment (Head sea condition-symmetrical flooding)

WH=11.7 cm	Flooding Mass=2.1 kg	Flooding Time=20 s
GM=7.81 cm	ω=6.3 r/s (1.0 hertz)	TS2929S.DAT

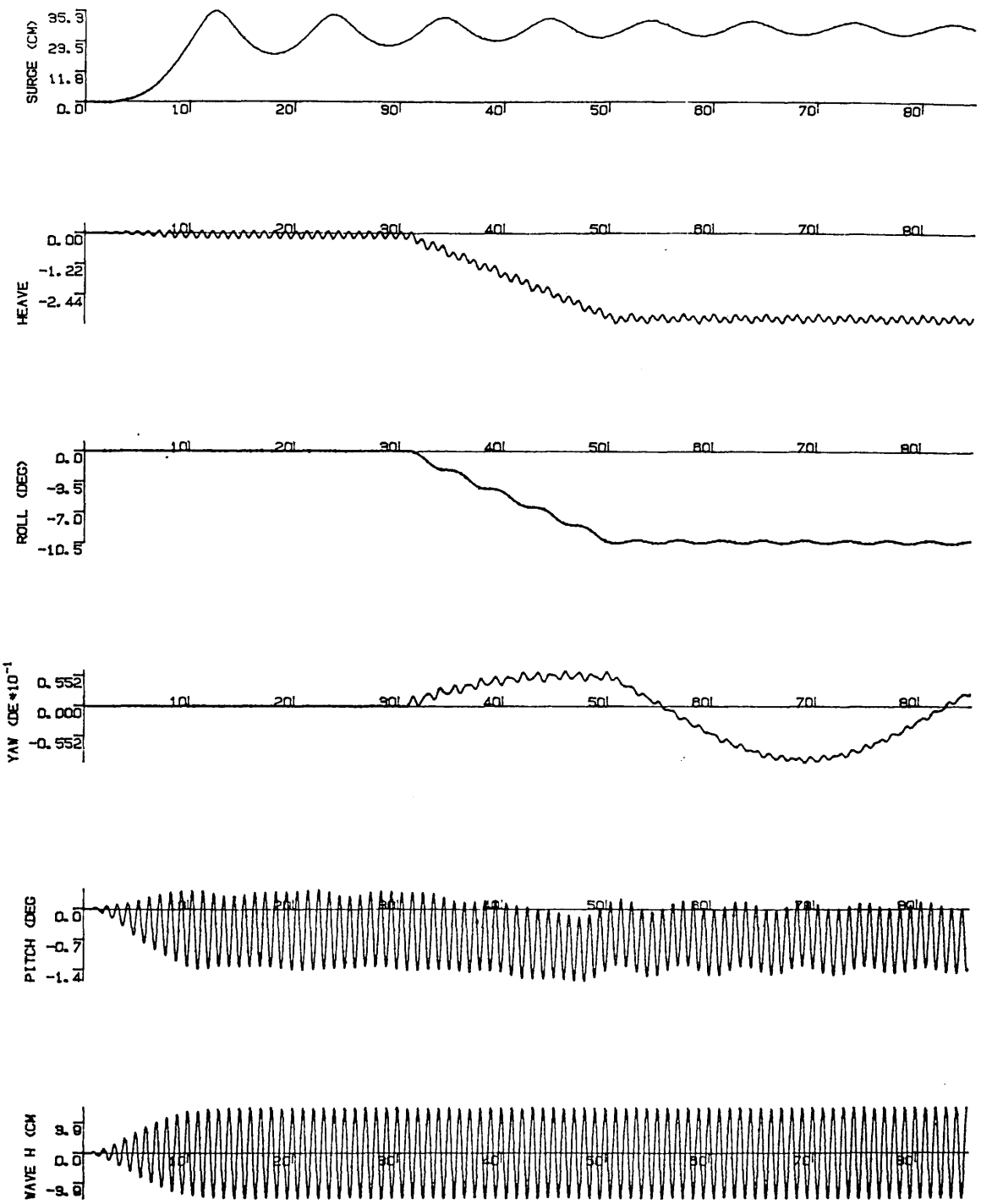

Fig.5.36 Motion response simulation (Head sea condition-symmetrical flooding)
WH=11.7 cm Flooding Mass=2.1 kg Flooding Time=20 s
GM=7.81 cm ω=6.3 r/s (1.0 hertz)

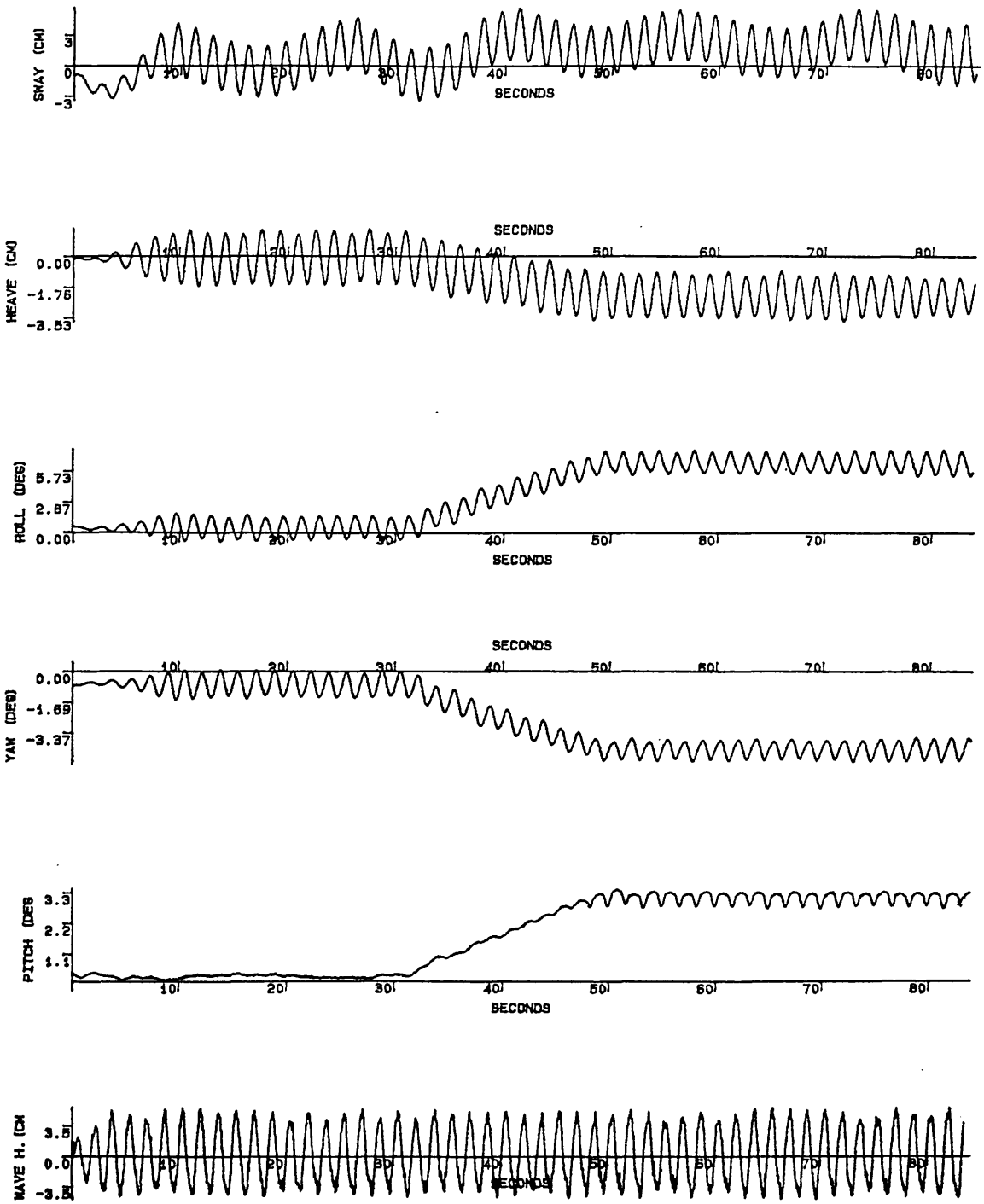

Fig.5.37 Motion response experiment (Beam sea condition-asymmetrical flooding)
WH=9.6 cm Flooding Mass=1.2 kg Flooding Time=20 s
GM=7.81 cm ω=3.8 r/s (0.6 hertz) TS2931S.DAT

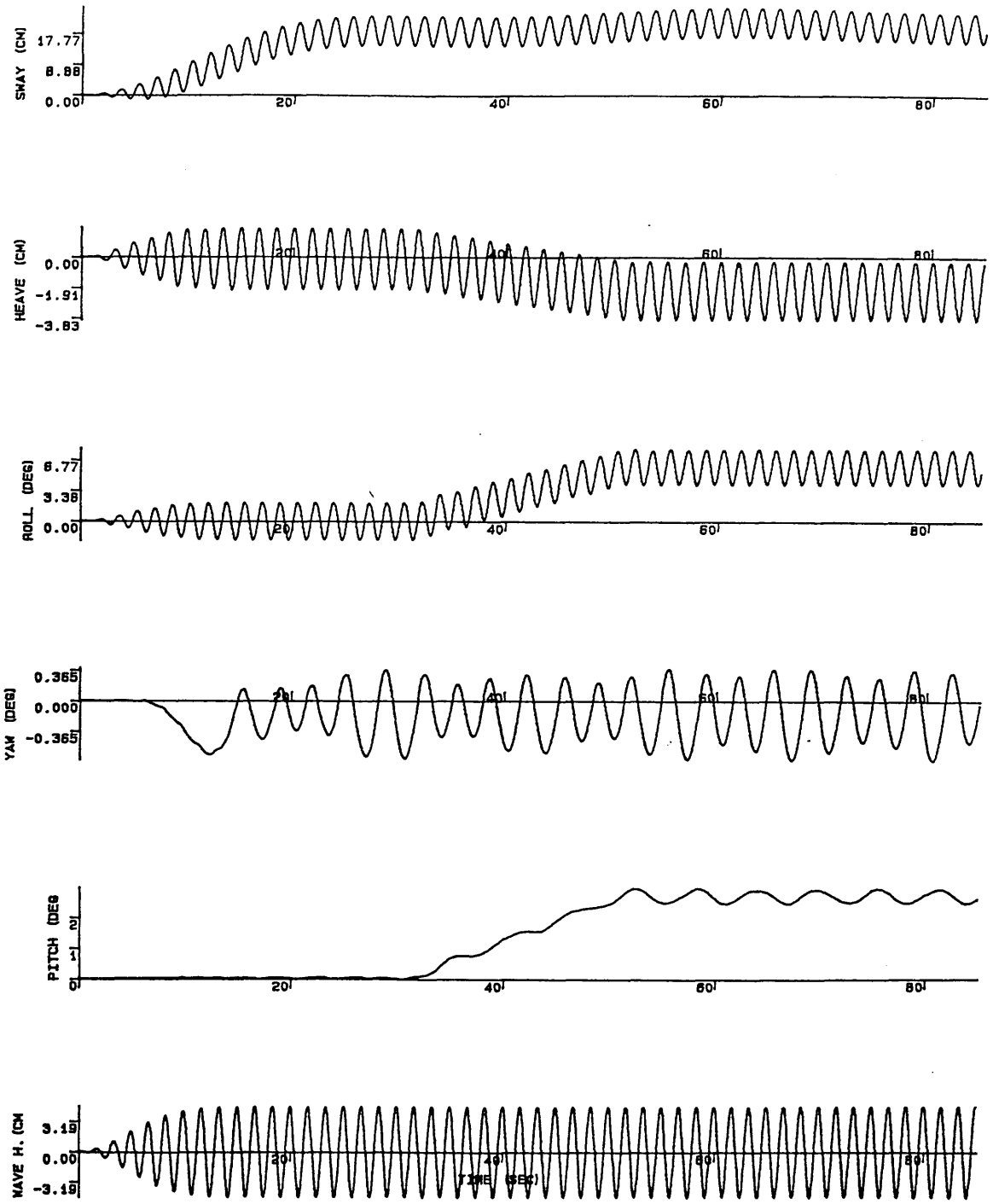

Fig.5.38 Motion response simulation (Beam sea condition-asymmetrical flooding)
WH=9.6 cm Flooding Mass=1.2 kg Flooding Time=20 s
GM=7.81 cm ω=3.8 r/s (0.6 hertz)

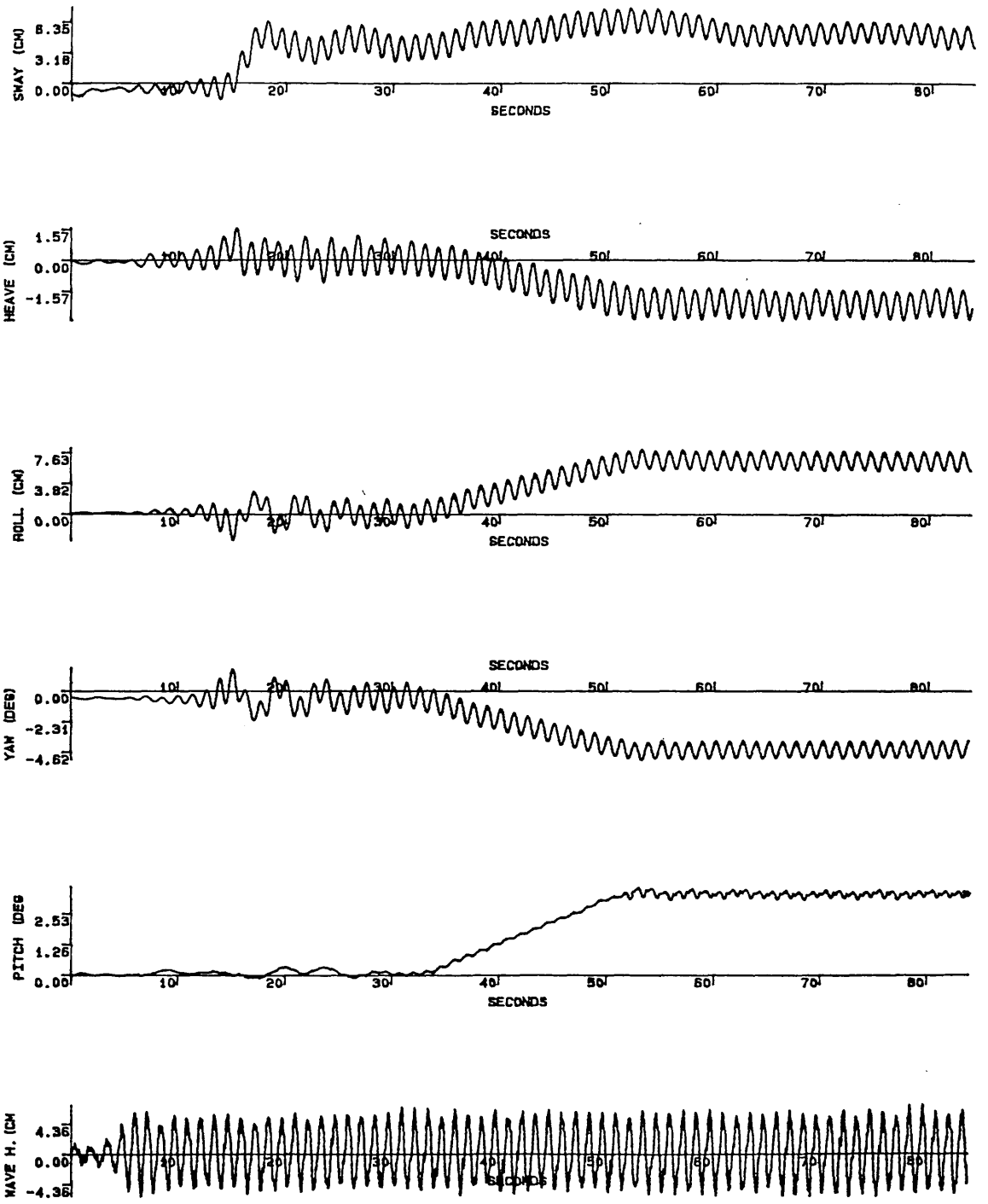

Fig.5.39 Motion response experiment (Beam sea condition-asymmetrical flooding)
WH=10.1 cm Flooding Mass=1.2 kg Flooding Time=20 s
GM=7.81 cm ω=5.0 r/s (0.8 hertz) TS2932S.DAT

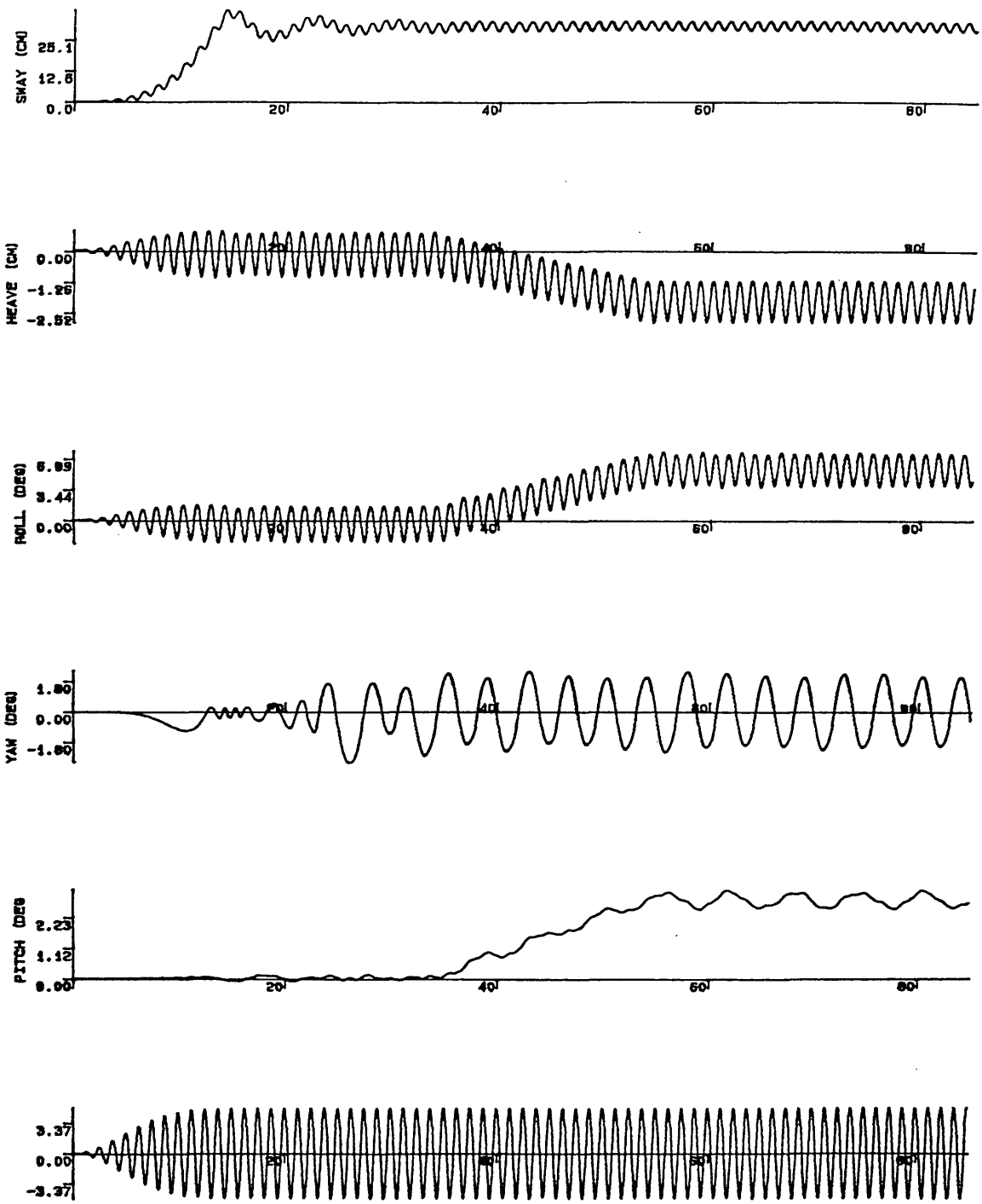

Fig.5.40 Motion response simulation (Beam sea condition-asymmetrical flooding)
WH=10.1 cm Flooding Mass=1.2 kg Flooding Time=20 s
GM=7.81 cm ω=5.0 r/s (0.8 hertz)

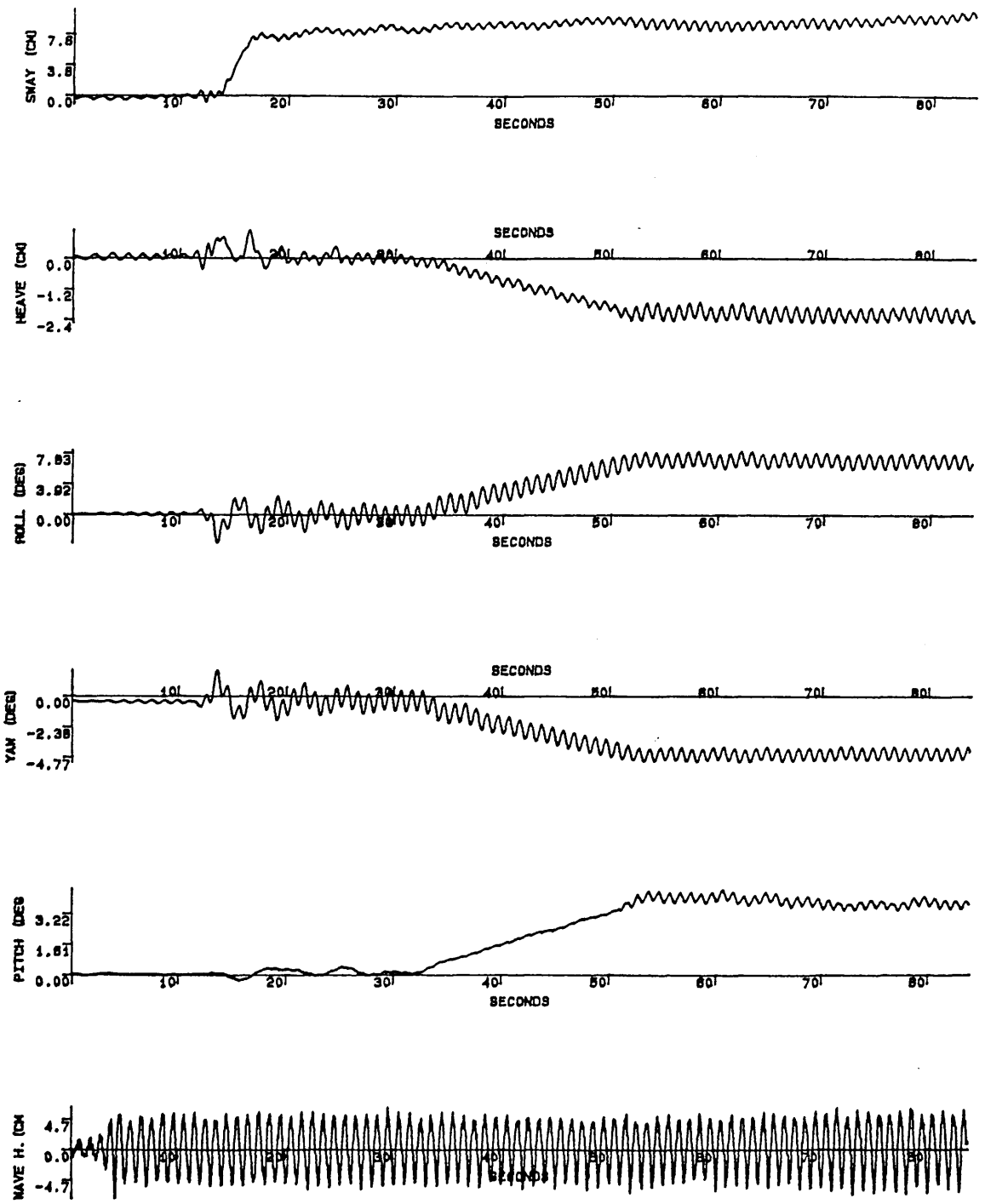

Fig.5.41 Motion response experiment (Beam sea condition-asymmetrical flooding)

WH=11.4 cm	Flooding Mass=1.2 kg	Flooding Time=20 s
GM=7.81 cm	ω=6.3 r/s (1.0 hertz)	TS2933S.DAT

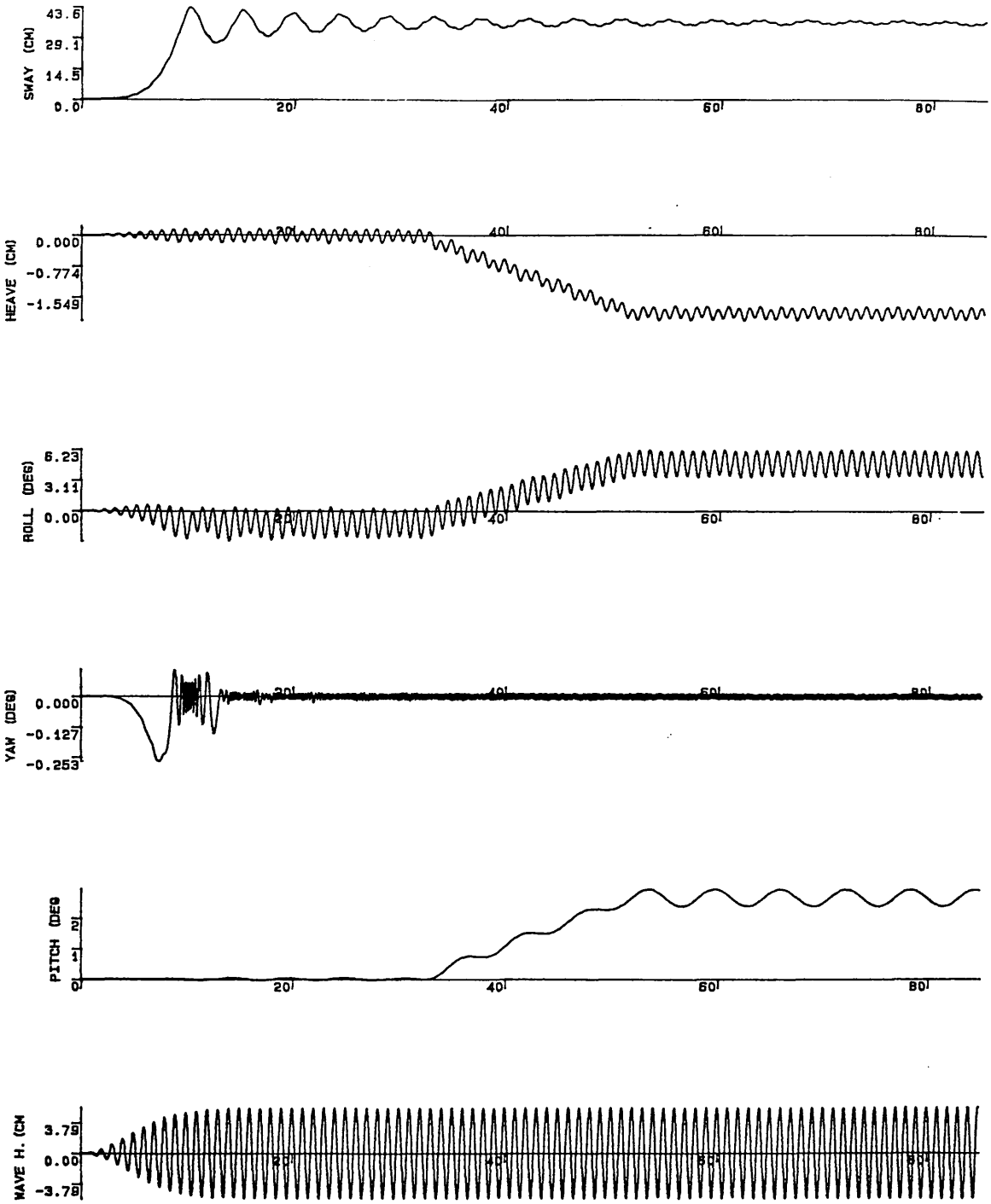

Fig.5.42 Motion response simulation (Beam sea condition-asymmetrical flooding)
WH=11.4 cm Flooding Mass=1.2 kg Flooding Time=20 s
GM=7.81 cm ω=6.3 r/s (1.0 hertz)

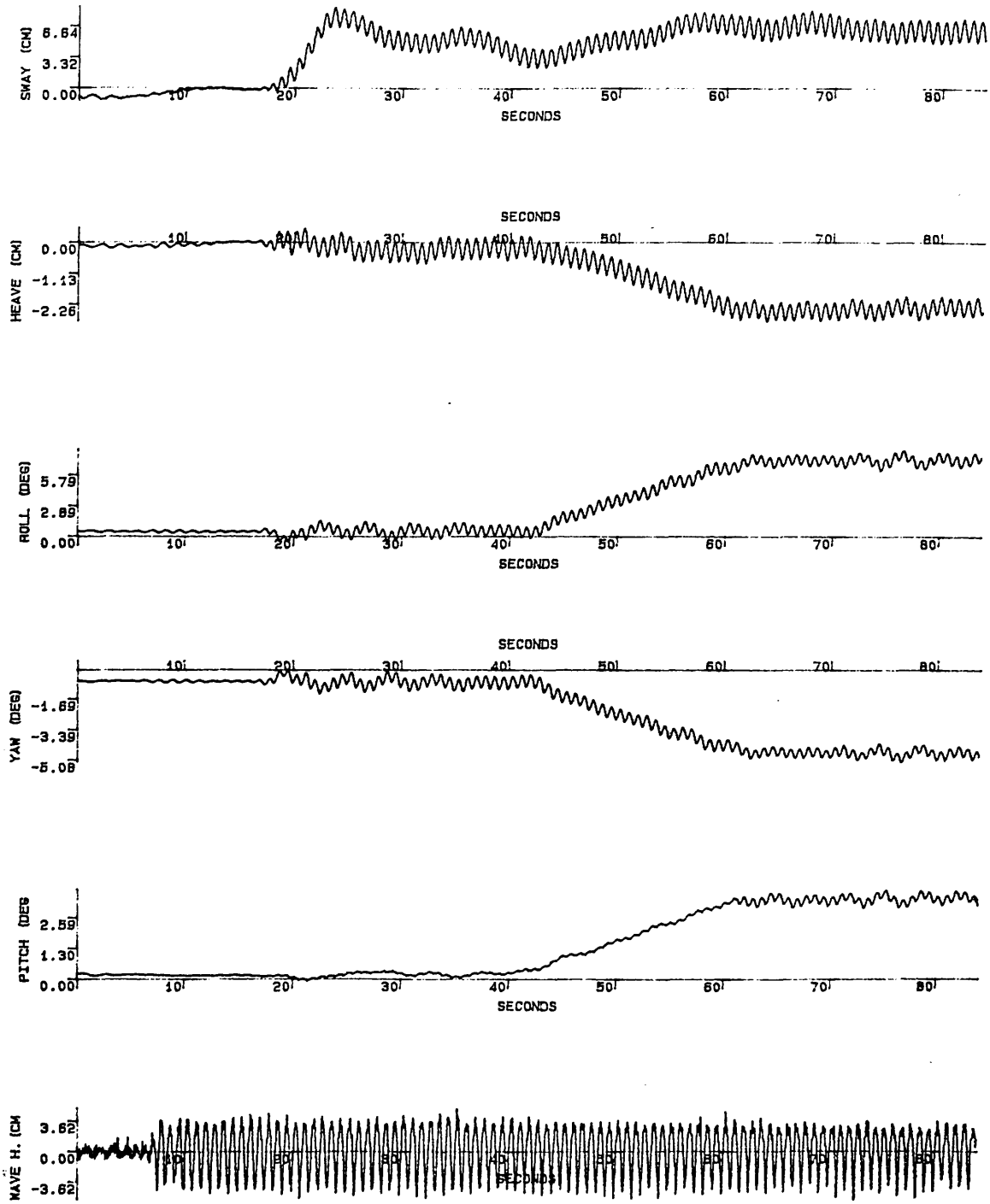

Fig.5.43 Motion response experiment (Beam sea condition-asymmetrical flooding)

WH=8.8 cm	Flooding Mass=1.3 kg	Flooding Time=20 s
GM=7.81 cm	ω=7.5 r/s (1.2 hertz)	TS2934S.DAT

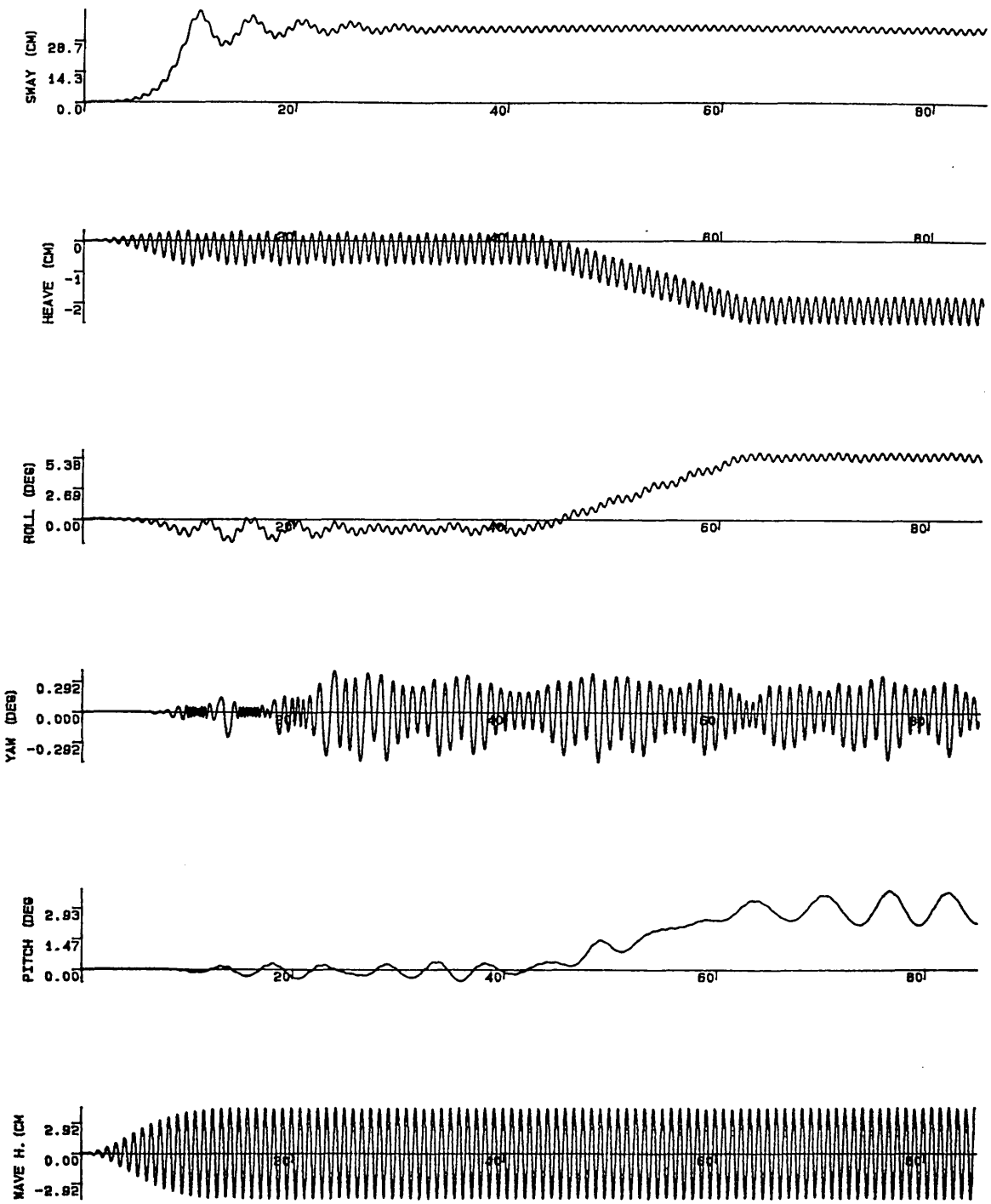

Fig.5.44 Motion response simulation (Beam sea condition-asymmetrical flooding)
WH=8.8 cm Flooding Mass=1.3 kg Flooding Time=20 s
GM=7.81 cm ω=7.5 r/s (1.2 hertz)

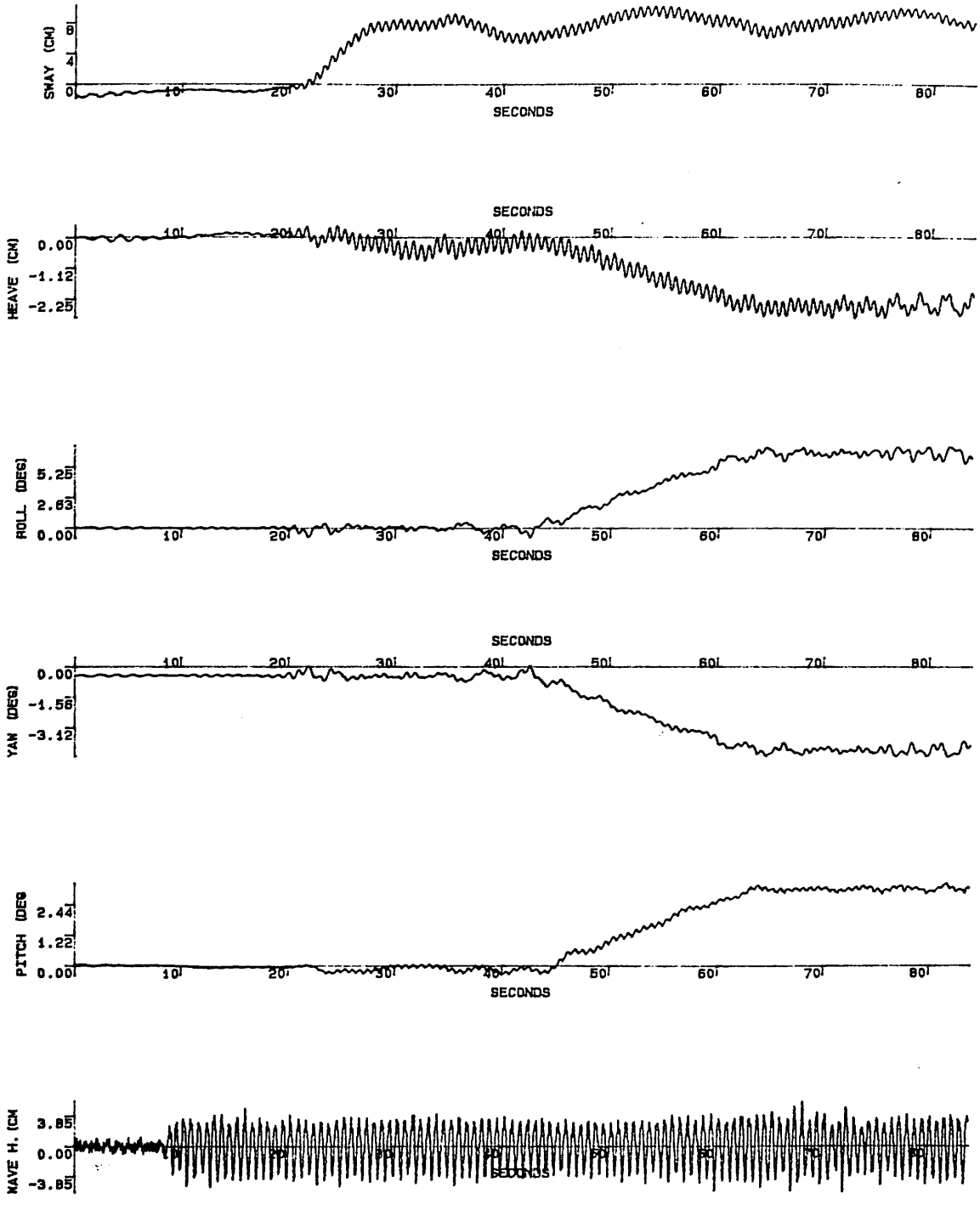

Fig.5.45 Motion response experiment (Beam sea condition-asymmetrical flooding)

WH=8.1 cm	Flooding Mass=1.4 kg	Flooding Time=20 s
GM=7.81 cm	ω=8.8 r/s (1.4 hertz)	TS2935S.DAT

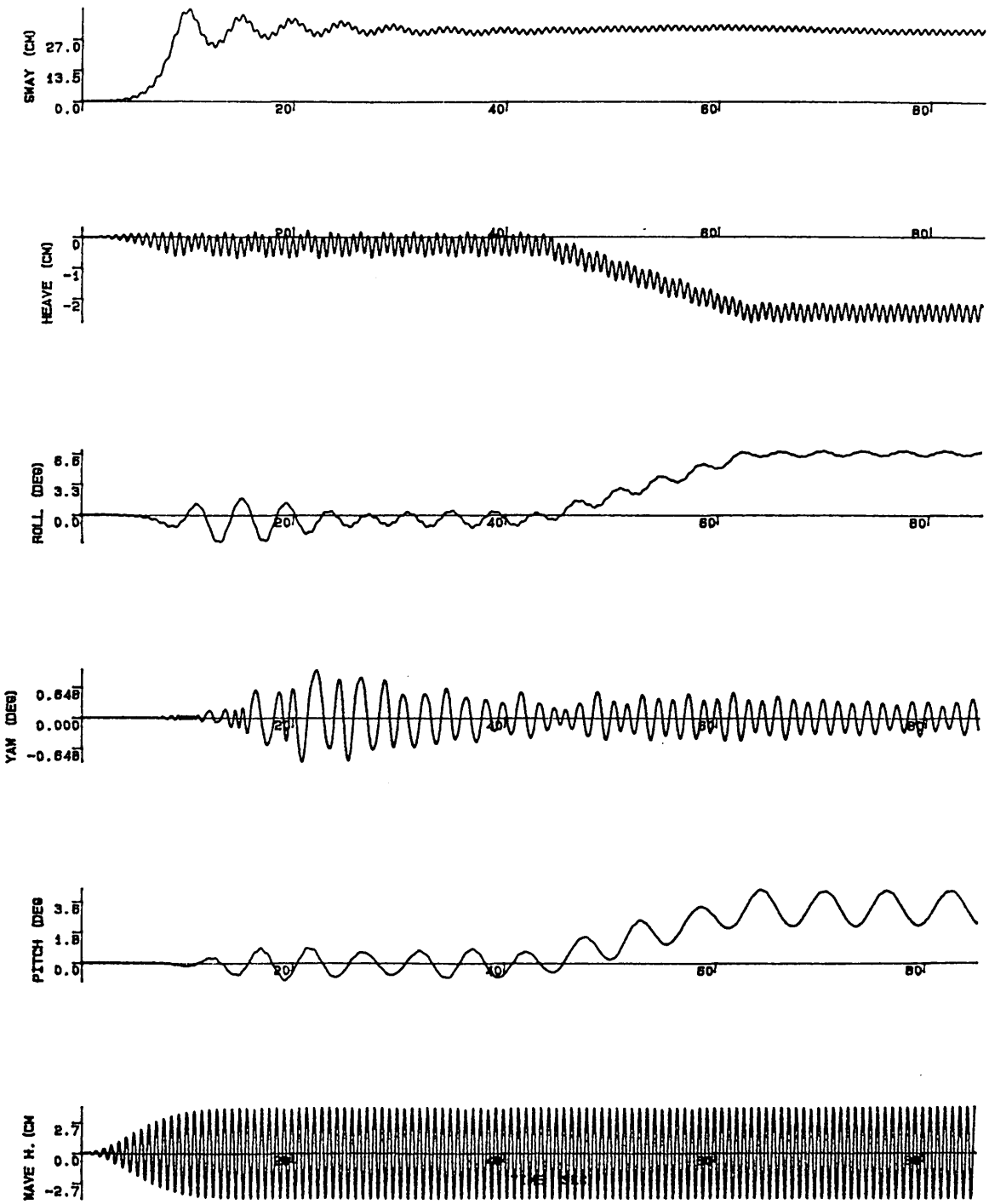

Fig.5.46 Motion response simulation (Beam sea condition-asymmetrical flooding)
WH=8.1 cm Flooding Mass=1.4 kg Flooding Time=20 s
GM=7.81 cm ω=8.8 r/s (1.4 hertz)

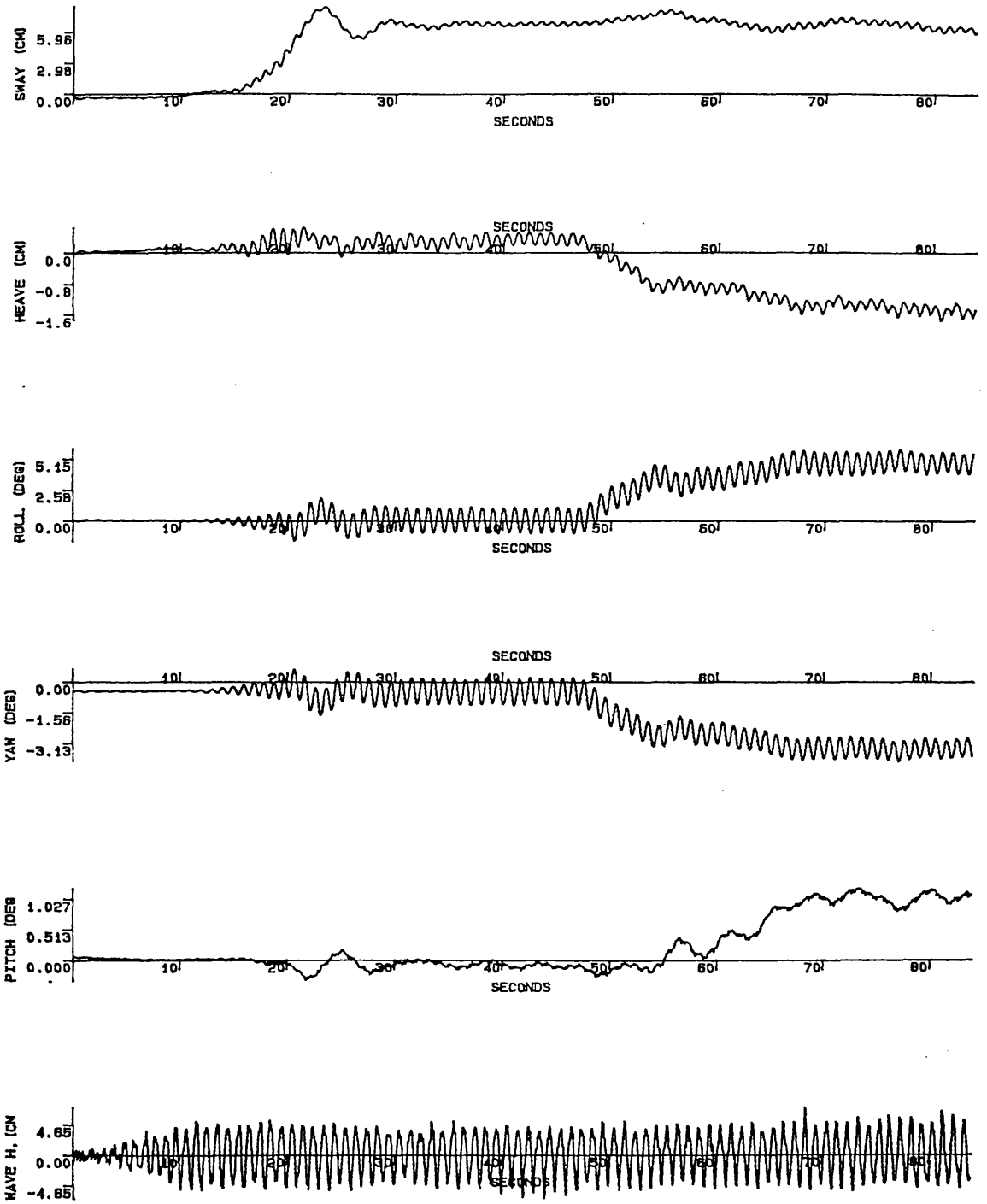

Fig.5.47 Motion response experiment (Beam sea condition-symmetrical flooding)

WH=9.8 cm	Flooding Mass=0.9 kg	Flooding Time=10 s
GM=7.81 cm	ω=6.3 r/s (1.0 hertz)	TS2939S.DAT

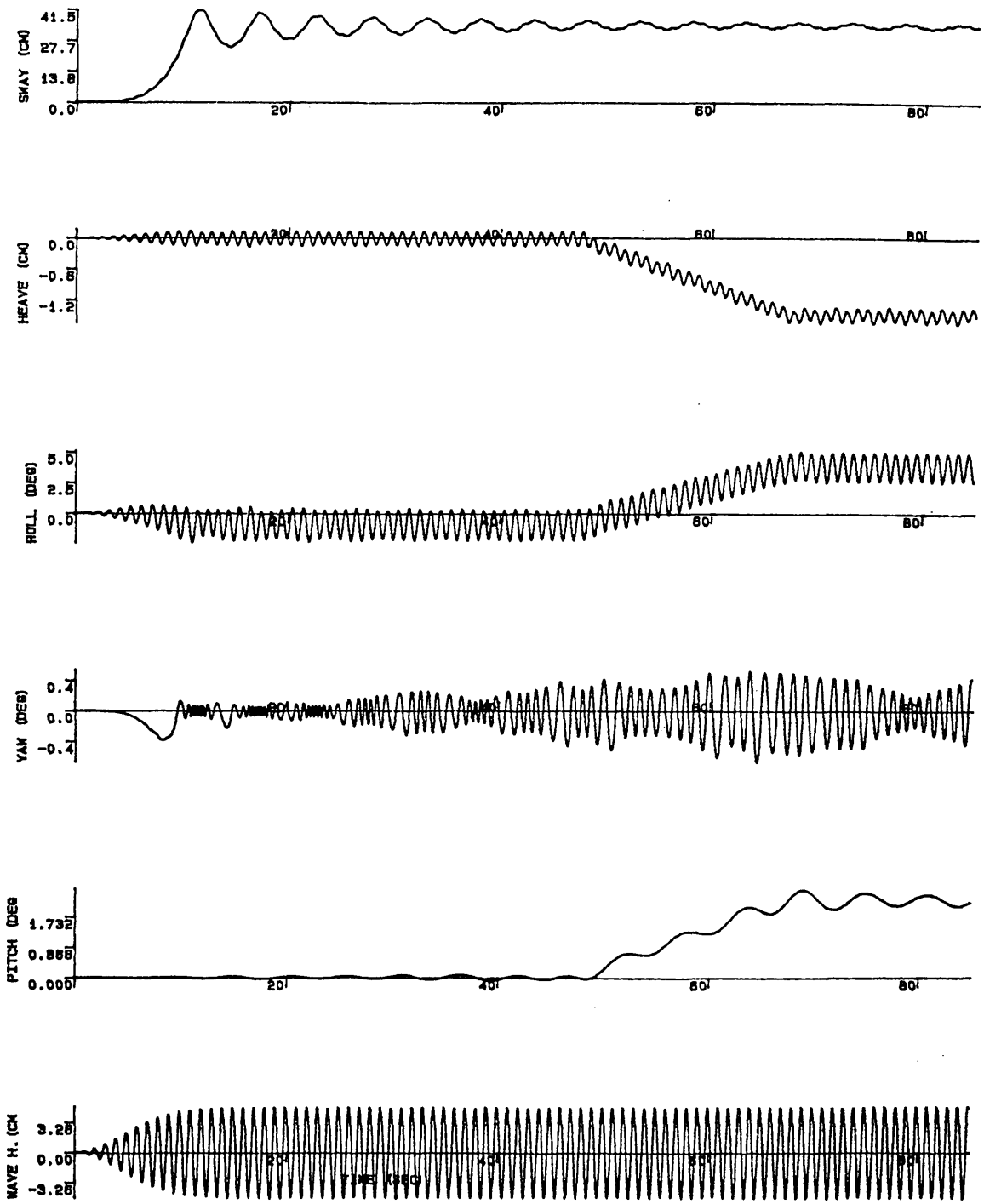

Fig.5.48 Motion response simulation (Beam sea condition-symmetrical flooding)
WH=9.8 cm Flooding Mass=0.9 kg Flooding Time=10 s
GM=7.81 cm ω=6.3 r/s (1.0 hertz)

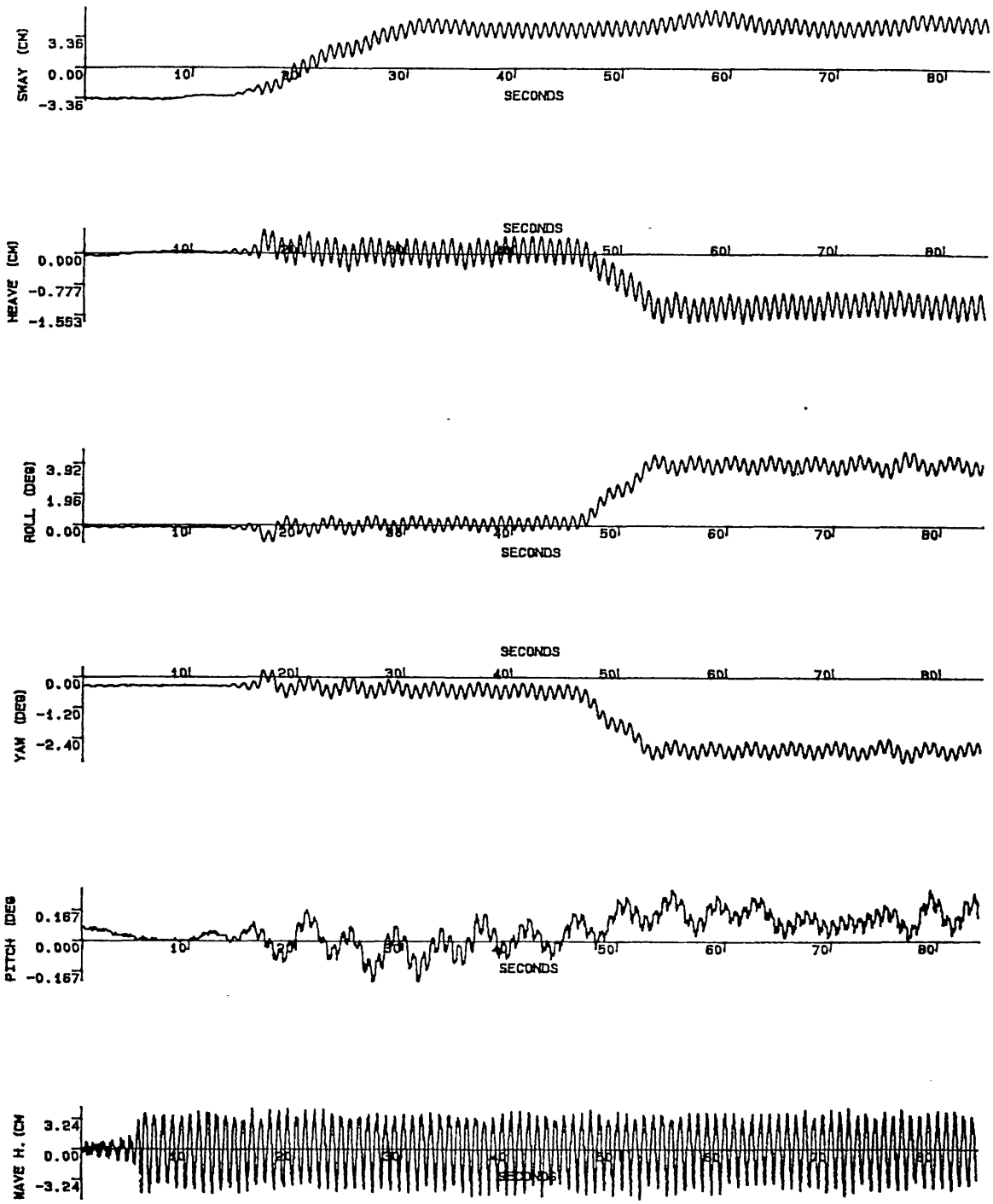

Fig.5.49 Motion response experiment (Beam sea condition-symmetrical flooding)
WH=8.2 cm Flooding Mass=0.9 kg Flooding Time=10 s
GM=7.81 cm ω=7.5 r/s (1.2 hertz) TS2940S.DAT

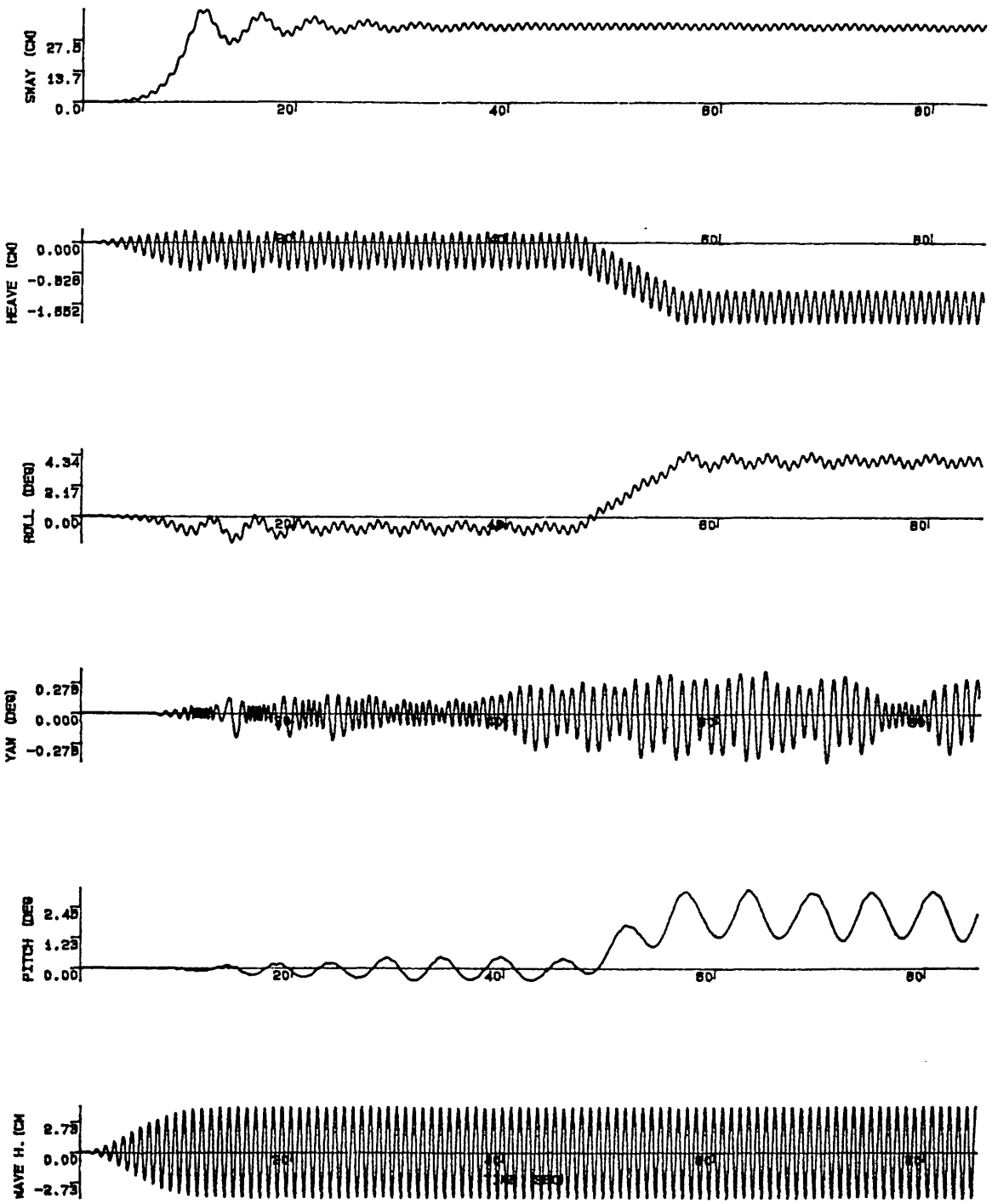

Fig.5.50 Motion response simulation (Beam sea condition-symmetrical flooding)
WH=8.2 cm Flooding Mass=0.9 kg Flooding Time=10 s
GM=7.81 cm ω=7.5 r/s (1.2 hertz)

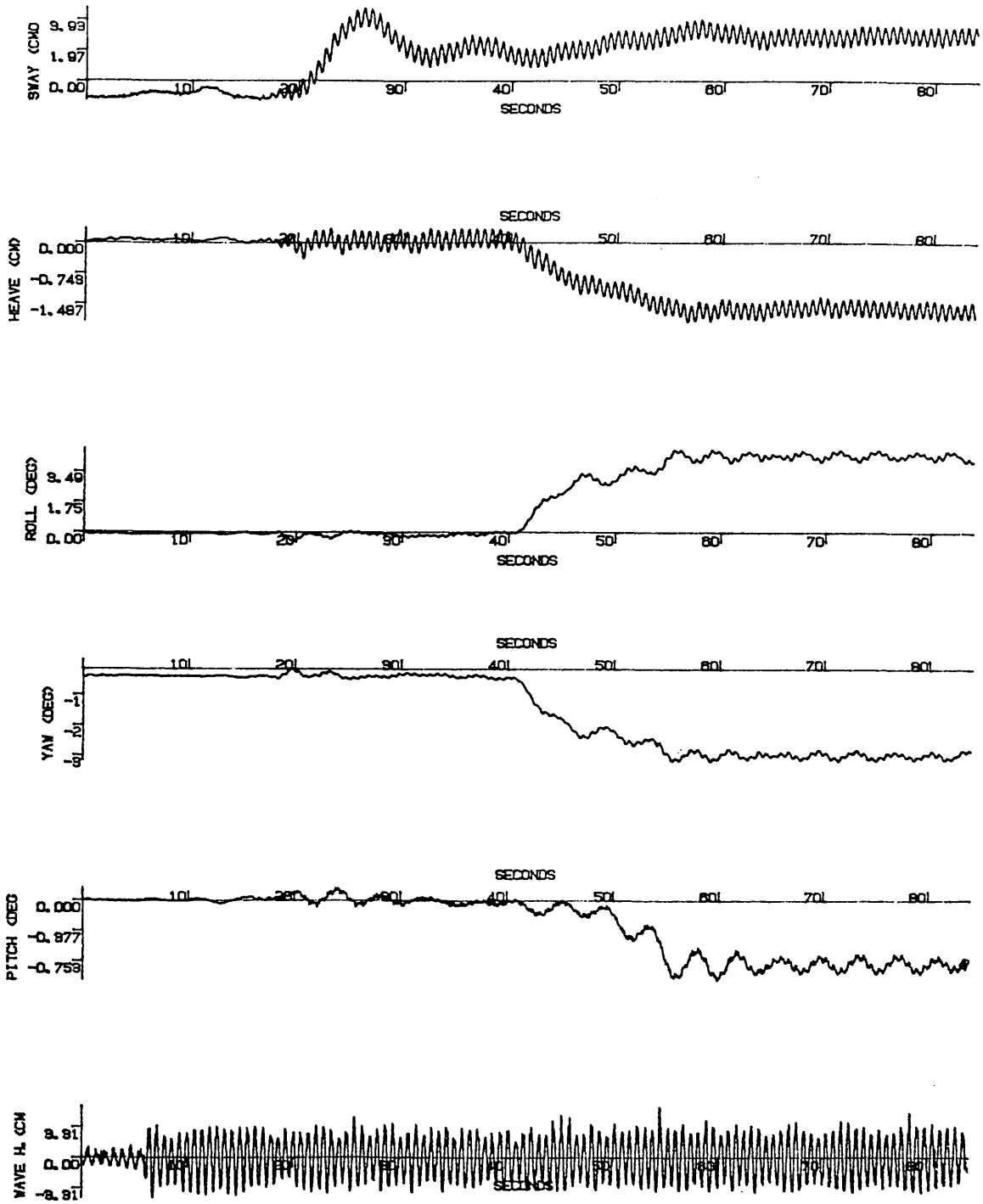

Fig.5.51 Motion response experiment (Beam sea condition-symmetrical flooding)

WH=7.0 cm	Flooding Mass=0.9 kg	Flooding Time=10 s
GM=7.81 cm	ω=8.8 r/s (1.4 hertz)	TS2941S.DAT

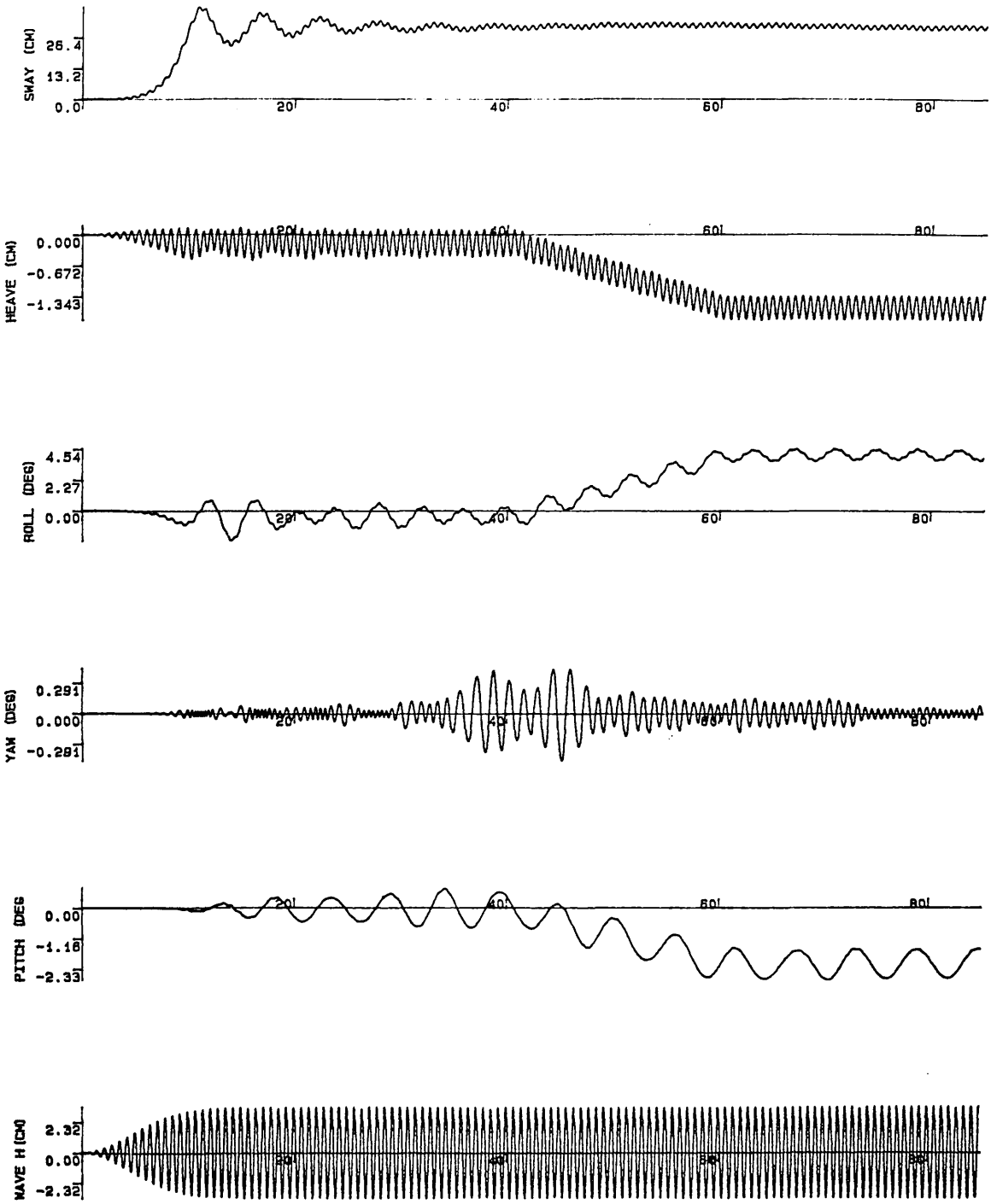

Fig.5.52 Motion response simulation (Beam sea condition-symmetrical flooding)
WH=7.0 cm Flooding Mass=0.9 kg Flooding Time=10 s
GM=7.81 cm ω=8.8 r/s (1.4 hertz)

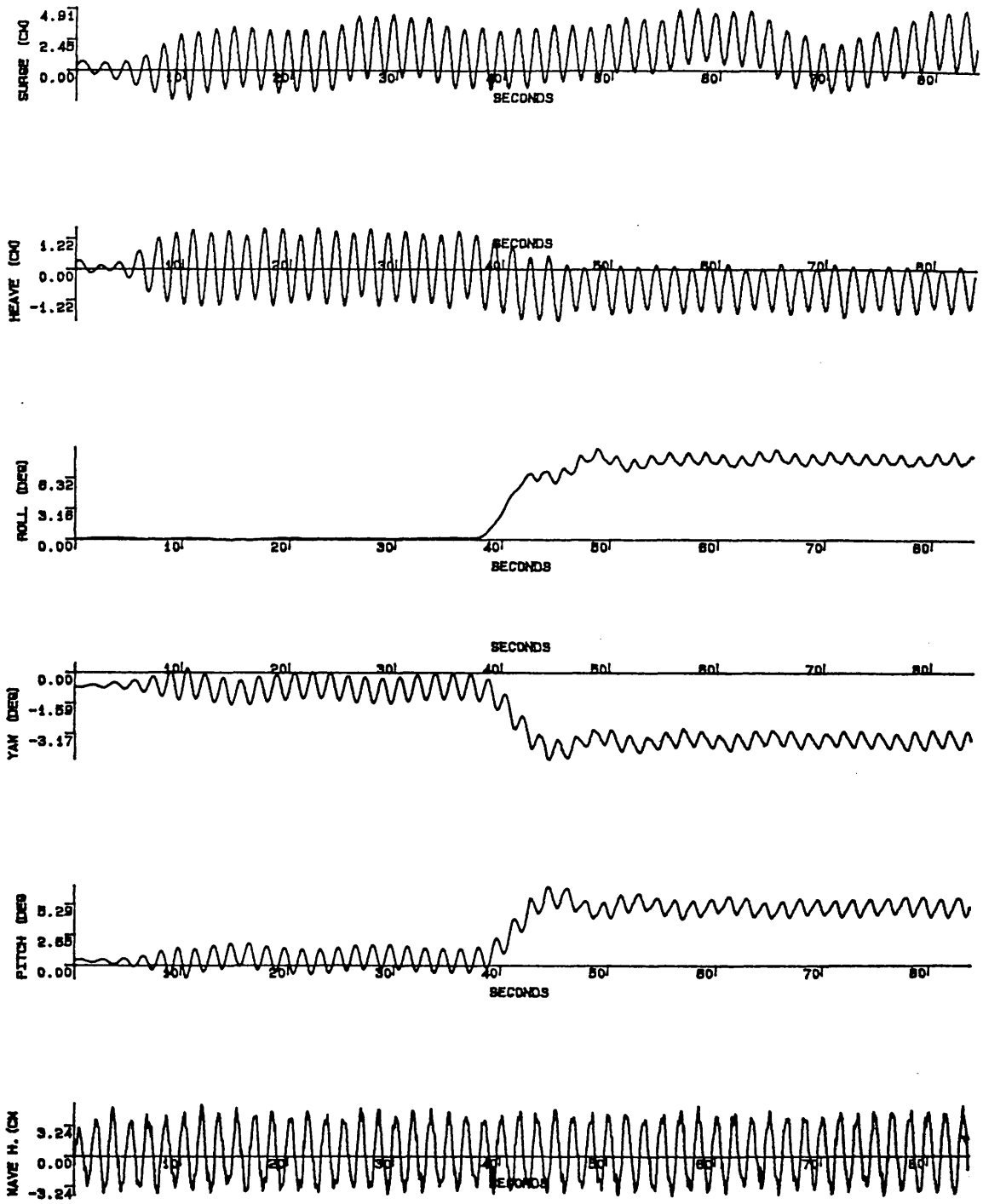

Fig.5.53 Motion response experiment (Head sea condition-asymmetrical flooding)
WH=8.2 cm Flooding Mass=0.6 kg Flooding Time=10 s
GM=2.29 cm ω=3.8 r/s (0.6 hertz) TS2957S.DAT

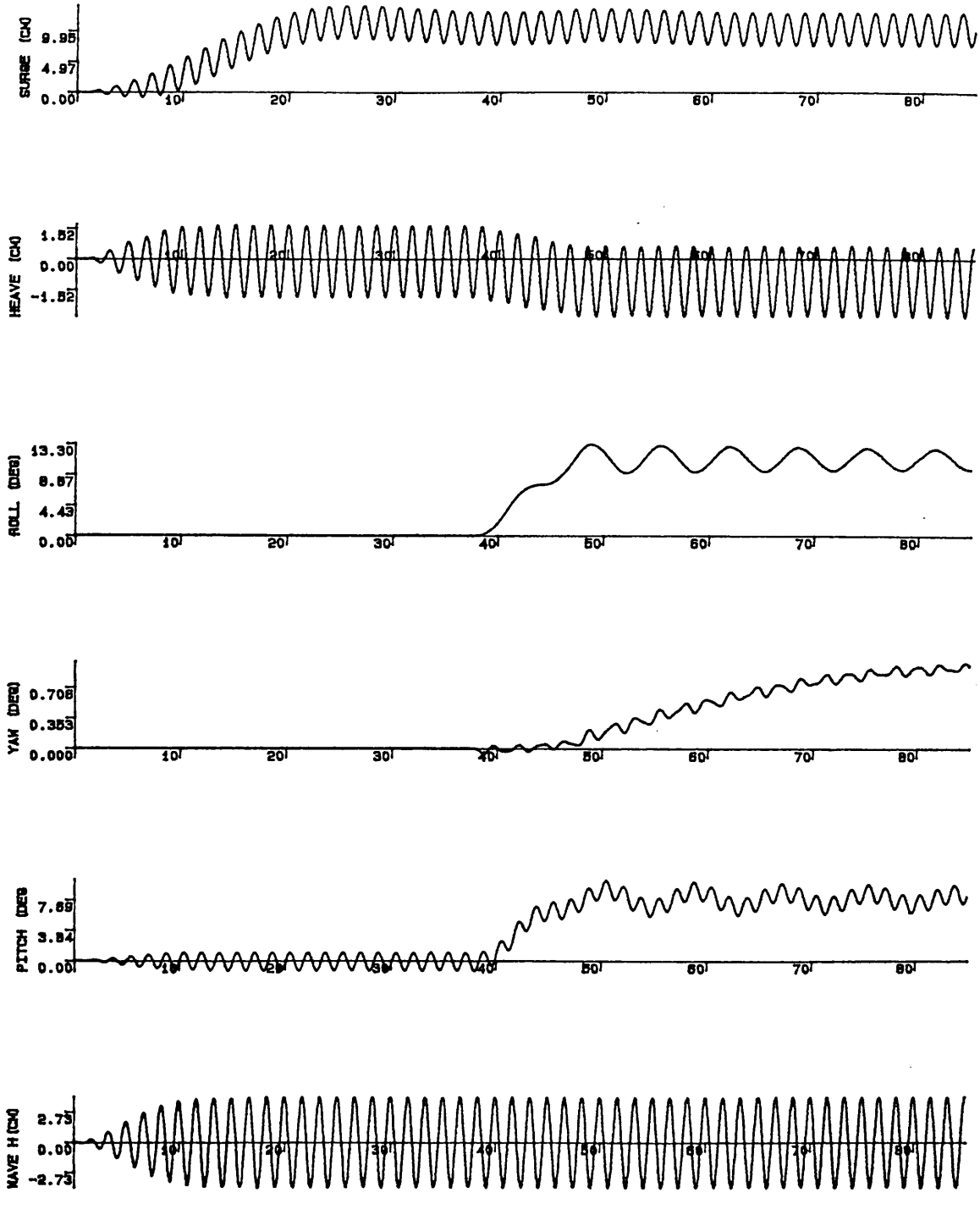

Fig.5.54 Motion response simulation (Head sea condition-asymmetrical flooding)
WH=8.2 cm Flooding Mass=0.6 kg Flooding Time=10 s
GM=2.29 cm ω=3.8 r/s (0.6 hertz)

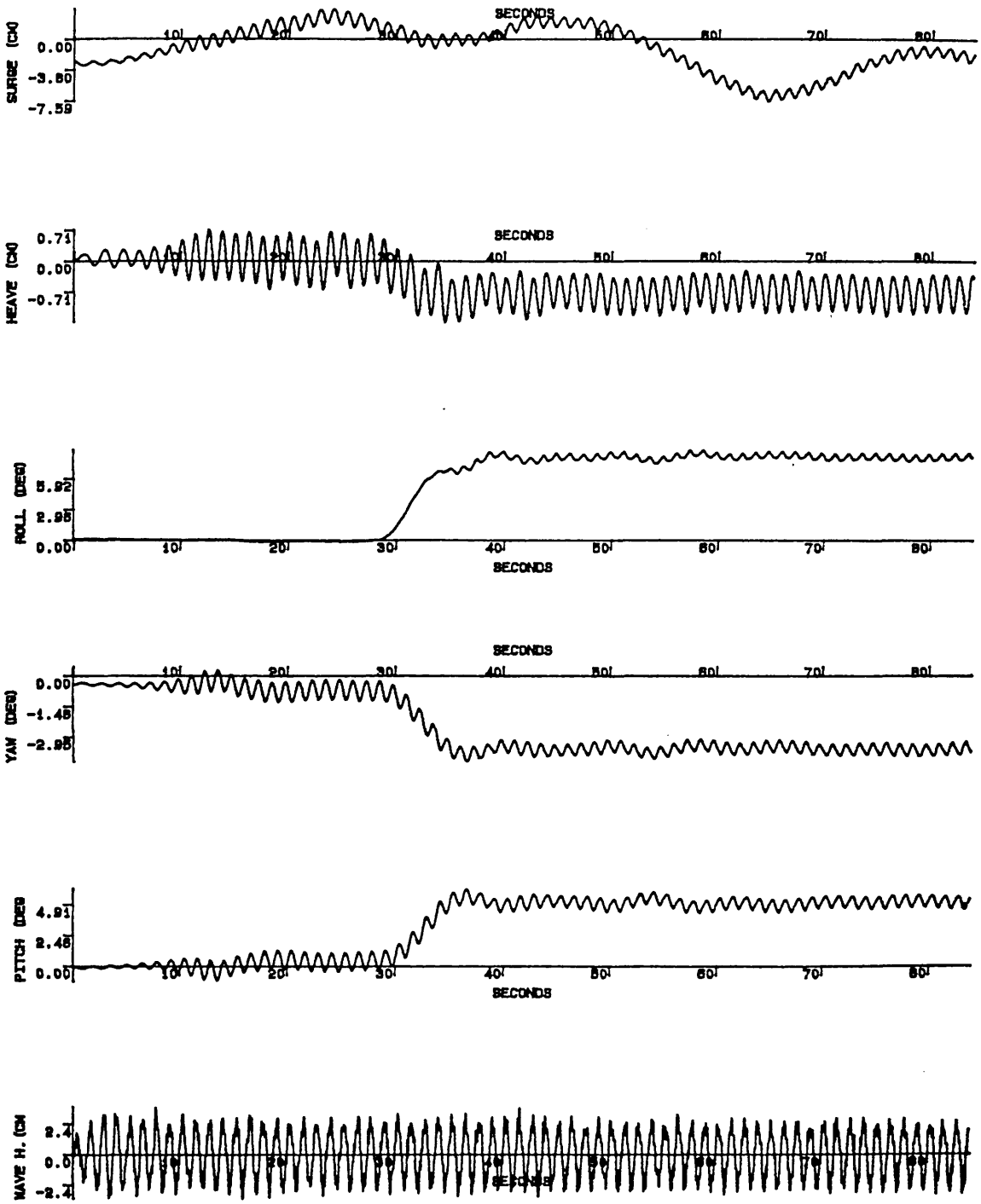

Fig.5.55 Motion response experiment (Head sea condition-asymmetrical flooding)
WH=10.1 cm Flooding Mass=0.6 kg Flooding Time=10 s
GM=2.29 cm ω=5.0 r/s (0.8 hertz) TS2958S.DAT

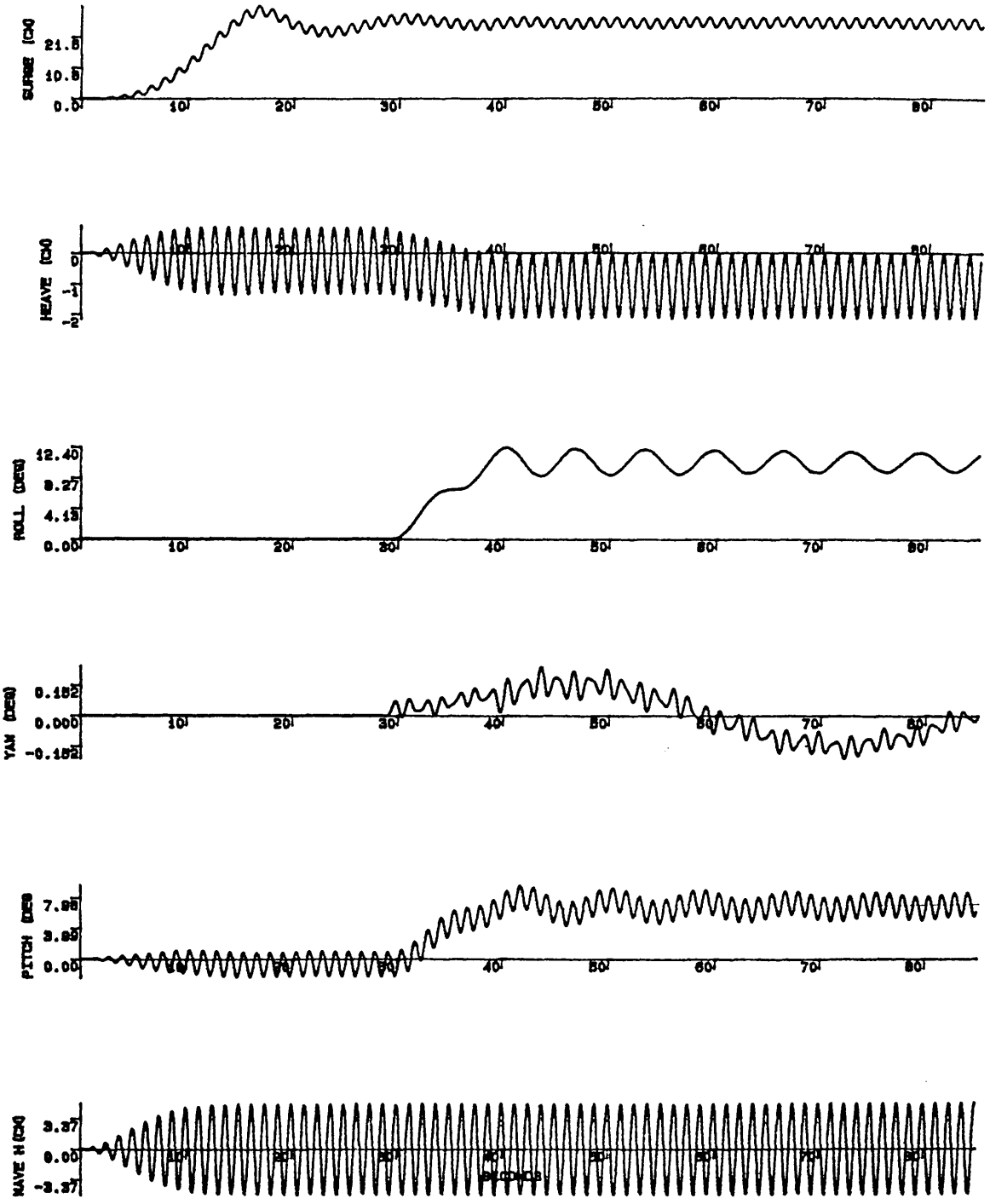

Fig.5.56 Motion response simulation (Head sea condition-asymmetrical flooding)
WH=10.1 cm Flooding Mass=0.6 kg Flooding Time=10 s
GM=2.29 cm ω=5.0 r/s (0.8 hertz)

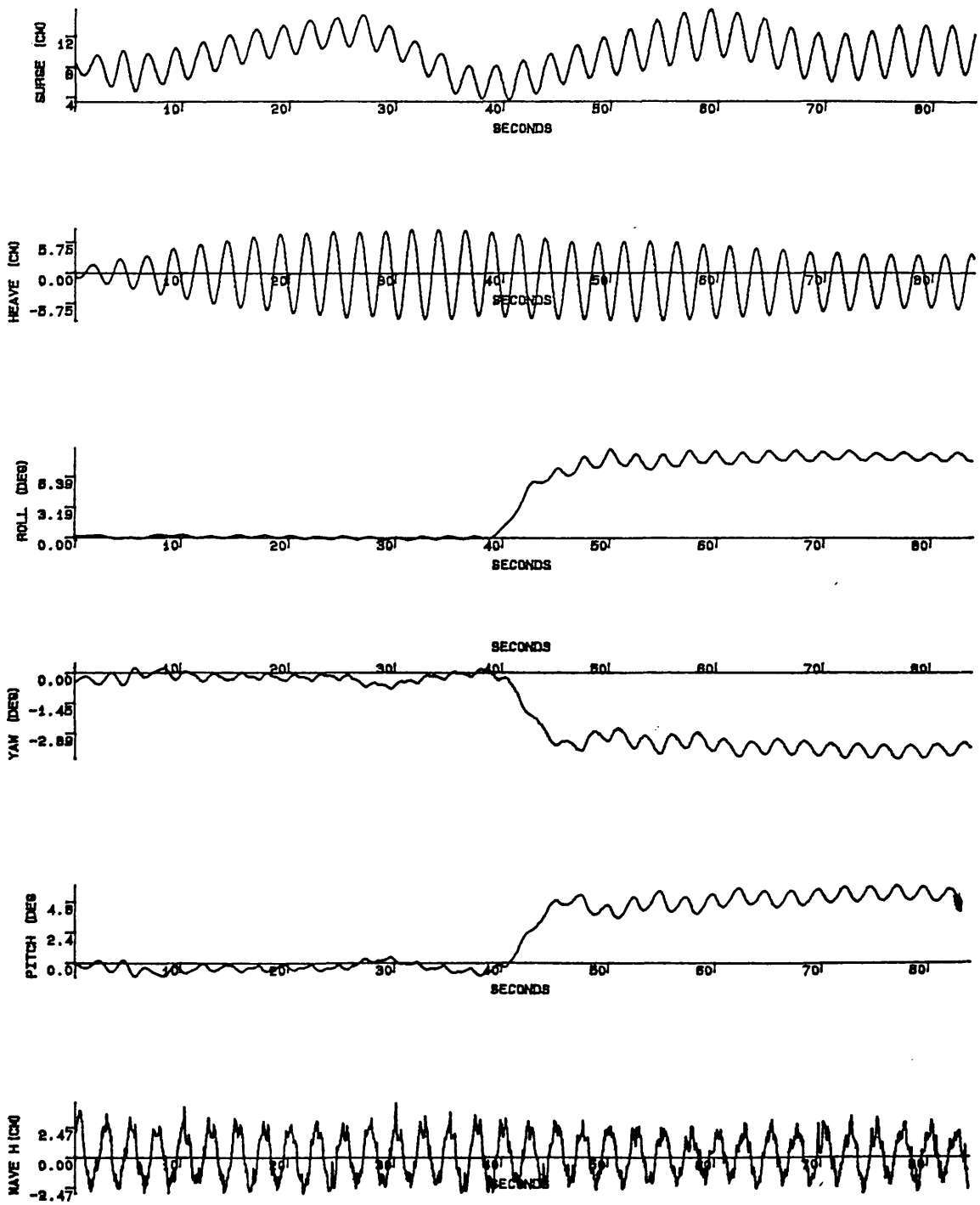

Fig.5.57 Motion response experiment (Head sea condition-asymmetrical flooding)

WH=4.7 cm	Flooding Mass=0.4 kg	Flooding Time=10 s
GM=2.29 cm	ω=2.5 r/s (0.4 hertz)	TS2959S.DAT

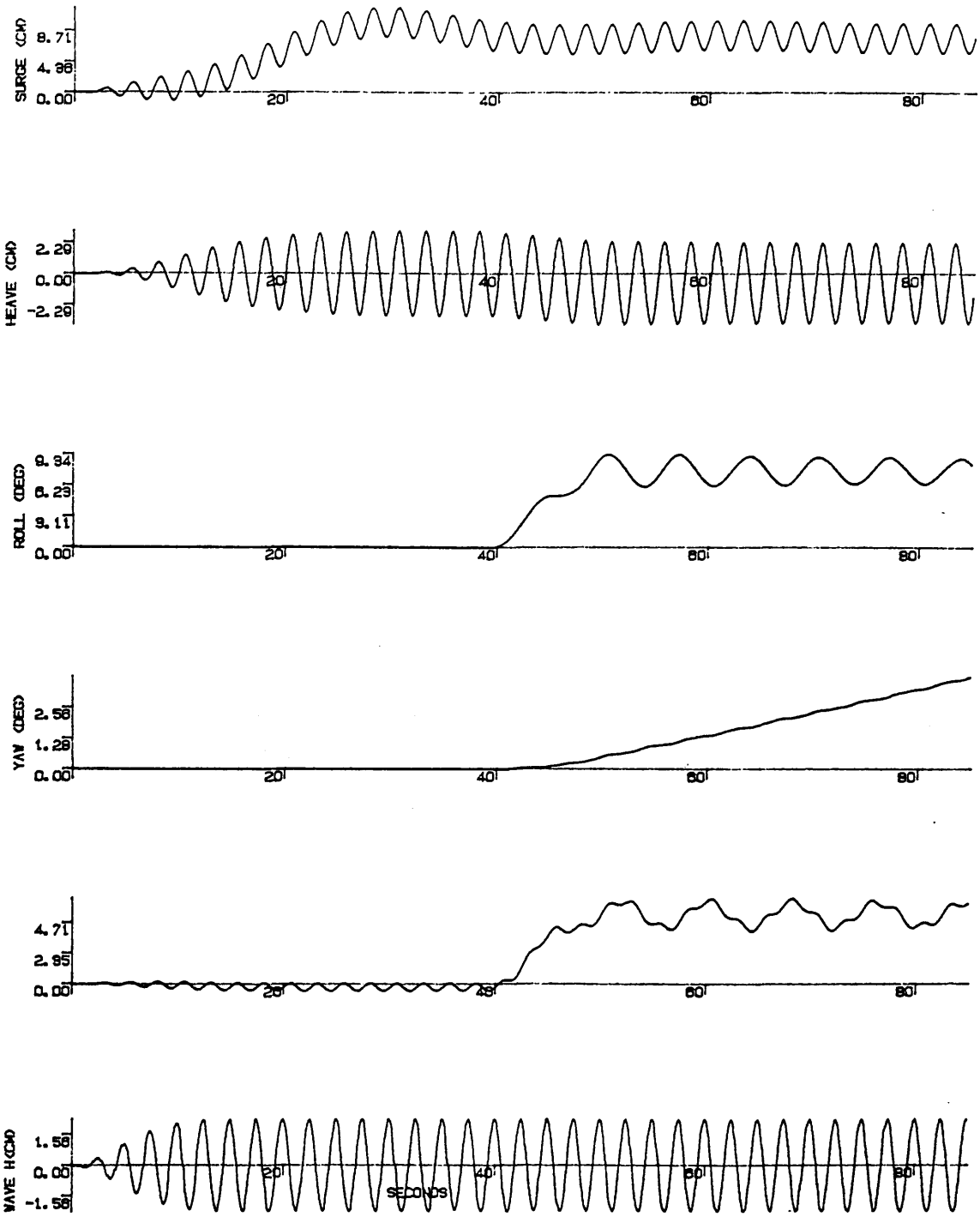

Fig.5.58 Motion response simulation (Head sea condition-asymmetrical flooding)
WH=4.7 cm Flooding Mass=0.4 kg Flooding Time=10 s
GM=2.29 cm ω=2.5 r/s (0.4 hertz)

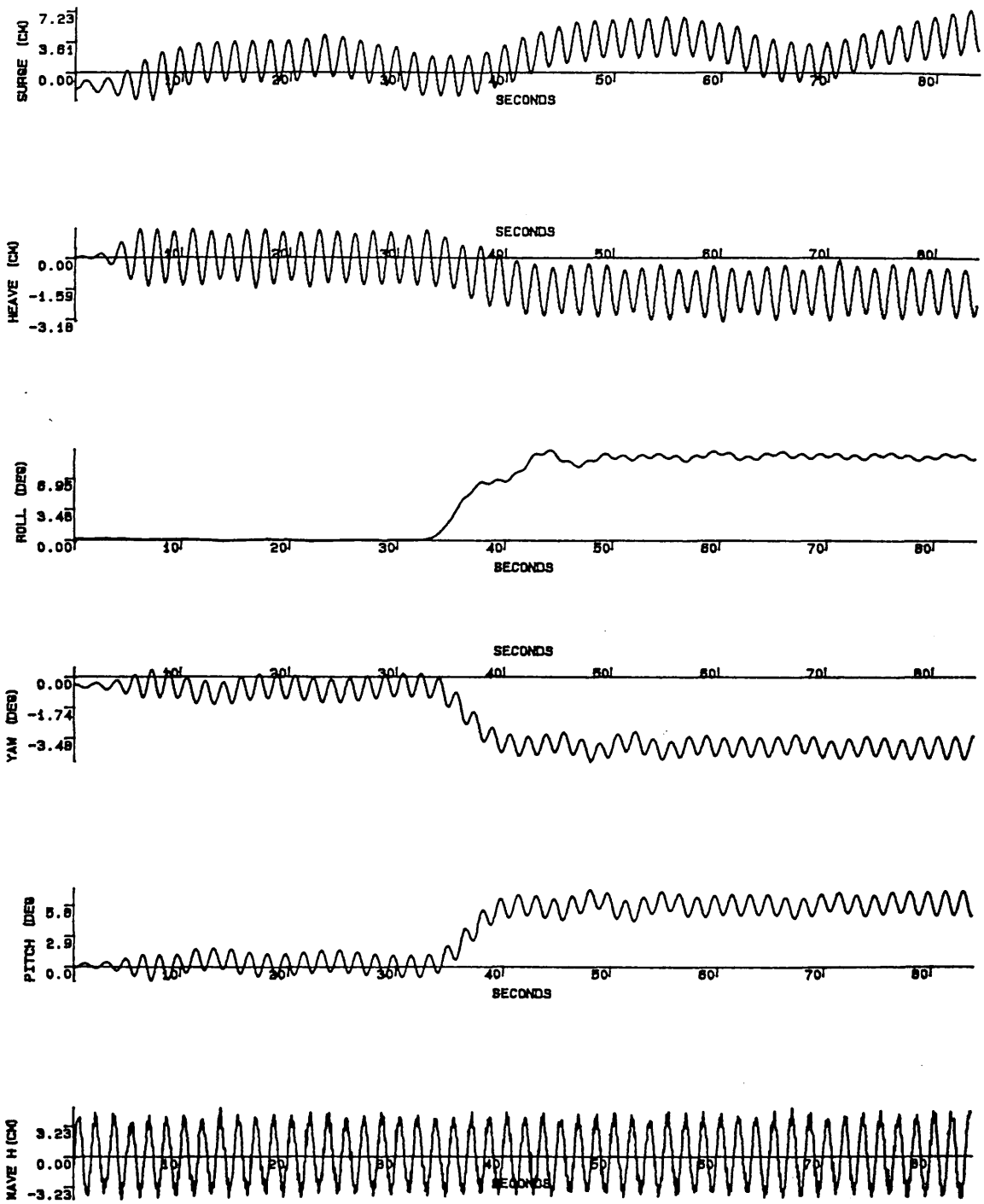

Fig.5.59 Motion response experiment (Head sea condition-asymmetrical flooding)
WH=7.8 cm Flooding Mass=0.6 kg Flooding Time=10 s
GM=2.29 cm ω=3.8 r/s (0.6 hertz) TS2960S.DAT

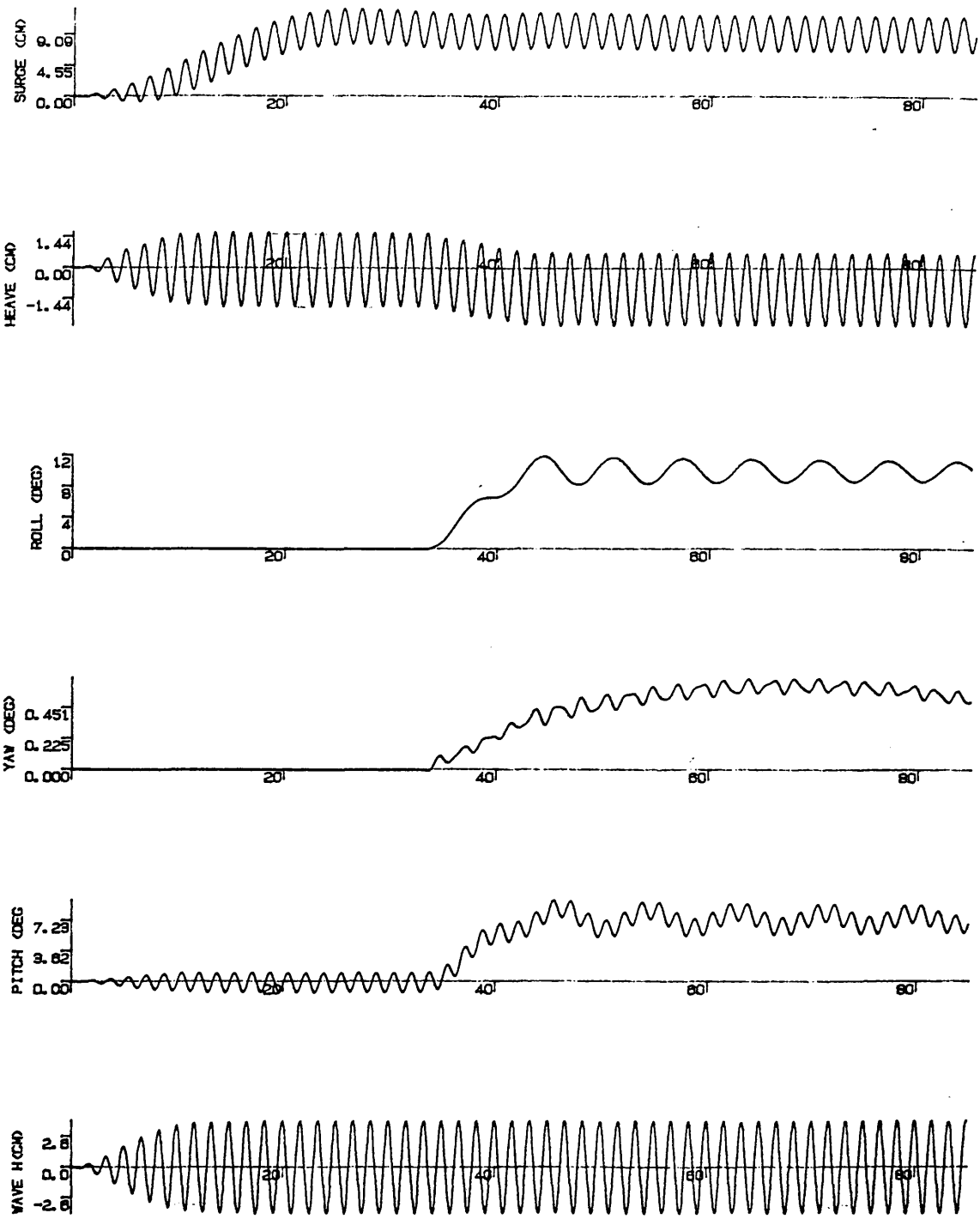

Fig.5.60 Motion response simulation (Head sea condition-asymmetrical flooding)
WH=7.8 cm Flooding Mass=0.6 kg Flooding Time=10 s
GM=2.29 cm ω=3.8 r/s (0.6 hertz)

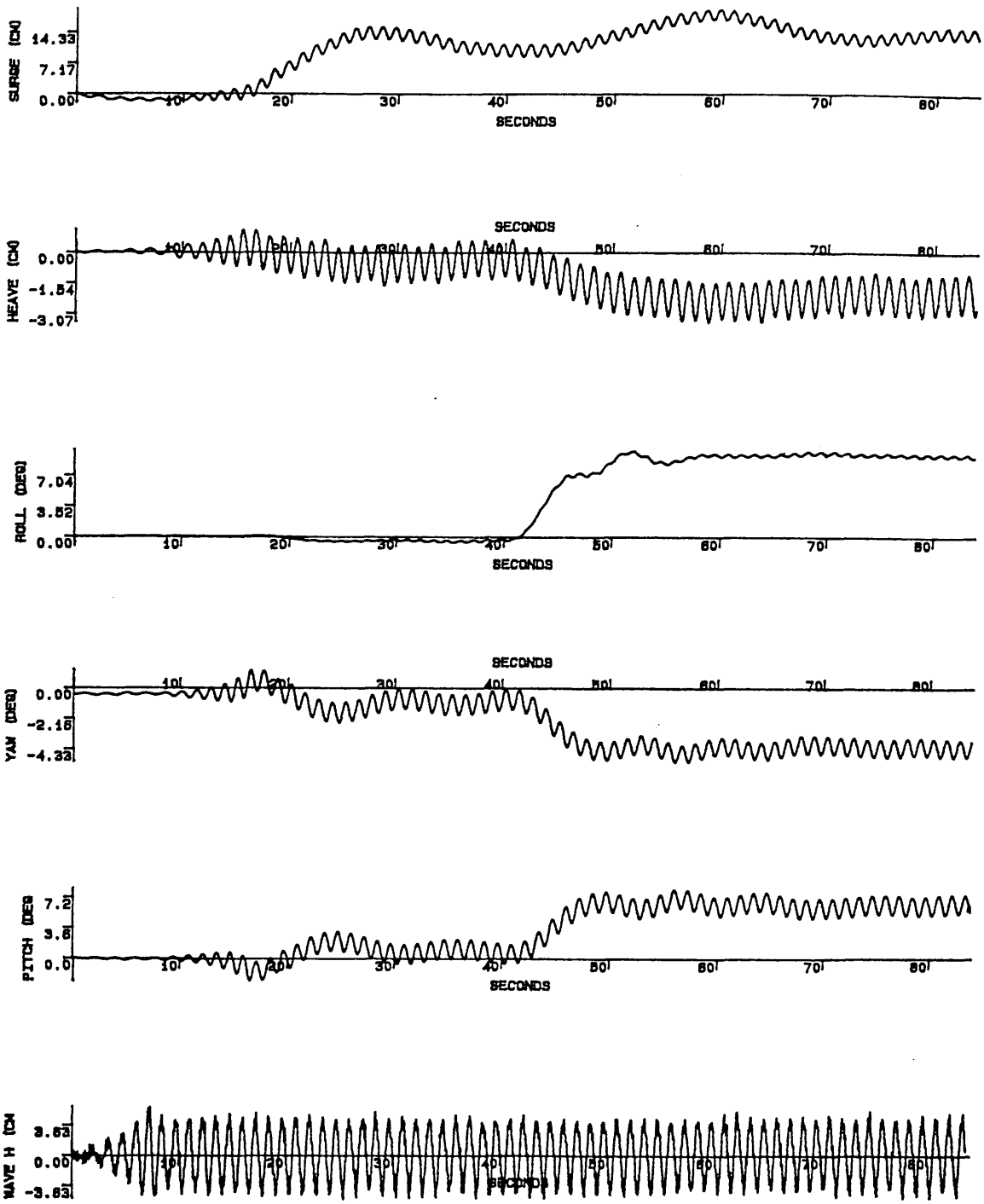

Fig.5.61 Motion response experiment (Head sea condition-asymmetrical flooding)
WH=8.8 cm Flooding Mass=0.5 kg Flooding Time=10 s
GM=2.29 cm ω=5.0 r/s (0.8 hertz) TS2961S.DAT

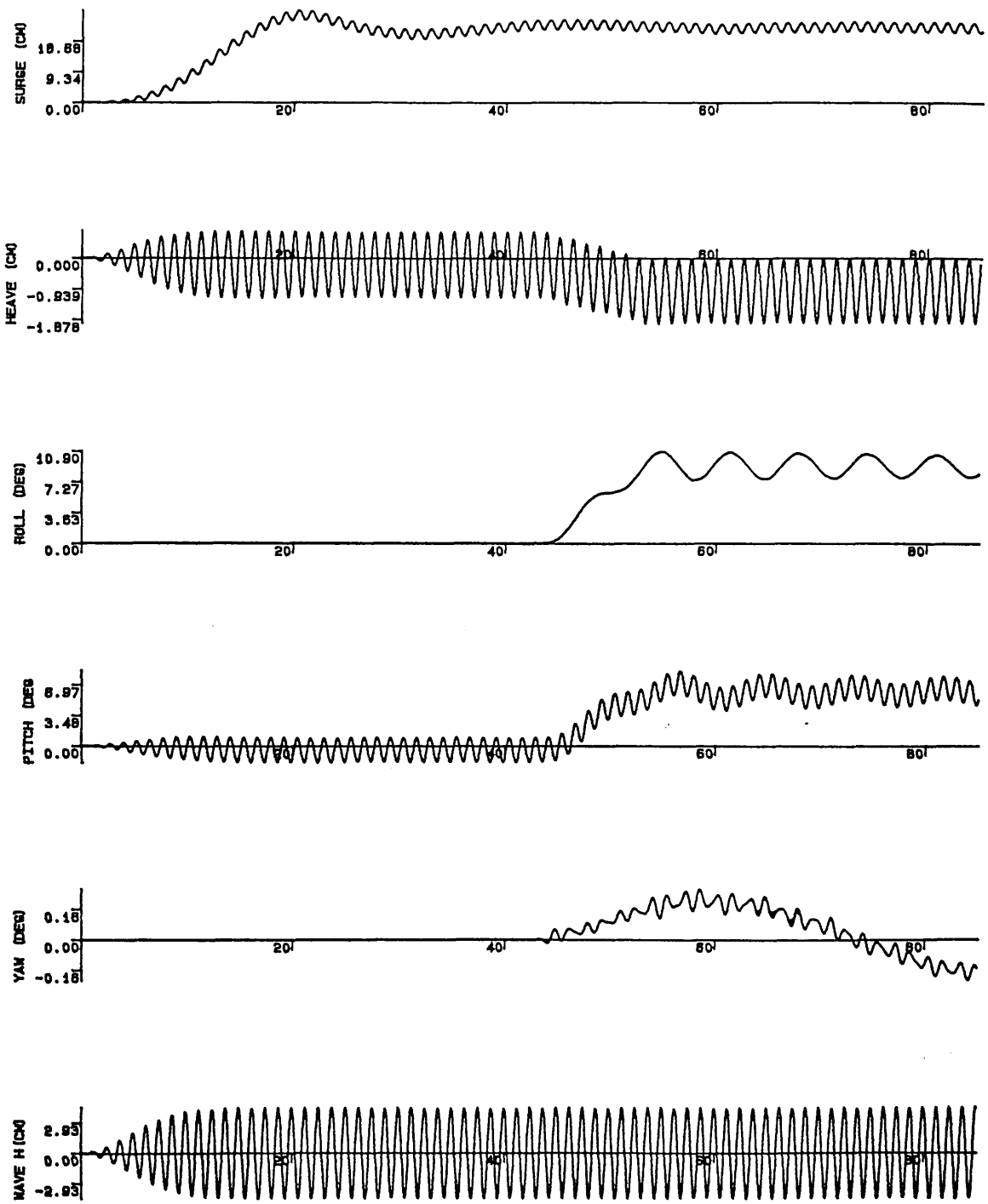

Fig.5.62 Motion response simualtion (Head sea condition-asymmetrical flooding)
WH=8.8 cm Flooding Mass=0.5 kg Flooding Time=10 s
GM=2.29 cm ω=5.0 r/s (0.8 hertz)

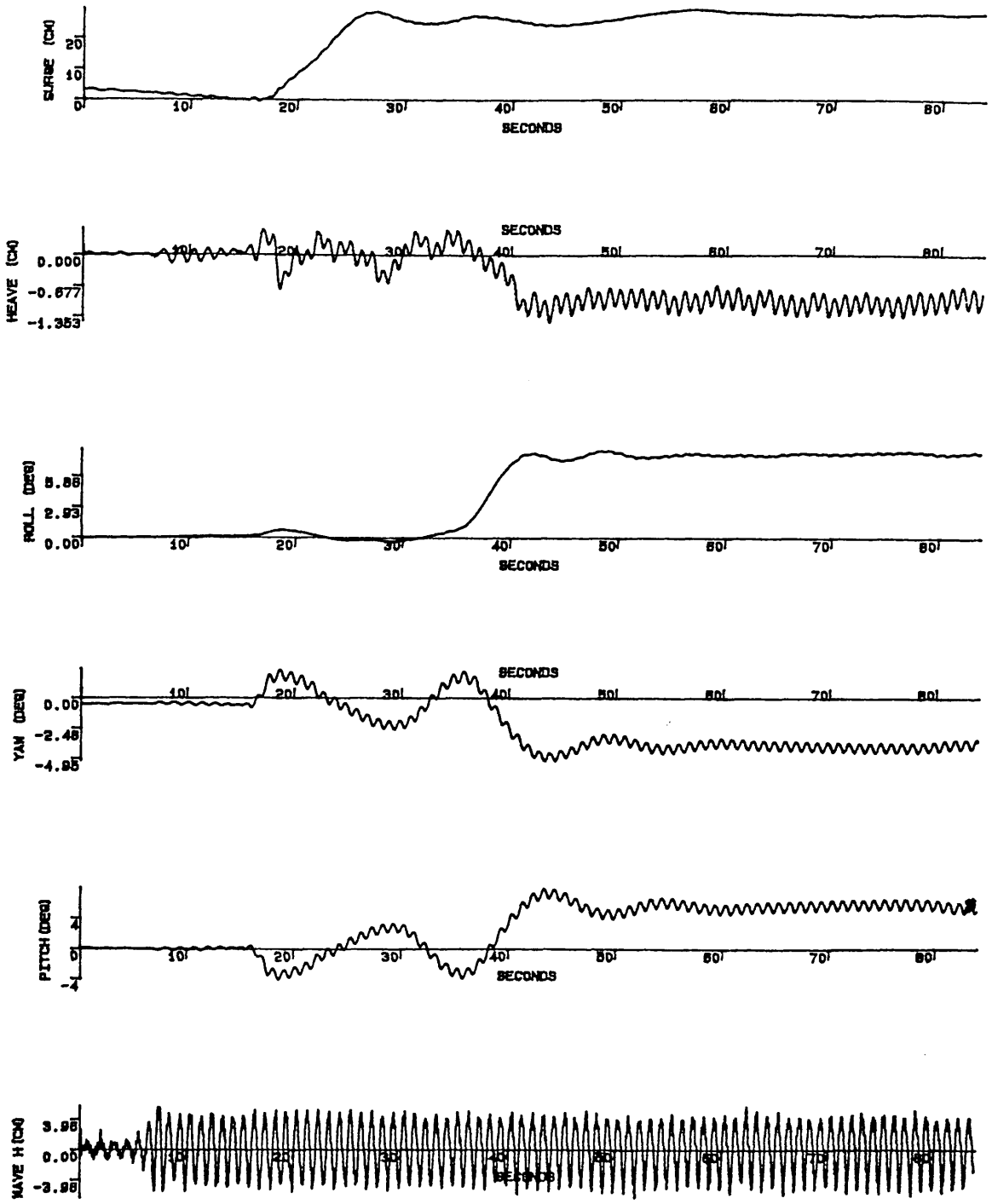

Fig.5.63 Motion response experiment (Head sea condition-asymmetrical flooding)

WH=9.6 cm Flooding Mass=0.4 kg Flooding Time=5 s

GM=2.29 cm ω=6.3 r/s (1.0 hertz) TS2962S.DAT

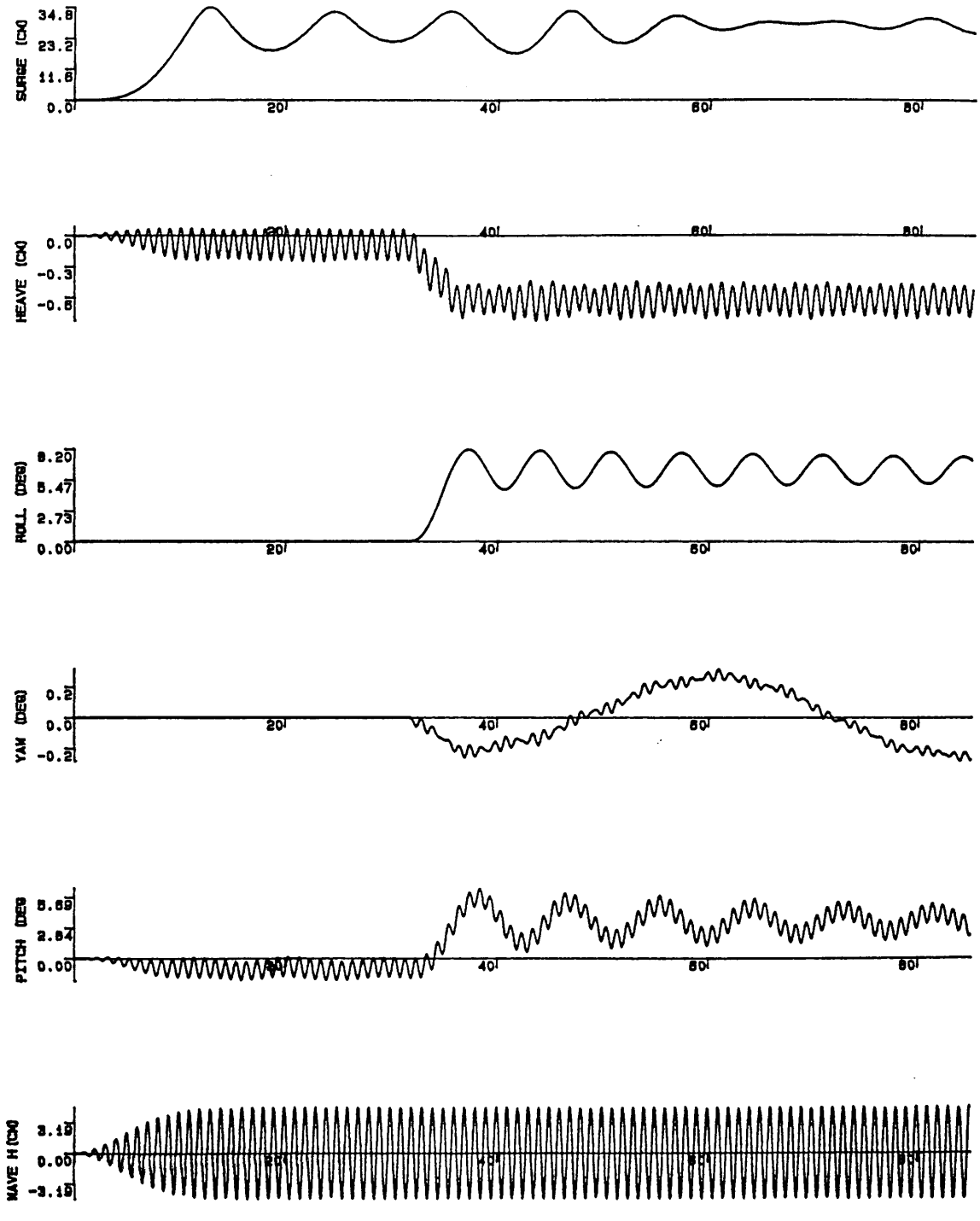

Fig.5.64 Motion response simulation (Head sea condition-asymmetrical flooding)
WH=9.6 cm Flooding Mass=0.4 kg Flooding Time=5 s
GM=2.29 cm ω=6.3 r/s (1.0 hertz)

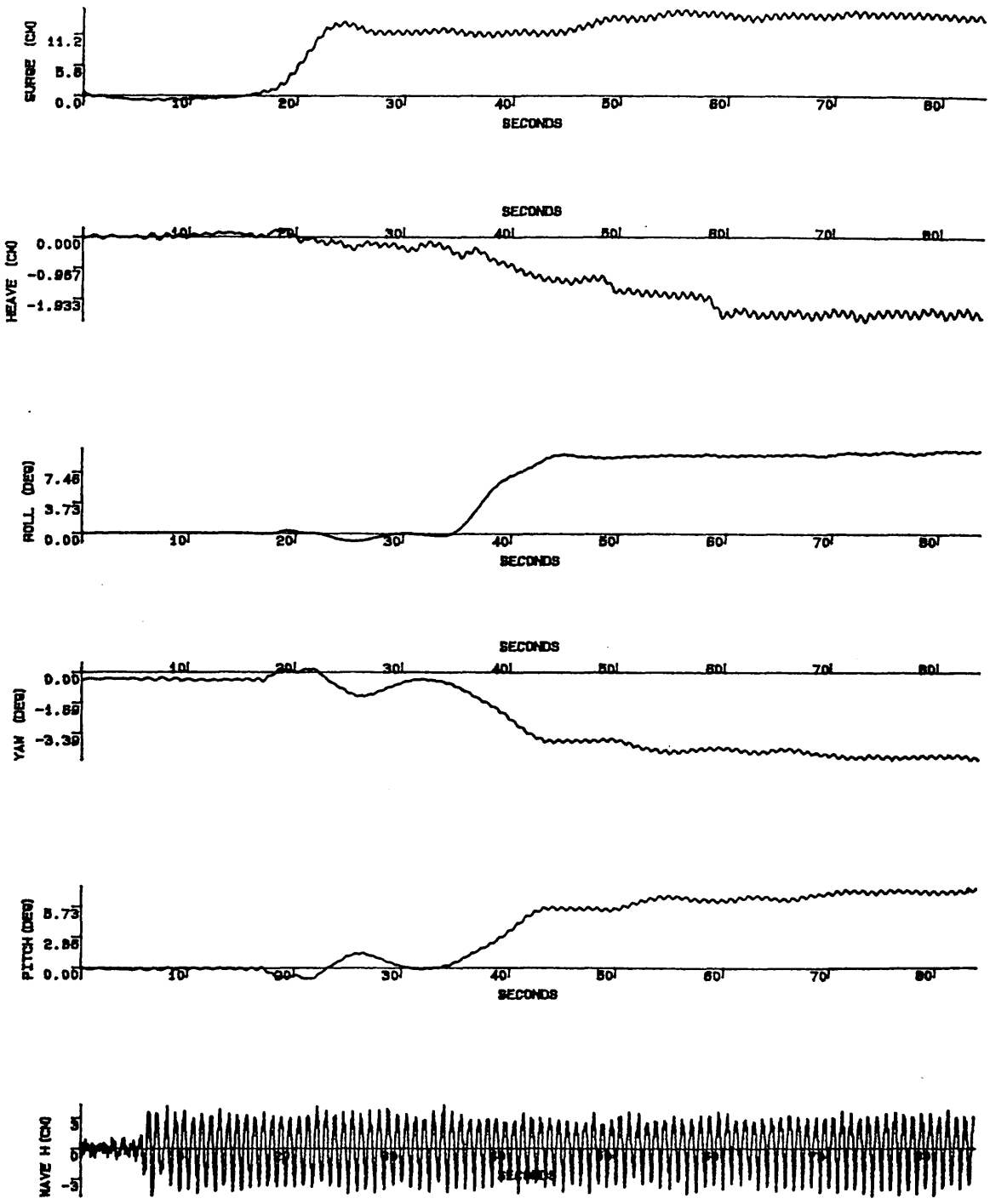

Fig.5.65 Motion response experiment (Head sea condition-asymmetrical flooding)

WH=7.3 cm	Flooding Mass=0.5 kg	Flooding Time=10 s
GM=2.29 cm	ω=7.5 r/s (1.2 hertz)	TS2963S.DAT

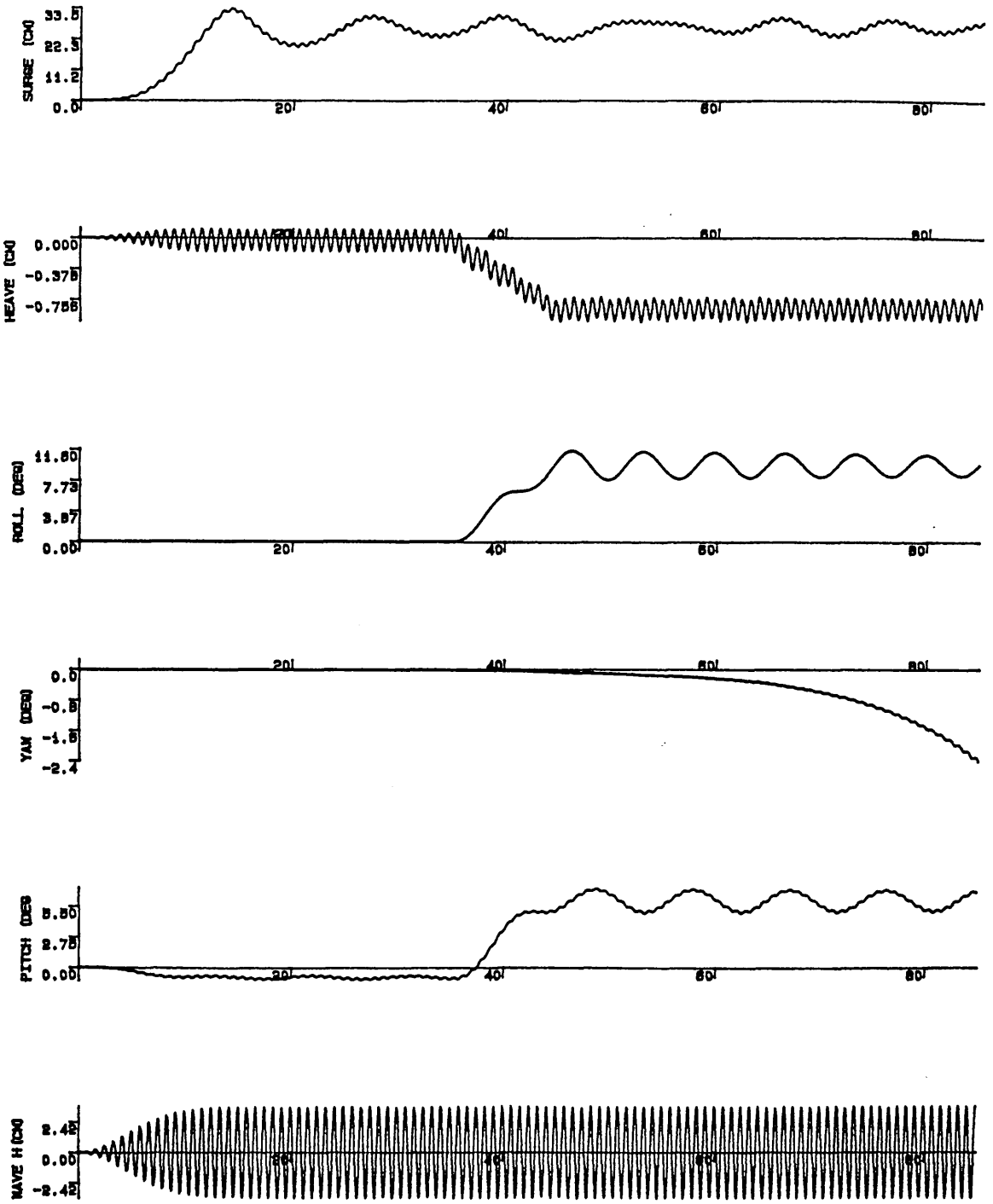

Fig.5.66 Motion response simulation (Head sea condition-asymmetrical flooding)
WH=7.3 cm Flooding Mass=0.5 kg Flooding Time=10 s
GM=2.29 cm ω=7.5 r/s (1.2 hertz)

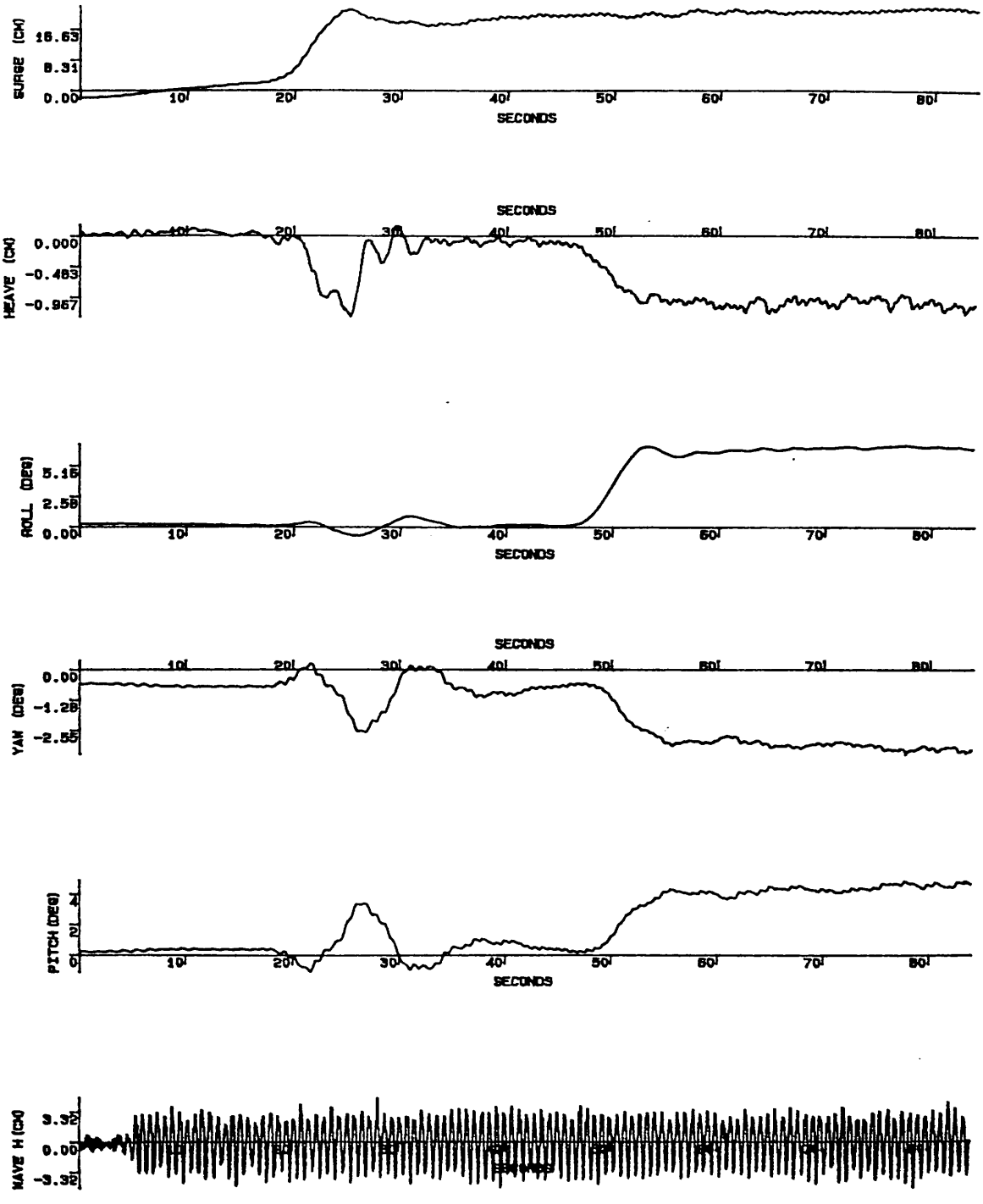

Fig.5.67 Motion response experiment (Head sea condition-asymmetrical flooding)

WH=6.6 cm	Flooding Mass=0.3 kg	Flooding Time=5 s
GM=2.29 cm	ω=8.8 r/s (1.4 hertz)	TS2964S.DAT

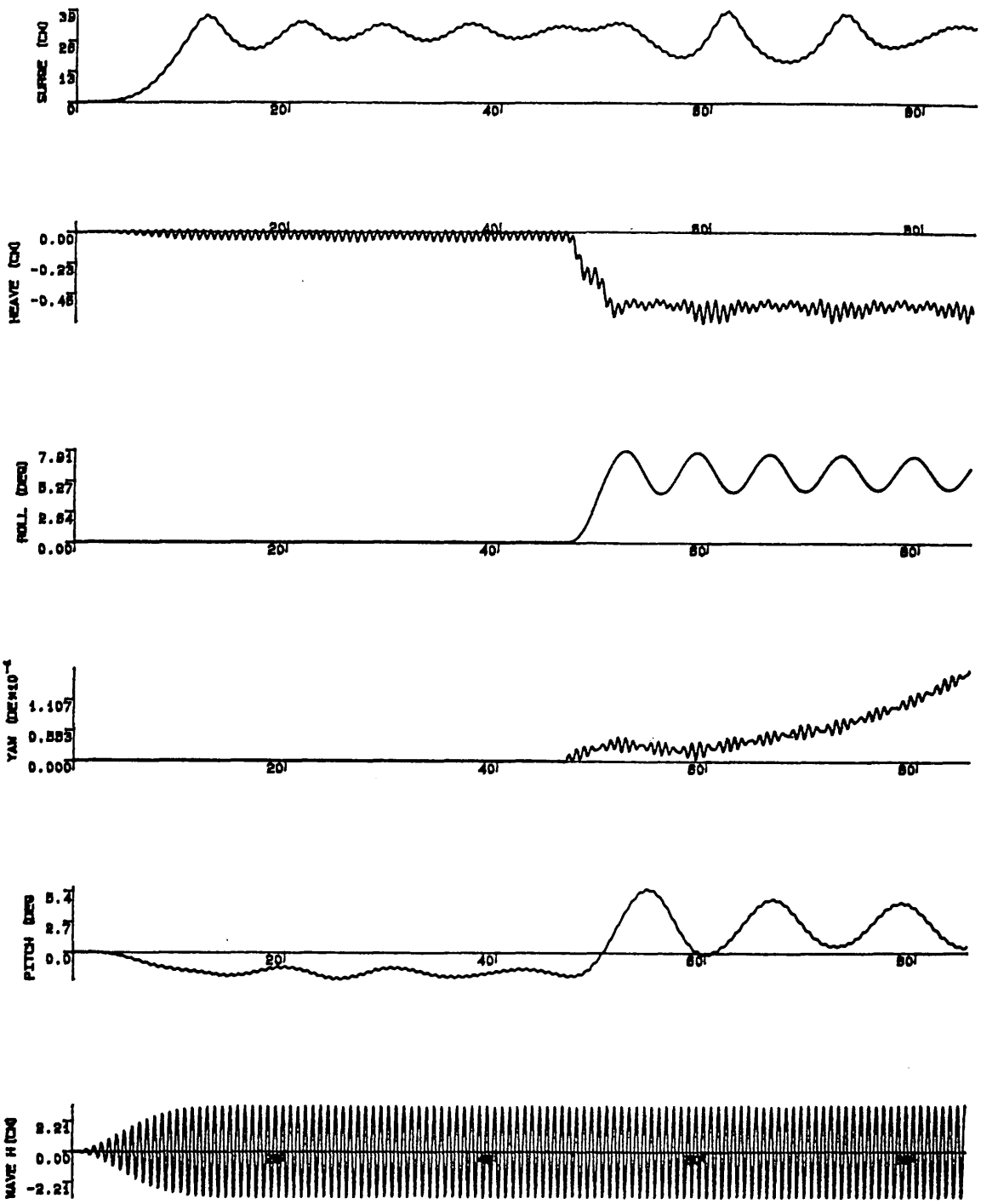

Fig.5.68 Motion response simulation (Head sea condition-asymmetrical flooding)
WH=6.6 cm Flooding Mass=0.3 kg Flooding Time=5 s
GM=2.29 cm ω=8.8 r/s (1.4 hertz)

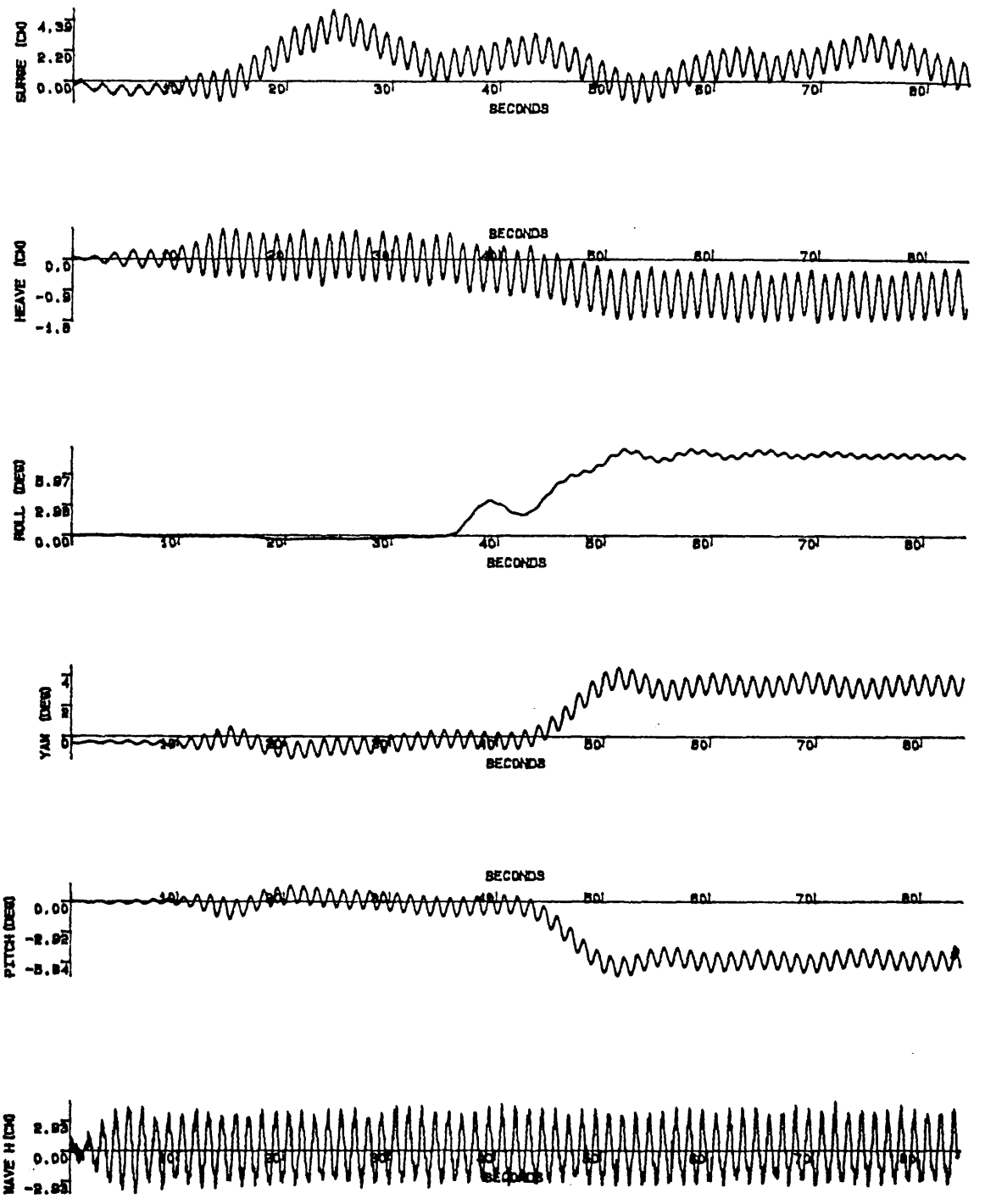

Fig.5.69 Motion response experiment (Head sea condition-asymmetrical flooding)

WH=6.8 cm	Flooding Mass=0.4 kg	Flooding Time=5 s
GM=2.29 cm	ω=5.0 r/s (0.8 hertz)	TS2967S.DAT

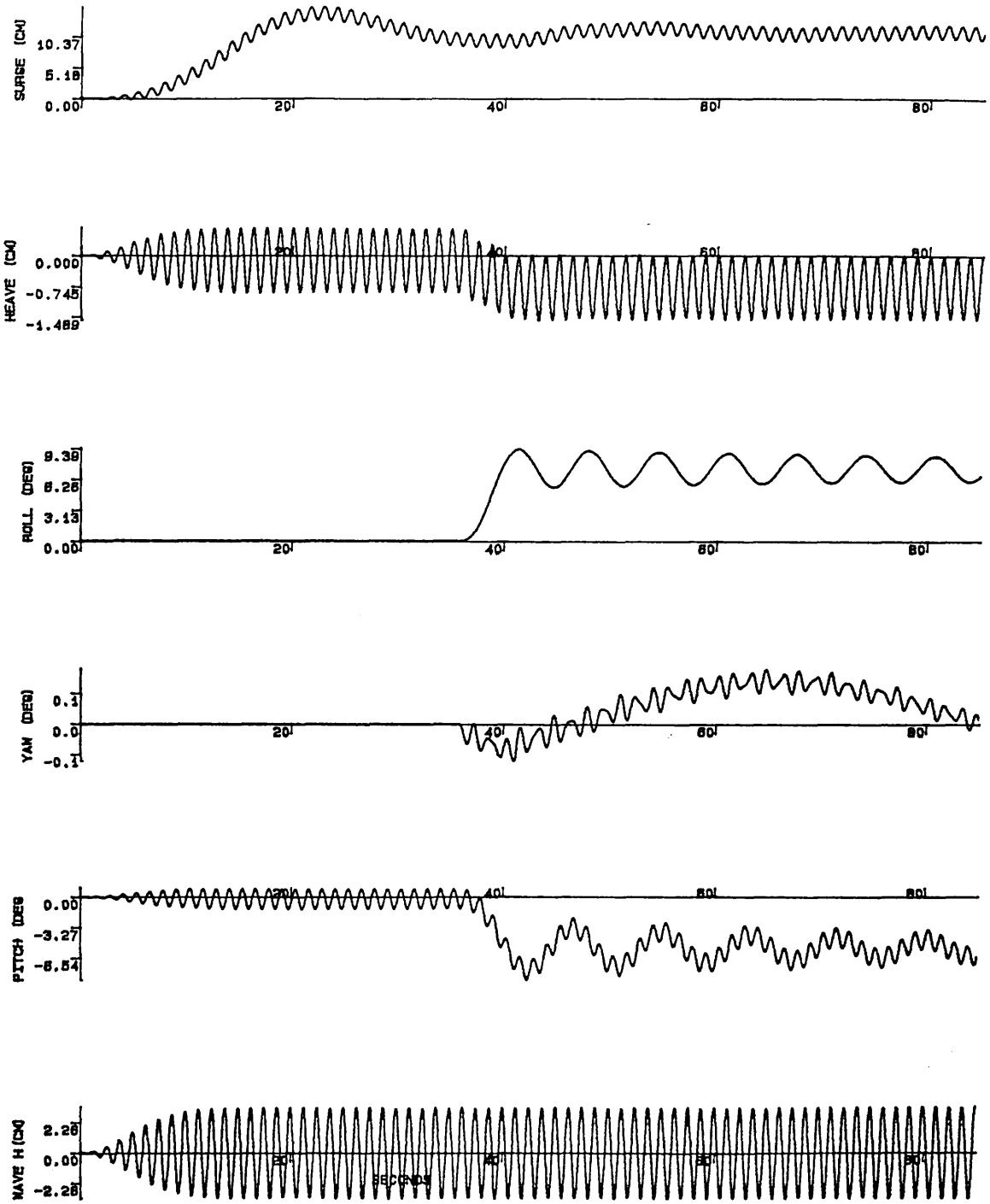

Fig.5.70 Motion response simulation (Head sea condition-asymmetrical flooding)
WH=6.8 cm Flooding Mass=0.4 kg Flooding Time=5 s
GM=2.29 cm ω=5.0 r/s (0.8 hertz)

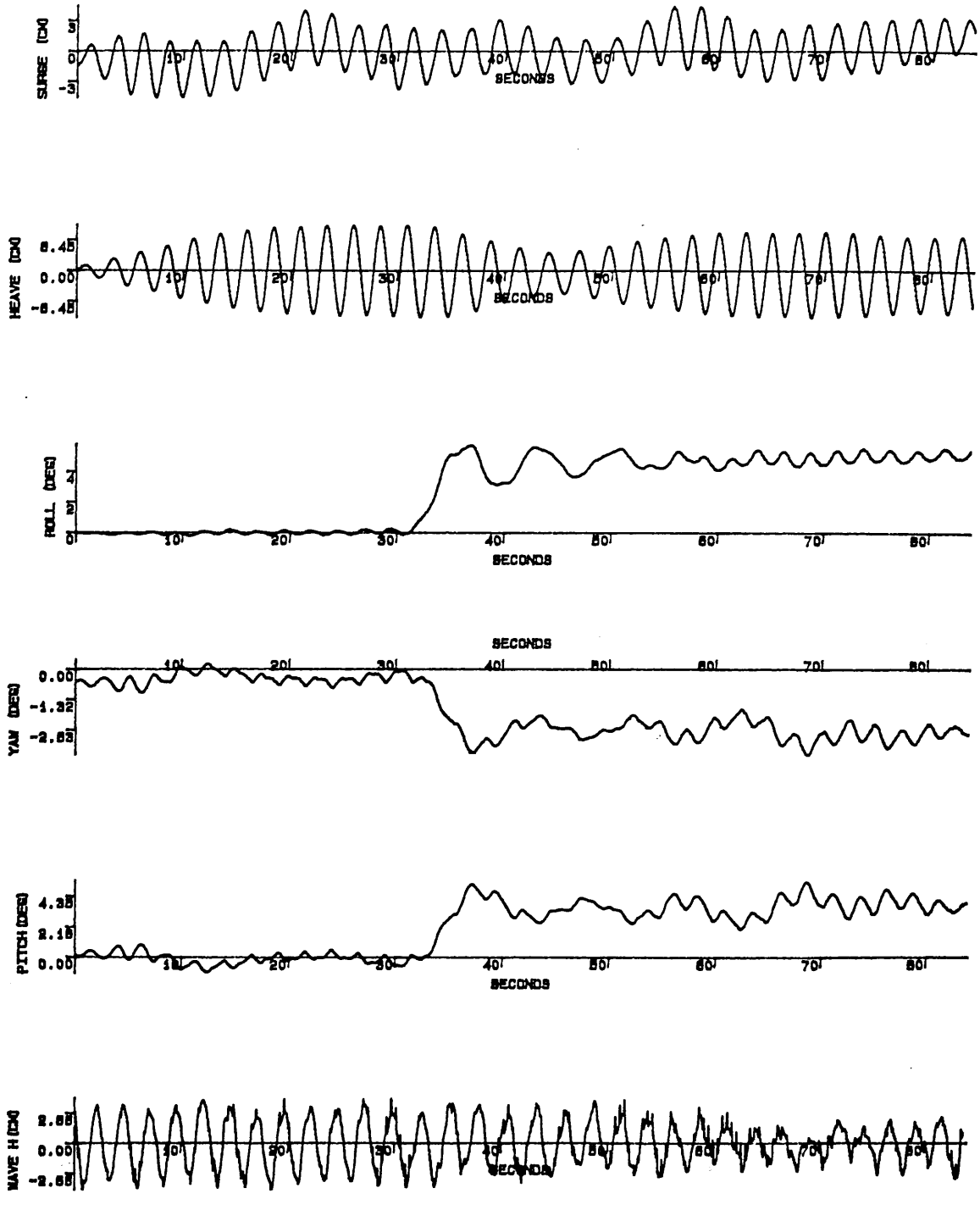

Fig.5.71 Motion response experiment (Head sea condition-asymmetrical flooding)
WH=6.2 cm Flooding Mass=0.4 kg Flooding Time=5 s
GM=2.29 cm ω=2.5 r/s (0.4 hertz) TS2968S.DAT

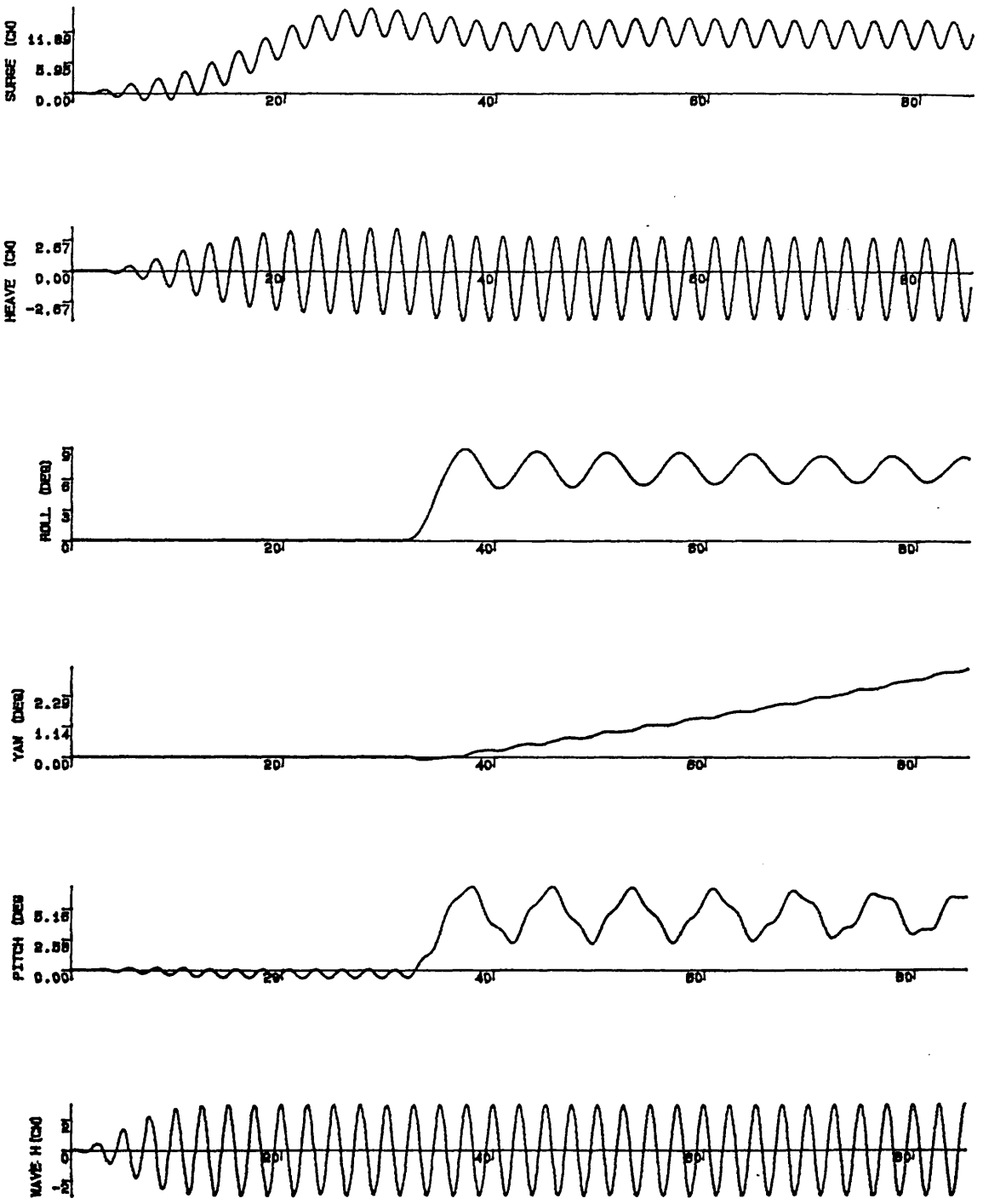

Fig.5.72 Motion response simulation (Head sea condition-asymmetrical flooding)
WH=6.2 cm Flooding Mass=0.4 kg Flooding Time=5 s
GM=2.29 cm ω=2.5 r/s (0.4 hertz)

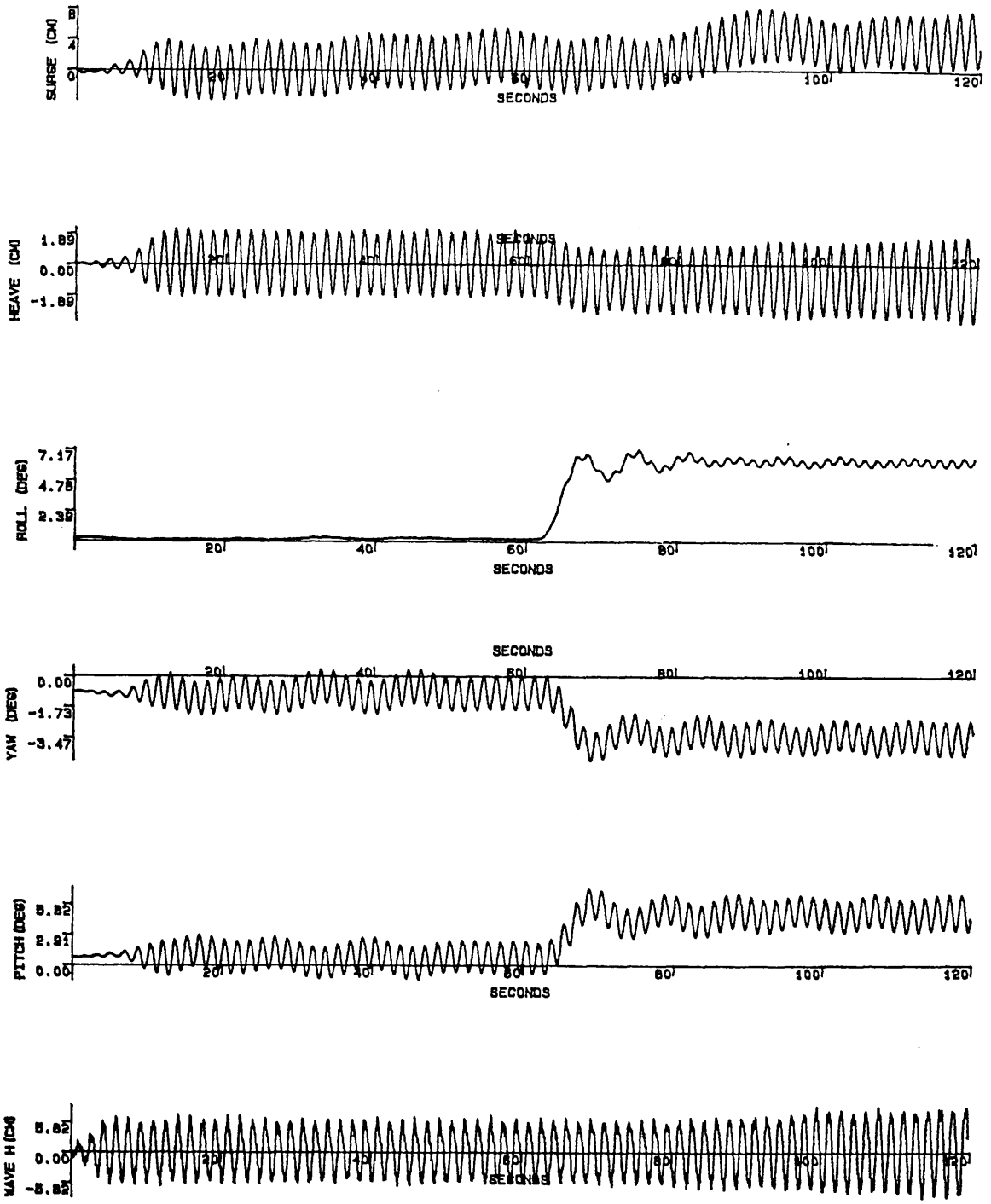

Fig.5.73 Motion response experiment (Head sea condition-asymmetrical flooding)

WH=12.3 cm Flooding Mass=0.3 kg Flooding Time=5 s

GM=2.29 cm ω=3.8 r/s (0.6 hertz) TS2969S.DAT

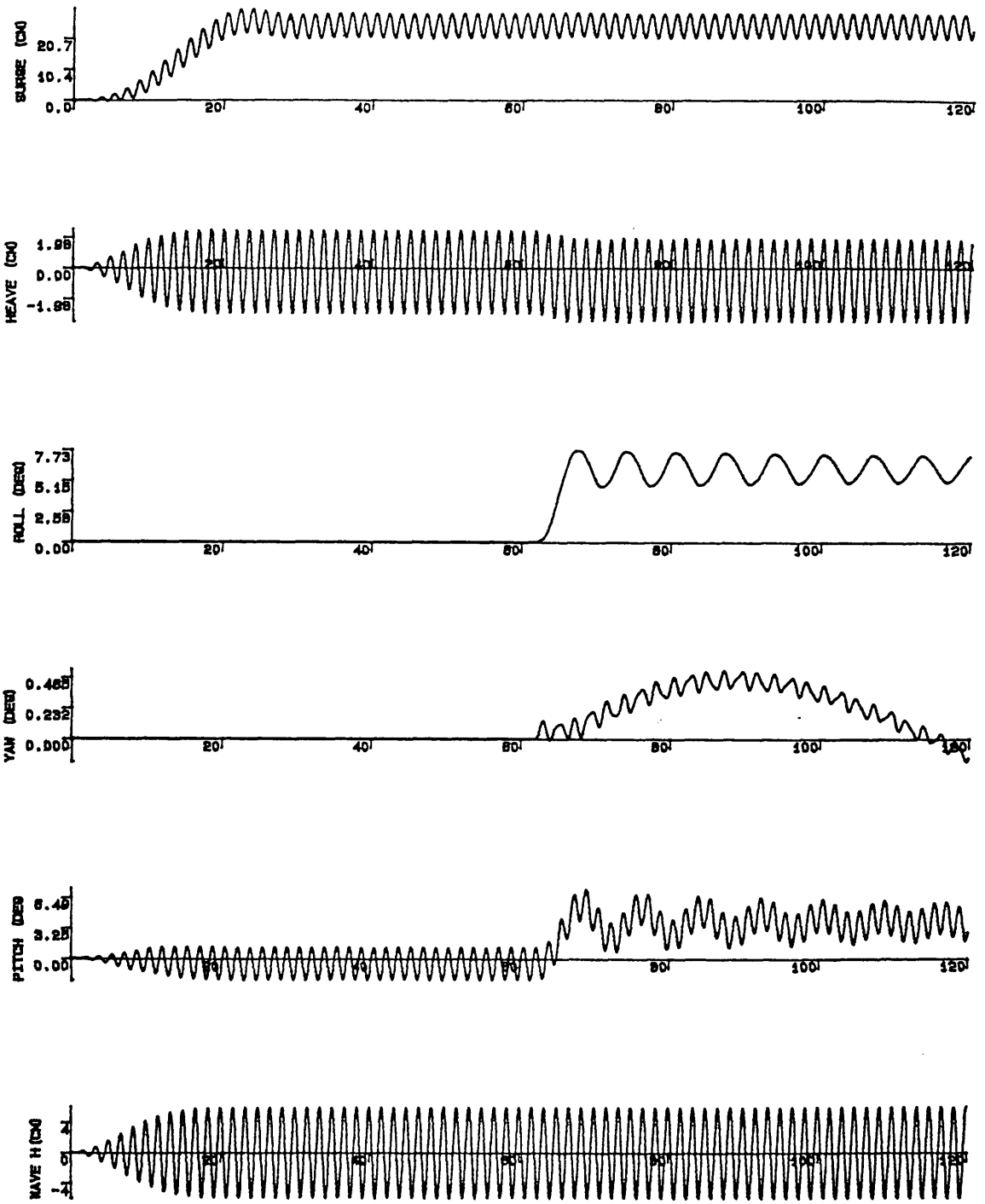

Fig.5.74 Motion response simulation (Head sea condition-asymmetrical flooding)
WH=12.3 cm Flooding Mass=0.3 kg Flooding Time=5 s
GM=2.29 cm ω=3.8 r/s (0.6 hertz)

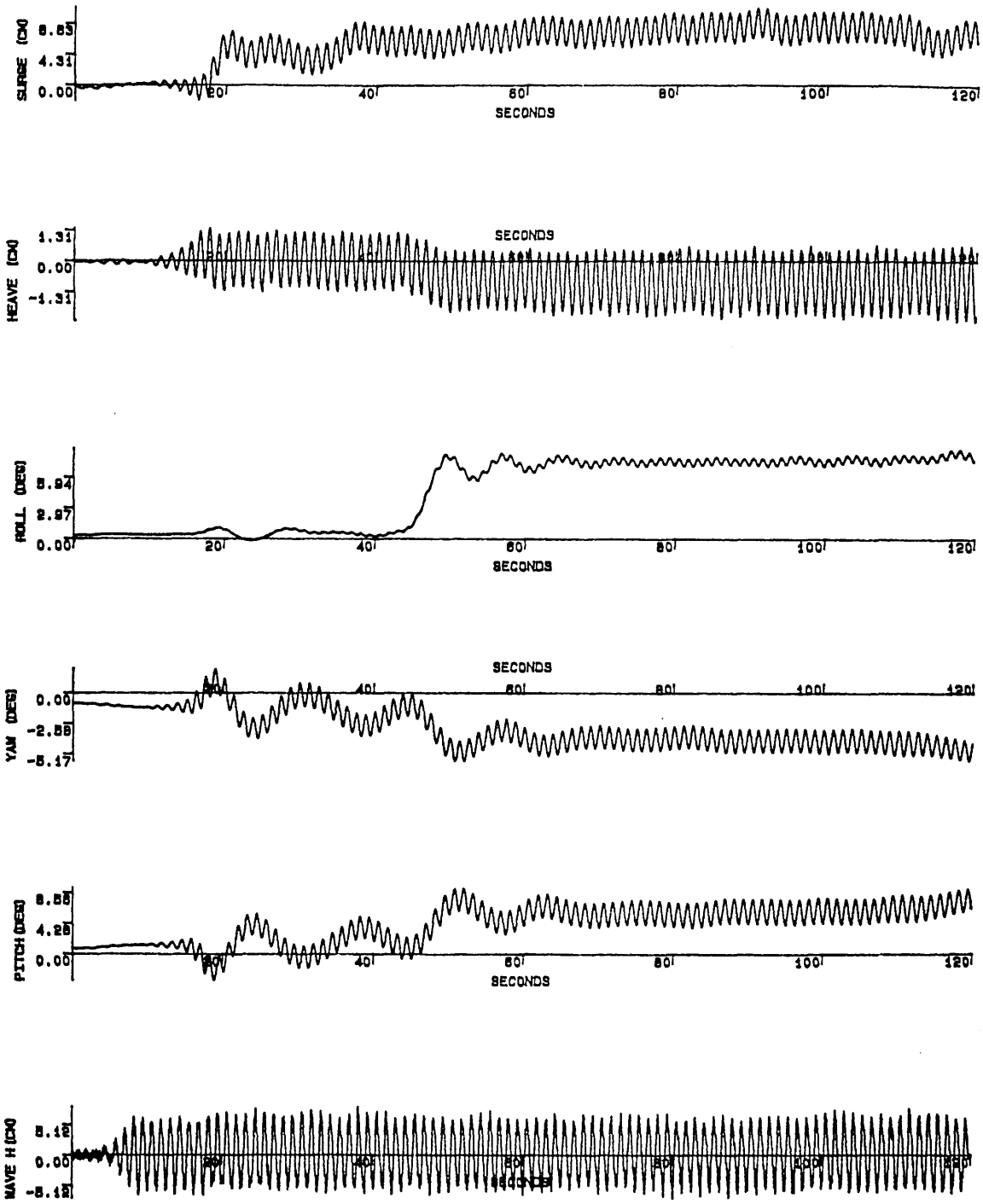

Fig.5.75 Motion response experiment (Head sea condition-asymmetrical flooding)
WH=12.9 cm Flooding Mass=0.4 kg Flooding Time=5 s
GM=2.29 cm ω=5.0 r/s (0.8 hertz) TS2970S.DAT

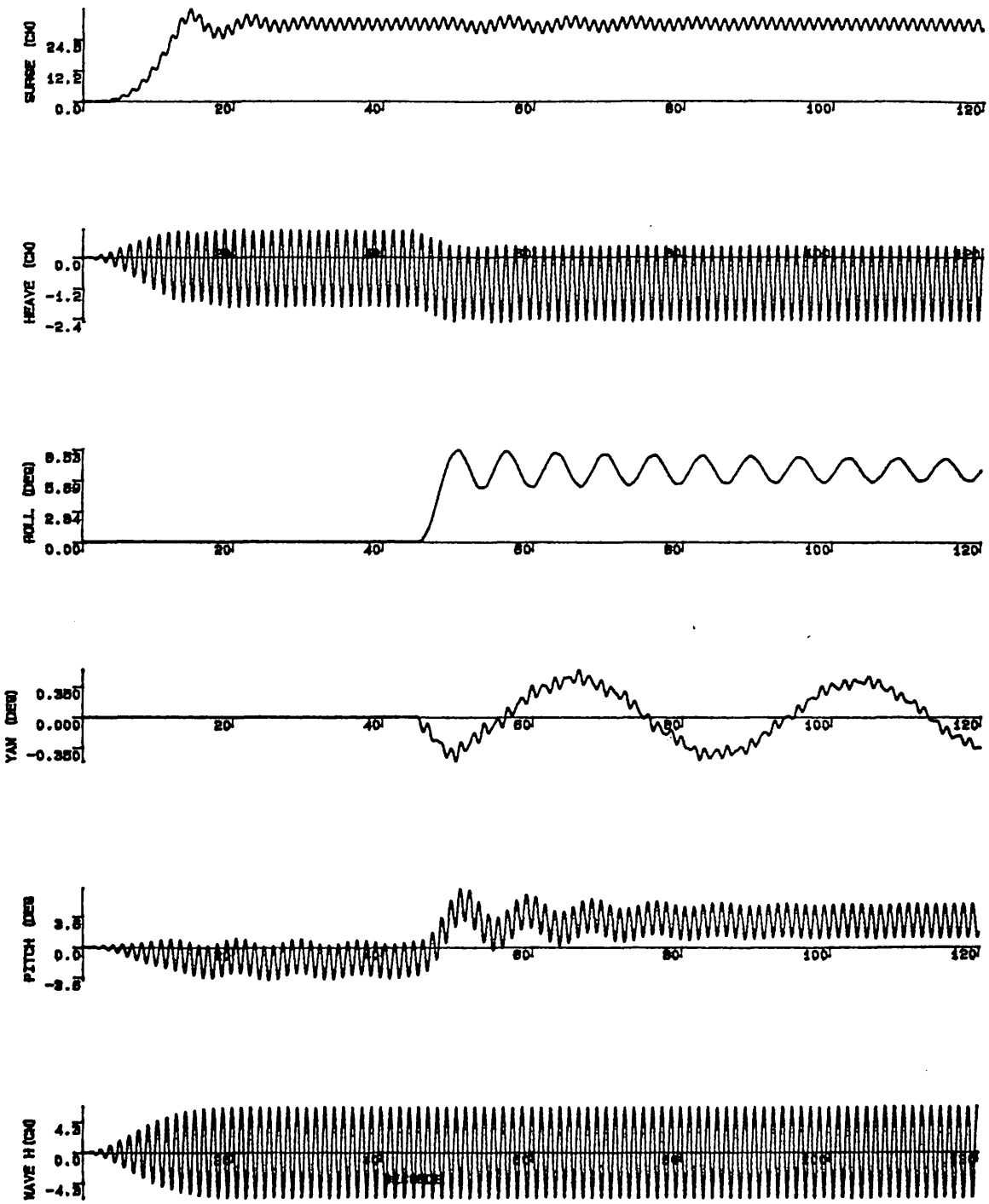

Fig.5.76 Motion response simulation (Head sea condition-asymmetrical flooding)
WH=12.9 cm Flooding Mass=0.4 kg Flooding Time=5 s
GM=2.29 cm ω=5.0 r/s (0.8 hertz)

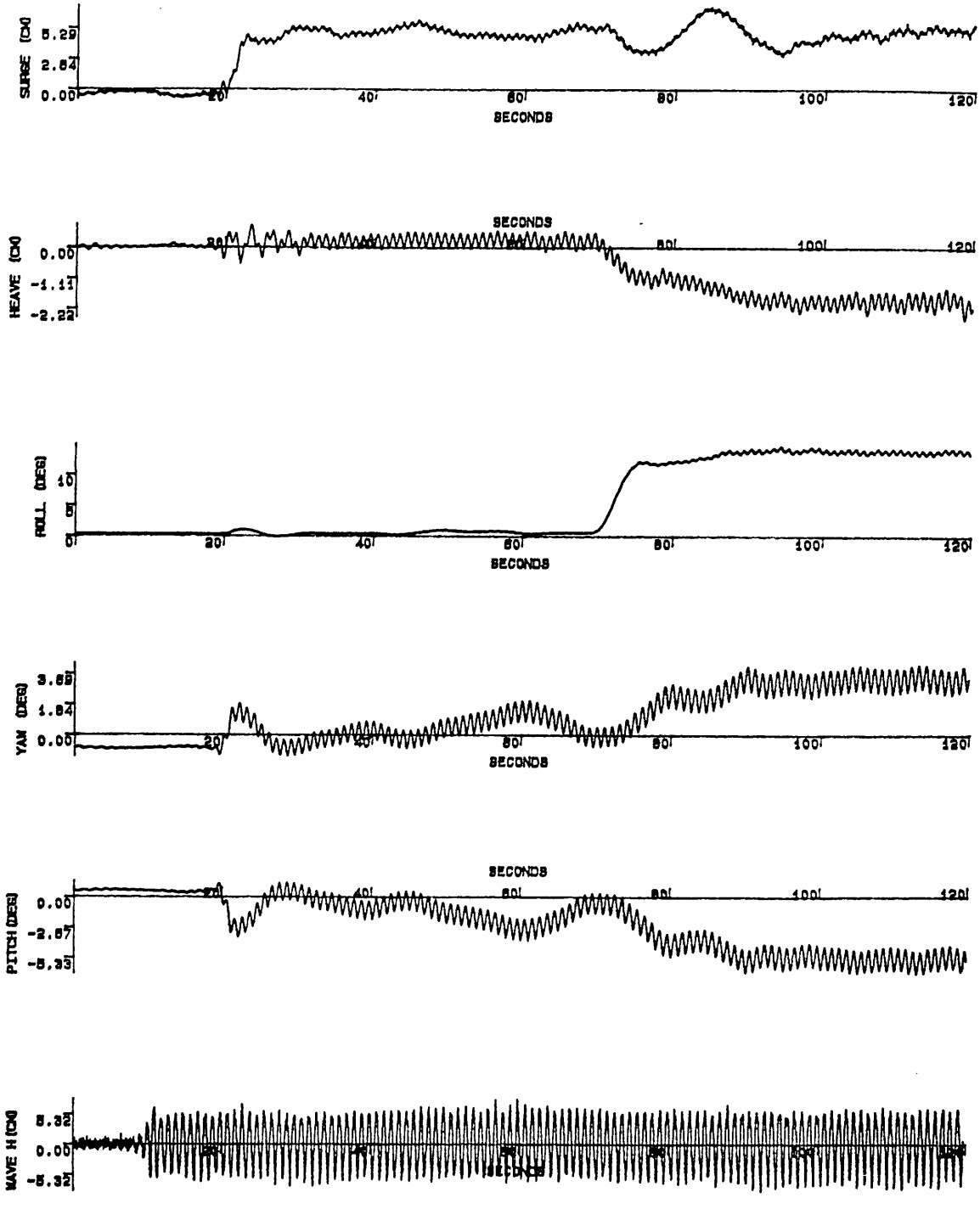

Fig.5.77 Motion response experiment (Head sea condition-asymmetrical flooding)

WH=12.3 cm	Flooding Mass=0.3 kg	Flooding Time=5 s
GM=2.29 cm	ω=6.3 r/s (1.0 hertz)	TS2971S.DAT

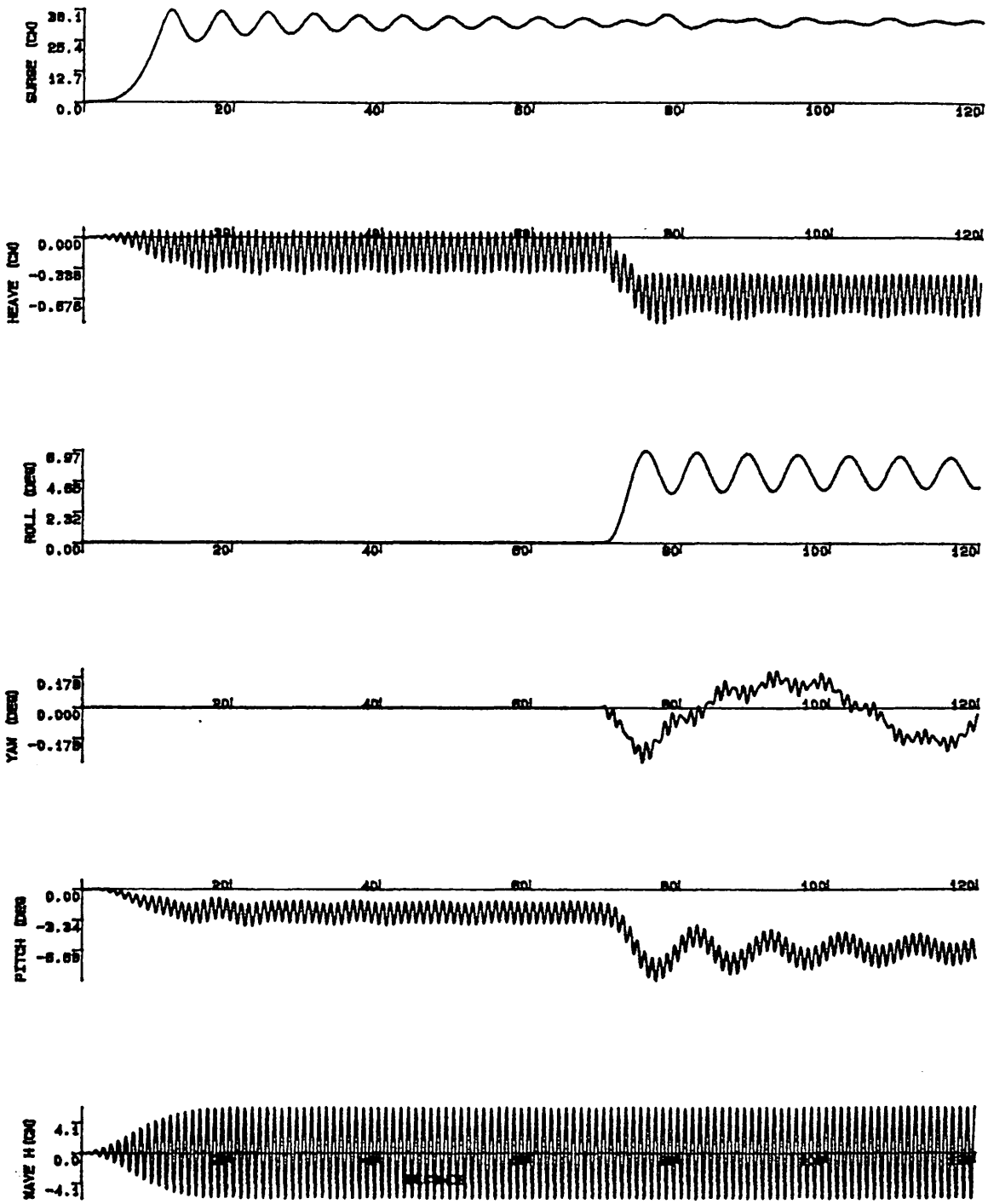

Fig.5.78 Motion response simulation (Head sea condition-asymmetrical flooding)
WH=12.3 cm Flooding Mass=0.3 kg Flooding Time=5 s
GM=2.29 cm ω=6.3 r/s (1.0 hertz)

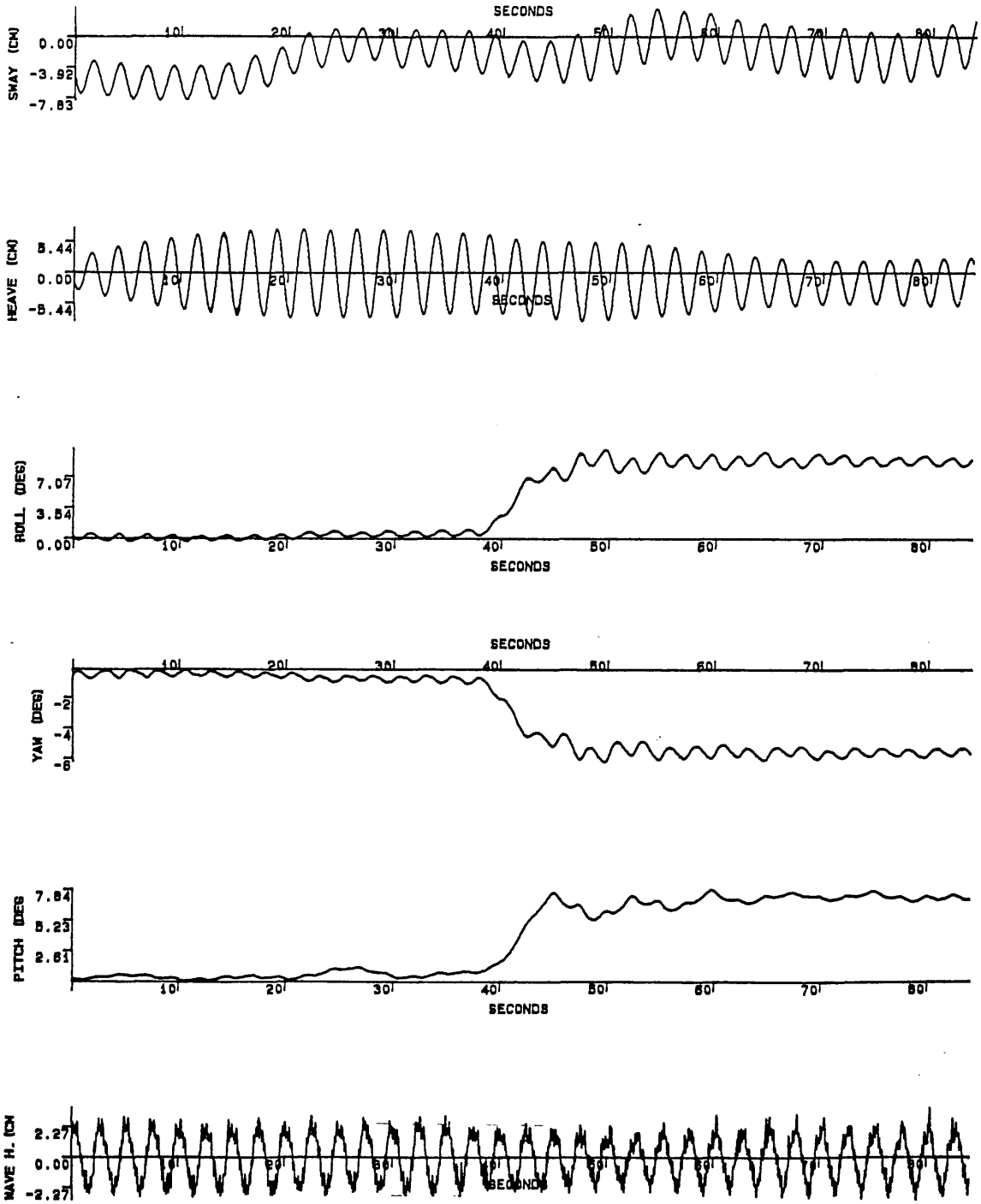

Fig.5.79 Motion response experiment (Beam sea condition-asymmetrical flooding)
WH=5.3 cm Flooding Mass=0.5 kg Flooding Time=10 s
GM=2.29 cm ω=2.5 r/s (0.4 hertz) TS2972S.DAT

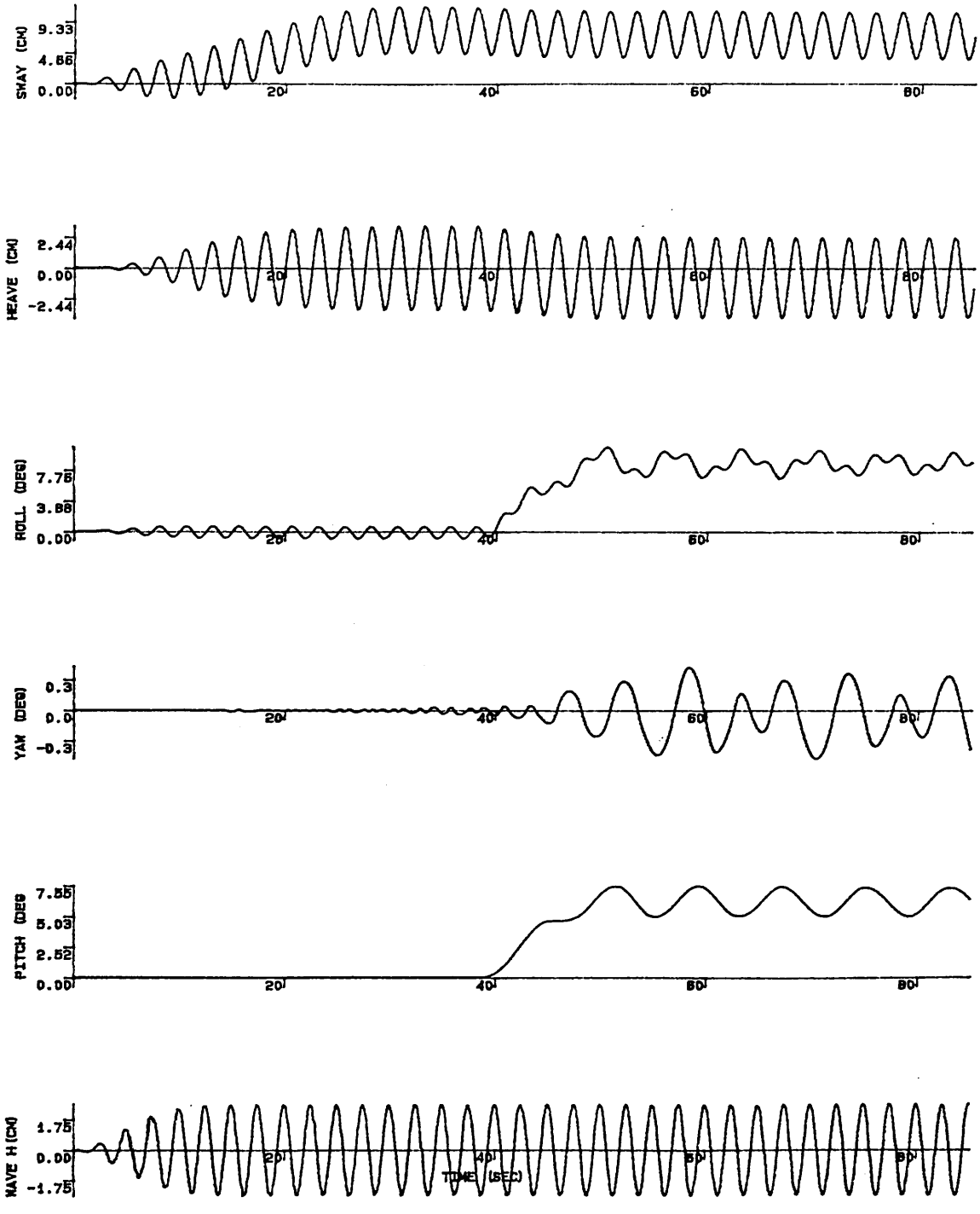

Fig.5.80 Motion response simulation (Beam sea condition-asymmetrical flooding)
WH=5.3 cm Flooding Mass=0.5 kg Flooding Time=10 s
GM=2.29 cm ω=2.5 r/s (0.4 hertz)

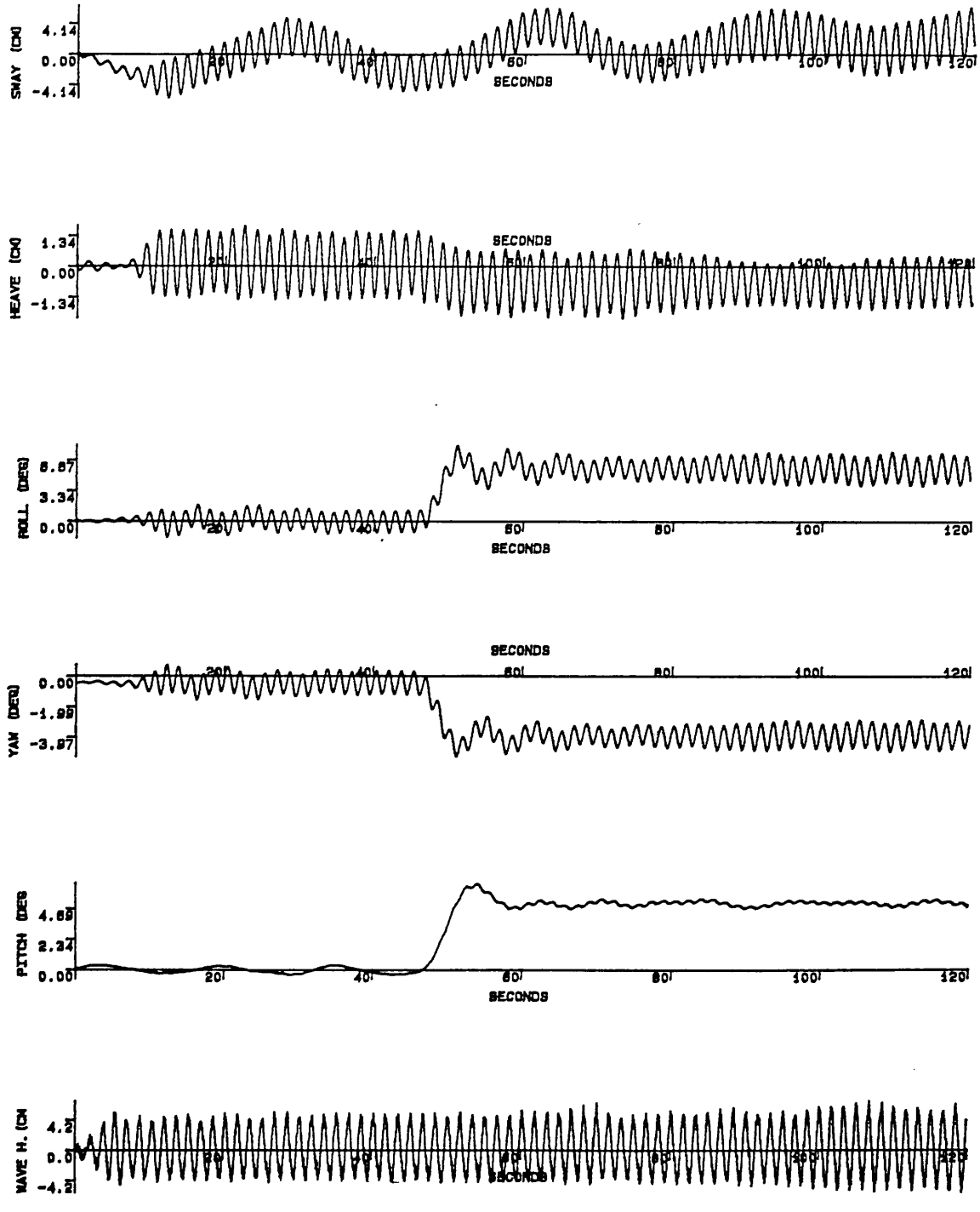

Fig.5.81 Motion response experiment (Beam sea condition-asymmetrical flooding)
WH=10.2 cm Flooding Mass=0.2 kg Flooding Time=5 s
GM=2.29 cm ω=3.8 r/s (0.6 hertz) TS2974S.DAT

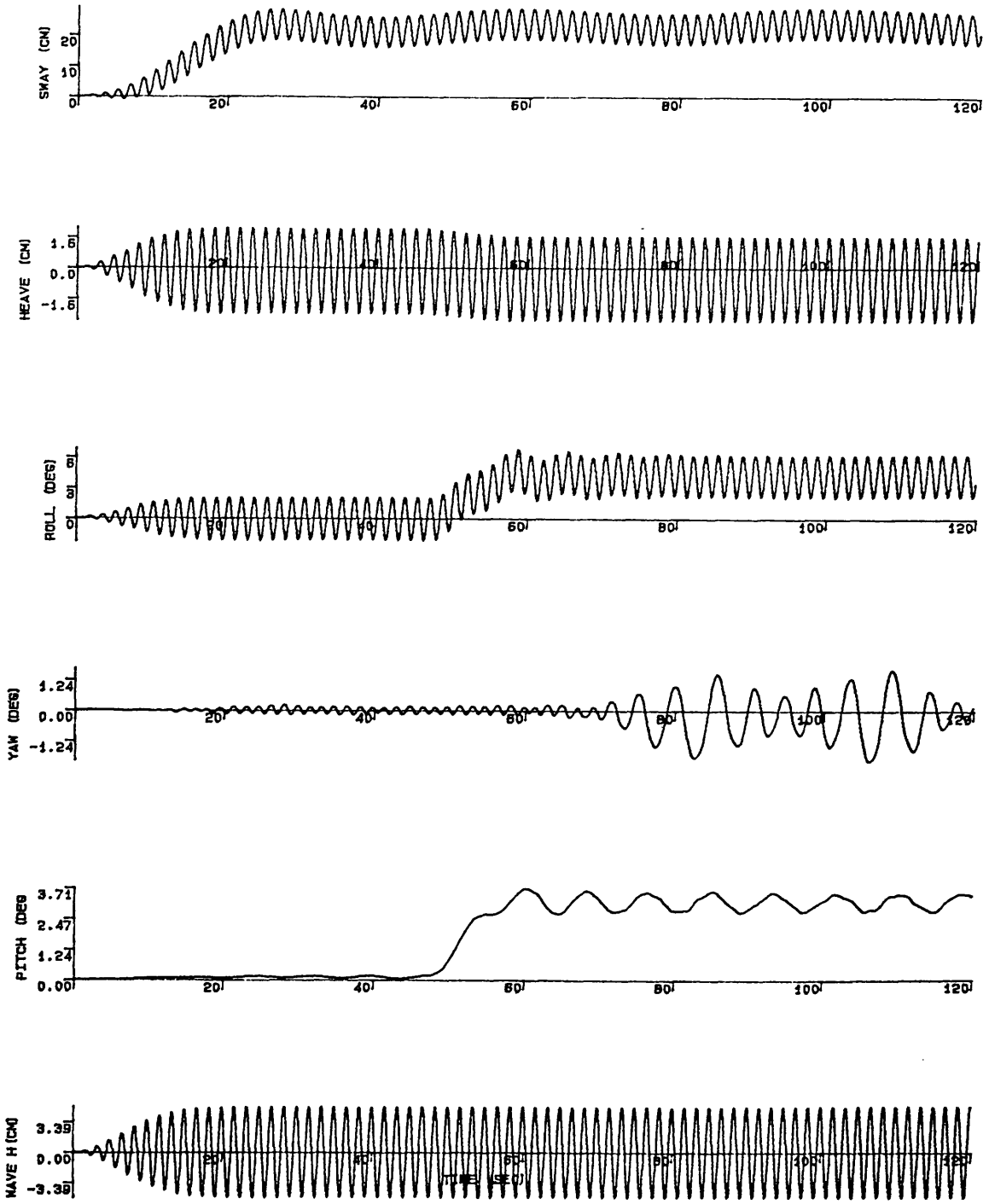

Fig.5.82 Motion response simulation (Beam sea condition-asymmetrical flooding)
WH=10.2 cm Flooding Mass=0.2 kg Flooding Time=5 s
GM=2.29 cm ω=3.8 r/s (0.6 hertz)

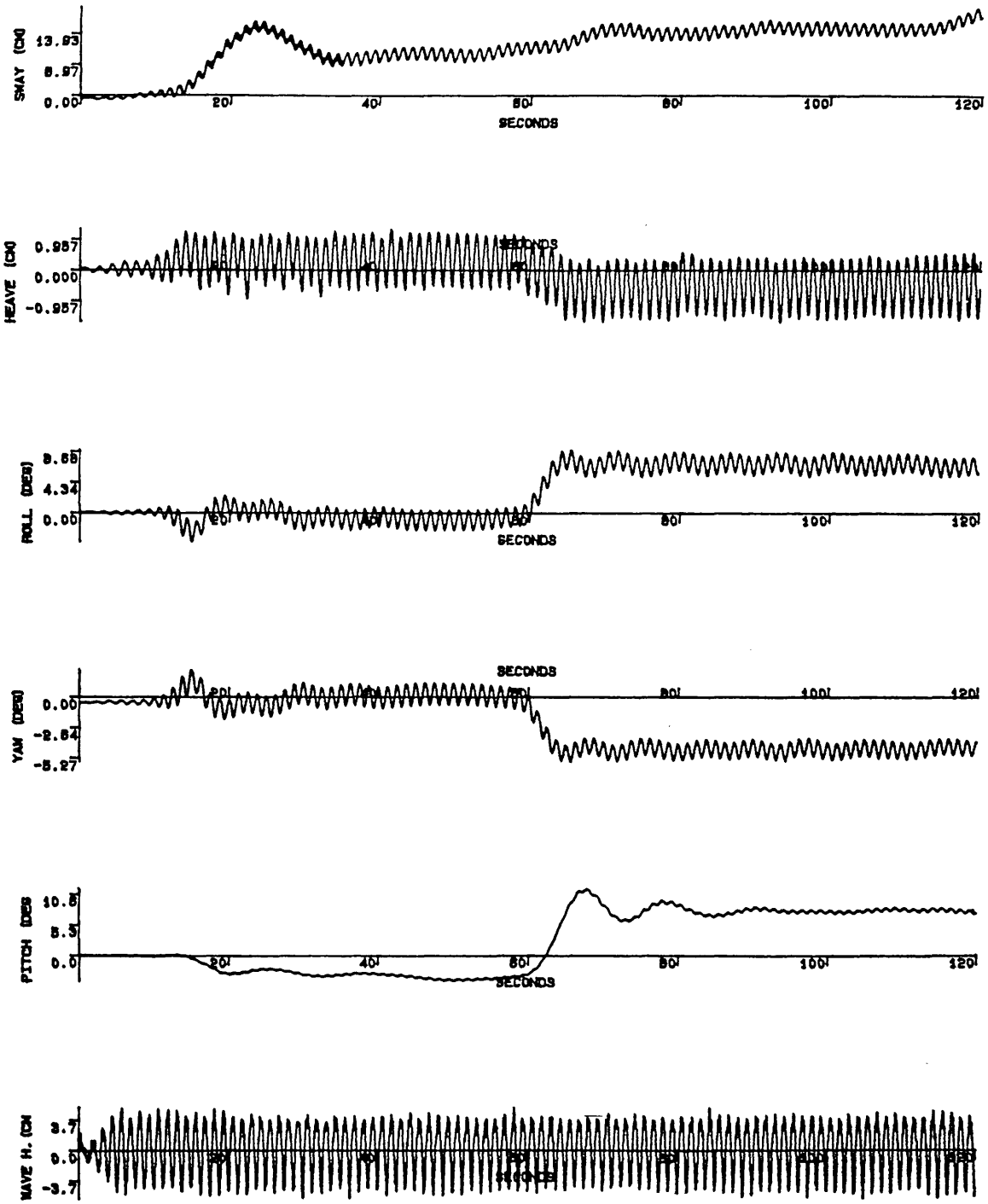

Fig.5.83 Motion response experiment (Beam sea condition-asymmetrical flooding)

WH=9.4 cm	Flooding Mass=0.2 kg	Flooding Time=5 s
GM=2.29 cm	ω=5.0 r/s (0.8 hertz)	TS2975S.DAT

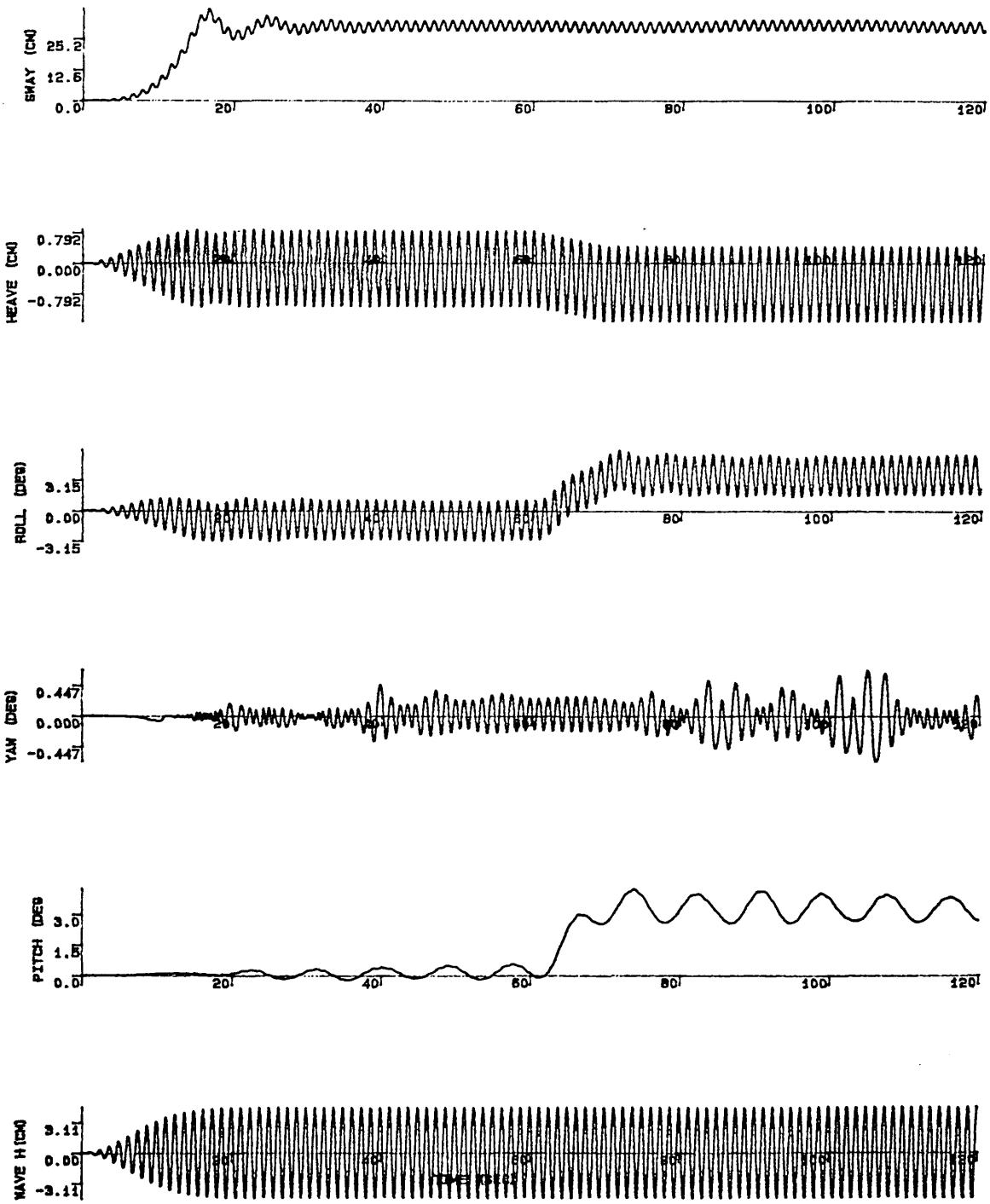

Fig.5.84 Motion response simulation (Beam sea condition-asymmetrical flooding)
WH=9.4 cm Flooding Mass=0.2 kg Flooding Time=5 s
GM=2.29 cm ω=5.0 r/s (0.8 hertz)

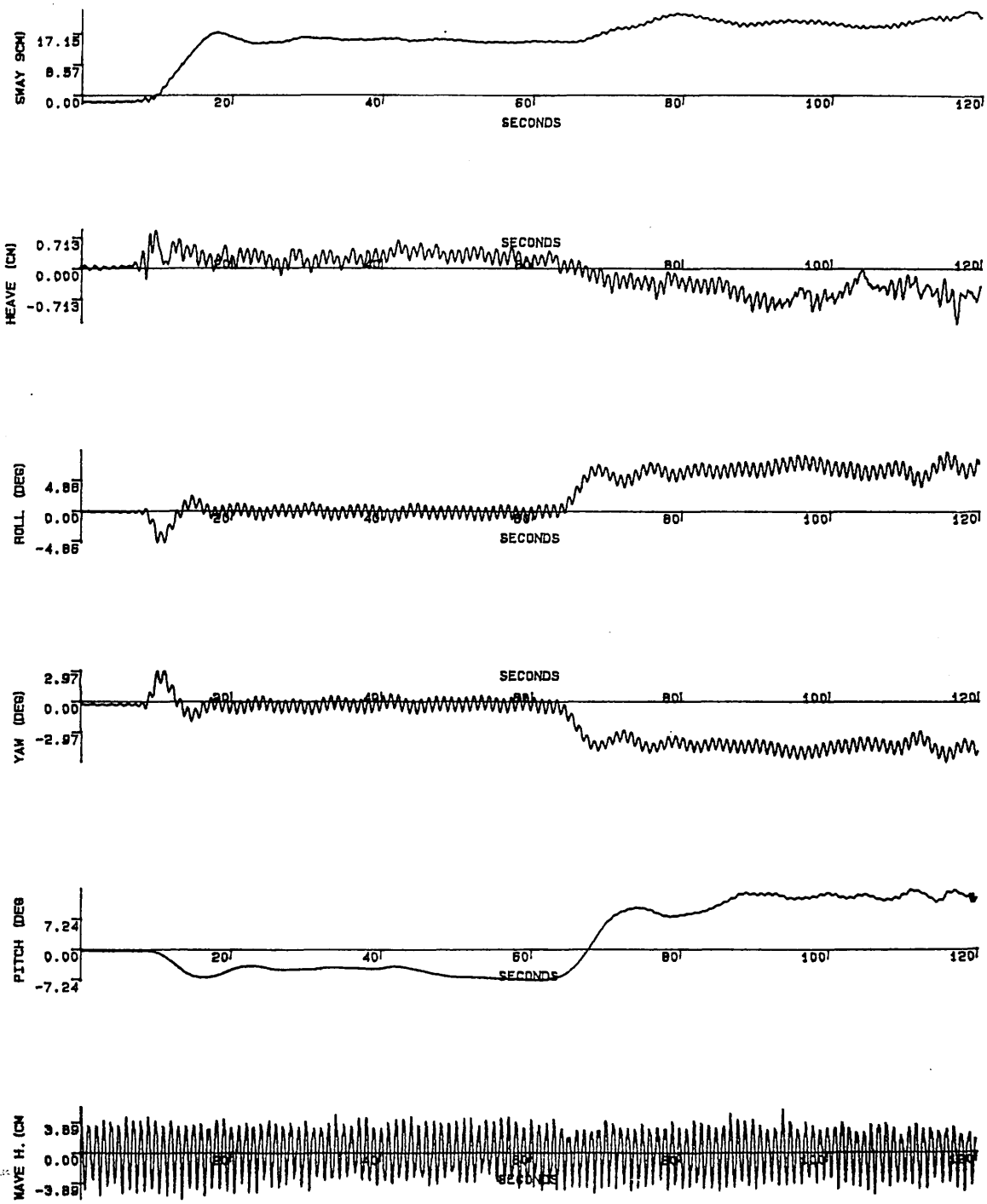

Fig.5.85 Motion response experiment (Beam sea condition-asymmetrical flooding)
WH=7.4 cm Flooding Mass=0.2 kg Flooding Time=5 s
GM=2.29 cm ω=6.3 r/s (1.0 hertz) TS2976S.DAT

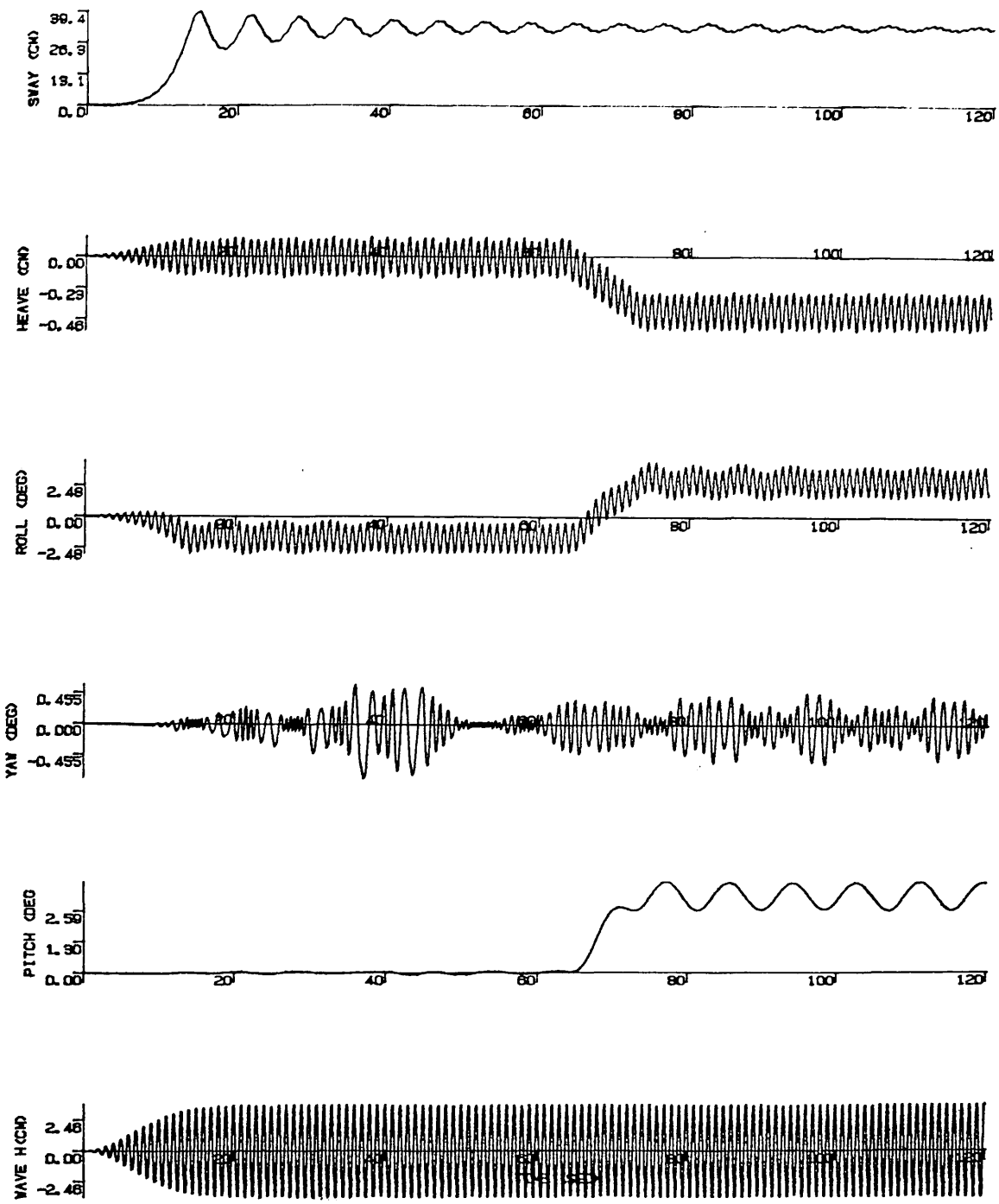

Fig.5.86 Motion response simulation (Beam sea condition-asymmetrical flooding)
WH=7.4 cm Flooding Mass=0.2 kg Flooding Time=5 s
GM=2.29 cm ω=6.3 r/s (1.0 hertz)

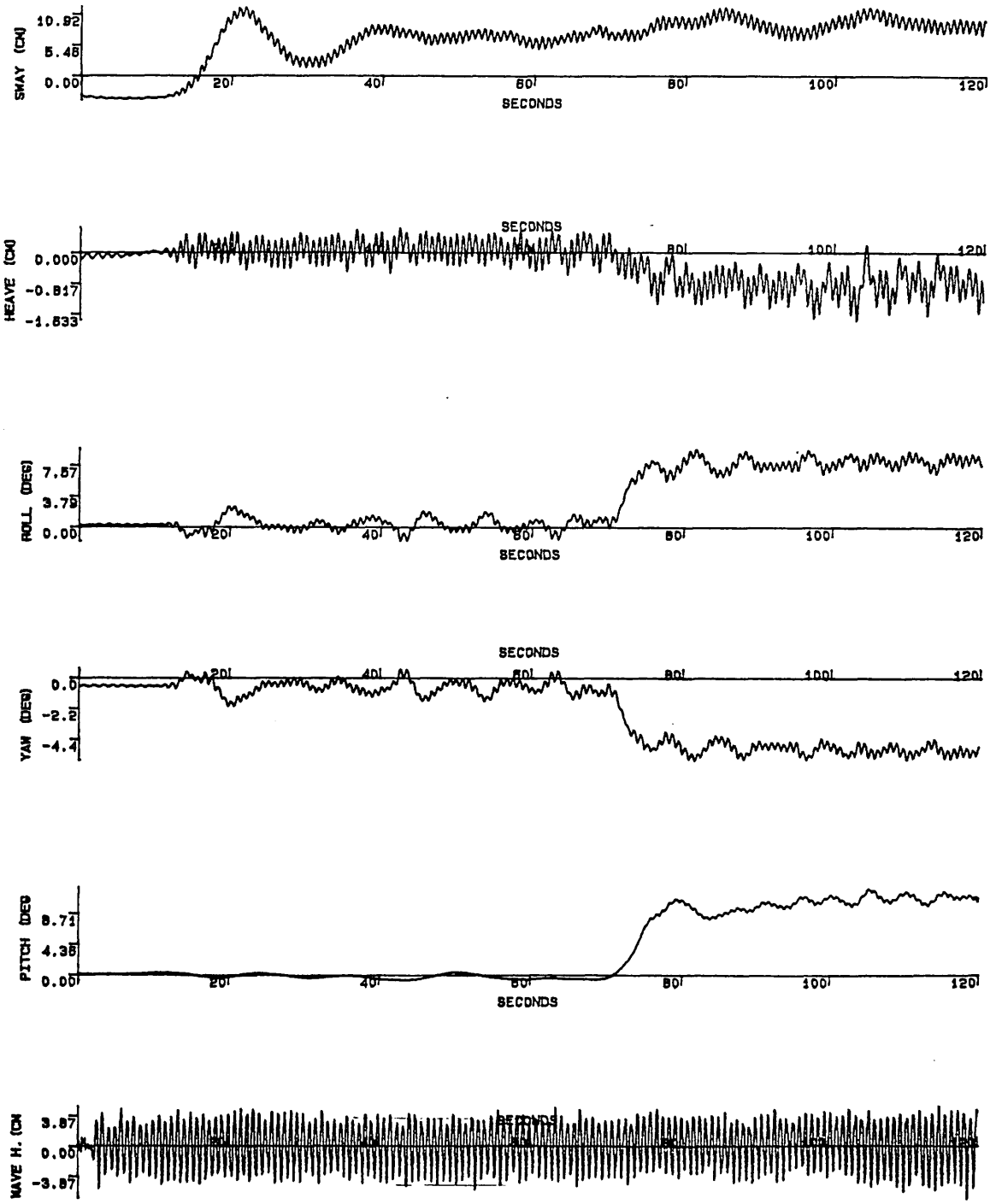

Fig.5.87 Motion response experiment (Beam sea condition-asymmetrical flooding)

WH=8.6 cm	Flooding Mass=0.2 kg	Flooding Time=5 s
GM=2.29 cm	ω=7.5 r/s (1.2 hertz)	TS2977S.DAT

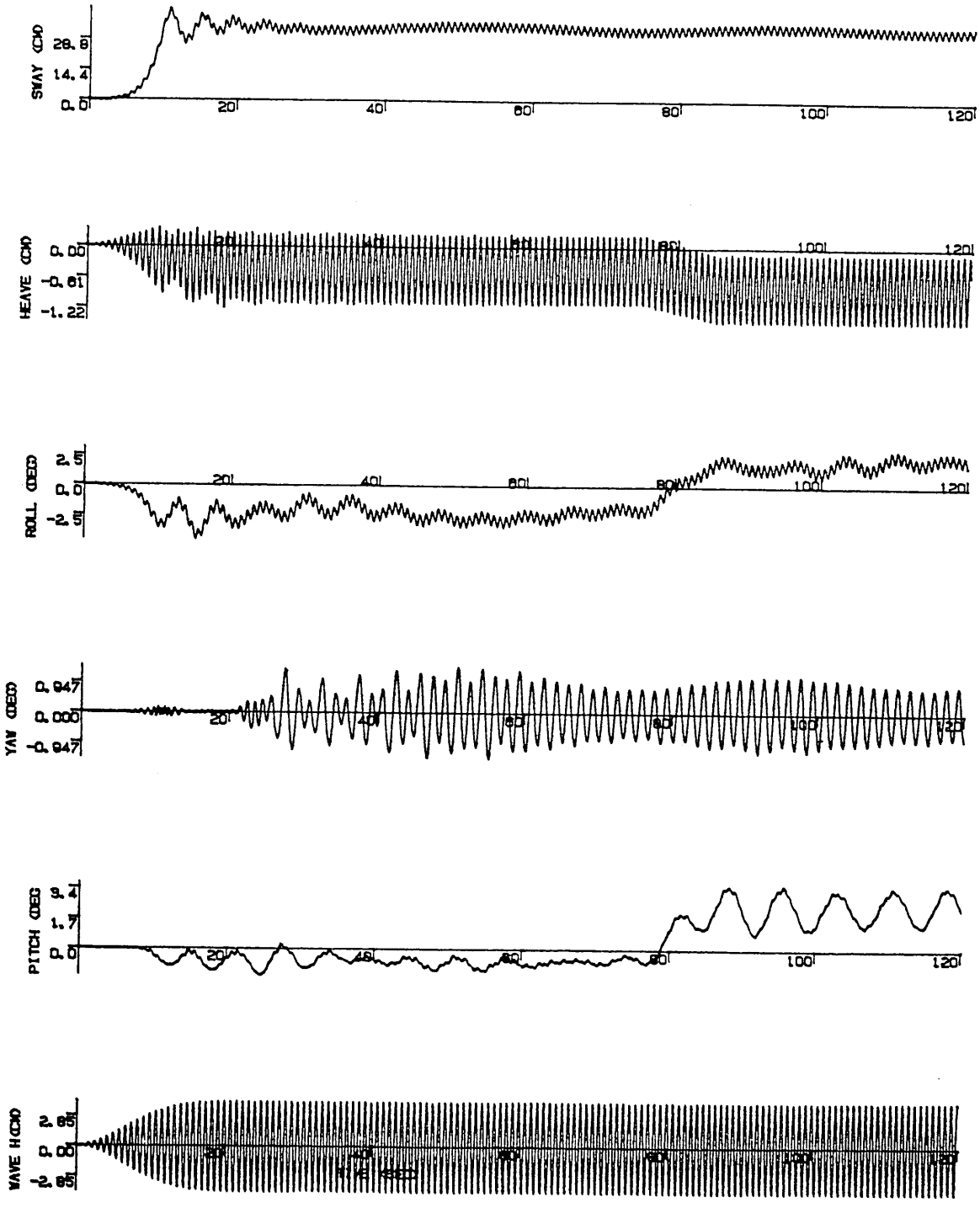

Fig.5.88 Motion response simulation (Beam sea condition-asymmetrical flooding)
WH=8.6 cm Flooding Mass=0.2 kg Flooding Time=5 s
GM=2.29 cm ω=7.5 r/s (1.2 hertz)

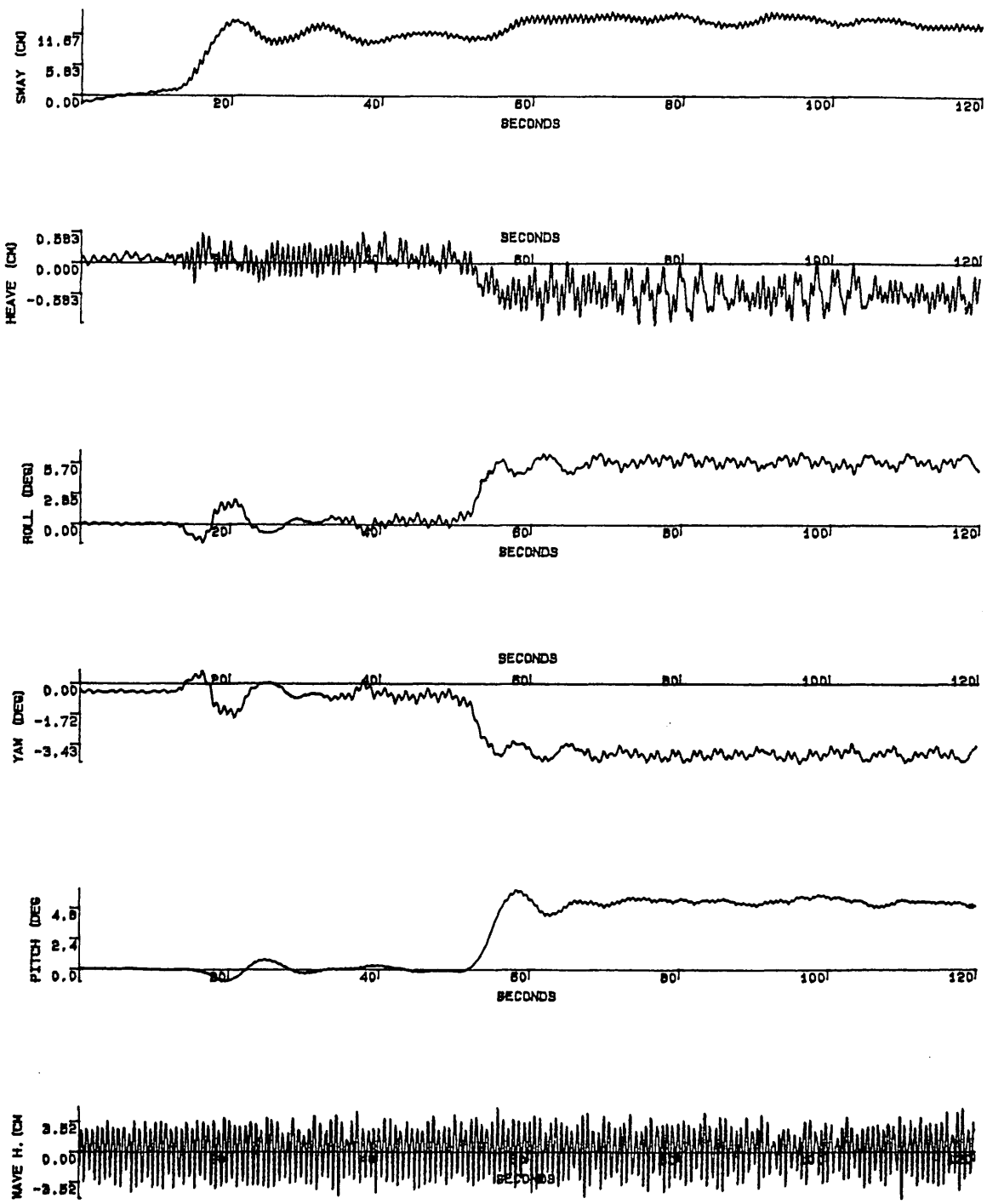

Fig.5.89 Motion response experiment (Beam sea condition-asymmetrical flooding)

WH=7.0 cm	Flooding Mass=0.2 kg	Flooding Time=5 s
GM=2.29 cm	ω=8.8 r/s (1.4 hertz)	TS2978S.DAT

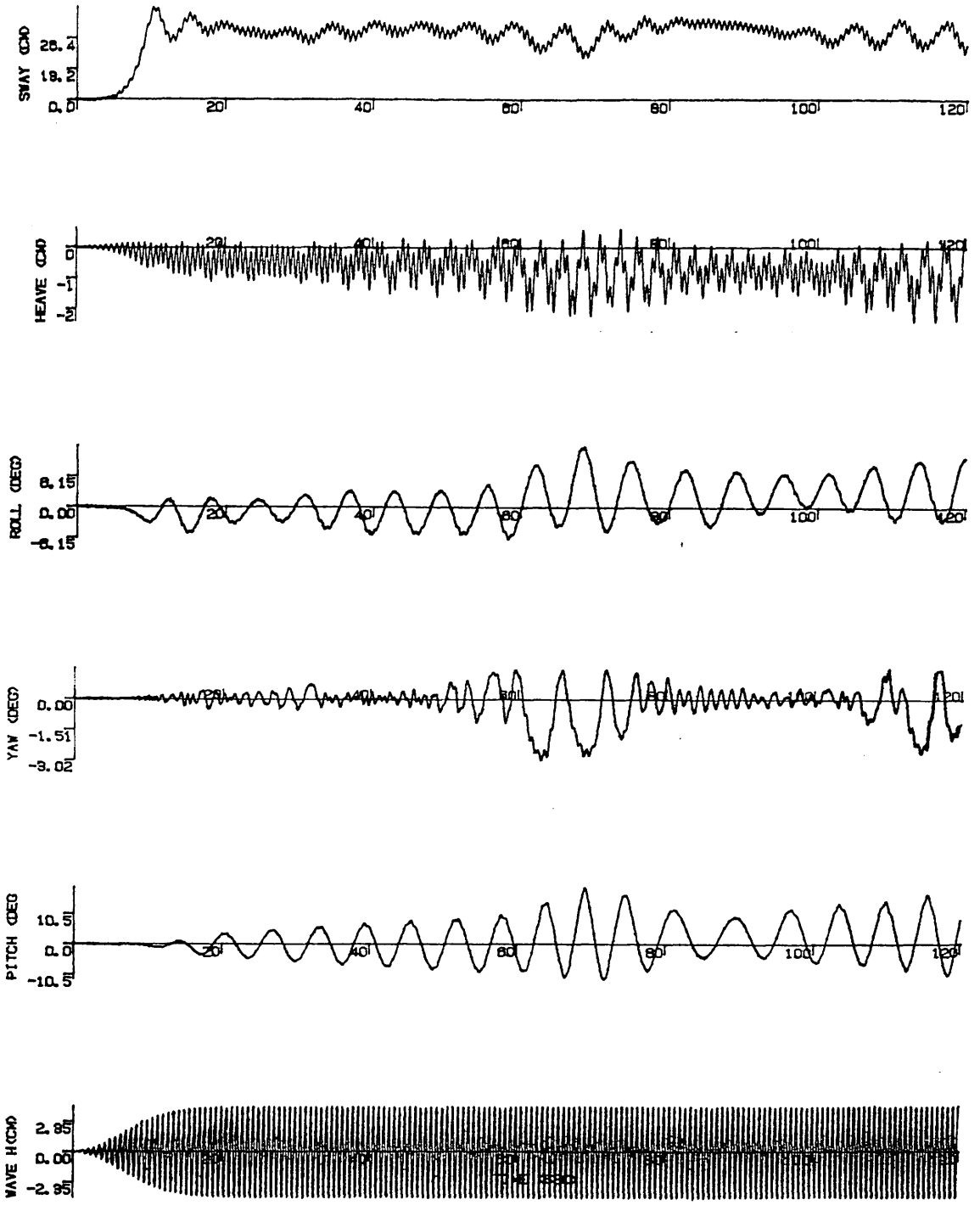

Fig.5.90 Motion response simulation (Beam sea condition-asymmetrical flooding)
WH=7.0 cm Flooding Mass=0.2 kg Flooding Time=5 s
GM=2.29 cm ω=8.8 r/s (1.4 hertz)

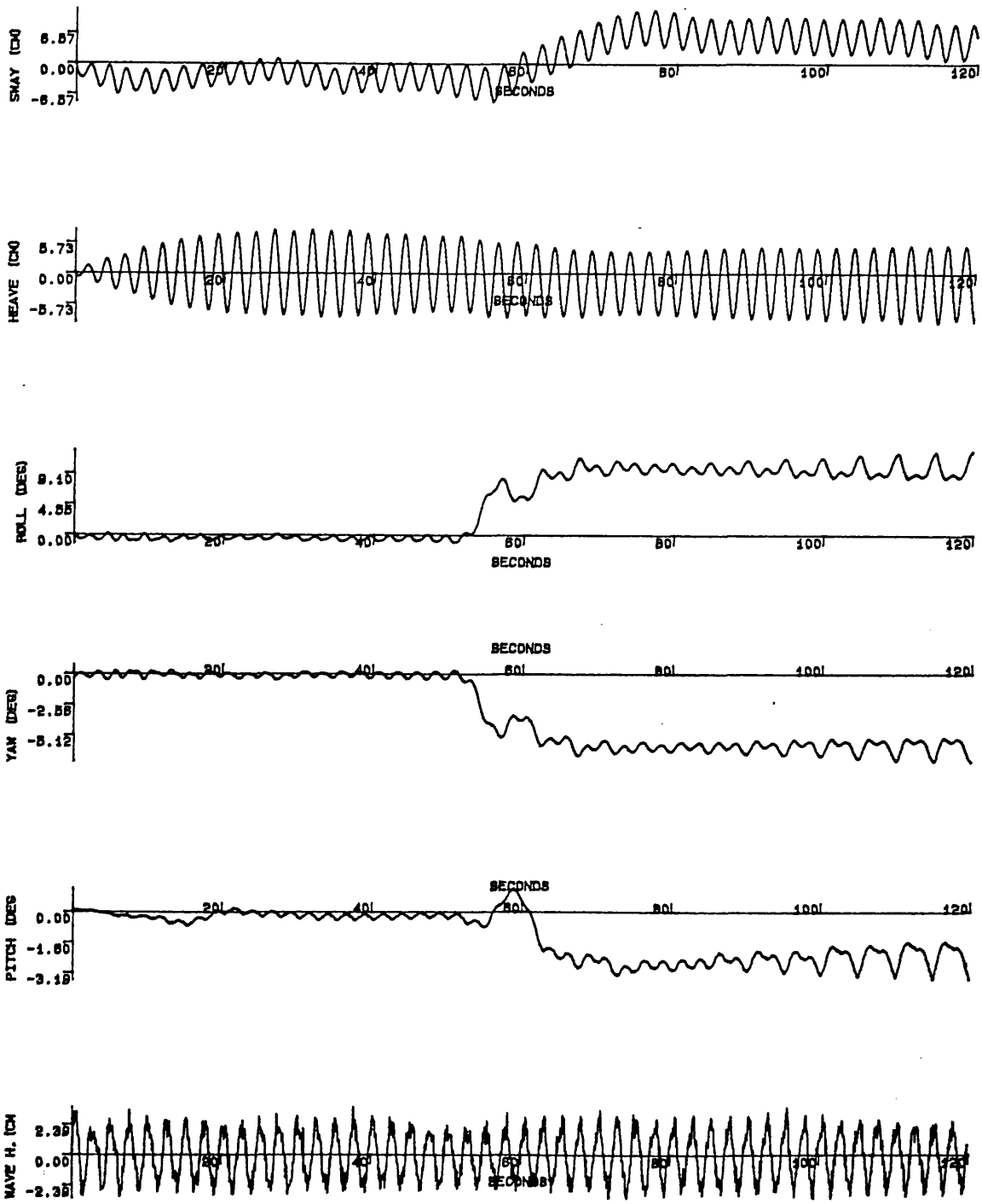

Fig.5.91 Motion response experiment (Beam sea condition-symmetrical flooding)

WH=5.5 cm	Flooding Mass=0.3 kg	Flooding Time=5 s
GM=2.29 cm	ω=2.5 r/s (0.4 hertz)	TS2979S.DAT

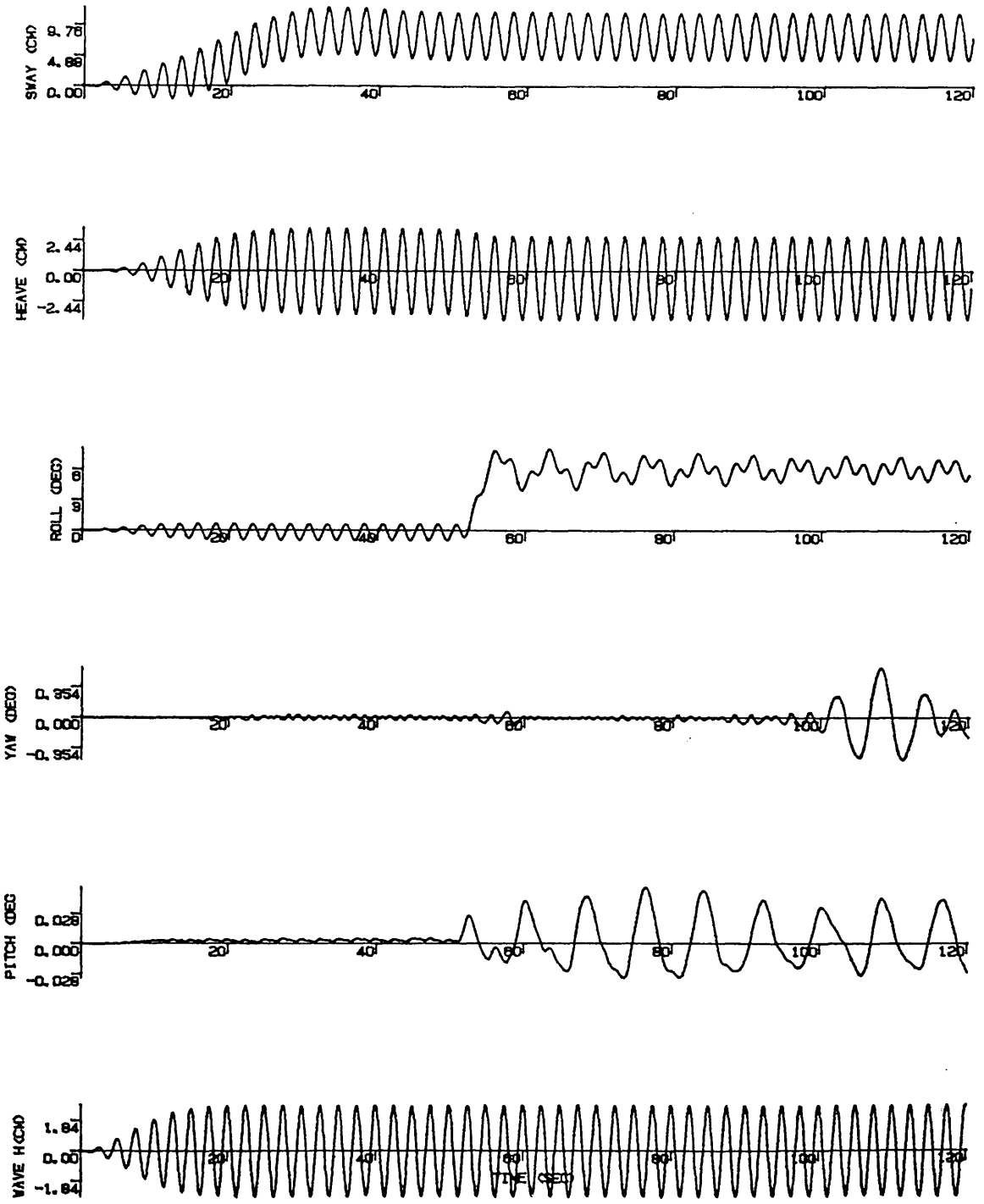

Fig.5.92 Motion response simulation (Beam sea condition-symmetrical flooding)
WH=5.5 cm Flooding Mass=0.3 kg Flooding Time=5 s
GM=2.29 cm ω=2.5 r/s (0.4 hertz)

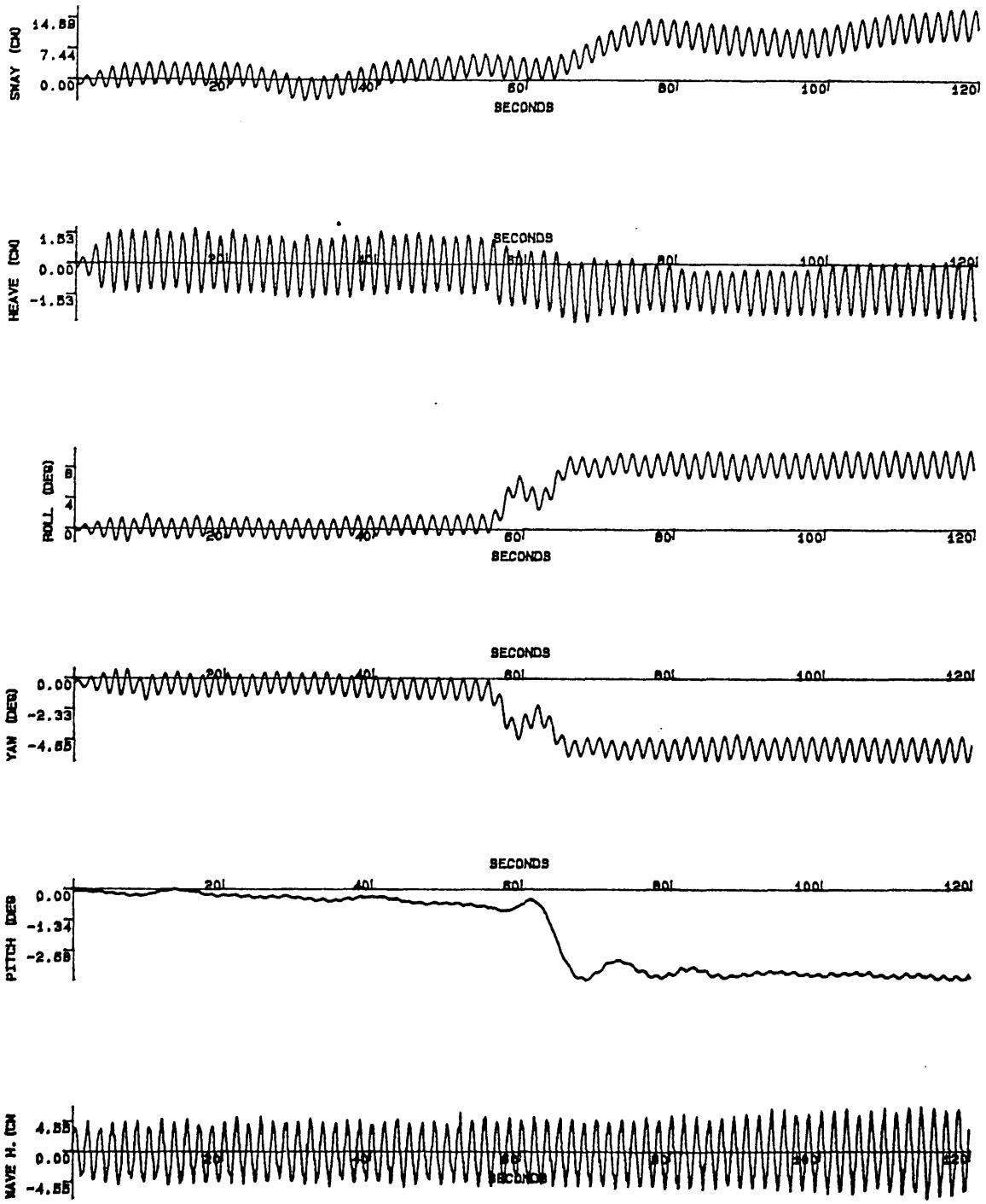

Fig.5.93 Motion response experiment (Beam sea condition-symmetrical flooding)
WH=10.1 cm Flooding Mass=0.3 kg Flooding Time=5 s
GM=2.29 cm ω=3.8 r/s (0.6 hertz) TS2980S.DAT

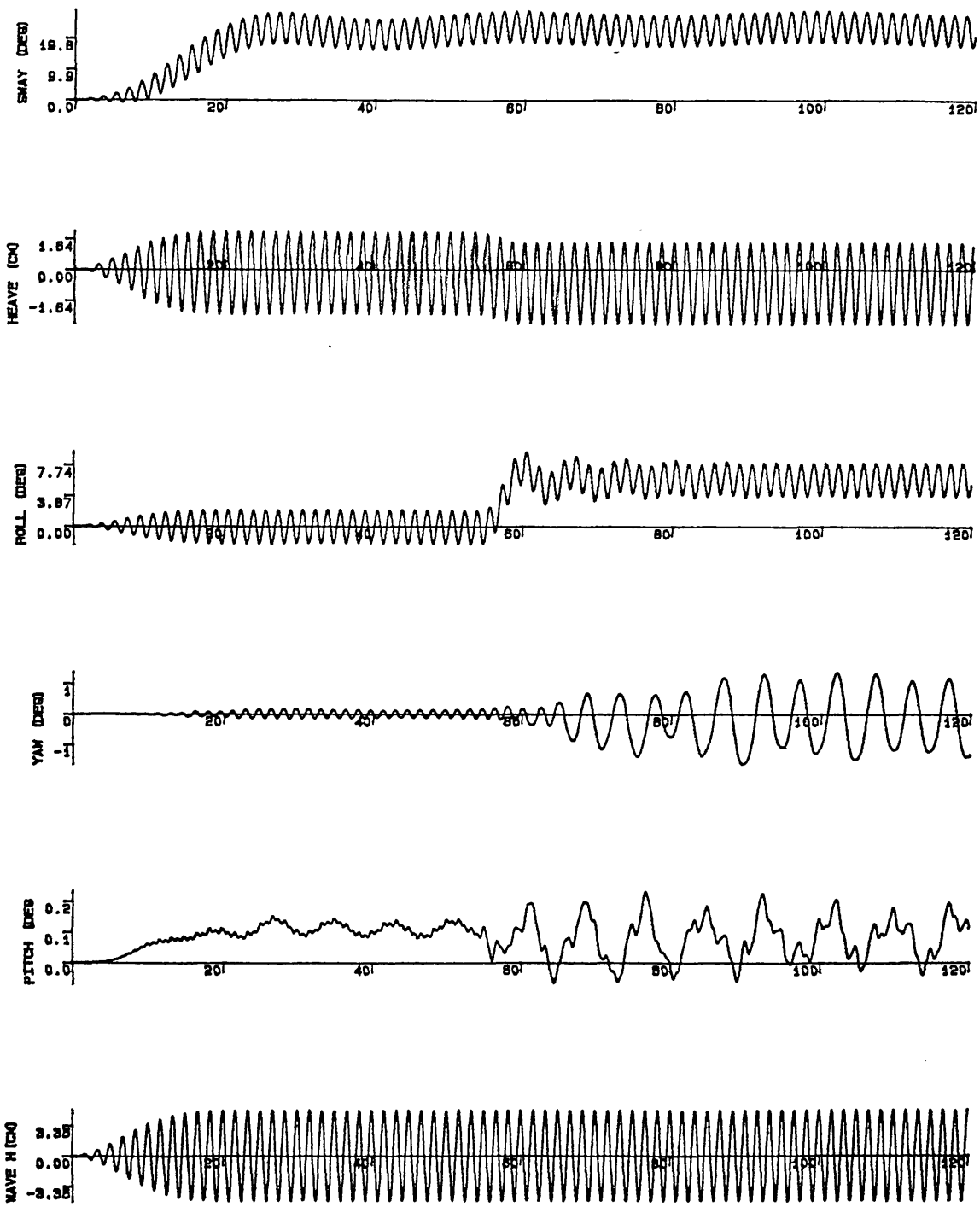

Fig.5.94 Motion response simulation (Beam sea condition-symmetrical flooding)
WH=10.1 cm Flooding Mass=0.3 kg Flooding Time=5 s
GM=2.29 cm ω=3.8 r/s (0.6 hertz)

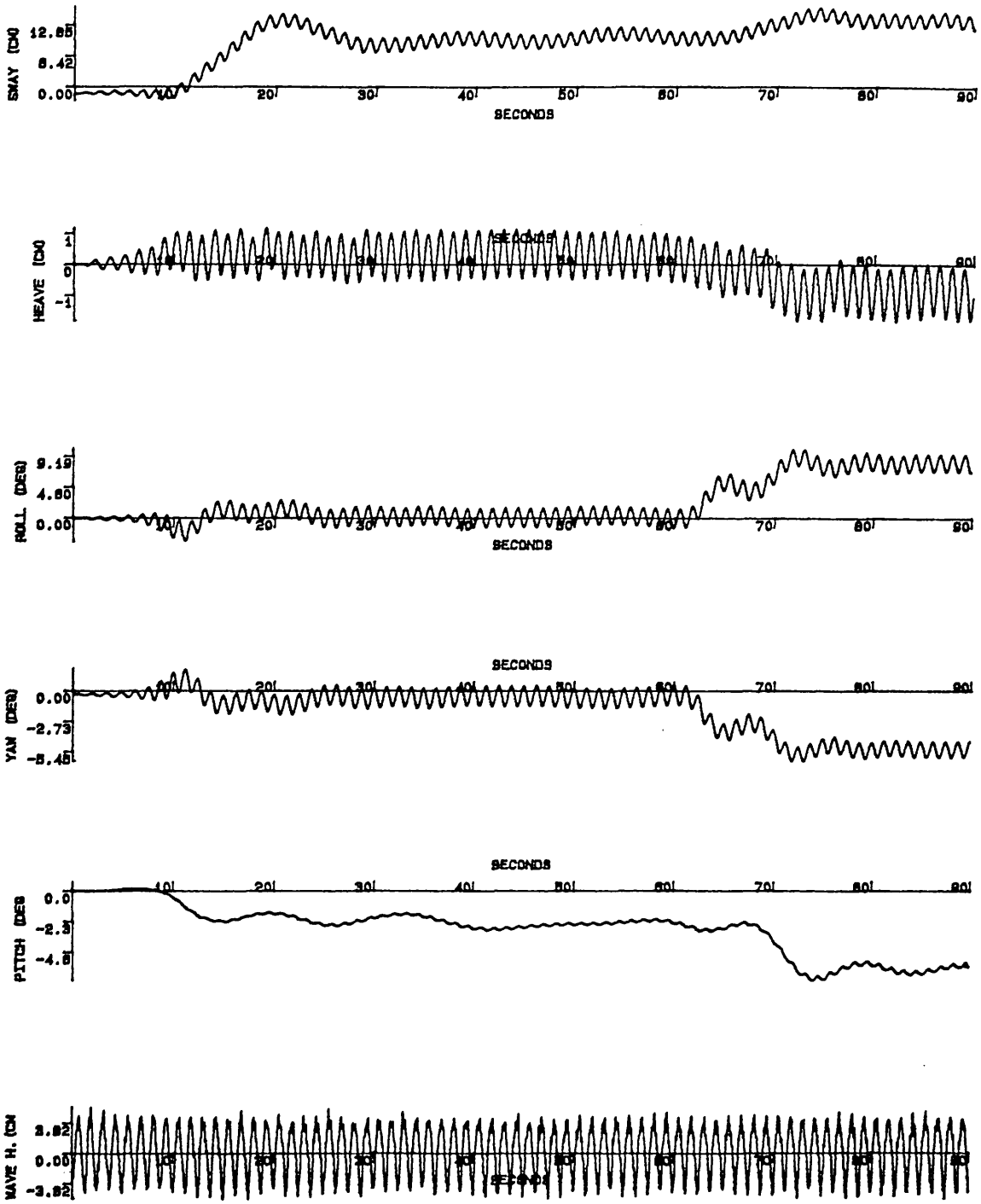

Fig.5.95 Motion response experiment (Beam sea condition-symmetrical flooding)

WH=8.9 cm	Flooding Mass=0.3 kg	Flooding Time=5 s
GM=2.29 cm	ω=5.0 r/s (0.8 hertz)	TS2981S.DAT

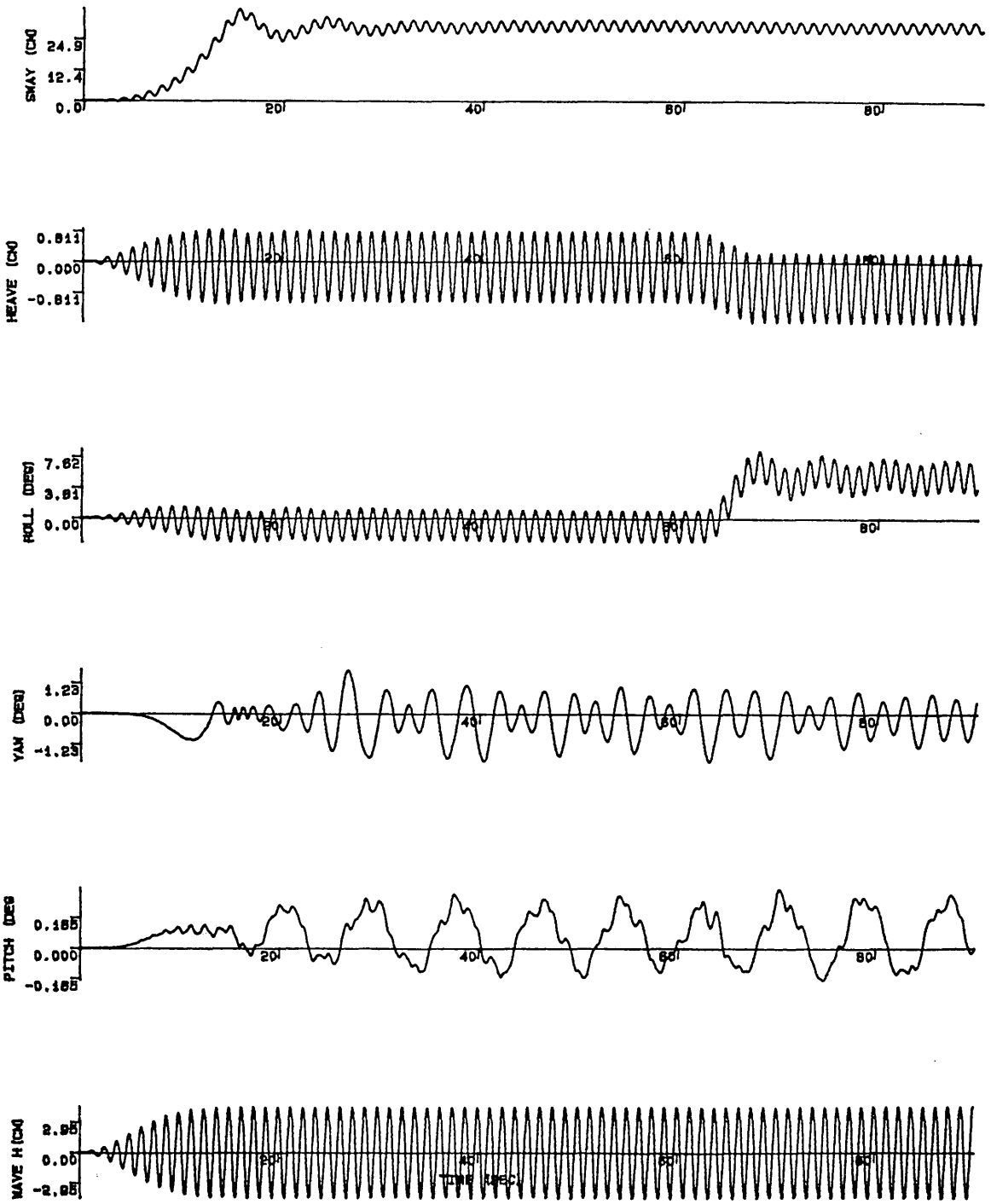

Fig.5.96 Motion response simulation (Beam sea condition-symmetrical flooding)
WH=8.9 cm Flooding Mass=0.3 kg Flooding Time=5 s
GM=2.29 cm ω=5.0 r/s (0.8 hertz)

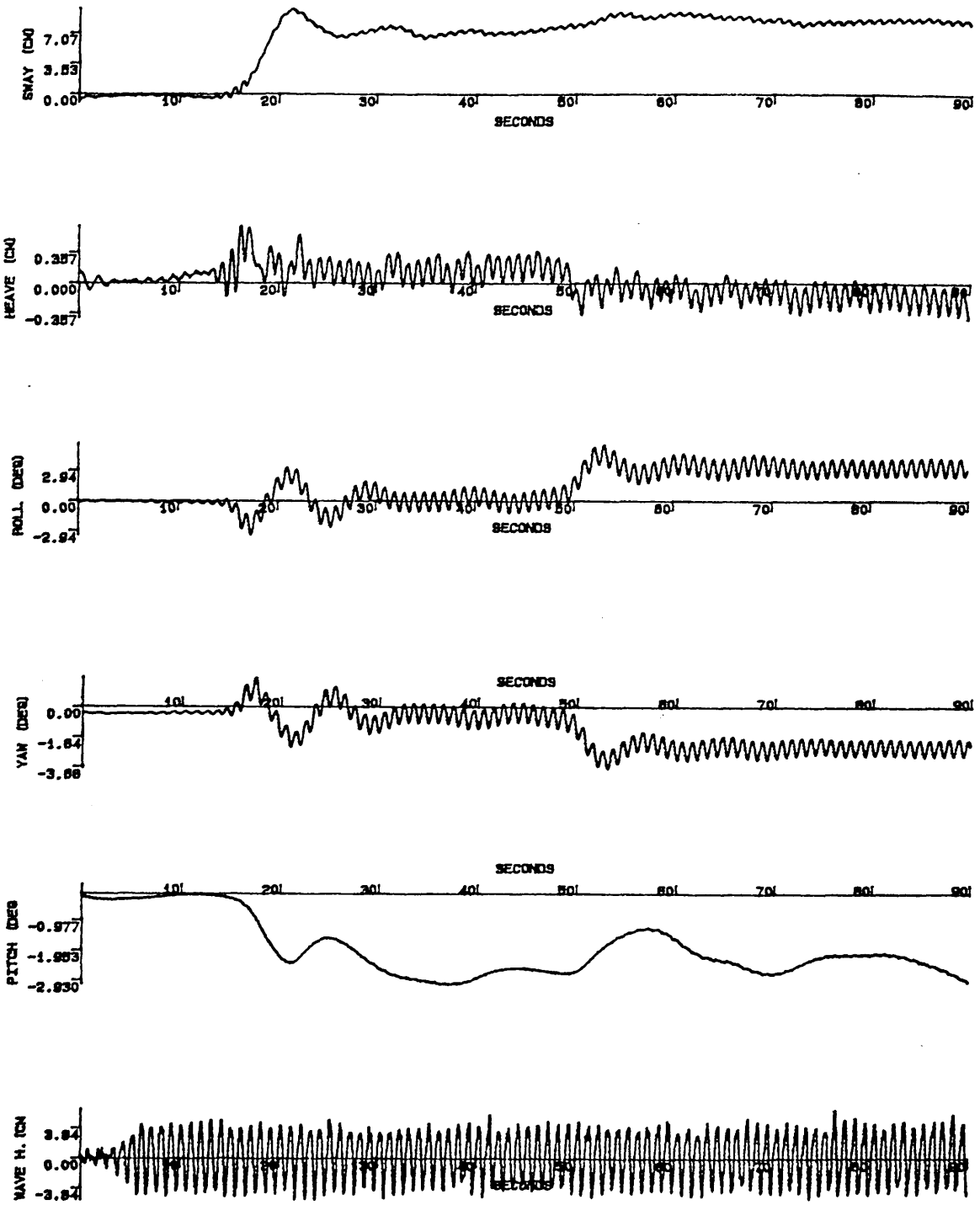

Fig.5.97 Motion response experiment (Beam sea condition-symmetrical flooding)
WH=8.9 cm Flooding Mass=0.3 kg Flooding Time=5 s
GM=2.29 cm ω=6.3 r/s (1.0 hertz) TS2982S.DAT

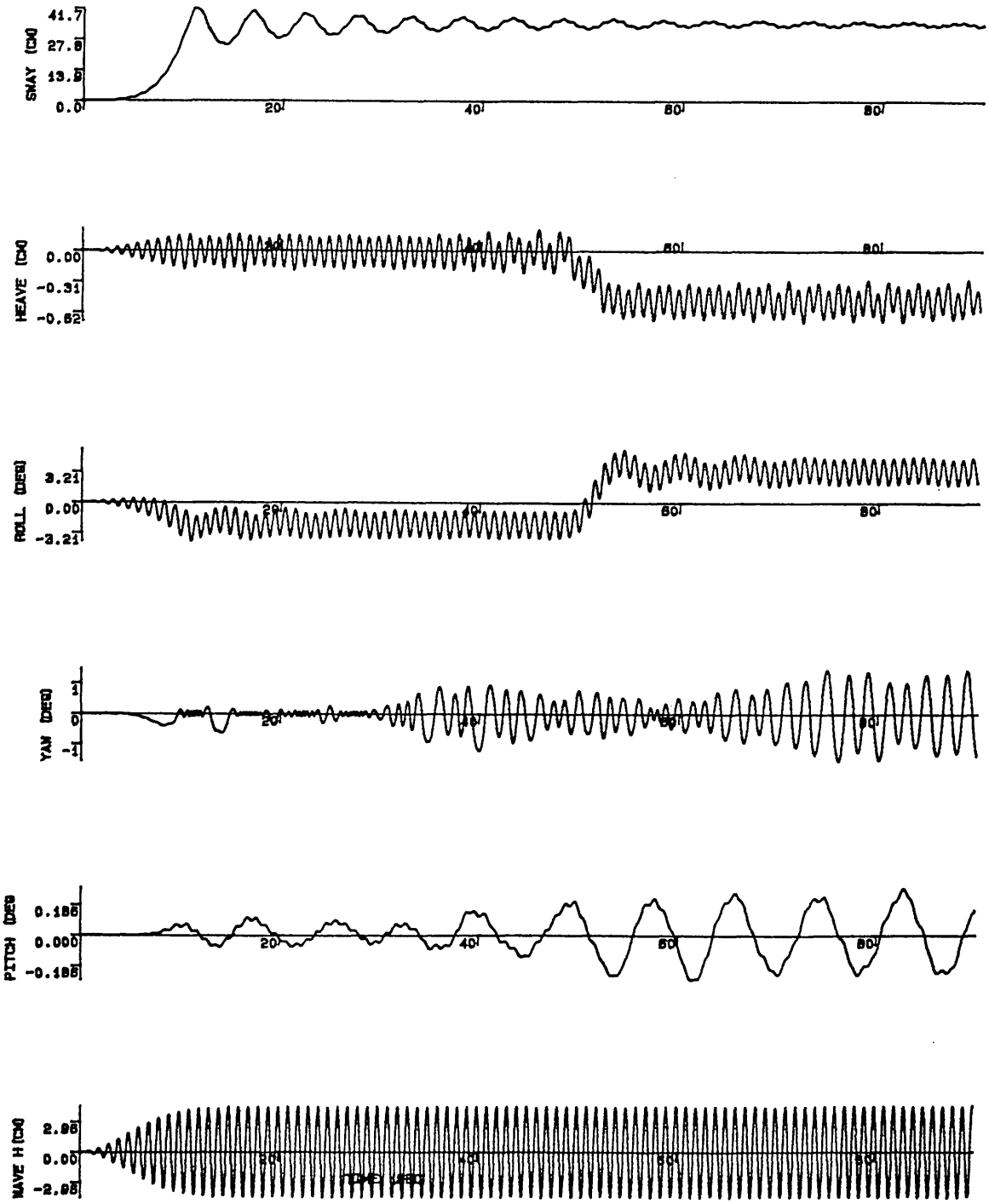

Fig.5.98 Motion response simulation (Beam sea condition-symmetrical flooding)
WH=8.9 cm Flooding Mass=0.3 kg Flooding Time=5 s
GM=2.29 cm ω=6.3 r/s (1.0 hertz)

CHAPTER 6

PARAMETRIC STUDIES

6.1 INTRODUCTION

This chapter presents the results of an extensive parametric study to investigate various non-linear aspects of the prediction of the large amplitude motion responses of a semi-submersible. The investigations were carried out for the particular semi-submersible geometry using a numerical simulation technique in the time-domain. The simulations were performed for the model during intact, progressive and post-flooding conditions under the combined loading of regular waves, steady wind and current for two different heading angles.

The main objectives of the parametric studies were to investigate the following aspects, which can non-linearly influence the motion responses and which can not be studied by linear frequency-domain prediction techniques. These aspects are the effects of flooding time and mass, non-linear wave-exciting and rigid-body induced motion (i.e. added mass and damping) forces, non-linear restoring forces, steady wind and current, variation of GM, initial position of the semi-submersible on motion responses.

Thus, this chapter is intended to provide some insight into the physical effects of the non-linear terms in the motion equations which are associated with the wave-excitation forces, rigid-body induced motion forces and restoring forces. Since the resulting motion responses could have a steady component as well as the oscillatory one, the force and motion phenomenon were also highlighted through the computation of these components.

6.2 PRESENTATION OF PARAMETRIC STUDIES

This section provides general information on the parametric studies. The aspects mentioned as the objectives of this chapter in the previous section were investigated under the following subtitles:

i) Effects of flooding time and mass on the roll response

ii) Effects of non-linear wave excitation and restoring forces on the motion behaviour

iii) Effects of coupling between heave and roll modes of motion

iv) Effects of steady wind and current on the motion behaviour

v) Effects of second-order forces

- First-order relative wave elevation
- Non-linear drag force

vi) Effects of non-linear added mass and damping force on motion behaviour

vii) Effect of different GM in steady and oscillatory motion behaviour

viii) Effect of initial condition on motion behaviour

Among the effects listed above, v is associated with the second-order phenomenon. Therefore, a brief definition of the second-order steady forces and their components is presented prior to considering the effects of second-order forces. Parametric studies were carried out for the semi-submersible model which was described in more detail in Chapter 5. A general arrangement of the model is shown in Fig.2.2.

Head and beam sea conditions were considered in the parametric studies. In most of the computations, the wave frequency range varied from 1 to 10 rad/s (0.12 to 1.19 r/s in full scale). The wave heights varied from 5 to 30 cm (3.5 to 21 m in full scale).

When the effects of steady wind and current were taken into account, it was assumed that they acted as in the same direction as the waves. Based on some full scale measurements, a typical value of 6.16 m/s (51.5 m/s in full scale) for the steady wind velocity and 0.1 m/s (0.8 m/s in full scale) for the steady current velocity were selected.

In damaged conditions, the model was assumed to be damaged at one or two of the inner columns. The flooding time varied from 5 to 15 s (41 to 125 s in full scale) while the flooding mass was varied from 1.5 to 5 kg (514 to 1715 t in full scale).

For the investigation of varying GMs, three different loading condition were tested. These conditions yielded corresponding GM values of 1.9, 3.8 and 7.9 cm in model scale. The highest GM value was used in the parametric studies presented in the other sections of the chapter.

6.2.1 THE EFFECT OF FLOODING TIME AND MASS ON THE ROLL RESPONSE

The non–linear motion equations given in Section 4.5 were applied to a semi-submersible model in the presence of no wind or current. As defined in more detail by Söylemez (1988), 110 computer simulations were carried out. The objective of this investigation was to determine the effect of size of flooded compartment and flooding time on motion response amplitudes.

Tabulated results of the computations for the above defined damaged condition (i.e. semi-submersible was assumed to be damaged at the inner columns) are given in Tables 6.1 and 6.2 and Figs.6.1-3 for the roll motion response. Although it is not very significant in the tables but quite clear in Figs.6.1-3, the general trend of the findings is that as the flooding time increases, the motion amplitudes in the transient region decrease. This group of studies also indicated that the transient motion displacement during progressive flooding can be significantly higher than that during post-flooding (Figs.6.1–3).

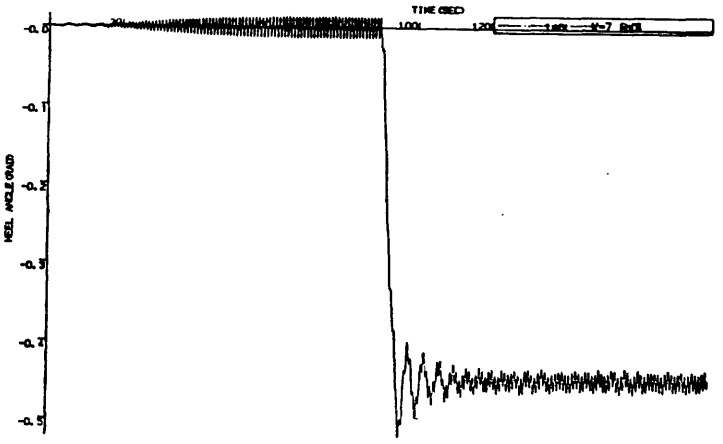

Fig.6.1 Motion response simulation of roll
WH=10 cm Flooding Mass=5 kg Flooding Time=5 s
GM=7.9 cm ω=7 rad/s

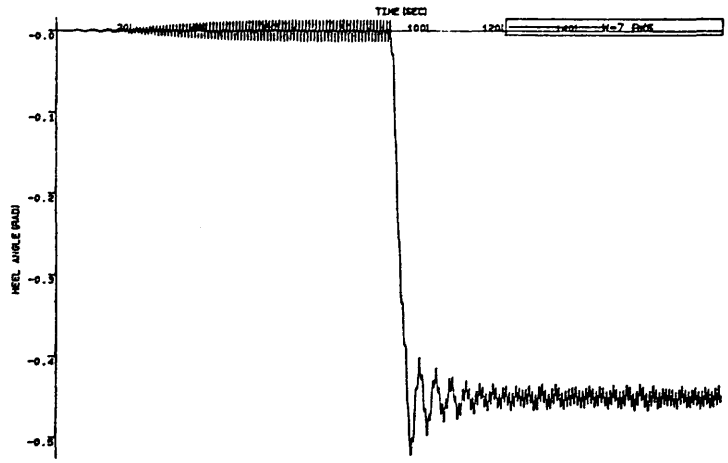

Fig.6.2 Motion response simulation of roll
WH=10 cm Flooding Mass=5 kg Flooding Time=10 s
GM=7.9 cm ω=7 rad/s

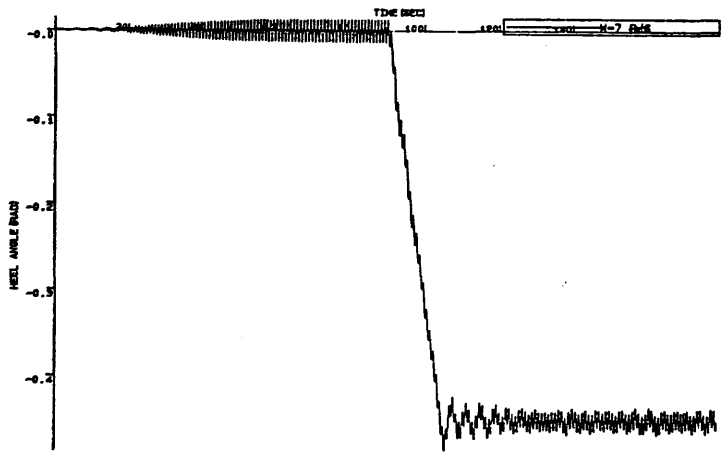

Fig.6.3 Motion response simulation of roll
WH=10 cm Flooding Mass=5 kg Flooding Time=15 s
GM=7.9 cm ω=7 rad/s

Freq (rad/s)	Roll Displacements in Intact Condition (deg)	Roll Displacements in Post Flooding Condition (deg)		
		Flooding Time=5 s	Flooding Time=10 s	Flooding Time=15 s
1	0.325	8.300	8.300	8.021
2	2.120	9.983	10.225	9.834
3	1.948	10.070	9.774	9.940
4	2.120	10.385	10.137	9.983
5	2.005	10.225	9.920	9.877
6	1.490	9.822	9.483	9.167
7	0.802	9.167	8.855	8.820
8	0.218	8.905	8.626	8.251
9	0.097	8.709	8.709	8.467
10	0.160	8.840	8.467	8.403
	Wave Height = 10 cm Water Mass in Flooded Compartment = 1.5 kg			

Table 6.1- The Effect of Flooding Time on Roll Response Predictions

6.2.2. EFFECTS OF NON-LINEAR WAVE EXCITATION AND RESTORING FORCES ON MOTION BEHAVIOUR

In order to show these two effects, the results of the computations for the heave and roll motion responses are provided in Tables 6.3 and 6.4 for two different wave heights (10 and 30 cm). In these computations, the model was in intact condition and no effect of wind or current was taken into account.

In table 6.3, linear displacements were obtained from the solution of the linear small amplitude motion equations in the frequency-domain whereas non-linear displacements were obtained from the solution of the large amplitude non-linear motion equations in the time-domain. In the latter solution, the two force terms were obtained through an actual non-linear modelling while in the former solution the non-linear effects were neglected.

In general, the heave and roll response values obtained from the non-linear model are higher than the response values obtained from the linear model. This trend becomes strong in the resonance regions. For instance, in the heave resonance region (2.5 rad/s) the non-linear formulation yields response values which are about 45% higher than the linear formulation for the extreme wave height of 30 cm in model scale. In the roll resonance region (1.5 rad/s), the non-linear formulation gives roll response displacement about 14% higher than does linear theory.

Table 6.4 shows the effects of non–linearities in wave excitation forces and stiffness terms independently. Since the heave stiffness remains constant during large amplitude oscillations in single degree of freedom due to the geometrical configuration of the semi-submersible, heave displacements compared in the Table 6.4, show the effect of non–linear heave excitation forces only.

Freq (rad/s)	Roll Displacements in Intact Condition (deg)	Roll Displacements in Post Flooding Condition (deg)		
		Flooding Time = 5 s	Flooding Time = 10 s	Flooding Time = 15 s
1	1.328	27.622	27.542	27.067
2	6.767	28.098	28.109	28.109
3	6.043	28.762	28.648	28.648
4	6.446	29.817	29.794	27.892
5	6.043	28.648	28.086	28.000
6	5.605	29.209	29.089	27.399
7	2.380	29.885	29.863	27.622
8	0.724	29.404	29.284	27.267
9	0.371	28.648	28.545	27.301
10	0.498	29.404	29.284	27.267
	Wave Height = 30 cm Water Mass in Flooded Compartment = 5 kg			

Table 6.2- The Effect of Flooding Time on Roll Response Predictions

Freq (rad/s)	Linear Heave Displacements (m)		Non-Linear Heave Displacements (m)		Linear Roll Displacements (deg)		Non-Linear Roll Displacements (deg)	
	Hw=10 cm	Hw=30 cm	Hw=10 cm	Hw=30 cm	Hw=10 cm	Hw=30 cm	Hw=10 cm	Hw=30 cm
1	0.050	0.149	0.050	0.151	0.390	1.170	0.325	1.328
2	0.056	0.166	0.058	0.159	1.972	5.917	2.120	6.767
3	0.016	0.049	0.018	0.071	1.904	5.711	1.948	6.043
4	0.017	0.052	0.017	0.053	2.064	6.193	2.120	6.446
5	0.009	0.026	0.009	0.026	1.927	5.780	2.005	6.043
6	0.001	0.002	0.001	0.002	1.422	4.266	1.490	5.605
7	0.004	0.013	0.004	0.013	0.688	2.064	0.802	2.380
8	0.006	0.016	0.005	0.016	0.115	0.344	0.218	0.724
9	0.003	0.010	0.003	0.010	0.183	0.550	0.097	0.371
10	0.001	0.003	0.001	0.003	0.206	0.619	0.160	0.498

Table 6.3- Comparison of Linear and Non-linear Motion Response Predictions

Freq (rad/s)	Heave Displacements (m)		Roll Displacements (deg)		Roll Displacements (deg)	
	Linear Heave Excitation Forces	Non-Linear Heave Excit. Forces	Linear Roll Excitation Forces	Non-Linear Roll Excit. Forces	Linear Stiffness	Non-Linear Stiffness
1	0.149	0.151	1.170	1.585	1.170	1.516
2	0.166	0.159	5.917	5.925	5.917	8.595
3	0.049	0.071	5.711	5.882	5.711	6.505
4	0.052	0.053	6.193	6.47	6.193	6.606
5	0.026	0.026	5.780	5.994	5.780	5.884
6	0.002	0.002	4.266	4.484	4.266	4.216
7	0.013	0.013	2.064	2.36	2.064	2.078
8	0.016	0.016	0.344	0.722	0.344	0.336
9	0.010	0.010	0.550	0.394	0.550	0.539
10	0.003	0.003	0.619	0.502	0.619	0.596
	Heave Stiffness Constant		Roll Stiffness Constant		Linear Roll Excit. Moment	
	Wave Height = 30 cm					

Table 6.4- The Effect of Non-linear Wave Excitation forces and of Non-linear Stiffness on Motion Responses

6.2.3 EFFECT OF COUPLING BETWEEN THE HEAVE AND ROLL MODE OF MOTION

The hydrodynamic coupling between heave and roll motions is one of the most important aspects in simulating large amplitude motions. In Table 6.5, the results of the computations for the coupled and uncoupled cases are provided for the intact condition. As shown in the table the inclusion of the coupling indicates the higher motion responses for both modes of the motions.

Freq (rad/s)	Uncoupled Heave (cm)	Coupled Heave (cm)	Uncoupled Roll (deg)	Coupled Roll (deg)
1	5.00	5.13	0.33	0.44
2	5.80	6.31	2.12	3.30
3	1.80	2.69	1.95	2.06
4	1.70	1.94	2.12	2.21
5	0.90	0.99	2.01	2.17
6	0.05	0.06	1.49	1.58
7	0.40	0.48	0.80	0.82
8	0.50	0.58	0.22	0.24
9	0.30	0.37	0.10	0.10
10	0.09	0.11	0.16	0.18
	Wave Height = 10 cm			

Table 6.5- Effect of Coupling Between Different Mode of Motions

6.2.4 EFFECTS OF STEADY WIND AND CURRENT

The environmental effects caused by wind and current influence the motion responses. When the effects are combined with the effect of the waves, large amplitude motions could occur and this aspect can be investigated through time-domain analysis.

In order to explore the effects, the steady wind and current were formulated and combined with the wave effects in the program. The method for the wind force calculation is given in Appendix A while that for the current is represented in Section 3.2.6.

The results of the computations for the intact model's motion responses in surge heave and pitch motions are presented in Figs.6.4., 6.6 and 6.7. The results presented in Figs.6.4 and 6.7 excluding wind and current effects do not include drag forces.

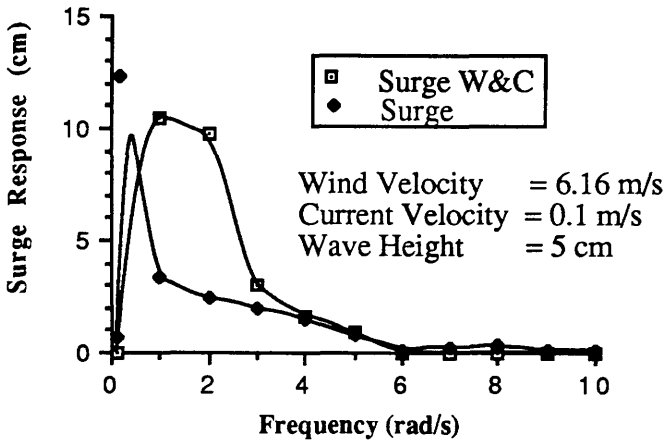

Fig.6.4 Effect of wind and current and current loading on surge response predictions (GM=7.9 cm)

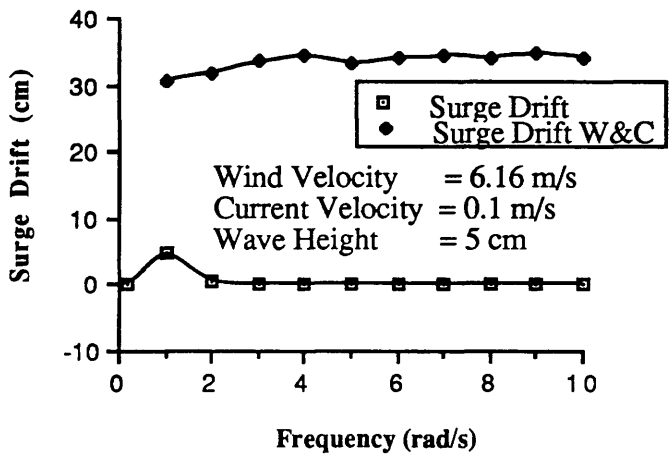

Fig.6.5 Effect of wind and current loading on surge drift predictions (GM=7.9 cm)

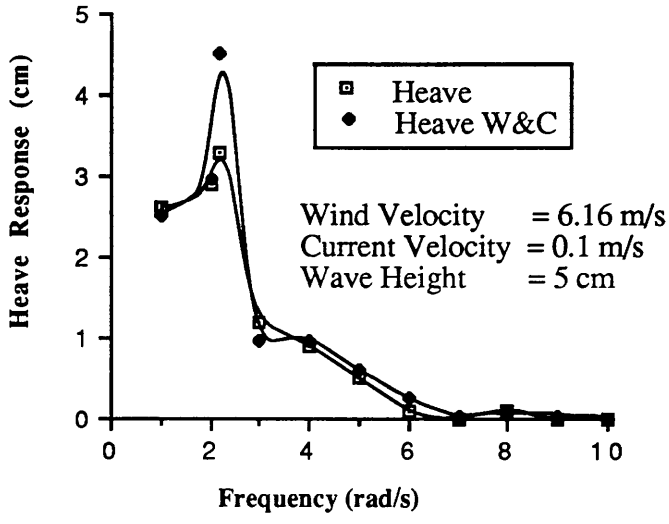

Fig.6.6 Effect of wind and current loading on heave response predictions (GM=7.9 cm)

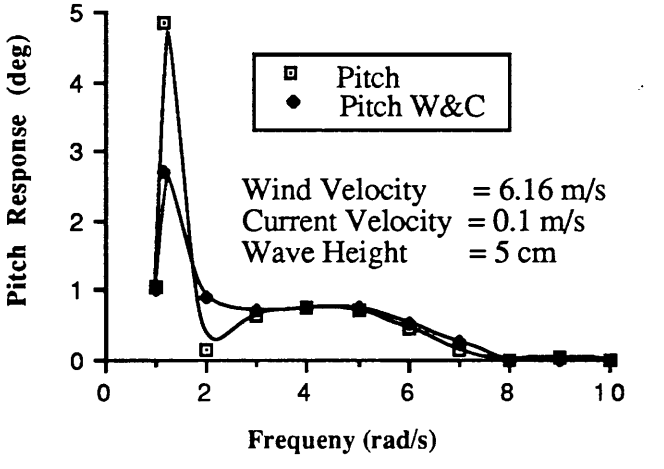

Fig.6.7 Effect of wind and current loading on pitch response predictions (GM=7.9 cm)

The effect of steady wind and current on first order oscillatory and steady drift motions was also investigated. This investigation showed that steady wind and current forces alter the mooring stiffness characteristics and this in turn causes significant changes in motion response characteristics, except for heave motions (see Figs.6.4-6.7).

6.2.5 EFFECTS OF SECOND-ORDER STEADY FORCES

When a floating structure is subjected to the surface waves, hydrodynamic forces and moments are exerted on its body. These forces and moments will have first-order,oscillatory components as well as small second-order, steady (mean) or low frequency components due to various non-linear effects (Pinkster 1980).

The first-order forces (or moments) are linearly proportional to wave height and cause the oscillatory motions of the structure with frequencies equal to the frequencies in the wave spectrum. The second-order forces (or moments) are linearly proportional to the square of the wave height and can cause large amplitude resonant behaviour of motions with very low damping. In a general definition, the term of second-order contains the product of two first-order terms which can be wave height, particle velocity,pressure, current velocity or vessel's motion response.

In spite of their small magnitudes, the second-order forces may have important effects on semi-submersibles. Depending on the mode of excitation, the motion response of the vessel can be magnified resulting in large excursions from the mean position when the vessel's has a long natural period.

Semi-submersibles experience relatively large second order forces in the vertical direction as well as large drift forces in the horizontal direction because of their small waterplane area and large submerged hulls. These forces are thought to be responsible for the long period roll or steady tilt behaviour and heave phenomena of semi-submersibles (Numata et al. 1976, Martin and Kuo 1979, Atlar 1986).

In the most general case, the second-order forces can be grouped into two main categories based on the flow characteristics as follows:

i) Potential flow forces

ii) Viscous flow forces

The most comprehensive discussion of the second-order potential forces is given by Pinkster (1980) who presented five contributions involved in these forces as follows:

i) Relative wave elevation
ii) Pressure drop
iii) Product of first-order translational motion and pressure
iv) Product of first-order rotational motion and inertia forces
v) Second-order potential

Later Standing et al. (1981a,1981b) introduced a 6th component to the steady forces due to the non-linear restoring effects. On the other hand, Morison's equation has the advantage of taking account of the viscous effect. By using this approach, several researchers introduced a 7th component to the steady forces associated with the viscous effects (Pijfers 1977, Ferretti 1980, Lundgreen 1982, Chakrabarti 1983).

In the following, these seven components are briefly defined based on the above references. By referring to these components, the components incorporated in the time-domain simulation program developed in the thesis are identified.

i) *First component of the Second-Order Steady Forces due to First Order Relative Wave Elevation*

First order relative wave elevation between the mean waterline of the structure and instantaneous free surface gives rise to the first component of the second-order steady forces.

$$-\frac{1}{2}\rho\, g \int_{WL} \zeta_r^{\,2}\, \boldsymbol{n}\, dl \tag{6.1}$$

where

ζ_r Relative wave elevation

dl Line element of the waterline

This second-order force component was also introduced as wave elevation drift force by Chakrabarti (1984b). Chakrabarti (1984a) gave a broad theoretical explanation of the steady drift forces on vertical cylinders.

ii) *Second Component of the Second-Order Steady Forces due to Pressure Drop*

The quadratic term in Bernoulli's equation gives rise to a steady second-order component when the first-order potential is used to calculate the pressure acting on the surface of the structure

$$-\iint_{S_o} -\frac{1}{2}\rho \left|\nabla \phi^{(1)}\right|^2 \boldsymbol{n}\, dS \tag{6.2}$$

where

∇	Vector operator
ϕ	Velocity potential
$\boldsymbol{n}$	Unit normal vector to surface (positive outward)
dS	Surface element of S_O

Chakrabarti (1984b) named this component the velocity head drift force.

iii) *Third Component of the Second-Order Steady Forces due to Product of Gradient of First-Order Pressure and First-Order Motion*

This component represents the change in the force due to first order motions through the pressure field (see Standing et al. 1981b).

$$-\iint_{S_o} -\rho\,(X^{(1)}.\nabla\,\phi_t^{(1)})\,\boldsymbol{n}\,ds \tag{6.3}$$

where

$\phi_t^{(1)}$ Derivation of the first-order velocity potential with respect to time

$X^{(1)}$ First-order motion vector of surface element ds relative to the fixed co-ordinate system

iv) *Fourth Component of the Second-Order Steady Forces due to Products of First-Order Angular Motions and Inertia Forces*

The first-order rotation on the direction of the fluid pressures acting at right angles to the structure's instantaneous surface gives rise to the fourth component of the second-order steady forces (See Standing 1981a). Therefore, this term takes the structure's rotational oscillations into account in the calculation of first-order wave exciting forces acting on a floating vessel.

$$\alpha^{(1)} \wedge (M \ddot{X}_g^{(1)}) \tag{6.4}$$

where

$\alpha^{(1)}$ First-order angular motion vector

$\ddot{X}_g^{(1)}$ First-order acceleration vector of the centre of gravity relative to the fixed co-ordinate system

Contribution from the products of first-order angular motions and inertia forces is defined by Chakrabarti (1984b) as rotational inertia drift force.

v) *Fifth Component of the Second-Order Steady Forces due to Second-Order Potential*

This component arises due to the second-order velocity potentials and is expressed as:

$$-\iint_{S_O} -\rho\ (\phi_{w_t}^{(2)} + \phi_{d_t}^{(2)})\, \boldsymbol{n}\, dS \tag{6.5}$$

where

$\phi_{w_t}^{(2)}$ Derivative of second-order potential of undisturbed incoming waves with respect to time

$\phi_{d_t}^{(2)}$ Derivative of second-order diffraction potential incoming waves with respect to time

vi) *Sixth Component of the Second-Order Steady Forces due to Non-linear Hydrostatic Stiffness*

This component of the second order steady forces was defined by Standing et al. (1981a-1981b) in the following form:

$$-\tfrac{1}{2}\,\rho\ g\ z_c\ A\ (\eta_4^2 + \eta_5^2)\ (0,0,1) \tag{6.6}$$

where

z_c	Heave motion
A	Water plane area
η_4	Roll motion response
η_5	Pitch motion response
$(0,0,1)$	Normal vector components

The equation given above by Standing et al. (1981b) represents the changes in the buoyancy force due to second-order motions.

vii) *Seventh Component of the Second-Order Steady Forces due to Non-linear Viscous Drift Force*

Morison's formula has the advantage of taking into account the viscous effect of the flow. In this formula, the flow velocity in the viscous drag term may have a constant part and a harmonic part. The constant part is induced by the mass transport of the waves (Stokes drift) and a possible current, whereas the harmonic part is induced by the wave particle motions (Pijfers and Brink 1977).

The constant velocity components induce steady "wave-current drag" forces at a submerged location in terms of the form and friction factor (Ludgren et al. 1982, Ferretti et al. 1980). The latter is a very small part of the form drag.

Since the wave particle velocity is harmonic, the drag forces induced by this velocity at a submerged location have a zero-mean over one period. However, because of the changing surface elevation along the splash zone of a vertical cylinder, a mean "wave-drag" force in the horizontal direction arises due to the horizontal wave particle velocities (Pijfers and Brink 1977). This component is obtained when the drag forces acting on vertical cylinders are calculated by integrating the forces up to the splash (instantaneous water) zone.

When Morison's formula is used in the frequency-domain analysis, it is necessary to linearise the viscous drag term (Naess and Hoff 1984). However, this linearisation process removes the mechanism which induced the steady component associated with the viscous effect. Whereas in the time-domain calculations, this non-linear drag term can be taken into account without linearisation since the numerical methods are employed to solve the motion response equations.

Chakrabarti 1984 calculated this force component for a fixed vertical cylinder and presented it in the following form:

$$\frac{\bar{F}}{\rho\, g\, C_D\, D\,/\,k^2} = \frac{(k\,H)^3}{12\pi}\left[\frac{1}{\sinh\,2kd} + C_1(kH)\coth\,2kd\right] \tag{6.7}$$

where

H	Wave height
d	Water depth
C_1	A coefficient function of kH

Among the seven above defined steady force components, the first component was taken in the time-domain solution by taking the upper limit of the wave-induced force and moment integrations up to the instantaneous free surface. The second component due to pressure drop was not taken into account since the Morison approach is used. The third and fourth components were automatically taken into account in the time-domain simulations since the translational and rotational oscillatory motions of the structure were considered in the calculations of the wave-exciting forces and moments at every time step. Since the fifth component is derived from the second-order potentials, the calculations presented in this thesis ignore this component. The contributions of the sixth component due to non-linear stiffness were taken into account in the simulation.

The seventh component due to viscous effect was also incorporated in the motion equation through the non-linear drag term in the Morison approach.

In addition to the above components, centripetal forces arising from rotational motions as explained in the formulation of non-linear added mass calculations given in Section 4.2 were taken into account in the time-domain formulations. These forces also contribute to the second-order steady forces acting on the structure.

Having highlighted the physics of the second-order force components, in the following sections a set of computations is presented for the semi-submersible model under consideration to investigate the effects of these forces.

In these computations particular emphasis is placed on the prediction of steady tilt behaviour of the model. This phenomenon has been reported by several investigators (Numata et al. 1976, De Souza 1976, Martin and Kuo 1979, Atlar 1986) during several model experiments. In these tests, it was noted that especially at low values of GM, the models developed a "steady tilt" in regular waves which could be as high as 10^0-15^0 and that the model made roll oscillations about this tilt angle. It was conjectured that the main forces responsible for this behaviour were the steady potential vertical forces (Ogilvie 1963, Lee and Newman 1971) (i.e. due to pressure drop component) on the lower hulls and steady horizontal forces on the columns induced by both the viscous and potential effects. These phenomena was observed in both directions (i.e. bi-stable tilt) or in one direction (preferred tilt).

In none of the above mentioned investigations has this non-linear steady behaviour been looked at in the time-domain. Therefore, it would be most appropriate to explore various aspects of this behaviour by the simulation program developed in this thesis. However, steady vertical forces on the lower hulls are neglected in the formulation of the simulation program.

6.2.6 THE EFFECT OF NON-LINEAR DRAG FORCE AND FIRST-ORDER RELATIVE WAVE ELEVATION

Figs.6.8 and 6.9 shows the results of the first groups of computations for the model in intact condition under the effect of beam waves for two different wave heights (10 and 30 cm). In these computations, the forces acting on the vessel were evaluated by integrating them up to still water level. In the figures a minus sign indicates the steady tilt in the leeward direction while a positive sign indicates the seaward tilt. As shown in both Figs.6.8 and Fig.6.9 the steady tilt could develop in both directions over the frequency range tested and its magnitude increases with increasing wave height.

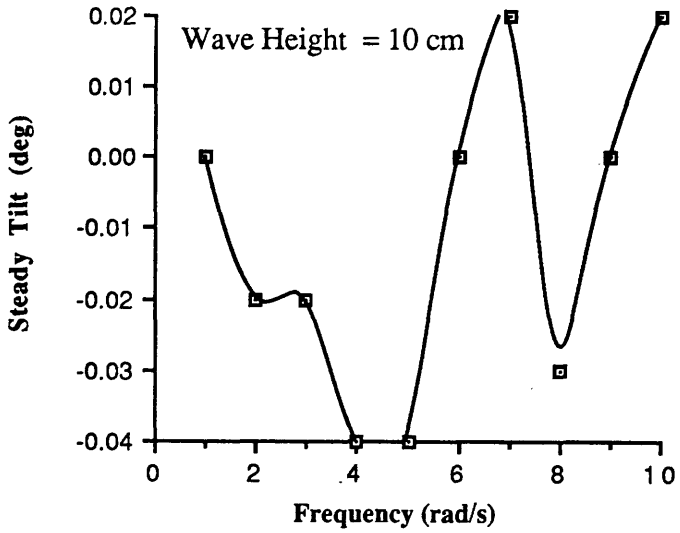

Fig.6.8 Steady Tilt Angle (Integration up to the Still Water Level)

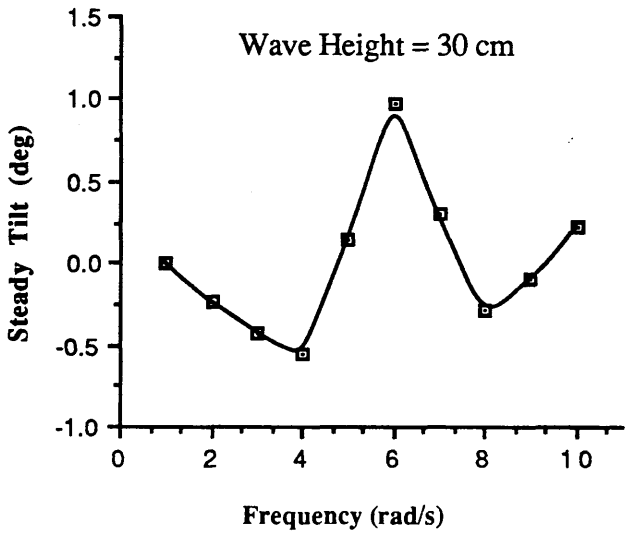

Fig.6.9 Steady Tilt Angle (Integration up to the Still Water Level)

The results of the second group of computations for the same wave conditions were presented in Figs.6.10 and 6.11. In this case, the forces were integrated up to the instantaneous water level which allowed the effect of relative wave elevation (i.e. first component) and non-linear viscous drag (i.e. seventh component) as well as others as indicated earlier in the chapter.

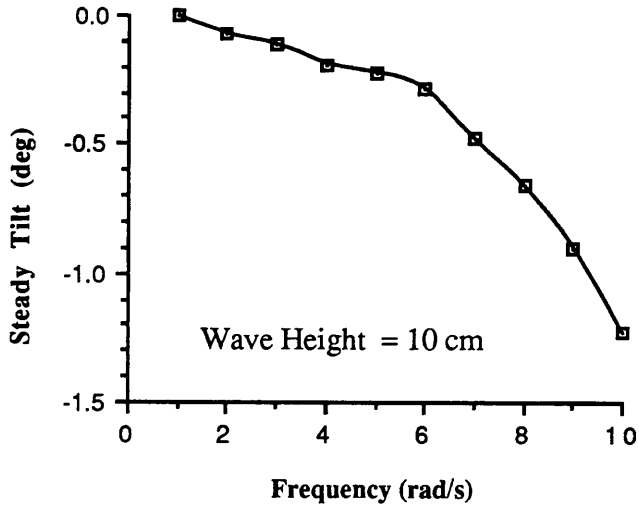

Fig.6.10 Steady Tilt Angle (Integration up to the Wave Elevation)

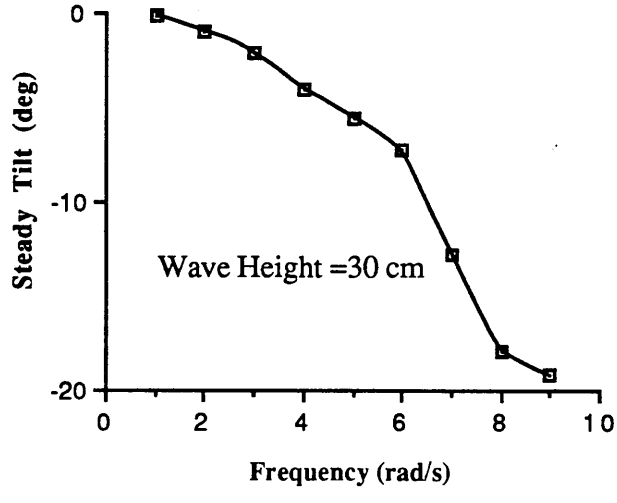

Fig.6.11 Steady Tilt Angle (Integration up to the Wave Elevation)

Comparison of Figs.6.10 and 6.11 with Figs.6.8 and 6.9 indicates that the inclusion of the first and seventh components increases the magnitude of the steady tilt as well as changing its bi-stable character. As shown in Figs.6.10 and 6.11, steady tilt occurred always in the leeward direction over the entire frequency range with the same model as reported by Atlar (1986).

Fig.6.12 compares the steady tilt predictions obtained from non-linear time-domain analysis with the test measurements for the semi-submersible configuration given in Chapter 5. As noticed in this figure the predicted steady tilt values were underestimated for the frequency range from 4.5 to 6.5 rad/s. This underestimation is attributed to the vertical component of the second-order force acting on the lower hulls which were not considered in the formulation of the simulation program.

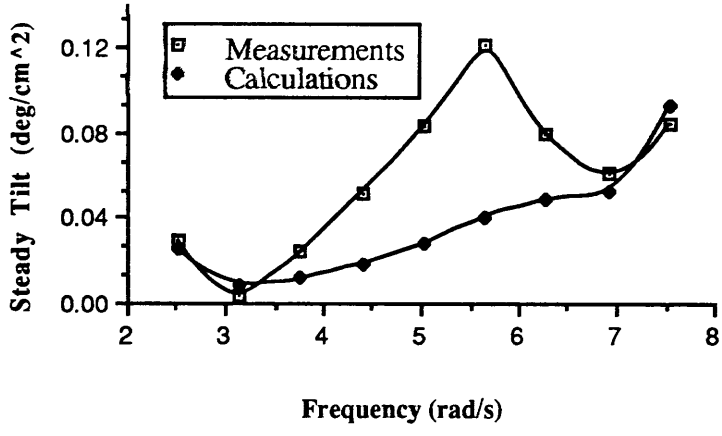

Fig.6.12 Comparison of steady tilt angle predictions with measurements

6.2.7 THE EFFECT OF NON-LINEAR ADDED MASS AND DAMPING FORCE

The parametric studies described in the preceding sections took into account the non-linearities due to the time and position dependent wave forces, non–linear restoring forces, and also non-linear damping forces in a simplified form.

Subroutine AMAS was written to calculate the non-linear added mass and damping forces which were formulated in Section.4.2. Having included the AMAS into the simulation program, computations in every time step increased the CPU time significantly. Therefore, only a few wave frequencies were tested in order to investigate the effect of non-linear added mass and damping. Table 6.6 shows the effect of non-linear added mass and the damping force on roll response amplitudes for 1,5 and 8 rad/s.

Frequency (rad/s)	Roll Response (deg) Linear Added Mass and Damping	Roll Response (deg) Non-Linear Added Mass and Damping
1	0.32	0.16
5	1.95	1.96
8	0.23	0.30
	Wave Height = 10 cm	

Table 6.6 Effect of Non-linear Added Mass and Damping

Comparisons between the results obtained both for the linear and the non-linear case show that there is no significant change in the motion response amplitudes results by including non-linear added mass and damping forces for the intact condition especially for the frequency of 5 rad/s. The roll response amplitude significantly decreased at 1 rad/sec both for intact and damage cases whereas the roll response increased at 8 rad/s.

The significant decrease in roll magnitude shown in Table 6.6 for frequency of 1 rad/s which coincides with the natural roll frequency of the platform is due to the effect of an increase in non-linear damping forces.

6.2.8 THE EFFECT OF DIFFERENT GMs ON MOTION BEHAVIOUR

In order to investigate the effects of different GM values on roll and pitch motions, cross-curves of stability for roll and pitch motions are generated for different KG values. Figs.C.3-8 show the cross curves of stability for three different KGs for roll and pitch oscillations.

The application of different GMs in the solution of the roll motion equation resulted in changes in the oscillation amplitudes and increased the steady tilt. At 1 rad/s reduction in GM value increased the response amplitude significantly as shown in Figs.6.14-15.

The response amplitudes obtained from the differential equations with linear and non-linear hard and soft spring characteristics are discussed in theoretical detail by Stoker (1950). Wilson (1984) gives some insight concerning the physical response of inherently

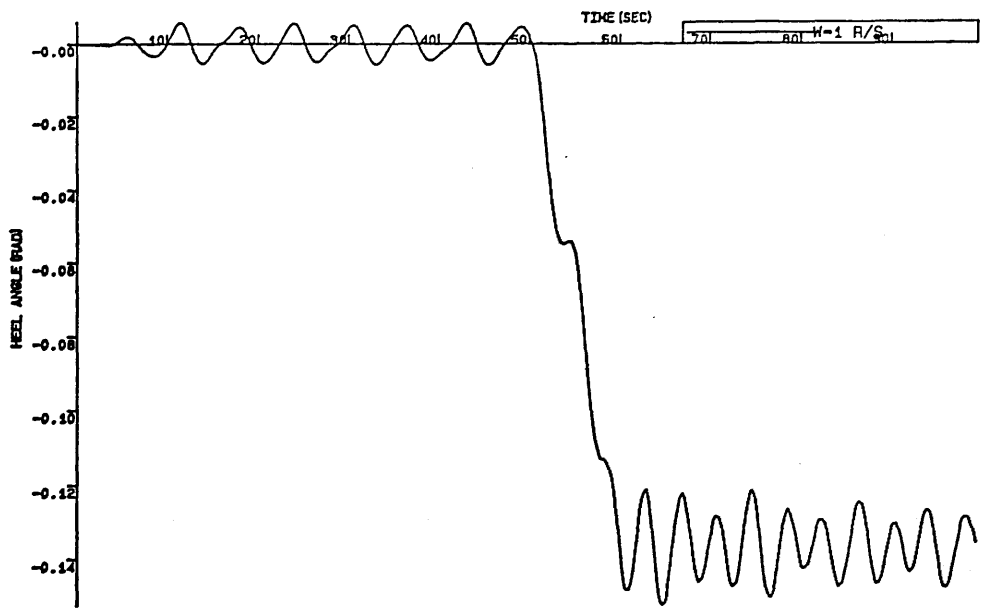

Fig.6.13 Motion response simulation of roll
WH=10 cm Flooding Mass=1.5 kg Flooding Time=10 s
GM=7.9 cm ω=1 rad/s

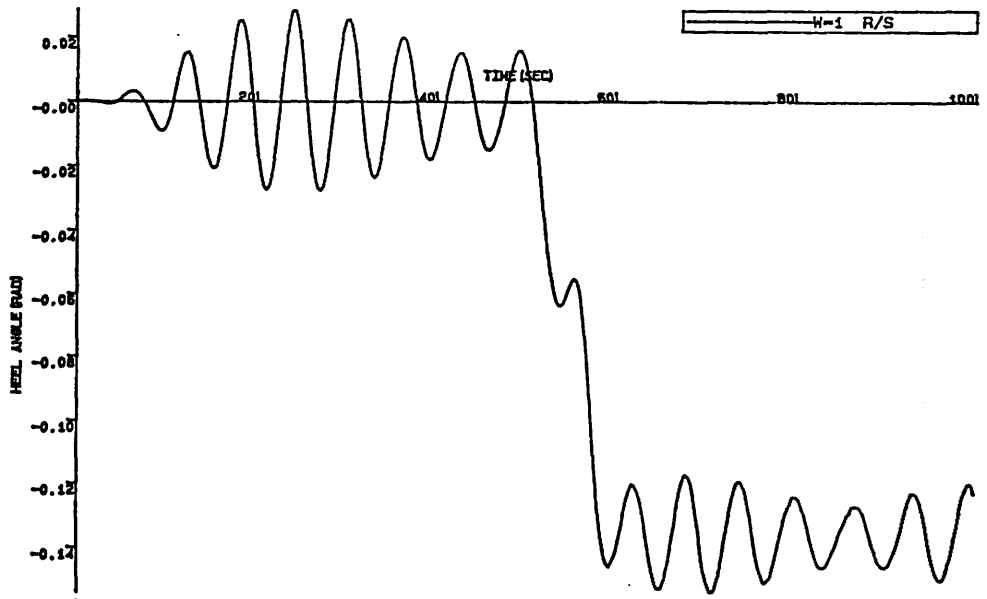

Fig.6.14 Motion response simulation of roll
WH=10 cm Flooding Mass=1.5 kg Flooding Time=10 s
GM=3.8 cm ω=1 rad/s

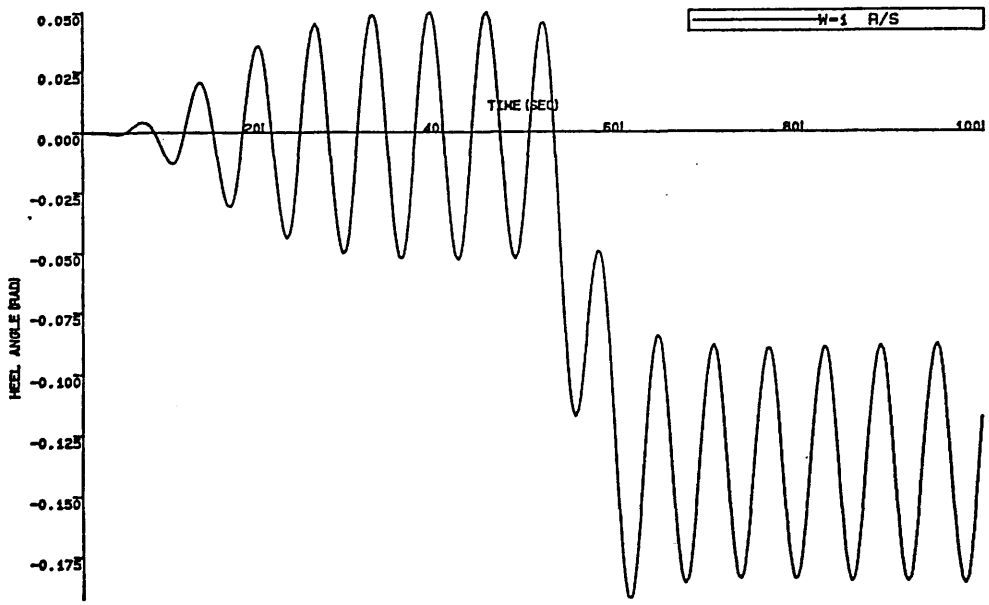

Fig.6.15 Motion response simulation of roll
WH=10 cm Flooding Mass=1.5 kg Flooding Time=10 s
GM=1.9 cm ω=1 rad/s

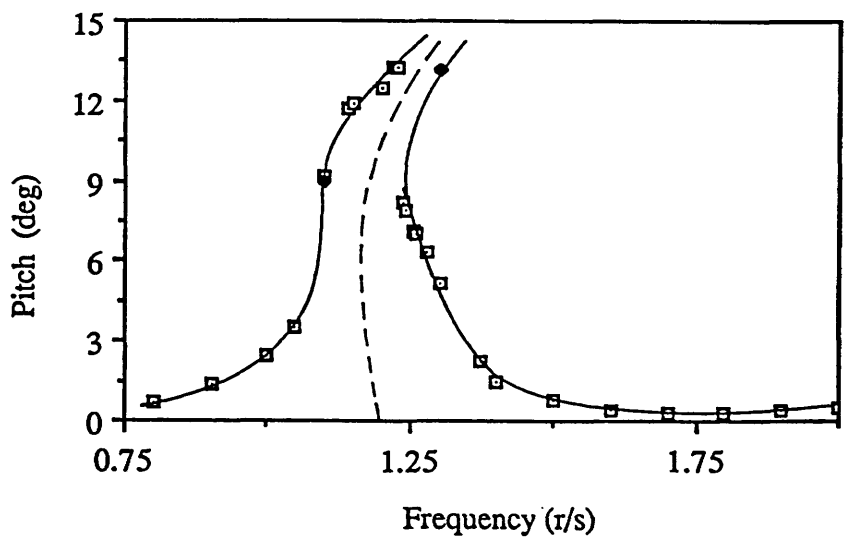

Fig.6.16 Effect of non-linear restoring moments on pitch response values
GM=3.8 cm WH=15 cm

non-linear cable-stayed systems such as moored ship or moored landing ship tank. The effect of non-linear pitch restoring moment on the motion response amplitude of the semi-submersible at the resonant frequency is shown in Fig.6.16. As seen in Fig.6.16, the pitch restoring moment has soft spring characteristics for small amplitude motions and hard spring characteristics for large amplitude motions. This figure is also an example of incipient jumps or erratic changes in the response amplitudes of non-linear equations. More theoretical background on this subject is given by Bishop et al. (1986). Theoretical investigations into the non-linear stiffness or restoring force of an offshore structure was carried out by Virgin and Bishop (1988). Bishop and Virgin (1987) described a combined numerical and geometric approach to study the dynamic behaviour of a moored semi-submersible based on solutions of the differential equations which are non-linear in stiffness term only. Data presented in Fig.6.16 was obtained from the numerical time-domain simulations.

Fig.6.17 shows the importance of the initial conditions on the motion response amplitude. As can be seen from Fig.6.17, the pitch response of a semi-submersible with 15^0 initial list angle is about three times larger than that of a semi-submersible with 0^0 initial list angle.

Investigations into the effect of GM on the pitch motion response values and the steady list angle under wave loading only, and under wave,wind and current loading were presented in Figs.6.18-21. It was found that the effect of different metacentric heights is not significant for higher frequencies so far as the magnitude of the motion amplitudes are concerned.

Table 6.7 shows the effects of variation of GM on steady tilt and oscillatory roll motions.

Freq (rad/s)	GM = 7.9 cm Wave Height = 10 cm Roll Resp. (deg)		GM = 3.8 cm Wave Height = 10 cm Roll Resp. (deg)		GM = 1.9 cm Wave Height = 10 cm Roll Resp. (deg)	
	Oscillatory	Steady	Oscillatory	Steady	Oscillatory	Steady
1	0.44	0.00	1.59	0.00	2.99	-0.08
2	3.30	-0.07	1.36	-0.10	1.19	-0.16
3	2.06	-0.11	1.76	-0.20	1.69	-0.34
4	2.21	-0.20	2.13	-0.35	2.15	-0.60
5	2.17	-0.22	2.08	-0.48	2.13	-0.69
6	1.58	-0.28	1.70	-0.63	1.78	-1.04
7	0.82	-0.50	0.99	-1.30	1.07	-2.46
8	0.24	-0.69	0.31	-2.39	0.44	-6.34
9	0.10	-0.90	0.15	-3.51	0.40	-12.93
10	0.18	-1.22	0.55	-7.70	1.16	-15.51

Table 6.7- Effect of Variations of GM in Steady and Oscillatory Motions

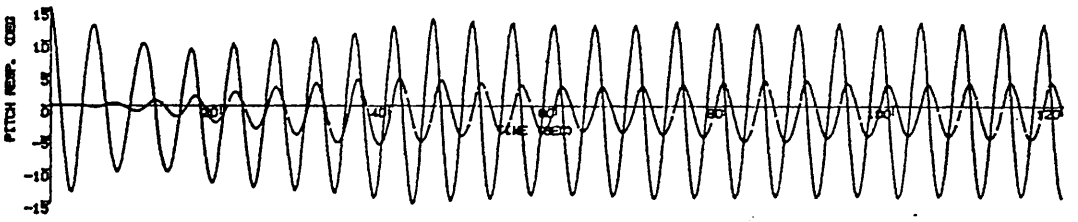

Fig.6.17 Effect of initial condition on pitch response
GM=3.8 cm HW=15 cm ω=1.3 rad/s

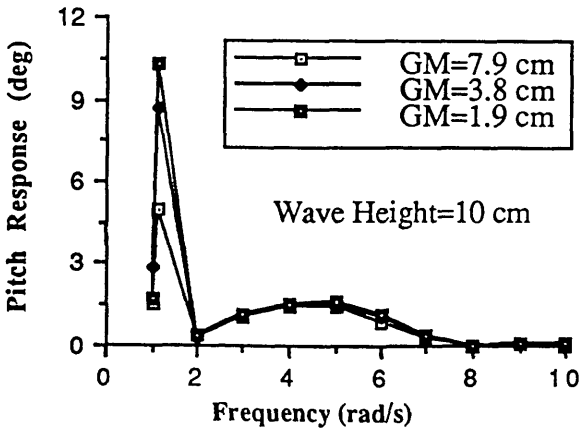

Fig.6.18 Effect of different GMs on pitch response predictions

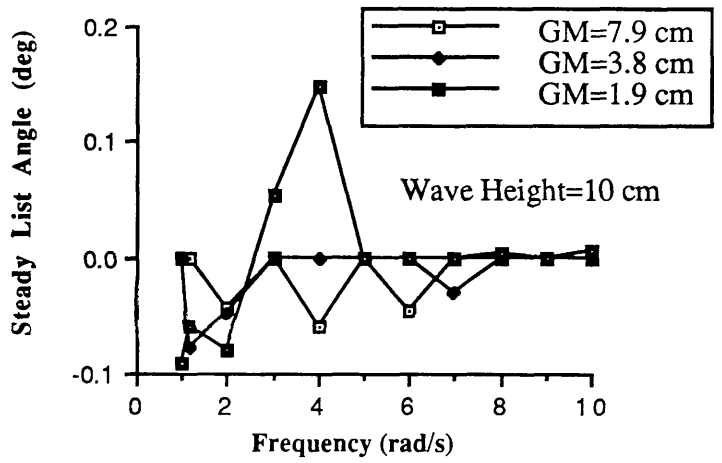

Fig.6.19 Effect of different GMs on steady list angle predictions

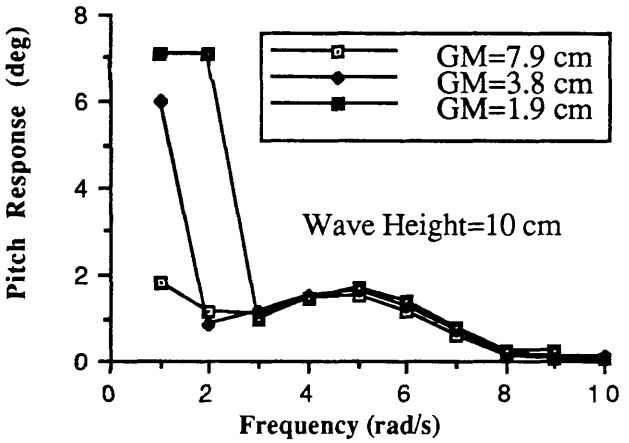

Fig.6.20 Effect of different GMs on pitch response predictions (Wind&Current)

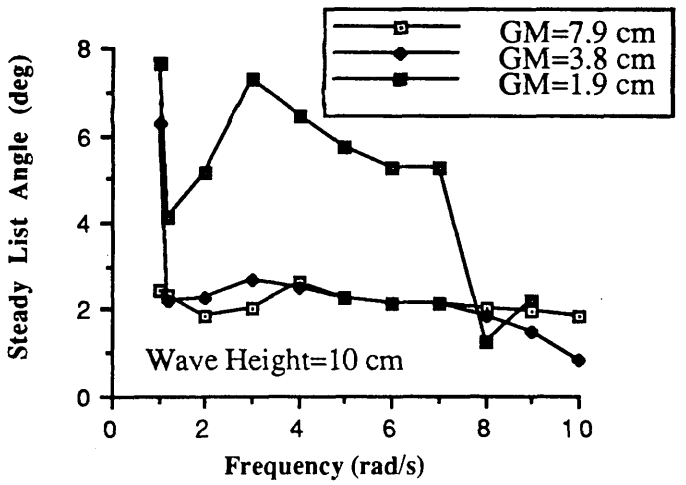

Fig.6.21 Effect of different GMs on steady list angle predictions (Wind&Current)

6.3 DISCUSSION OF RESULTS

The parametric studies were performed to determine the effect of the size of the flooded compartment and the flooding time in motion amplitudes. Tables 6.1 and 6.2 show that as the flooding time decreases the motion amplitudes increase. The parametric calculations carried out in this study revealed that transient motion displacements during progressive flooding can be significantly higher than those during post-flooding.

The effects of various non-linear terms in the motion equations were studied systematically. Table 6.3 shows comparisons between the solutions of linear small amplitude motion equations and the solutions of large amplitude non-linear equations of the semi-submersible geometry in intact condition. As can be seen from Table 6.3, heave and roll response values obtained from non-linear large amplitude motion equations are higher than the response values obtained with linear motion equations, except when wave frequencies are 9 and 10 rad/sec. In the heave resonance region, non-linear formulations yield response which is about 45% higher than does small amplitude linear theory for the extreme wave height of 30 cm in model scale. In the roll resonance region, non-linear formulations give a roll displacement about 14% higher than does linear theory. The effects of non-linearities in wave excitation forces and in stiffness terms are also illustrated in Table 6.3. Table 6.4 shows that non-linear wave force and non-linear stiffness terms equally affect the response values.

The heave and roll amplitudes obtained from the solutions of uncoupled and coupled non-linear equations are compared in Table 6.5. The motion amplitudes given in this table were obtained for a wave height of 10 cm. Table 6.5 shows that solutions obtained from uncoupled motion equations are significantly less than those obtained from coupled equations. Table 6.7 shows the effect of variation of GM on steady tilt and oscillating roll motions.

The effect of non-linear pitch restoring moment on the motion response amplitude is shown in Fig.6.16. Fig.6.17 shows the importance of the initial conditions on the motion response amplitude. As can be seen from Fig.17, pitch response of a semi-submersible with 15^0 initial list angle is about three times larger than that of a semi-submersible with 0^0 initial list angle.

The effect of steady wind and current on first order oscillatory and steady drift motions was also investigated. This investigation showed that steady wind and current forces alter the mooring stiffness characteristics and this, in turn, causes significant changes in motion response characteristics, except in heave motions (see Figs.6.4-7 and Figs.6.18-21).

The effect of GM on the pitch motion response values and on steady list angle was also investigated under wave and wave,wind and current loading (see Figs.6.18-21). These figures suggest that the effect of small GM was amplified with the inclusion of drag forces into the wave force calculations particularly for the steady motions. For oscillatory motions, responses in the resonance region are mostly affected by increasing the GM.

CHAPTER 7

CONCLUSIONS

7.1 GENERAL

The general aim of the study reported in this thesis was to develop a prediction technique to simulate the motion response of a damaged platform under wave, wind and current forces. This objective was achieved through the development of a computer program based on the technique presented in Chapter 3 and 4. This program was successfully validated through the simulation of test measurements. Some parametric studies were conducted in order to investigate the effects of various non-linearities in motion response predictions.

It is expected that designers and certifying bodies will benefit from this study in their motion simulation work on the determination of several aspects of dynamic stability including the assessment of adequacy of watertight openings.

Conclusions of the study are presented and discussed below. Recommendations for the future work on the subject are given at the end of this chapter.

7.2 CONCLUSIONS OF CHAPTER TWO

Since the purpose of the study was to develop a prediction technique in order to determine the motion response of a damaged platform in waves utilising a time-domain solution technique one has to choose an accurate as well as computationally efficient method of calculating hydrodynamic forces.

At the beginning of the study, hydrodynamic forces were calculated using the Morison approach. A number of computer routines were developed to calculate heave motions for head and beam sea conditions, as well as sway and surge motions of the semi-submersible platform. Following these calculations, the coupled heave-pitch and heave-roll motions of the semi-submersible using the Morison approach were formulated and calculated using a new set of computer programs. The motion response values calculated using the Morison approach were also re-calculated utilising the computer programs based on 2-D source-sink distribution method developed by another research

student in the Department of Naval Architect and Ocean Engineering, Glasgow University. Comparisons of the Morison approach with the 2D source-sink distribution technique showed that there is reasonably good agreement between the two methods for coupled heave-pitch and heave-roll motions. Comparisons of forces for head and beam sea conditions were also conducted and it was shown that there is also good agreement between the two methods. Additionally, the effect of columns on the hulls was investigated using 2-D source-sink distribution method.

The step-by-step technique to solve the coupled motion equations in the time-domain for the simulation of large amplitude motions of a semi-submersible in intact and damaged conditions requires the calculation of the hydrodynamic, hydrostatic and wave exciting forces many times over a given wave cycle. One has to select an appropriate method to determine these values so that the computational task becomes feasible.

Although both methods have advantages and disadvantages (e.g. while Morison equation considers viscous forces, the 2D source-sink does not; while the 2D approach can take into account the interaction effect between members the Morison approach can not; the application of strip theory is also questionable in the case of members which do not have uniform cross-sections such as columns) the two methods produced results in good agreement with each other for this particular semi-submersible geometry.

Having regard to the computing and storage requirements and limitations, the Morison approach was chosen and implemened in the time-domain motion simulation of a damaged platform in waves.

Since the Morison approach was found to correlate well with the 2-D source-sink distribution technique and also to be considerably more efficient in terms of CPU time than the 2-D source-sink method, the Morison's approach was chosen to derive wave and motion induced forces to simulate the coupled non-linear motions of a semi-submersible in intact, progressive and post-flooding conditions.

7.3 CONCLUSIONS OF CHAPTER THREE

The formulations derived in the previous sections were used in developing a computer program which predicts the non-linear large amplitude motions of a floating platform in six degrees of freedom. This computer program is described in Section 4.8. The calculation procedure derived in Chapter 3 provides a very efficient means of calculating wave forces and moments during the time-domain simulations of a floating platform experiencing large amplitude motion in intact, progressive flooding and damaged conditions.

7.4 CONCLUSIONS OF CHAPTER FOUR

In this chapter, a general method to obtain the loading on the circular cylindrical members of offshore structures due to rigid body motion was presented. Rigid body induced motions and total external forces were combined to obtain motion equations. Non-linear, coupled six degrees of freedom equations were reduced to a first order differential equation system so that a numerical solution using the Runge-Kutta method could be employed to obtain the motion responses in the time-domain.

Some examples from simulation studies were presented to illustrate various aspects during the development of the motion program. The results of parametric studies obtained using these equations were presented in Chapter 6. Several difficulties encountered during the development of the time-domain simualtion program were explained. Particular emphasis was given to the application of ramp functions which are necessary to obtain quick convergence in the time-domain simulation.

The formulations and the computational procedures given in this chapter provide useful tools for the investigataion of the non-linear dynamic stability characteristics of floating structures in waves for intact, damaged and post-flooding conditions in six degrees of freedom.

7.5 CONCLUSIONS OF CHAPTER FIVE

The experimental setup for intact and damaged simulation tests of a twin–hulled semi-submersible model and the measurements carried out during inclination, natural period and motion tests were described in Chapter 5.

The primary objectives of these tests were to compare the calculated motion responses with the measurements in order to verify the computer simulation method, and to study the motions of the model semi-submersible under intact, progressive flooding and post-flooding conditions.

Comparison of the test results with the numerical simulations shows good agreement for heave, roll and pitch motions. The measured first-order oscillatory motion responses for surge and sway modes correlated well with those obtained numerically but second-order steady displacements for surge and sway motions predicted using the stiffness characteristics of a catenary mooring system are larger than experimental measurements. This discrepancy was due to the fact that the model was moored to the tank walls by means of harnesses which possessed high stiffness characteristics. Similarly, the yaw motion simulation on the computer differed from experimental measurements which showed first-order oscillatory response about a mean position. This may be attributed to highly non-linear behaviour of the mooring lines or to the reflected waves between tank walls. This first-order oscillatory response was not observed in the numerical simulations during intact condition period since there was no yawing moment acting on the platform due to its symmetrical geometry with respect to the wave direction.

During the post-flooding simulation, as can be seen in some of the figures, i.e. Fig.5.13, there is an oscillatory roll motion in head sea condition. This could be due to the effects of piping used to flood the model and/or green water on the deck, which would have introduced assymmetry in the model and/or the reflected waves between tank walls.

The effect of free surface in the flooded compartment was also investigated and it was found that it had a negligible effect on the GM.

It was noticed that the smaller the GM, the higher the probability of capsize of a platform under post-flooding condition. During the experiments in which a maximum

roll angle was measured as 10^0 and the maximum pitch angle was measured as 15^0.(see Fig.5.85), green water on the decks was observed. These two typical experiments suggest that a platform with a smaller GM (2.29 cm in model scale or 1.6 m in full scale) could be capsized even with a flooded compartment volume of 1% of the total displacement.

Although GM is an important parameter in determining the capsize phenomenon in waves, the effects of the downflooding angle and the green water in deck should also be considered since they all contribute towards the occurrence of the capsize.

Although reasonable agreement was found between theoretical predictions and experimental measurements, further investigations into the time-domain simulation both theoretically and experimentally is essential for a through understanding of the points given in Section 7.7.

7.6 CONCLUSIONS OF CHAPTER SIX

The parametric studies carried out during the investigation reported in this chapter show that non-linear coupled large amplitude motion equations yield higher responses than those obtained from linear uncoupled motion equations as the wave excitation frequencies approach the natural oscillation frequencies. For example, as seen in Table 6.5, coupled heave and roll responses are 33% and 36% higher than the uncoupled heave and roll responses respectively.

The integration of wave exciting forces acting on the columns up to the wave surface makes a significant contribution to the steady motions (Figs.6.8-11).

It was concluded that in the resonance regions the non-linear heave and roll motion equations yield 45% and 14% higher response values than those obtained by the linear heave and roll motion equations respectively.

The inclusion of static wind and current loading causes significant changes in oscillatory and steady motion characteristics, except in heave motions, due to changes in mooring stiffness. A large steady tilt angle occurs as the GM values decrease particularly at high wave frequencies.

These parametric studies have also revealed that the non-linear drag force which gives rise to steady motions does increase in the higher frequency range.

7.7 RECOMMENDATIONS FOR FUTURE WORK

With this recently completed work as a foundation, some extension of the study by incorporating the following aspects is recommended.

i) *Mooring Effects*: The stiffness terms currently used in the motion response equations take into account the effects of non-linear hydrostatic stiffness and the non-linear mooring stiffness due to large steady and oscillatory translational and oscillatory displacements of the platform. The effects of the mooring line failure, its location and the configuration should be considered during transient and post mooring damaged conditions.

ii) *Wind and Wave-Drift Effects*: Effects of dynamic wind and gust, and second-order steady wave forces due to pressure drop on the motions of the platform should be investigated. The wind velocity variations obtained from recent measurements carried out in various offshore locations should be incorporated into the analysis.

iii) *Interference Effects*: The effect of wave inertia, added-mass and damping coefficients which take into account the interference between the members of the structure should also be incorporated into the analysis.

iv) *Effect of Upper Deck Buoyancy*: An improved analytical technique needs to be developed and incorporated into the analysis routines to take into account the effects of both the buoyancy and the hydrodynamic loads of the deck on the motion responses of a mobile platform experiencing large amplitude oscillations during intact or damaged conditions.

v) *Effects of Multi-Directional Random Seas*: An application of multi-directional random seas in the motion response analysis should be considered.

vi) *Effects of Different Semi-Submersible Configurations*: The non-linear time-domain simulation programs developed during this study and the results given in this thesis were based on the semi-submersible geometry shown in Fig.2.2. However, it is also recommended that the non-linear motion characteristics of different semi-submersible configurations be determined systematically to arrive at general conclusions and recommendations for the safety of mobile platforms.

7.8 CLOSURE

This thesis describes research which was aimed at providing an accurate tool to predict the behaviour of a damaged platform under extreme environmental conditions. By the use of this analytical tool, this study has made a contribution to the understanding of some non-linear effects in the motion response simulation of platforms through time-domain simulations.

It is hoped that the work presented in the thesis will enable designers and certifying authorities to assess the safety of mobile platforms in extreme environmental and damaged conditions.

APPENDIX A

CALCULATION OF WIND FORCES

In this appendix, a method of wind force prediction recommended by the American Bureau of Shipping (ABS 1973) is summarised. This method is adopted in the calculation of wind forces acting on the semi-submersible.

The total wind force on the object can be predicted using the following equation.

$$F = \frac{1}{2} \rho \, c_h \, c_s \, A_p v^2 \qquad \text{(A.1)}$$

where

ρ	Density of air (1.225 kg/m^3 for dry air)
c_h	Height coefficient from Table A.1
c_s	Shape coefficient from Table A.2
A_p	Characteristic area of the body
v	Wind velocity

Height (metres)	c_h
0.0 - 15.3	1.00
15.3 - 30.5	1.10
30.5 - 46.0	1.20
46.0 - 61.0	1.30
61.0 - 76.0	1.37
76.0 - 91.5	1.43
91.5 -106.5	1.48
106.5 -122.0	1.52
122.0 -137.0	1.56
137.0 -152.5	1.60
152.5 -167.5	1.63
167.5 -183.0	1.67
183.0 -198.0	1.70
198.0 -213.5	1.72
213.5 -228.5	1.75
228.5 -244.0	1.77
244.0 -256.0	1.79
256.0	1.80

Table A.1 Height Coefficient

Object	c_s
Cylinders	0.5
Hull (surface type)	1.0
Deck house	1.0
Isolated structural shapes (cranes, angles, channels, beams,etc.)	1.5
Under deck areas (smooth surfaces)	1.0
Under deck areas (exposed beams and girders)	1.3
Rig derrick (each face)	1.3

Table A.2 Shape Coefficient

If several members of an offshore structure are located in a plane normal to the wind direction, as in the case of a plane truss or a series of columns, the solidification effect must be taken into account. The wind force given in Eq.A.1 then becomes:

$$F = \frac{1}{2} \rho \, c_{DE} \, \theta \, A_{PE} \, v^2 \qquad \text{(A.2)}$$

where

c_{DE} Effective force coefficient from Table A.3

θ Solidity ratio defined as the projected exposed area of the frame normal to the direction of the force divided by the area enclosed by the boundary of the frame normal to the direction of the force

A_{PE} Projected area enclosed by the boundaries of the frame

Solidity Ratio	Effective Force Coefficient		
	Flat-side Members	Circular Sections	
		Re<4.2x10	Re>4.2x10
0.1	1.9	1.2	0.7
0.2	1.8	1.2	0.8
0.3	1.7	1.2	0.8
0.4	1.7	1.1	0.8
0.5	1.6	1.1	0.8
0.75	1.6	1.5	1.4
1.0	2.0	2.0	2.0

Table A.3 Effective Force Coefficient

If two or more parallel frames or members are located behind each other in the wind direction, the shielding effect must be taken into account.

The wind force on a shielded member can be calculated as:

$$F = \frac{1}{2} \rho C_D A_p v^2 \eta$$

or

$$F = \frac{1}{2} \rho C_{DE} \theta A_{PE} v^2 \eta \qquad \text{(A.3)}$$

where

C_D	Drag coefficient
η	Shielding factor

If more than two members are located in line with the wind direction, the wind force on the third and subsequent members should be taken to be equal to the wind load on the second member.

Spacing ratio α	Value of η for an aerodynamic solidity ratio β, of							
	0.1	0.2	0.3	0.4	0.5	0.6	0.7	0.8 and over
up to 1.0	1.0	0.96	0.90	0.80	0.68	0.54	0.44	0.37
2.0	1.0	0.97	0.91	0.82	0.71	0.58	0.49	0.43
3.0	1.0	0.97	0.92	0.84	0.74	0.53	0.54	0.48
4.0	1.0	0.98	0.93	0.86	0.77	0.67	0.59	0.54
5.0	1.0	0.98	0.94	0.88	0.80	0.71	0.64	0.60
6.0 and over	1.0	0.99	0.95	0.90	0.83	0.75	0.69	0.66

Spacing ratio α: The distance, centre to centre, of the frames, beams or girders divided by the least overall dimension of the frame, beam or girder measured at right angles to the direction of the wind. For triangular or rectangular framed structures diagonal to the wind, the spacing ratio should be calculated from the mean distance between the frames in the direction of the wind.

Aerodynamic solidity ratio $\beta = \phi \cdot a$

where

ϕ	solidity ratio, see B1.2.2
a	constant a = 1.6 for flat-sided members; = 1.2 for circular sections in subcritical range and for flat-sided members in conjunction with such circular sections; = 0.5 for circular sections in the supercritical range and for flat-sided members in conjunction with such circular sections.

Table A.4 The shielding factor η

The wind load calculations were carried out for the semi-submersible structure for heel and list angles of 0^{o}, 5^{o}, 10^{o} and 15^{o} in order to take into account the wind forces for head and beam sea condition in the time-domain simulation. Lift force due to wind acting on the vessel was not considered in the calculations. Fig.A.1 shows the general arrangement of the superstructure which the wind load calculations are based on. Fig.A.6 shows perspective view of the superstructure and the dimensions of each element.

Results of the calculated head and beam wind force and moments are plotted in Figs.A.2-5. Third order polynomial curves were fitted through the results in order to define continuous functions to be used in the time-domain simulations.

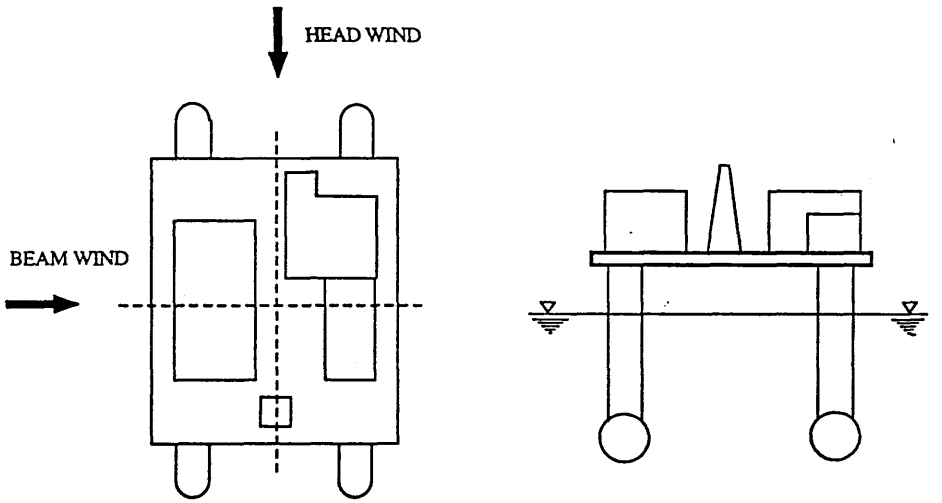

Fig.A.1 General arrangement of the superstructure

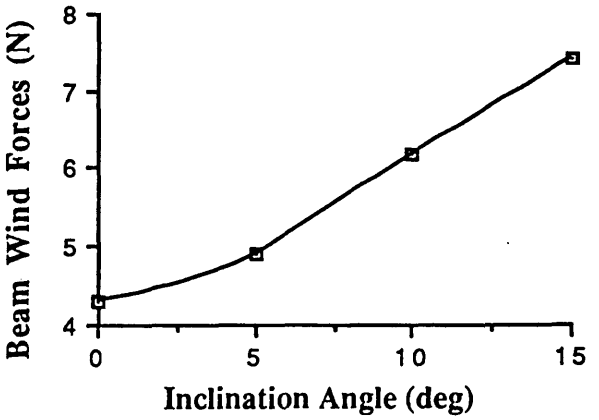

Fig.A.2 Wind forces obtained for the beam sea condition

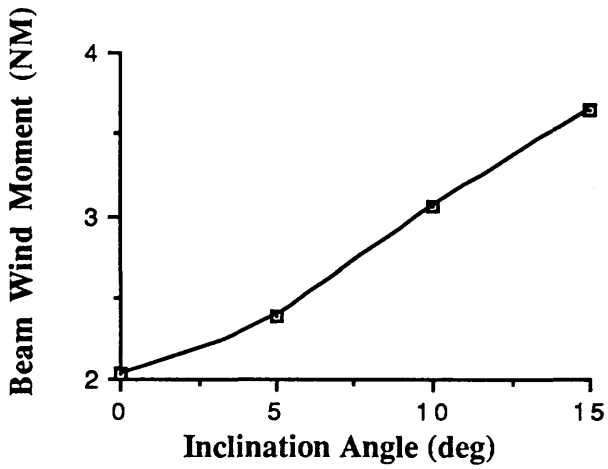

Fig.A.3 Wind moments obtained for the beam sea condition

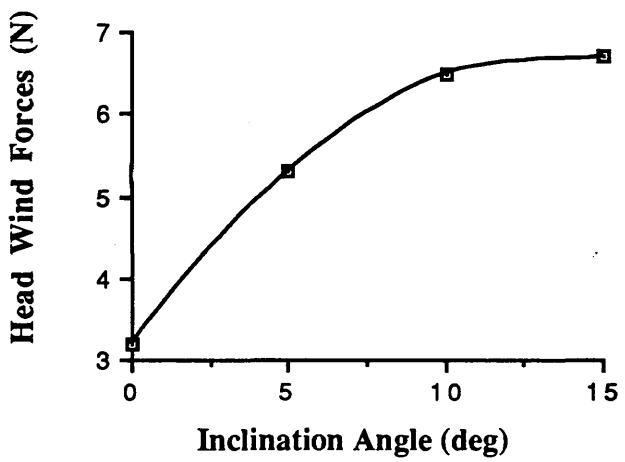

Fig.A.4 Wind forces obtained for the head sea condition

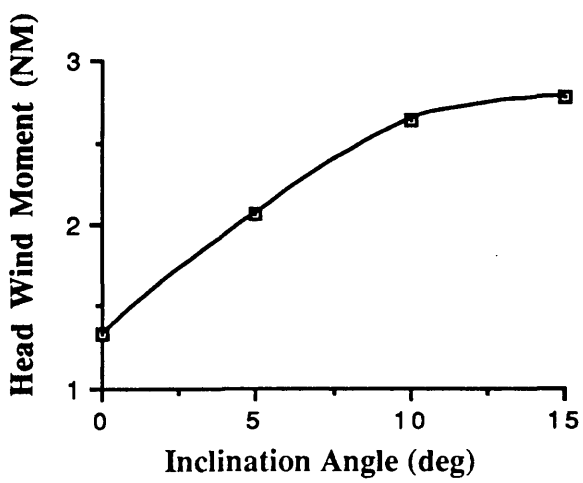

Fig.A.5 Wind moments obtained for the head sea condition

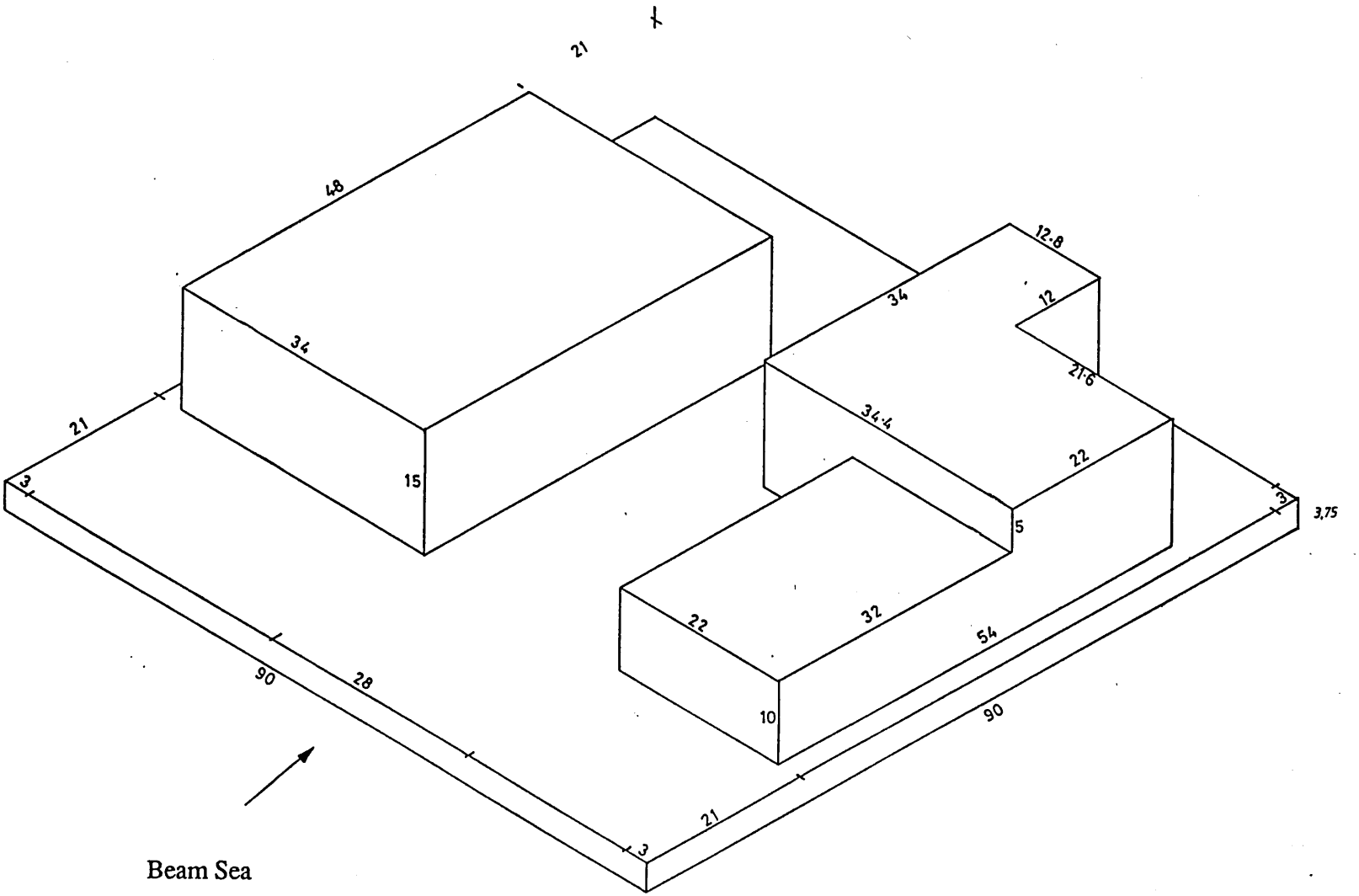

Fig.A.6 Dimensions of the superstructure

(Model dimensions in cm, Scale:1/70)

APPENDIX B

CALCULATION OF YAW RESTORING MOMENT

In this appendix, a set of formulations to calculate the yaw restoring moments is presented. In the time-domain simulations, the yaw restoring moments are calculated from the non-linear mooring forces measured during the experiments of a similar semi-submersible which was tested with catenary moorings at the Hydrodynamics Laboratory.

In calculating the yaw restoring moment, the semi-submersible is assumed to be moored by four cables from the corner columns at an angle of 45^0 with respect to the wave reference system axis. Fig.B.1 shows the mooring forces acting on the corner columns in surge and sway directions.

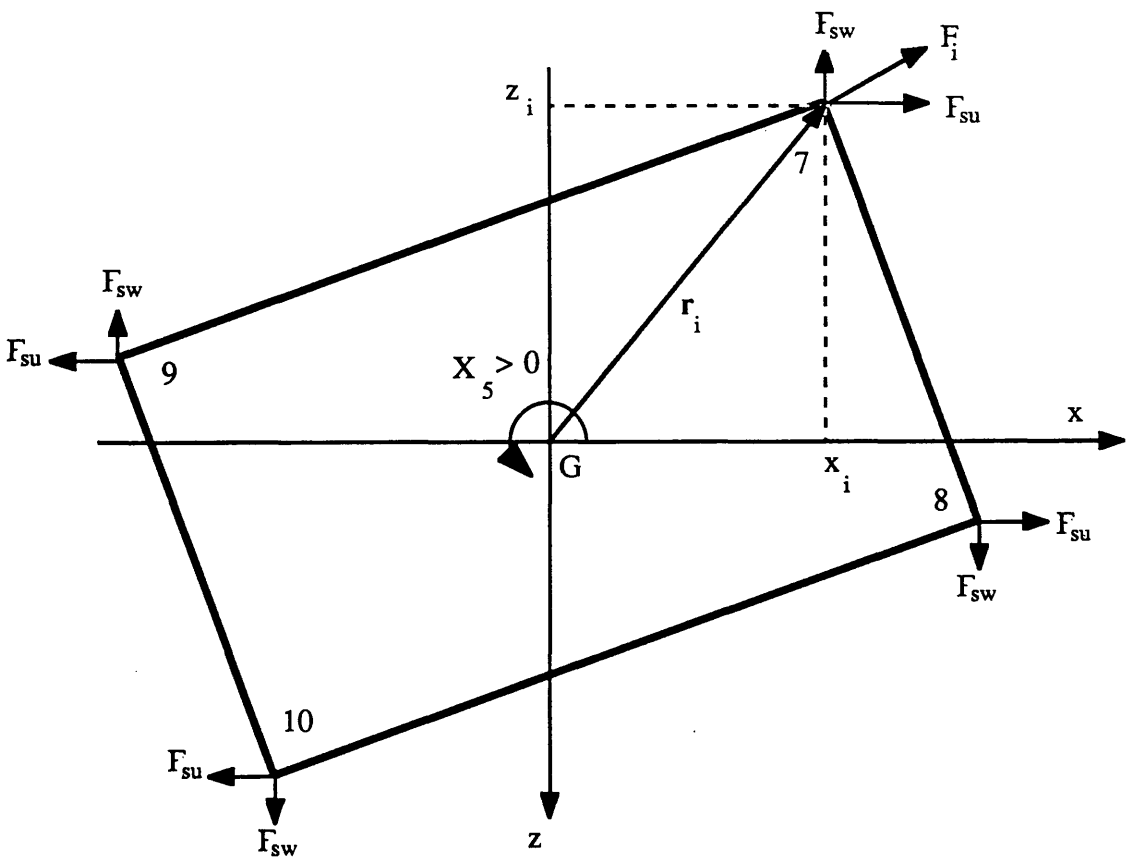

Fig.B.1 Mooring forces acting on the corner columns of the semi–submersible

Anti-clockwise rotation is the positive yaw displacement and the mooring force characteristics in sway and surge direction are assumed to be similar.

Restoring moments due to the mooring forces can be calculated using the following equation:

$$M = \sum_{i=1}^{m} r_i \wedge F_i \tag{B.1}$$

Since there are only four cables to moore the semi-submersible for this particular case, Eq.(B.1) takes the following form:

$$M = \sum_{i=7}^{10} r_i \wedge F_i \tag{B.2}$$

where

r_i Position vector of the ith node with respect to the wave reference system

F_i Mooring forces acting on the ith node

Mooring forces are taken from Fig.B.2 for instantaneous displacements of surge and sway motions. Since the experimental measurements give the total mooring force in one direction surge or sway forces used in the calculations are obtained by dividing the mooring force values by two as follows:

$$F_{su} = \frac{1}{2} S_{su}(x)\, i \tag{B.3}$$

$$F_{sw} = \frac{1}{2} S_{sw}(z)\, j \tag{B.4}$$

where

$S_{su}(x)$ Surge forces

$S_{sw}(z)$ Sway forces

In general, r_i position vector is given in the following form.

$$r_i = x_i\, i + y_i\, j + z_i\, k \tag{B.5}$$

and

$$F_i = F_{su_i}\, i + F_{sw_i}\, j \tag{B.6}$$

If Eq.(B.6) is expressed in an explicit form for mooring forces acting on each node:

$$F_7 = F_{su_7}\, i - F_{sw_7}\, k \tag{B.7}$$

$$F_8 = F_{su_8}\, i + F_{sw_8}\, k \tag{B.8}$$

$$F_9 = - F_{su_9}\, i - F_{sw_9}\, k \tag{B.9}$$

$$F_{10} = - F_{su_{10}}\, i + F_{sw_{10}}\, k \tag{B.10}$$

Vertical forces due to mooring lines are ignored, therefore cross production in Eq.(B.1) takes the following form:

$$M = \sum_{i=7}^{10} \begin{vmatrix} i & j & k \\ x_i & y_i & z_i \\ F_{su} & 0 & F_{sw} \end{vmatrix} \tag{B.11}$$

Yaw restoring moment due to mooring forces is the j th component of Eq.(B.2).

$$M_{yaw} = \sum_{i=7}^{10} (F_{su}\, z_i - F_{sw}\, x_i) \tag{B.12}$$

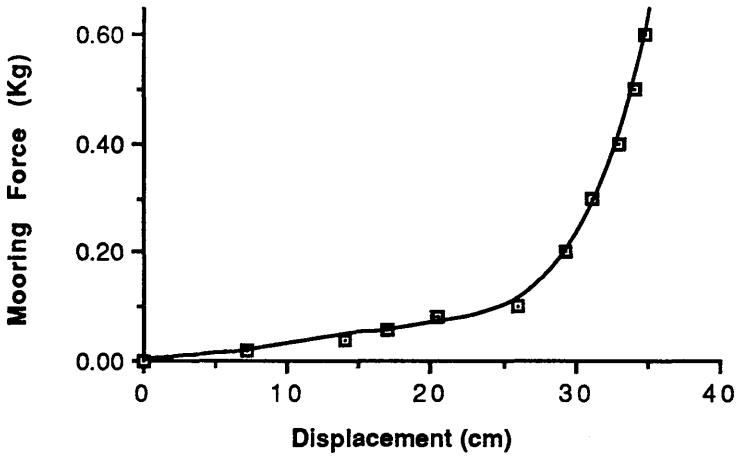

Fig.B.2 Mooring force characteristics for sway and surge motions

APPENDIX C

CALCULATION OF NON-LINEAR ROLL AND PITCH RESTORING MOMENTS

In order to solve the large amplitude non-linear roll and pitch motion equations for a semi-submersible, roll and pitch restoring coefficients are needed as well as the other hydrodynamic properties for any given heel or list angle. For this purpose, program ROSTP was written, which generates the data for restoring forces for a given semi-submersible configuration.

Calculations of stability cross curves were based purely on geometric considerations. In program ROSTP, the centre of gravity; G is supposed to be fixed and the displacement is allowed to vary as the vessel inclines, hence both the displacement and the righting arm values are calculated for each waterline. Basically, there are four main sections in the program to calculate the volume of hulls and columns, the buoyancy centre of the vessel and GZ values which are obtained by using the geometrical relationship between the coordinates of the buoyancy centre and the centre of gravity. A flow-chart given in Fig.C.1 shows the calculation steps in program ROSTP.

In order to use the stability data which was generated by program ROSTP at any given time step, another subroutine called INT was written. This program interpolates and extrapolates GZ values from the stability cross curves using instantaneous displacement and heel (or list) angle of the vessel.

The linear interpolation technique is used in subroutine INT. When solving large amplitude roll and pitch motions, restoring moments as a function of GZ values for a given instantaneous displacement and heel (or list) angle, are calculated by calling subroutine INT. However, different types of interpolation methods can be applied for greater accuracy in obtaining GZ values which may have a very non-linear trend as a function of angular motions. A flow-chart for subroutine INT is given in Fig.C.2.

Figs.C.3-8 show cross curves of stability for angles increasing from 5^0 to 60^0 for heel and from 5^0 to 20^0 for list. Stability cross curve data presented in Figs.C.3-7 were prepared in block data form so that easy access to the data was possible during the calculation of roll and pitch restoring moments in the time-domain simulations. At each time step, the displacement of the vessel was calculated by taking into account the vessel's instantaneous position. This information was then transferred to interpolation routine INT. Using the instantaneous angular motion values and displacements, the corresponding GZ value was obtained by iteration and returned to the subroutine which calculates the roll and pitch restoring moments.

Since there were three different GMs chosen during this study, three different data blocks were generated for each GM. Therefore, the time-domain simulation program requires appropriate data for other GM values which are different than those three GM values, viz. 7.9 cm, 3.8 cm and 1.9 cm (5.53 m, 2.66 m and 1.33 m in full scale). The selected GM values include possible maximum and minimum metacentric heights for the semi-submersible geometry chosen for the study. On the other hand, in order to avoid this restriction for the GM values, program ROSTP can be used as a subroutine for the main program and instead of interpolating or extrapolating instantaneous GZ values, they can be calculated at every time-step for the corresponding underwater geometry of a given semi-submersible configuration. However, this will require a longer CPU time to solve the motion equations. Nevertheless, direct use of program ROSTP in the time-domain simulations will provide more accurate GZ values.

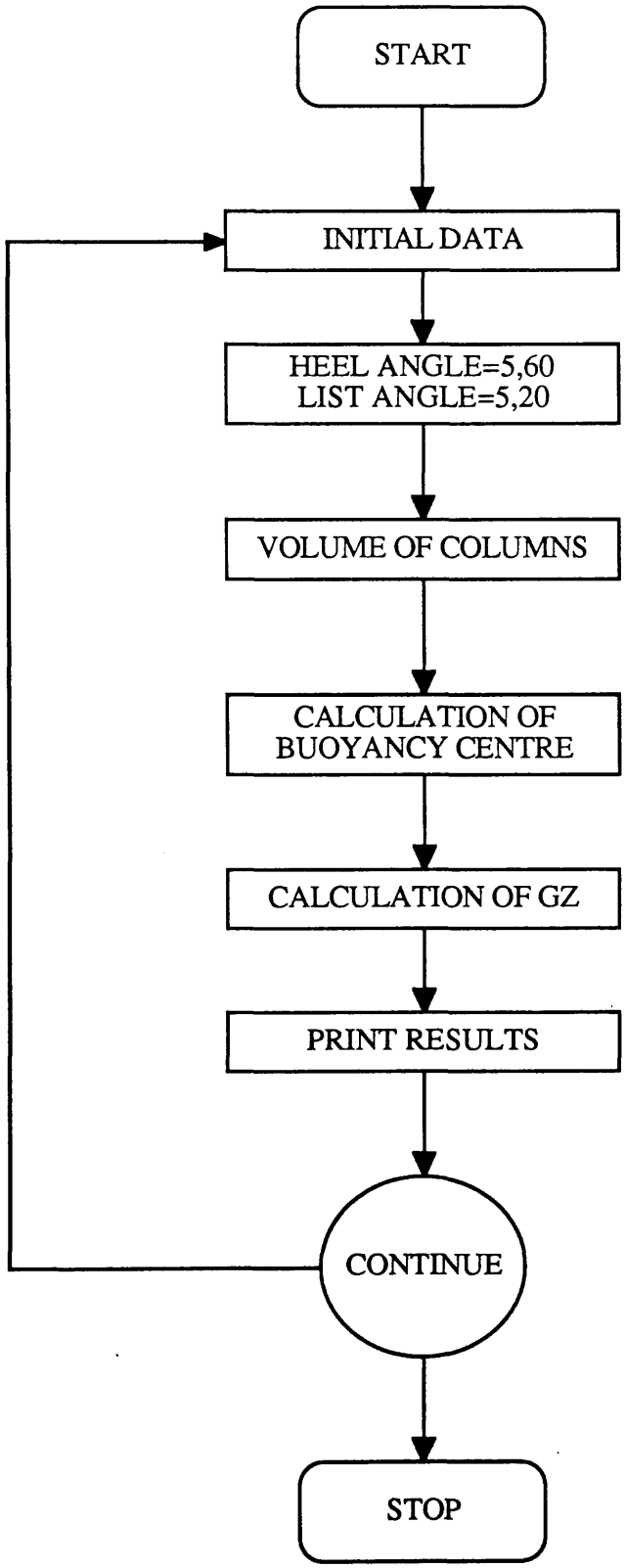

Fig.C.1 Flow-Chart of Program ROSTP

SUBROUTINE INT

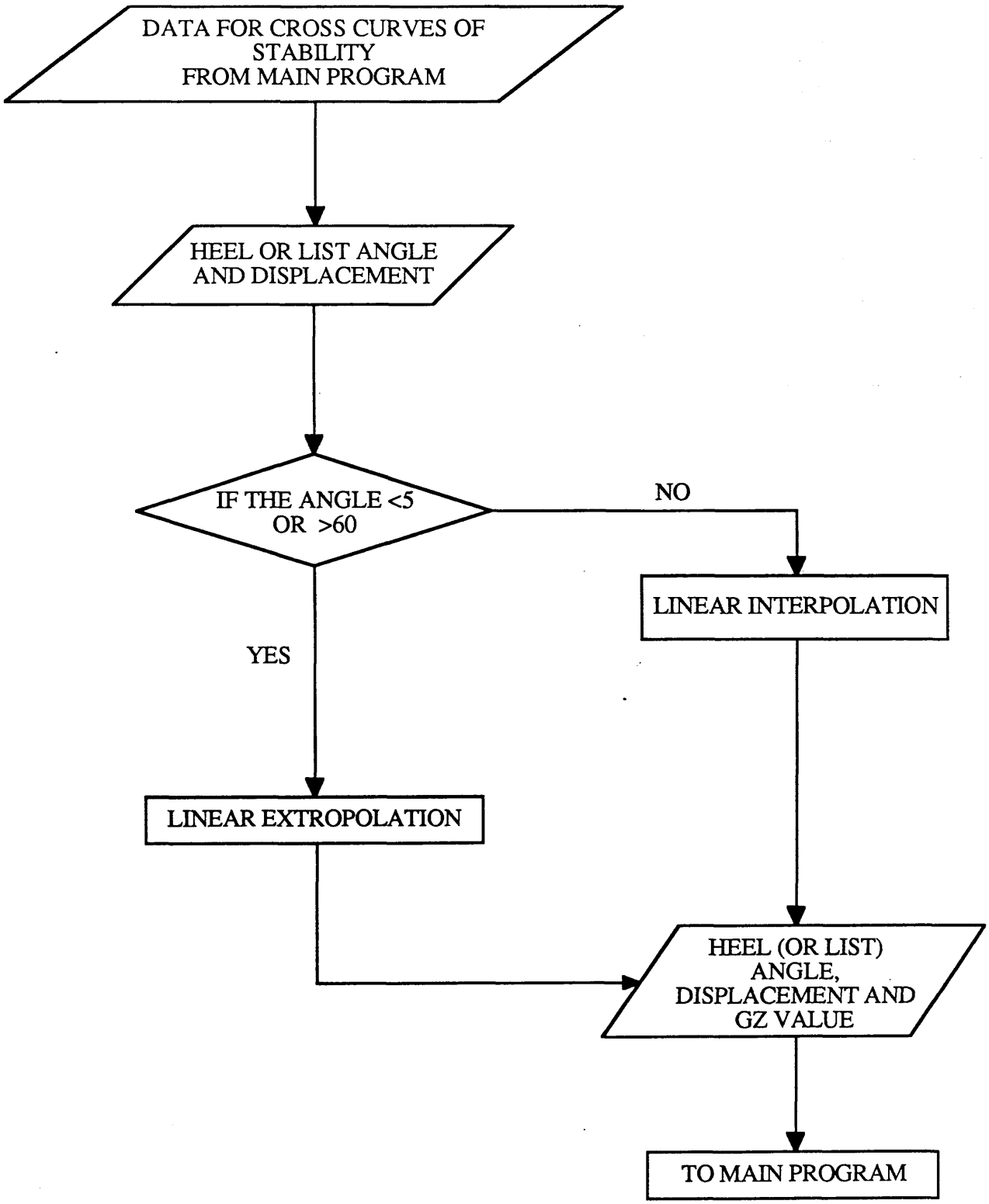

Fig.C.2 Flow-Chart of Subroutine INT

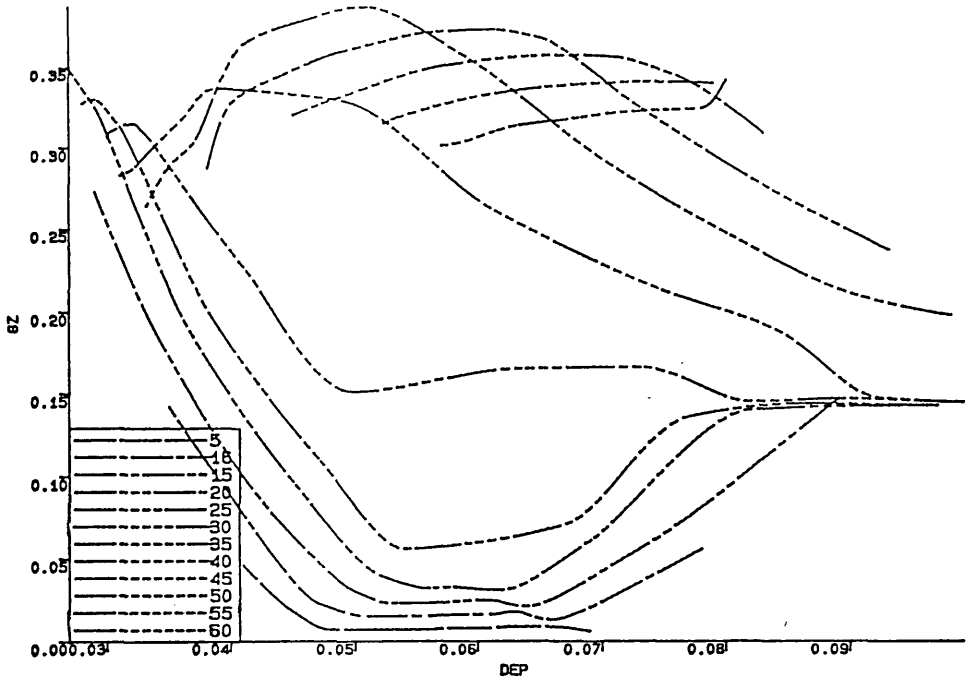

Fig.C.3 Transverse cross curves of stability

KG=22 cm GM=7.9 cm in model scale

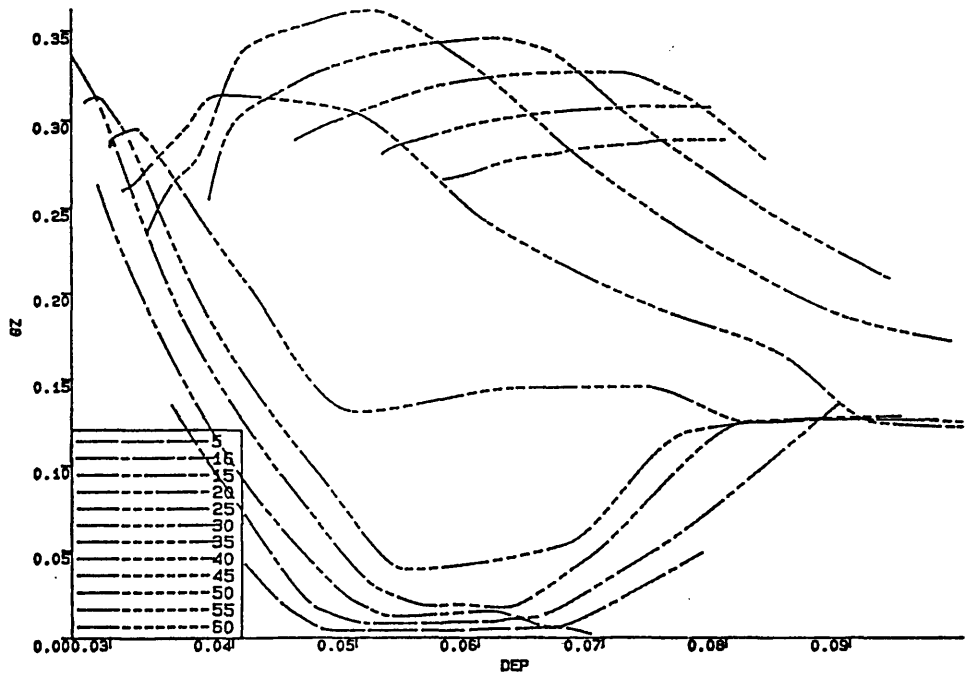

Fig.C.4 Transverse cross curves of stability

KG=26 cm GM=3.8 cm in model scale

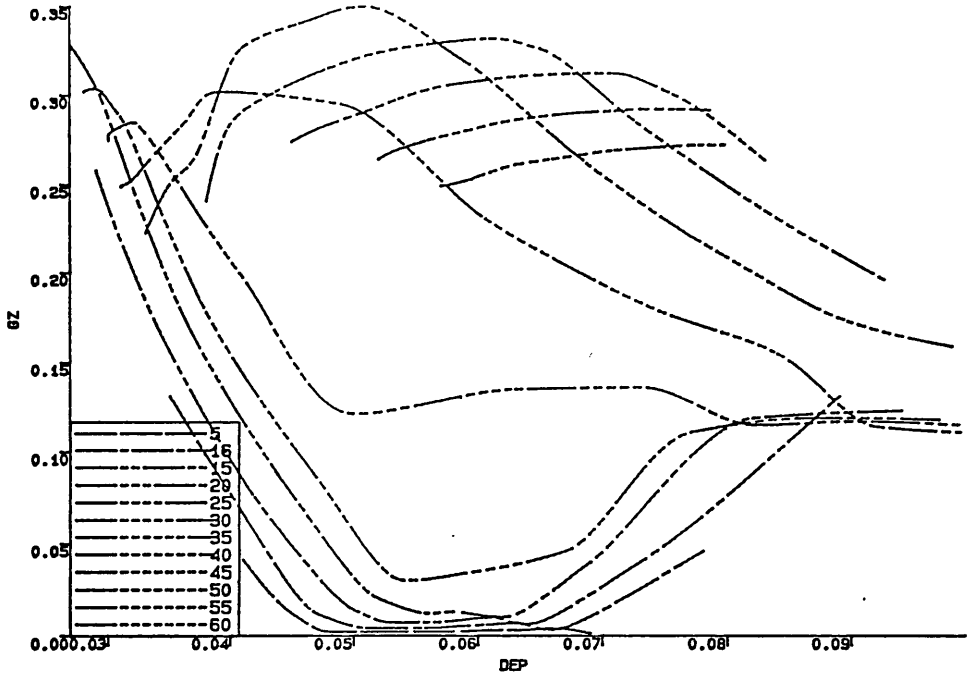

Fig.C.5 Transverse cross curves of stability

KG=28 cm GM=1.9 cm in model scale

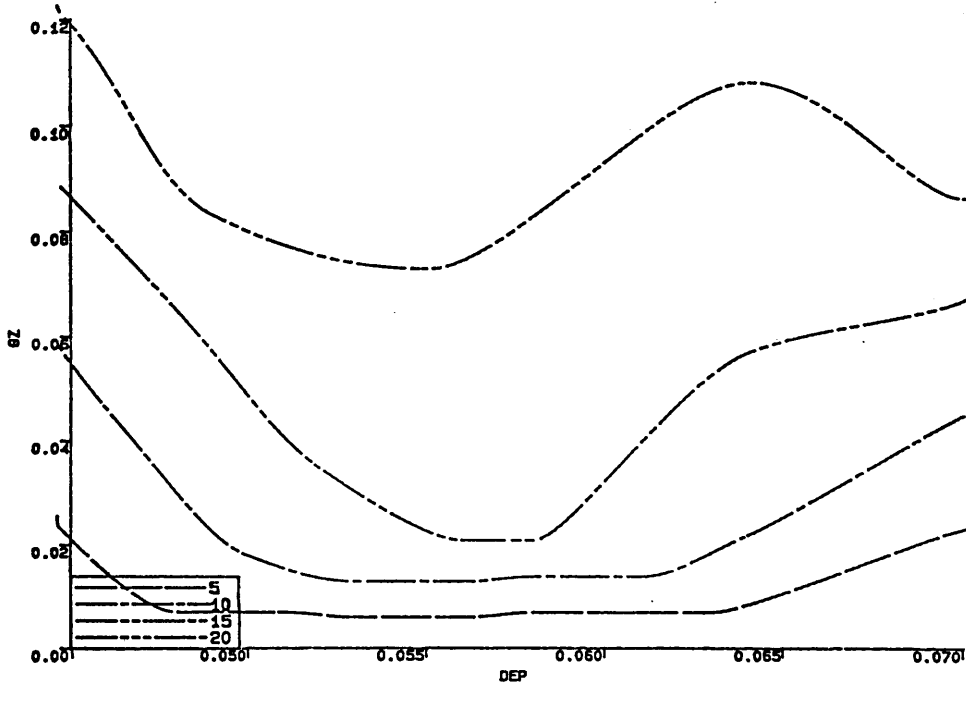

Fig.C.6 Longitudinal cross curves of stability

KG=26 cm GM=7.9 cm in model scale

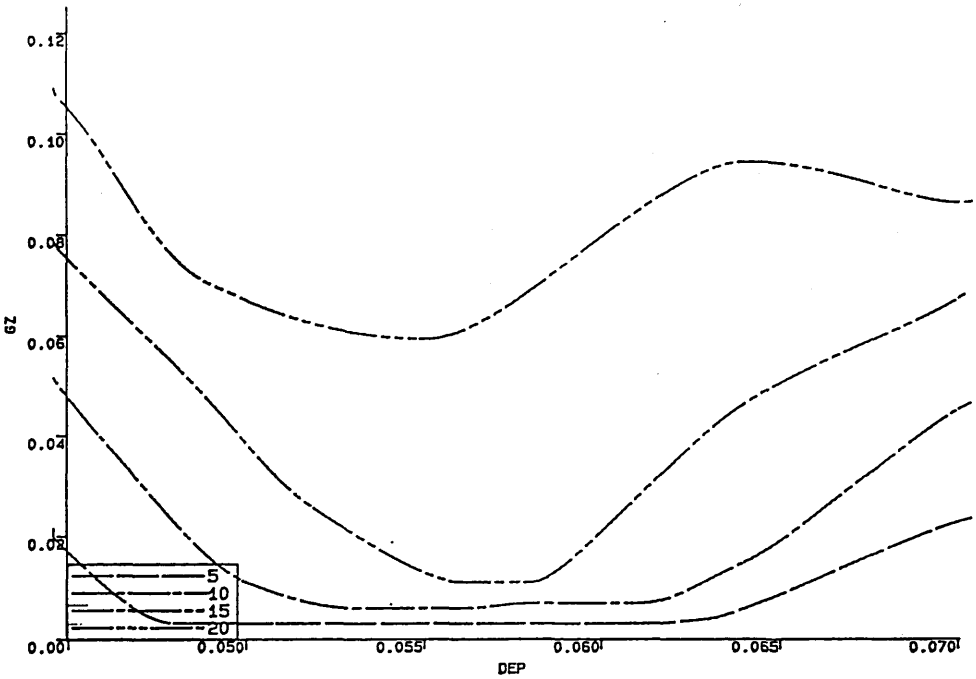

Fig.C.7 Longitudinal cross curves of stability
KG=28 cm GM=3.8 cm in model scale

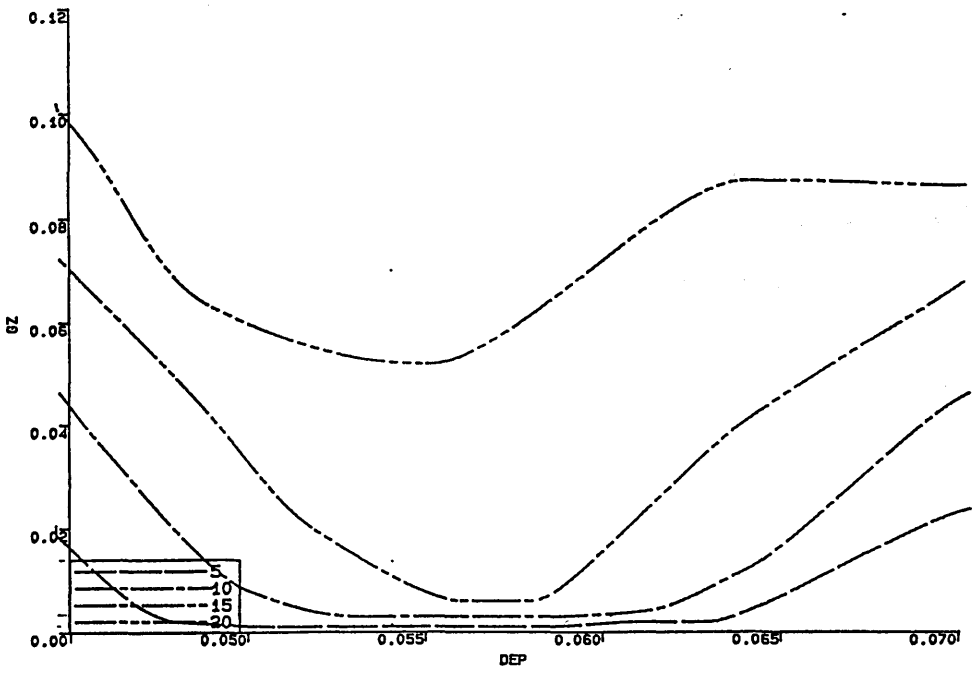

Fig.C.8 Longitudinal cross curves of stability
KG=28 cm GM=1.9 cm in model scale

REFERENCES

Abicht, W., Damage stability and subdivision of semisubmersible drilling rigs, *2nd Int. Conference on Stability of Ships and Offshore Vehicles*, Tokyo, Oct. 1982.

Adachi, H. and Kagemoto, H., Transient motions of a semi-submersible after damages, *Proc. of the Int. Conference on Stationing and Stability of Semi-Submersibles*, Glasgow 1986.

Atlar, M. and Lai, P.S.K. *A Two Dimensional Method for Estimating Hydrodynamic Loads and Motions of a Twin-Hulled Semi-Submersible Associated with Some Hydrodynamic Aspects in Regular Seas*, Report NAOE-85-34, Glasgow University, Glasgow, 1985 b.

Atlar, M., *Method for Predicting First-Order Hydrodynamic Loads on Single and Twin Sections by the Frank Close-Fit Technique,* Report NAOE-85-41, Glasgow University, Glasgow, 1985 a.

Atlar, M., Towards the understanding of the steady tilt phenomenon in semi-submersibles, *Ph.D. Thesis*, University of Glasgow, 1986.

Bishop, S. R. and Virgin, L. N., The onset of chaotic motions of a moored semi-submersible, *Proceedings of the 6th Int. Conference on Offshore Mechanics and Arctic Engineering*, OMAE, pp.319-323, 1987.

Bishop, S. R., Leung, L. M. and Virgin, L. N. Predicting incipient jumps to resonance of compliant marine structures in an evolving sea-state, *J. Offshore*

Brebbia, C. A. and Walker, S., *Dynamic Analysis of Offshore Structures*, Newnes-Butterworths, 1979.

Chakrabarti, S. K. and Cotter, D. C., Nonlinear Wave Interaction with a Moored Floating Cylinder, *Proc. of the 16th Annual Offshore Tech. Conf.*, Paper No. OTC 4814, Houston, pp.325-334, 1984b.

Chakrabarti, S. K., *Hydrodynamics of Offshore Structures*, CMP and Springer-Verlag, New York, 1987.

Chakrabarti, S. K., Steady Drift Force on Vertical Cylinder-Viscous vs. Potential, *Applied Ocean Research*, **6**, No.2, pp.73-82, 1984a.

Chen, H. H., Shin, Y. S. and Wilson, J. L., Towards rational stability criteria for semisubmersibles- A pilot study, *Third Int. Conference on Stability of Ships and Ocean Vehicles*, Gdansk, pp. 61-68, Sept. 1986.

Clauss, G. F., Stability and dynamics of semisubmersible after accidental damage, *Offshore Technology Conference*, Houston, OTC 4729, pp.159-171, May 1984.

Dahle, E. A., Intact and damaged stability of rigs and crane vessels, *Norwegian Maritime Research*, **9**, No. 3, pp. 33-42, 1981.

Dahle, L. A., Mobile platform stability: Project synthesis with recommendations for new philosophies for stability regulations, *Offshore Technology Conference*, Houston, OTC 4988, May 1985.

De Souza, P. M. F. M. and Miller, N. S., The intact and damaged stability of two semi-submersible models under wind and wave loading, *Offshore Technology Conference*, Houston, OTC 3298, pp.2147-2157, May 1978.

De Souza, P. M. F. M., *Dynamic response of semi-submersibles*, Departmental Report, Department of Naval Architecture and Ocean Engineering, University of Glasgow, NAOE-HL-76-03, 1976.

Dean, R. G., Relative validities of water wave theories, *Journal of Waterways and Horbors Division*, Proc. of ASCE, **96**, No. WW1, pp. 105-119, Feb. 1970.

Dean, R. G., Stream function representation of nonlinear ocean waves, *Journal of Geophysical Research*, **70**, No.18, pp.4561-4572, Sep. 1965.

Deepwater Drilling Report: Innovative semi-submersible will service fixed platforms and aubsea pipe lines,*Ocean Industry*, **17**, pp. 66-68, June 1982.

Deepwater Drilling Report: New Generation semi-submersible for deepwater hostile environment, *Ocean Industry*, **17**, pp. 37-44, Aug. 1982.

Dudgeon, E. H., Hydrodynamic Model Studies of the Ocean Ranger Marine Disaster, *Proc. of the Int. Conference on Stationing and Stability of Semi-Submersibles*, Glasgow 1986.

Eatock Taylor, R. and Jefferys, E.R. Variability of hydrodynamic load predictions for a tension leg platform, *Ocean Engineering,* **13**, No 5, pp.449-490, 1986.

Faltinsen, O. and Michelsen, F., Motions of large structures in waves at zero Froude Number, *Int. Symposium on the Dynamics of Marine Vehicles and Structures in Waves,* University College London, 1974.

Faulkner, D., Incecik, A. and Lang, C., Design evaluation of a multi-purpose semi-submersible, Paper read at the IESIS on 10th Jan., 1989.

Ferretti, C. and Berta, M. Viscous effect contribution to drift forces on floating structures, *Proc. First Int. Symp.on Ocean Engineering and Ship Handling*, SSPA, Gothenborg, 1980.

Garrison, C. J., Hydrodynamic loading of large offshore structures: Three-Dimensional Source Distribution Methods, Chapter 3 of *Numerical Methods in Offshore Engineering*, Zienkiewicz, O. C., Lewis, R. W. and Stagg, K. G. (Eds.), John Wiley, pp.87-140, 1978.

Goodfellow Associates Limited, *Offshore Engineering: Development of Small Oilfields*, Graham & Trotman Limited, 1986.

Hallam, M. G., Heaf, N. J., and Wootton, L. R., *Dynamics of Marine Structures: Method of Calculating the Dynamic Response of Fixed Structures Subject to Wave and Current Action,* Report UR8, CIRIA Underwater Engineering Group, London, 1978.

Hineno, M., Takegawa, H., Oda, T.,and Abe, M., The effect of low frequency roll motion of under-deck clearance of semi-submersible platform, *2nd Int. Conference on Stability of Ships and Offshore Vehicles*, Tokyo, Oct. 1982.

Hogben, N. and Standing, G., Wave loads on large bodies, *Int. Symposium on the Dynamics of Marine Vehicles and Structures in Waves,* University College London, 1974.

Hooft, J. P., Hydrodynamic Aspects of Semi-Submersible Platforms, *Ph. D. Thesis,* Netherlands Ship Model Basin, Pub. No. 400, Wageningen, 1972.

Huang, X. and Naess, A., Dynamic response of a heavily listed semi-submersible platform, *2nd Int. Sym. on Ocean Engineering and Ship Handling*, 1983.

Huang, X., Hoff, J. R. and Naess, A., On the behaviour of semisubmersible platforms at large angles, *Offshore Technology Conference*, Houston, OTC 4246, pp.193-203, May 1982.

Huse, E. and Nadrelid, T., Hydrodynamic stability of semi-submersibles under extreme weather conditions, *Offshore Technology Conference*, Houston, OTC 4987, May 1985.

Incecik, A., Design Aspects of the Hydrodynamic and Structural Loading on Floating Offshore Platforms Under Wave Excitation, *Ph.D. Thesis,* University of Glasgow, 1982.

Incecik, A. *Structural Response and Optimum Design Analysis of Stable Floating Platforms Under Wave Excitation,* Report NAOE-HL-78-27, Glasgow University, Glasgow, 1978.

Incecik, A., Wu S-K, Söylemez, M., Effect of different mathematical models in calculating motion and structural response of offshore platforms, *Proc. of 3rd Int. Symposium on Integrity of Offshore Structures,* Glasgow, 1987.

Kagemoto, H., Takai, R. and Adachi, H., On the stability of semisubmersible oil drilling rigs (Part 2: Dynamic Stability), *Papers of Ship Research Institute*, 24, No. 6, Nov. 1987, (in Japanese).

Kim, C. H., and Chou, F., Motions of a Semi-Submersible Drilling Platform in Head Seas, *Marine Technology*, **10**, No 2, pp. 112-123, April 1973.

Kuo, C.,Lee, A. and Welya, Y., Semisubmersible intact stability-static and dynamic assessment and steady tilt in waves, *Offshore Technology Conference*, Houston, OTC 2976, May 1977.

Lee, C. M. and Newman, J. N. The vertical mean force and moment of submerged bodies under waves, *J. Ship Research*, 15, No. 3, pp 231-245, Sept. 1971.

Longuet-Higgins, M. S. and Stewart, R. W., The changes in amplitude of short gravity waves on steady non-uniform currents, *J. Fluid Mech.*, **10**, pp.529-549, 1961.

Lundgren, H., Sand, S. E. and Kirkegaard, J., Drift forces and damping in natural sea states, *Proc. Third Int. Conf. BOSS*, MIT, 1982.

MacCamy, R. C. and Fuchs, R. A., Wave forces on piles: A diffraction theory, *Technical Memorandum No. 69*, Beach Erosion Board, Corps of Engineers, Dec. 1954.

Martin, J. and Kuo, C., Calculations for the steady tilt of semi-submersibles in regular waves, *Trans. of RINA*, **122**, pp. 87-101, 1979.

Martinovich, W. M. and Praught, M. W., Stability requirements for semi-submersibles- A Designer's Viewpoint, *Proc of the Int. Conference on Stationing and Stability of Semi-Submersibles*, Glasgow 1986.

Mathisen, J., and Carlson, C. A., A Comparison of calculation methods for wave loads on twin pontoon semi-submersible, *Proceedings on Internatioal Symposium on Ocean Engineering-Ship Handling*, SSPA, Gothenburg, Sweden, Sept. 1980.

McIver, D. B., Taggart, S., Starsmore, N. and Lillywhite, P. A., The development of stability analysis of semi-submersibles, *Second International Symposium on Ocean Engineering and Ship Handling*, Gothenburg, SSPA, pp.363-374, 1983.

Miller, N. S., Effect of geometry and dimensions on natural heaving period in semi-submersibles and tethered buoyant platforms-some design considerations, *Lecture Notes*, Dept. of Naval Arch. and Ocean Eng., Glasgow University, Sept. 26-30, 1977.

Moncarz, P. D., Paulling, J. R., Taylor, R. K. and Thomas, J. M., *Stability of damaged platforms, Behaviour of Offshore Structures*, Amsterdam, pp.205-212, 1985.

Morison, J. R., O'Brien, M. P., Johnson, J.W., and Schaaf, S. A., The force exerted by surface waves on piles, *Petroleum Transactions,* AIME, **189**, pp. 149-147, 1950.

Mourelle, M. M., Jacob, B. P. and Ebecken, F. F., Nonlinear dynamic behaviour of semisubmersible platforms, *Proc. 6th. Int. Symp. on Offshore Engineering*, Coppe, Aug. 1987.

Muir Wood A. M., *Coastal Hydraulics*, Macmillan, 1969.

Naess, A., Hoff, J. R. and Herfjord, K., Modelling of the dynamic behaviour of damaged platforms by time simulation methods and model tests, *Behaviour of Offshore Structures*, Amsterdam, pp.195-203, 1985.

Naess, A.and Hoff, J. R., Time simulation of the dynamic response of heavily listed semisubmersible platforms in waves, *Norwegian Maritime Research*, No. 1, 1984.

NAG: *Fortran Library Manuals: Mark 7*, Numerical Algorithms Group, 1978.

Nakamura, I., Takaki, M., Park, R-S. and Harada, S., Hydrodynamic loads acting on a semisubmersible unit with a large list angle, *Trans. West Japanese Society of Naval Architects*, No.68, 1984, (in Japanese).

Numata, E. and McClure, A. C., Experimental study of stability limits for semisubmersible drilling platforms, *Offshore Technology Conference*, Houston, OTC 2285, May 1975.

Numata, E. and Michel, W. H., Experimental study of stability limits for semisubmersible drilling platforms, *Offshore Technology Conference*, Houston, OTC 2032, May 1974.

Numata, E., (Written discussion to Martin, J. and Kuo, C., 1979), *Trans. of RINA*, 122, pp. 87-101, 1979.

Numata, E., Michel, W. H. and McClure, A. C., Assessment of stability requirements for semisubmersible units, *SNAME Transactions*, 84, pp. 56-74, 1976.

Ogilvie, T. F., First and second order forces on a cylinder submerged under a free surface, *J. of Fluid Mech.*, **16**, pp.451-472, 1963.

Oo, K. M. and Miller, N. S., Semi-submersible design: The effect of differing geometries on heaving response and stability, *Trans. of RINA*, **119**, pp.97-119, 1977.

Östergaard, C. and Schellin, T. E. Comparison of experimental and theoretical wave on floating and compliant offshore structures, *Applied Ocean Research,* **9**, No 4, 1987.

Paulling, J. R. The sensitivity of predicted loads and responses of floating platforms to computational methods, *Integrity of offshore structures,* Eds. D. Faulkner, M. J. Cowling and P. Frieze, Elsevier Applied Science Publishers, Glasgow, 1981.

Paulling, J. R., Time domain simulation of semisubmersible platform motion with application to the tension-leg platform, *Proc. of Second Ship Technology and Research (Star) Symposium*, San Francisco, CA, May 25-27, 1977.

Pijfers, J. G. L. and Brink, A. W., Calculated drift forces of two semisubmersible platform types in regular and irregular waves, *Offshore Technology Conference*, Houston, OTC 2977, pp.155-164, May 1977.

Pinkster, J. A., Low Frequency, Second-Order Wave Exciting Forces on Floating Structures, *Doctoral Thesis*, MARIN Publ. No. 650, Wageningen, The Netherlands,1980.

Pinkster, J. A., Mean and Low Frequency Wave Forces on Semi-Submersibles, *Proc. of the 13th Annual Offshore Tech. Conf.*, Paper No. OTC 3951, Houston, 1981.

Rawson, K. J. and Tupper, E. C., *Basic Ship Theory,* Longmans Publication, 1968.

Rules for Building and Classing Offshore Mobile Drilling Units, American Bureau of Shipping, New York, 1973.

Rusaas, S., The capsizing of "Alexander L. Kielland", *2nd Int. Conference on Stability of Ships and Offshore* Vehicles, Tokyo, Oct. 1982.

Sarpkaya, T., and Isaacson., M., *Mechanics of Wave Forces on Offshore Structures,* Van Nostrand Reinhold, New York, 1981.

Sarpkaya, T., In-line and transverse forces on cylinders in oscillatory flow at high Reynolds numbers, *Offshore Technology Conference*, Houston, OTC 2553, pp.95-108, May 1976.

Shark, G., Shin, Y. S. and Spencer, J. S., Dynamic-Response-Based Intact and Residual Damage Stability Criteria for SemiSubmersible Units, *presented at the Annual Meeting*, New York, N.Y., SNAME, Nov. 1989.

Shields, D. R. and Zueck, R. F., Deepwater semi-submersible motion simulation, *Proc. The Marine Technology Societ's and IEEE,* Ocean Eng. Soc's Conf., *Ocean 84,* **2**, Wash. D. C., Sept. 1984.

Shields, D. R., Zueck, R. F. and Nordell, W. J., Ocean Model Testing of a Small Semi-Submersible, *Proc. of the 19th Annual Offshore Tech. Conf.*, Paper No. OTC 5454, Houston, 1987.

Sommerville, D. M. Y., *Analytical Geometry of Three Dimensions*, Cambridge University Press, 1939.

Söylemez, M. and Incecik, A., Prediction of large amplitude motions and stability of intact and damaged mobile platforms, *Offshore Technology Conference*, Houston, OTC 5628, May 1988.

Söylemez, M., *Motion Response Simulation of Damaged Floating Platforms*, Annual Report, Glasgow University, 1986.

Söylemez, M., *Motion Response Simulation of Damaged Floating Platforms*, Annual Report, Glasgow University, 1988.

Springett, C. N. and Praught, M. W., Semisubmersible design considerations-Some new developments, *Marine Technology*, 23, No.1, pp.12-22, Jan. 1986.

Standing, R. G. The sensitivity of structure loads and responses to environmental modelling, *Proc. of SUT Int. Conf. on Modelling the Offshore Environment,* London, 1987.

Standing, R.G., Dacunha, N.M.C. and Matten, R.B., *Mean Wave Drift Forces: Theory and Experiment*, NMI Report No. R124,OT-R-8175, 1981b.

Standing, R.G., Dacunha, N.M.C. and Matten, R.B., *Slowly–Varying Second-Order Wave Forces: Theory and Experiment*, NMI Report No. R138, OT-R-8211, Oct. 1981a.

Stoker, J. J., *Nonlinear Vibrations in Mechanical and Electrical Systems*, Interscience Publishers Ltd., London, 1950.

Takagi, M., Arai, S-I, Takezawa, S., Tanaka, K. and Takarada, N., A comparison method for calculating the motion of a semi-submersible, *Ocean Engineering,* **12**, No 1, pp. 45-97, 1985.

Takai, R., Kagemoto, H. and Adachi, H., On the stability of semisubmersible oil drilling rigs (Part 1: Static Stability), *Papers of Ship Research Institute*, 24, No. 6, Nov. 1987, (in Japanese).

Takaki, M., Higo, Y. and Nakamura, K., A study on the stabilizing method of semisubmersible platform with a large list in waves, *Trans. Soc. Naval Arch. Japan*, 204, 1987, (in Japanese).

Takarada, N., Nakajima, T. and Inoue, R., A phenomenon of large steady tilt of a semi-submersible platform in combined environmental loadings, *Third Int. Conference on Stability of Ships and Ocean Vehicles*, Gdansk, pp. 225-237, Sept. 1986.

Takarada, N., Obokata, J., Inoue, R.,Nakajima, T., and Kobayashi, K., The stability on semi-submersible platform in waves (on the capsizing of moored semi-submersible platform), *2nd Int. Conference on Stability of Ships and Offshore Vehicles*, Tokyo, Oct. 1982.

Taylor, Sir Geoffrey, The action of a surface current used as a breakwater, *Proc. R. Soc. (Series A)*, **231**, pp.466-478, 1955.

Vassalos, D., Konstantopoulos, G., Kuo, C. and Welaya, Y., A realistic approach to semisubmersible stability, *SNAME Transactions*, 93, pp. 95-128, 1985.

Virgin, L. N. and Bishop S. R., Catchment regions of multiple dynamic responses in nonlinear problems of offshore mechanics, *7th Int. Sym. on Offshore Mech. and Arctic Engineering*, OMAE, Houston, Tex., pp.15-22, Feb. 7-12, 1988.

Wilson, J. F. (Editor), *Dynamics of Offshore Structures,* Wiley Interscience, New York, 1984.